SMALL RESIDENCE MULTIZONE MODELING WITH PARTIAL CONDITIONING FOR ENERGY EFFICIENCY IN HOT AND HUMID CLIMATES

A Dissertation

by

SIMGE ANDOLSUN

Submitted to the Office of Graduate Studies of
Texas A&M University
in partial fulfillment of the requirements for the degree of

DOCTOR OF PHILOSOPHY

Chair of Committee,	Charles H. Culp
Committee Members,	Jeff S. Haberl
	Mark J. Clayton
	Liliana O. Beltran
	David E. Claridge
Department Head,	Ward V. Wells

August 2013

Major Subject: Architecture

ABSTRACT

The purpose of this study is to reduce the energy cost of the low-income households in the hot and humid climates of the U.S. and thereby to help them afford comfortable homes. In this perspective, a new HVAC energy saving strategy, i.e. "partial conditioning" was modeled and its potential to reduce the HVAC energy consumption of the low income homes in Texas was quantified. The "partial conditioning" strategy combined three primary ideas: 1) using historic courtyard building schemes to provide a buffer zone between conditioned spaces, 2) zoning and applying occupancy based heating/cooling in each zone, and 3) reusing the conditioned air returning from the occupied zones in the unoccupied zones before it is returned to the system. The study was conducted in four steps: 1) data collection, 2) baseline design and modeling, 3) partial conditioning design and modeling, and 4) analyses and recommendations.

First, a site visit was held to the Habitat for Humanity office in Bryan, Texas to collect data on the characteristics of the Habitat for Humanity houses built in Bryan. Second, a base-line Habitat for Humanity house was designed and modeled based on this information along with multiple other resources including International Energy Conservation Code 2012 and Building America benchmark definitions. A detailed comparison was made between the commonly used energy modeling tools (DOE-2.1e, EnergyPlus and TRNSYS) and a modeling method was developed for the estimation of the baseline energy consumption. Third, the "partial conditioning" strategy was introduced into the baseline energy model to simulate a partially conditioned atrium house. As the occupied zone and the direction of the airflow changed throughout the year in the partially conditioned house, this step required an innovative air loop model with interzonal air ducts that allowed for scheduled bi-directional airflow. This air loop was modeled with the AirflowNetwork model of EnergyPlus. Fourth, the modeling results were analyzed and discussed to determine the performance of the partial conditioning strategy in a hot and humid climate. It was found that partial conditioning strategy can provide substantial (37%-46%) reduction in

the overall HVAC energy consumption of small residences (∼1,000 ft^2) in hot and humid climates while performing better in meeting the temperature set points in each room. It was also found that the quantity of the energy savings that can be obtained with the partial conditioning strategy depends significantly on the ground coupling condition of the house for low rise residential buildings.

DEDICATION

To my mother, father, sister and Alper for making me feel special and loved.

ACKNOWLEDGEMENTS

First of all, I would like to thank my advisor, Dr. Charles H. Culp, for all his support, guidance and endless research ideas. In the future, I will always benefit from his constant encouragement in shaping us into independent thinkers and researchers during these graduate years. I would like to thank Dr. Jeff S. Haberl for sharing his depth of knowledge and experience in the building energy simulation field and for his continuous support and encouragement during my years at Texas A&M. I am also very grateful for the invaluable contributions of my committee members to my research, which significantly improved the quality of this dissertation.

I also would like to express my gratitude to my fellow research group members at Texas A&M who have provided me the best possible environment for scientific progress and social well-being: Mini Malhotra who endured hours of scientific discussions and has become a close friend and Jaya Mukhopadhyay who was always there for me to answer my questions.

I would like to thank American Society of Heating, Refrigerating and Air-conditioning Engineers (ASHRAE) for the ASHRAE Grant-in-aid award, the Texas A&M University Office of Graduate Studies for the Texas A&M Dissertation Fellowship and the Texas A&M Energy Systems Laboratory for their support.

Finally and very importantly, I am deeply grateful to my family for believing in me unconditionally which constantly encouraged me to do better in life. I appreciate their love, support and patience. I am thankful that they have always respected my choices and trusted my decisions which helped me become who I want to be. But above all, I am most grateful to Alper who supported me, helped me, bared with me throughout the last four years of my Ph.D. studies and taught me a variety of useful skills including the LaTex program which I used to write this dissertation. Most importantly, I am grateful to him for making me smile every day.

NOMENCLATURE

A_d	Cross-section area of an air duct (m^2)
A_s	Area of the slab (ft^2)
C	Air mass flow coefficient (kg/s-m at 1 Pa)
C_c	Correction factor for the DOE-2 ground coupling load (unitless)
C_d	Discharge coefficient
CFA	Conditioned floor area (ft^2)
COU	Coefficient of utilization
D2	Modeled with DOE-2
D_e	Circular equivalent of rectangular duct for equal length, fluid resistance, and airflow (mm)
D_h	Hydraulic diameter (mm)
$\triangle P$	Pressure difference across a crack or opening (Pa)
$\triangle P_r$	Reference pressure difference (Pa)
E	Maintained lighting level (fc)
$EGain$	Annual total heat gain from the equipment (kWh/day)
-eit	Ground coupled by external iteration of EnergyPlus and Slab
E_{mod}	Modified lighting level (Lux)
EP	Modeled with EnergyPlus
E_{thres}	Threshold lighting level (Lux)
$F2$	Perimeter conduction factor (Btu/hr-°F-ft)
FFA	Finished floor area (ft^2 or m^2)
f	Friction factor (dimensionless)
GCS	Ground coupled with Slab model
GCT	Ground coupled with TRNSYS slab-on-grade model
GCTh	Hourly TRNSYS slab/soil interface temperatures

GCTm	Monthly average TRNSYS slab/soil interface temperatures
GCW	Ground coupled with Winkelmann's slab-on-grade model
GI	Ground isolated
h	Friction loss of the air ducts (in.w.g./100 ft)
h_{fi}	Floor inside surface convection coefficient (kJ/hr.m^2.K)
$IGain$	Daily internal gain per dwelling unit (Btu/day)
-iit	Ground coupled by a single internal iteration of EnergyPlus and Slab
L	Effective leakage area (ft^2 or cm^2)
L_{actual}	The actual duct length (ft)
L_d	Duct length (m)
L_f	Fraction of the lights in the room that is on (0-1)
$L_{fitting}$	Virtual duct lengths to represent the pressure loss through the fittings (ft)
L_L	The maximum lighting level of the room (Watt)
LLF	Light loss factor
LR	Hourly lighting requirement of the room (Watt)
$\dot{m}$	Air mass flow rate (kg/s)
$\dot{m}_{max}$	Maximum air mass flow rate (kg/s)
n	Airflow exponent (dimensionless)
N_{br}	Number of bedrooms
N_{La}	Number of luminaires
O_f	Fraction of the hour that the room is occupied (0-1)
P	Perimeter length of a crack or opening (m)
P_{ducts}	Pressure loss in the air ducts (in.w.g.)
P_{exp}	Exposed perimeter (ft)

P_{furn}	External static pressure of a furnace (in.w.g.)
P_{sys}	Pressure loss in the air handling unit (in.w.g.)
Q	Airflow rate (cfm)
Q_{fm}(s)	Monthly average floor heat flux(es)
Q_{LOADS}	Floor heat flux at 70°F steady state zone air temperature
Q_{mod}	Floor heat flux at 78°F steady state zone air temperature
Q_r	Predicted airflow rate at $\triangle P_r$ (m^3/s)
$Q_{slab/zair}$	Heat transfer between the slab and the zone air
$Q_{soil/slab}$	Heat transfer between the soil and the slab
R_{carpet}	Resistance of the carpet (hr.ft^2°F/Btu)
R_{eff}	Effective resistance of the slab (hr.ft^2°F/Btu)
R_{fic}	Resistance of the fictitious insulation layer (hr.ft^2°F/Btu)
R_{film}	Resistance of the inside air film (hr.ft^2°F/Btu)
R_{slab}	Resistance of 4″ concrete (hr.ft^2°F/Btu)
R_{soil}	Resistance of the soil (hr.ft^2°F/Btu)
R_{us}	Actual slab resistance (hr.ft^2°F/Btu)
ρ	Air density (kg/m^3)
SA_{duct}	Duct surface area (m^2)
SLA	Specific leakage area (unitless)
TEL	The total effective length of the duct run (ft)
T_{am}(s)	Monthly average outside air temperature(s)
T_{fi}	Floor inside surface temperature (°C)
T_g(s)	Monthly average deep ground temperature(s) calculated by DOE-2 using Kasuda approach
T_{LOADS}	The 70°F default constant zone air temperature that DOE-2 uses

T_{mod}	78°F constant zone air temperature
TR	Modeled with TRNSYS
$T_{slab/soil}$(s)	Monthly average slab/soil interface temperature(s)
T_{zair}	Zone air temperatures
U_{eff}	The effective U-value of the slab (Btu/hr.ft^2°F)
$\dot{v}$	Air volume flow rate (m^3/s)
$\dot{v}_{max}$	Maximum air volume flow rate (m^3/s)
-wotEv	Evapotranspiration flag of Slab is off
-wtEv	Evapotranspiration flag of Slab is on

TABLE OF CONTENTS

LIST OF FIGURES

LIST OF TABLES

1. INTRODUCTION

1.1 Background

In the U.S., buildings account for 36% of the total energy use and 65% of the electricity consumption.[1] The residential sector accounts for the 23%[2] of the total primary energy consumption and 22% of the national CO_2 emissions.[3] The largest electricity consuming sector in the U.S. is the residential sector and it accounts for the 39% of the overall electricity produced in the country.[4]

Energy costs contribute to the overall financial burden of housing in the U.S.[5] The U.S. Department of Housing and Urban Development defines affordability as the condition that no more than 30% of a household's annual income is spent on housing.[6,7] In 2006, approximately 40 million households spent 30% or more of their incomes on housing.[6] According to the U.S. Environmental Protection Agency,[5] improving energy efficiency in housing can reduce the energy cost burden on low-income households by helping make homes more affordable. Approaching energy efficiency improvements comprehensively can provide other energy, environmental and economic benefits as well.[5] These benefits include increased employment and reduced demand for federal assistance program resources.[5] Considering the fact that a total of 38.6 million out of 111.1 million households are currently eligible for federal home energy assistance in the U.S.[8], it becomes clear that there is significant need for studies on energy efficient housing design in the U.S.

For energy efficient design of residential buildings, it is important to identify the primary determinants of energy consumption in these buildings. According to Yu *et al.*[9], there are seven determinants of building energy use. These determinants are:

1) building occupants' behavior and activities,

2) social and economic factors (e.g., degree of education, energy cost, etc.),

3) the required indoor environmental quality,

4) user-related characteristics (e.g., user presence, lighting requirement, equipment requirement, outside air requirement etc.),

5) building services systems and operation (e.g., space cooling/heating, hot water sup-

plying, etc.),

6) building related characteristics (e.g., type, shape, area, orientation, etc.),

7) climate (e.g., outdoor air temperature, solar radiation, wind velocity, etc.).

Occupants affect building energy use in multiple ways. For instance, the social and economic factors affect the occupants' attitude toward energy consumption.[9] They also determine the required indoor environmental quality.[9] They affect the building thermal load by using electric lighting and equipment, requiring ventilation or by simply being present in the building as well. Thus, they are very important parameters for building energy estimations. The occupant related features of buildings are, however, sources of significant uncertainty in energy modeling as human behavior is a complex phenomenon which is hard to predict. In search of eliminating this uncertainty, researchers conducted surveys and investigations to find out the occupants' typical behavioral schedules and utilized them in order to make more realistic energy estimations.[10–18] Studies were also conducted to use monitored occupant behaviors to develop occupancy-based energy saving strategies and control systems.[19,20] Among these studies, the ones that utilized residential occupant patterns in order to develop energy efficient HVAC systems[20] were noticeably rare.

Building systems and operation is another important factor that affects building energy consumption. Among these systems, HVAC systems are the most energy consuming devices accounting for approximately 10-20% of final energy use in developed countries.[21] In the U.S., HVAC energy consumption accounts for 50% of building consumption and 20% of the total national energy consumption.[21] Currently, residential buildings (22%) account for a higher weight in building energy consumption in the U.S. than commercial buildings (18%), and space conditioning is the primary cause of 53% of the total residential energy use.[21] Given this high impact of HVAC energy use on the overall building energy consumption in the U.S., it is a key factor for the current building energy codes to set HVAC minimum energy efficiency requirements in the promotion of energy efficiency.[22]

The energy regulations in the U.S. examine residential and commercial buildings sepa-

rately since the Model energy code[23] and the dual prescriptive-performance path for compliance (Title 24-1980) were introduced in the 1980s.[22] In 1992, the federal government passed the Energy Policy Act[24] which required the active intervention of the Department of Energy (DOE) in the development of building energy codes.[22] Based on DOE's determinations, the ASHRAE Standard 90.1-1989 for commercial buildings and the Council of America Building Officials (CABO) Model Energy Code (MEC 1992) for residential buildings were proposed.[22] Finally, the International Code Council (ICC) developed the International Energy Conservation Code (IECC) which has become the model for the code enforcement community in the last decade both for residential and commercial buildings.[22]

The HVAC related prescriptive measures in the current codes can be categorized under six groups, i.e. equipment minimum efficiencies, fluid distribution systems, HVAC control, ventilation, heat recovery and free cooling.[22] These measures describe the minimum requirements for energy efficiency for HVAC systems. The latest step in the development of energy codes in the U.S. attempts to standardize "beyond-code" programs on commercial buildings in order to increase energy efficiency above the energy codes. In this perspective, ASHRAE developed Standard 189.1-2009, "Standard for design of high-performance green buildings" in order to provide minimum requirements to reduce the overall impact of buildings on human health and the natural environment. This standard excludes low-rise residential buildings and there is currently no standard that regulates beyond code green building design practices for these buildings. Thus, the studies that achieve beyond code residential energy efficiency are highly required as they can provide guidance in preparation of a residential green building standard.

Building shape and climate are also considered significant factors in building energy consumption.[25–27] Traditional courtyard buildings have been a climatic solution in regions with predominantly warm seasons.[28] These buildings evolved into the contemporary atrium buildings that offer more amenities such as protection from rain and snow.[28] In buildings where an atrium building is included as part of the energy saving strategy, the overall energy consumption of the building has been found to be lower than a comparable building

built on more traditional lines.[29] Among these integrated strategies, using the atrium space as the plenum of the building was identified as the most energy efficient one in modern commercial schemes.[29] These atrium related strategies may offer significant energy saving potential for low-rise residential buildings as well. Further studies are required to quantify this potential.

The majority of the residential buildings in the U.S. are slab-on-grade (32%) one story buildings (69%).[30] Low-rise slab-on-grade residential buildings have long been an area of uncertainty in the field of building energy simulation. One of the primary reasons for this uncertainty is the inaccuracies in calculations of slab-on-grade heat transfer, which accounts for 30% to 50% of the total heat loss in these buildings.[31] The wide range of variation (25%-60%) between the results of the available slab-on-grade heat transfer models[32] makes it difficult to consistently estimate energy consumption for these buildings. Most of slab-on-grade heat transfer models available in the market are single zone models which assume identical floor temperatures for all rooms of the building. The aboveground sections of these buildings are also typically modeled as single zone which oversimplifies real life and disregards the effects of thermostat location, interior partitions, duct layout and the resulting variation in infiltration rates and air temperatures between the rooms.

The primary use of the residential electricity consumption in the U.S. is for space cooling[4], which is particularly high in hot and humid climates. This study proposes an occupancy based HVAC design strategy for low-income residential buildings in hot and humid climates. This strategy is designed integrated with an unconditioned atrium space which is used as a return plenum, and is estimated to provide energy savings beyond IECC 2012. For the simulation of this building, a multizone modeling approach was followed for both the aboveground and belowground heat transfer calculations. In this approach, the effects of thermostat location, interior partitions and duct layout were taken into account and the resulting differences in zone air temperatures and infiltration rates between the rooms were monitored.

1.2 Purpose and Objectives

Texas is the highest residential energy consuming state in the U.S. by being the 2nd most populous state in the country and having primarily a hot and humid climate.[33] The purpose of this study is to show that 20-50% HVAC energy savings above code can be achieved before any on-site energy generation in low income residences of Texas through innovative HVAC design based on occupant usage patterns. For this purpose, a case study was conducted following the steps below:

1) A site visit was made to the Bryan Habitat for Humanity office in Texas to collect information about the house plans, construction materials, electric lighting and equipment features of the Habitat for Humanity houses. Mr. Jim Davis, the Property Director of the Bryan/College Station Habitat for Humanity, provided information on these features along with the construction drawings of the houses.

2) A detailed comparison was made between three well-known energy modeling tools. i.e. DOE-2, EnergyPlus and TRNSYS with a focus on their slab-on-grade heat transfer models. A ground heat transfer modeling method was then selected for the modeling of low-rise slab-on-grade residential buildings.

3) The obtained features of the Bryan/College Station Habitat for Humanity houses were improved to obtain baseline houses in compliance with the current energy code (IECC 2012)[34], Building America Benchmark definitions[35] and the IES'[36] lighting requirements. The ground heat transfer model selected in the previous step was used in this step for the modeling of slab-on-grade heat transfer in the baseline houses.

4) A realistic duct layout was designed for the baseline houses and the air distribution through these ducts was modeled using the AirflowNetwork model of EnergyPlus which accounted for the conduction heat transfer through the ducts and the effect of the system airflows on infiltration rates and interzonal airflows.

5) An integrated design and modeling process was described for a new HVAC (heating, ventilating and air-conditioning) system design strategy (i.e. "partial conditioning") which integrates two energy efficiency measures previously suggested in literature (plenum atrium

and occupancy based heating/cooling) with a new airflow design idea, i.e. reuse of air.[37] This new idea is based on using the return air of the occupied zones as the supply air of the unoccupied zones before it is returned to the system.[37]

1.3 Expected Impact of the Study

Within the framework of the research objectives, this study provides multiple inputs to the building energy modeling field by:

1) indicating that the energy efficiency measures suggested for commercial buildings (i.e. the outside air systems, atrium plenum, etc.) can be applied in residential buildings effectively. This input is expected to provide information exchange between the different research areas within the energy efficient building design field leading to new inspirations.

2) indicating that mechanical ventilation brings more benefits than infiltration for residential buildings in hot and humid climates during the cooling season. This presents a strong and well-supported counterargument to the studies that support natural ventilation in these climates.

3) highlighting the significant areas of discrepancy between energy modeling tools for the simulation of low-rise slab-on-grade residential buildings and explaining the reasons for these variations. It is believed that these findings will provide significant guidance for building energy modelers and building energy code users and will contribute to the standardization of building energy modeling methods.

4) suggesting a multizone energy modeling method based on the coupled/combined use of multiple tools and models in order to improve the accuracy of building energy estimations for low-rise slab-on-grade residential buildings.

1.4 Organization of the Dissertation

This dissertation is divided into five sections which include: 1) introduction, 2) literature review, 3) methodology, 4) results and discussions, and 5) summary and conclusions.

Section 1 presents an introduction to the study by providing a background, establishing the need, and stating the purpose and objectives of this study.

Section 2 reviews the literature related to the multiple aspects of this study. The

topics covered in this section include global energy use, residential energy use in the U.S., housing characteristics and energy use in hot and humid regions of the U.S., the efforts on energy efficient housing in hot and humid climates, the effect of human behavior on residential energy use, courtyard/atrium buildings in hot and humid climates, integrated modeling methods for atrium buildings and slab-on-grade heat transfer modeling in low-rise residential buildings.

Section 3 describes the methodology applied in the study. This includes a detailed comparison of three well-known energy modeling tools for slab-on-grade residential buildings, design and modeling of a typical low-income house in Texas as the baseline and the design and modeling of the partially conditioned atrium house through a series of steps.

Section 4 presents an analysis and discussion on the results of the study. This includes comparison of the energy consumption estimations for the cases modeled in the study and quantification of the energy saving potential of the partial conditioning strategy in residential buildings in hot and humid climates.

Finally, Section 5 summarizes this study, discusses the key findings and presents a conclusion. Based on the limitation of this study, recommendations for future research are proposed.

2. LITERATURE REVIEW

2.1 Global Energy Use

From 1995 through 2007, world energy consumption increased by 26% from 366 Quads (1 Quad=1×10^{15} Btu) to 495 Quads.[33] The global recession that started in 2008 and contracted the marketed energy consumption by 1.2% in 2008 and by 2.2% in 2009. In 2009, after the recovery from the recession, the global energy use was estimated to return to its earlier economic growth path and reach 739 quads by the year 2035.[33]

In 2007, for the first time, the energy consumption of the non-OECD* countries exceeded those of the OECD countries by 1.5% due to the leading (with 20% share in global energy use) energy consumption of China and India.[33] The same year, a single OECD country i.e. the United States (U.S.), however, had a share higher than the sum of China's and India's consumption[33] despite its four times less population when compared to each of these two countries.[38]

2.2 Residential Energy Use in the U.S.

The share of the U.S. in global energy use depends on the level of its economic activity in all sectors except in the residential sector.[33] In the residential sector, the U.S. energy consumption depends primarily on the physical size of the buildings in the country.[33] In the last three decades (1980-2006), an increase occurred both in the number (41%) and size (45%) of the U.S. households, which resulted in a ∼32% increase in overall residential energy consumption.[4] In 2009, the average single-family house was 2,438 ft^2 in the U.S.[39] and the share of the residential energy consumption accounted for 22% of the overall U.S. energy consumption.[40] As the size of the houses increased, the percentage of the houses constructed with a central air-conditioning system also increased (from 46% in 1975 to 90% in 2005) in the U.S.[41] Currently, the residential sector is the largest electricity consuming sector in the U.S. (with 37% share) and the largest share of this electricity (20% of 37%) is used for space cooling.[4]

* Organization of Economic Co-operation and Development.

2.3 Housing Characteristics and Energy Use in Hot and Humid Regions of the U.S.

The hot and humid climate is observed in the southern region of the U.S. This region has the largest share (37%) in the U.S. housing stock[4] and uses more residential energy than the other regions.[42] The U.S. houses in the south are generally (71%) slab-on-grade buildings and almost all (99%) of them have a central air conditioner installed.[39] Heat pumps are the main heating system (with 53% market share) in these houses with electricity being the most popular (with 58% market share) heating fuel. Lower income families use 31% more energy per square foot than the higher income families in the southern region.[42] This is partly because their houses are smaller (∼2 times), older, more leaky and with a less efficient HVAC system when compared to those of the higher income families.[42] The lower income families in this region also devote a higher percentage (8.6%) of their income to paying their energy bills than the higher income households do (2.2%).[42] Texas, which is located in the southern region of the U.S., is the highest residential energy consumer and the second most populous state of the country and it ranks 3rd among all states of the U.S. in the number of low income households.[42]

2.4 Efforts on Energy Efficient Housing in Hot and Humid Climates

There have been multiple efforts that focused on reducing energy consumption of residential buildings in hot and humid climates. Among these studies, the ones that had a significant impact on this thesis were conducted by the BAIHP* team[43], the National Affordable Housing Network[44], Haberl *et al.*[45], Gardner[46], Kim[47], Kootin-Sanwu[48] and Malhotra.[49]

The BAIHP team, selected by the U.S.D.O.E. Building America program in 2009, conducted renovations on 41 affordable and middle income homes in Florida and Alabama and obtained up to 48% savings by applying multiple strategies (such as CFLs, ENERGY STAR ceiling fans and refrigerators, increased ceiling insulation, good air sealing, spectrally selective window tint, and a higher SEER HVAC system with a programmable thermostat).[43]

* Building America Industrialized Housing Partnership led by the University of Central Florida. This team included Florida Solar Energy Center researchers, personnel from subcontractors Florida Home Energy and Resources Organization, Calcs-Plus, Washington State University, Oregon Department of Energy, RESNET and other subcontractors.

The National Affordable Housing Network, partnered with Habitat for Humanity (HFH) affiliates and nonprofit builders in Texas, built more than 40 resource efficient houses in six less humid cities of Texas (including San Antonio, Longview, Abilene, Dallas and El Paso) and obtained up to 42% savings compared to the current practice by using multiple features.[44] These features included R-30 ceiling and R-18 wall insulation, double glazed fenestration with heat rejection glazing, under slab and above ceiling moisture barriers, controlled continuous ventilation with a high performance fan and a downsized HVAC system.[44] Haberl *et al.*[45] and Gardner[46] focused on more humid regions of Texas. Haberl *et al.*[45] conducted calibrated DOE-2 simulations and side by side measurements on two identical HFH houses in Houston and verified that increasing HVAC SEER from 10 to 12 reduces the annual electricity use by 11% and increases the annual natural gas use by 0.8% in these houses. Gardner[46] then conducted a case study near Houston to test the effectiveness of renewable energy products and green building materials in an affordable home and obtained a ∼50% lower overall electricity consumption when compared to similar houses of the same size. These studies showed that up to 50% overall energy savings can be obtained in low-income houses in Texas through combined application of conventional energy efficiency measures.

The studies of Kim[47] and Kootin-Sanwu[48] were particularly important for this study as they both worked on the energy performances of Bryan Habitat for Humanity houses. The early concepts of the partial conditioning strategy was modeled in the case study houses that Kim[47] and Kootin-Sanwu[48] studied. The final models were then produced by selecting a typical plan among the most current plans of the Habitat for Humanity houses built in Bryan, Texas.

Kim[47] worked on improving the accuracy of a 2000/2001 IECC compliant performance simulation using the DOE-2.1e simulation program to investigate the energy performance of a typical single-family house. He accomplished several objectives to achieve this purpose. These objectives included: 1) the development of an IECC-compliant simulation model, 2) the development and testing of specific improvements to the existing code-traceable model,

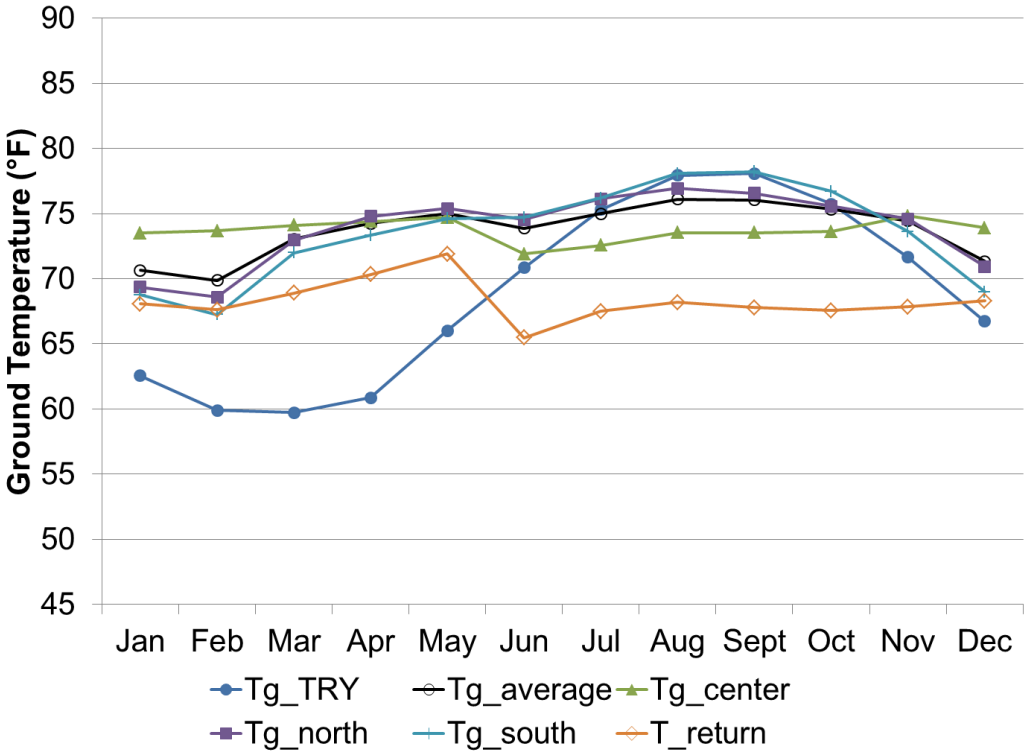

Figure 2.1: The monthly average ground temperatures of the Habitat for Humanity house studied by Kim.[47]

3) the calibration and installation of sensors in a case-study house, 4) the validation of the improved simulation model with measured data from the case-study house, and 5) using the validated model to simulate the energy-conserving features of single-family residences that cannot be simulated with existing versions of the DOE-2.1e program. The Habitat for Humanity house discussed in this study was in Bryan, Texas and detailed ground temperature measurements were conducted for this building. Fig. 2.1 shows the monthly averages of these temperatures.

Kootin-Sanwu[48] studied the energy consumption and environmental consumption by installing a 48 channel data logger to record 15-minute data in a 1,120 ft^2 Habitat for Humanity house in Bryan, Texas. The measured data included air conditioner, blower, clothes washer/dryer, refrigerator, and other appliances, natural gas monitoring for monitoring energy consumption. He also monitored environmental variables such as temperature, relative

humidity for return, supply, attic space, and outside air, horizontal solar radiation, carbon dioxide and wind speed. Kootin-Sanwu[50] also developed guidelines to reduce the costs of the same Habitat for Humanity house by carefully selecting and analyzing energy and water reducing design options that can be installed cost effectively by volunteer labor. He developed a monthly baseline using a PRISM (Princeton Score Keeping Method) analysis of 28 Habitat for Humanity houses in Bryan/College Station, Texas. He used various sensors to instrument and measure 15-minute energy use and environmental data from the case study house. He developed a detailed, calibrated building energy simulation model of the case study house using a modified version of the DOE 2.1e program. He then used this calibrated model to evaluate the energy conservation design options to determine the projected energy use.

Malhotra[49] investigated the feasibility of the off-grid, off-pipe design approach in six climate locations across the U.S. to achieve self-sufficiency in a 2,500 ft^2 IECC 2000/2001 compliant house for building energy, indoor water use, and household wastewater and sewage disposal using only on-site available renewable resources. She considered renewable resources such as solar radiation, wind, biomass for building energy needs; rainwater for indoor water use. In addition, the building site was considered for the disposal of household wastewater and sewage. Depending on the individual requirement of each location, she selected energy and water efficiency measures in order to reduce the building needs. For these reduced building needs, she sized the systems for self-sufficiency. These systems included solar thermal system for building's space heating and water heating needs, photovoltaic and wind power systems for building's electricity needs; rainwater harvesting system for indoor water needs; and septic system for the on-site disposal of household wastewater and sewage. Through this process, she developed an integrated analysis procedure for the analysis and design of off-grid, off-pipe homes, and demonstrated it for six U.S. climate locations. She found that achieving self-sufficiency for energy, water and sewage disposal was possible in all climates provided the systems for the collection and storage of renewable resources were large. Malhotra's[49] study has been an inspiration for this thesis showing

substantial energy reductions can be achieved in residential buildings in all climates of the U.S.

2.5 The Effect of Occupant Behavior on Residential Energy Use

The studies that looked into the effect of occupant behavior on building energy consumption in residential buildings primarily focused on producing or obtaining more realistic occupant behavior patterns for these buildings in order to improve the reasonableness of the energy estimations.[10–12,51] A few other studies focused on development of energy efficiency strategies based on occupanct patterns.[20]

Papakostas and Sotiropoulos[51] conducted surveys on occupant behaviors (i.e. household work, in-home entertainment, hobbies, sleeping, resting and eating) in Greek residences and obtained an average behavior for the Greek families to use them for the calculation of cooling loads and the simulation of occupants' behavior in building energy models.

Al-Mumin *et al.*[10] studied 30 residences in Kuwait and surveyed their occupancy patterns and operation schedules of electrical appliances. He then entered these values into the thermal simulation program, ENERWIN, to replace the default data which was based on the Western lifestyle and obtained a 21% increase in overall building energy consumption.

Emery and Kippenhan[12] presented the construction of four test houses by the University of Washington. They presented the measurement system employed in these houses, the energy consumption measured over a 15-year period, 1987-2002, the effectiveness of the simulation programs in predicting this energy consumption, and the effect of occupants on the heating energy consumption. They found that the occupants operated these test houses differently which resulted in significantly different total energy consumption in these houses. The other important difference (between 10 and 20 kWh/day) was observed between the hot water consumptions of these houses.

Tanimoto *et al.*[11] proposed a methodology to more accurately estimate the cooling demand in residential buildings by integrating probabilistic variations in occupant behavior. They conducted this study as a means of providing a better assessment of urban heat-

island effects caused by the use of residential air-conditioning units. Their methodology included two key features. The first was an algorithm that generated short-term events that are predicted to occur in a residential building based on published data on residential occupant behavior. The second was a Monte Carlo approach used for calculation of cooling load considering the stochastic variations in these short-term events and the consequences of turning the air-conditioning on or off.

Mozer[20] introduced a new approach to providing energy savings in residential buildings. In this approach, the house programs itself by observing the lifestyle and desires of the inhabitants, and learns to anticipate and accommodate their needs. The system he developed controlled the basic residential comfort systems (i.e. air heating, lighting, ventilation, and water heating) according to the usual occupant behavior. He also constructed a prototype system in an actual residence, and verified its performance. Mozer's[20] research showed that there are consistent occupant usage patterns in residential buildings and these patterns can be utilized to provide energy savings.

These studies indicate the fact that energy consumptions of residential buildings are influenced by the lifestyles of their occupants. The activity patterns, schedule profiles of lights and electrical devices as well as the A/C thermostat settings are significant parts of the occupants' lifestyle which play an essential role in the magnitude of the energy requirement.

2.6 Courtyard/Atrium Buildings in Hot and Humid Climates

The courtyard building is a historic building type that has been used by numerous urban civilizations.[52] In the middle of the 20th century, courtyard buildings were condemned as unsuitable for modern living and were destroyed in large numbers.[53] Today, with energy and health related concerns, there is a revival of interest in courtyard buildings since they are considered to have great potential to save energy by utilizing natural ventilation[54] and daylight[55], while providing a comfortable internal environment with satisfactory indoor air quality.

2.6.1 Residential Courtyard/Atrium Buildings

Courtyard house is the traditional house type of many Asian, North American, South American and European countries[56] and has been widely studied by various researchers. Mohsen[57], Muhaisen and Gadi[58], Nguyen *et al.*[59], Kubota *et al.*[60], Klote and Milke[61], Deng[62], Li[63], Zhang[64], Dili *et al.*[65], Sadafi *et al.*[66], Reynolds[52] and Rajapaksha *et al.*[67] were among these researchers. These researchers suggested either 1) proper selection of courtyard proportions, or 2) using a proper ventilation method for improving the performance of these buildings.

Mohsen[57] and United Nations Department of Economic and Social Affairs[68] suggested a compact courtyard layout for hot climates on the grounds that it provides mutual shading between surfaces with the consequence of reducing the thermal load on them. They found that the height of the courtyard is the most important factor for avoiding solar penetration. They recommended that the courtyard dimensions in plan do not exceed this height in order to provide the intended compact plan which is shaded during the day.[57,69] According to Muhaisen and Gadi[58], the deeper and the more elongated the courtyard is, the more preferable it is for reducing the cooling load in summer as a result of self-shading.

For residences, ASHRAE[70] recommended a reasonably tight building envelope and a properly designed and operated mechanically ventilated system to avoid poor humidity control, air moisture infiltration and the lack of control in ventilation rates. ASHRAE[70] recommended these features also to have the opportunity to recover the energy used to condition the ventilation air. Studies like that of Nguyen *et al.*[59] supported ASHRAE's suggestions by showing that, under extreme conditions, relying entirely on traditional passive means might not be enough to maintain indoor thermal comfort in courtyard houses. Especially the daytime ventilation did not appear to be favorable in summer in hot and humid climates due to the high outdoor temperatures.[59] Kubota *et al.*[60] showed that, in these climates, night ventilation can be used to effectively reduce indoor operative temperature and improve thermal comfort; however, the majority of occupants tend not to apply night ventilation due to insects, security risks and rain. Thus, Nguyen *et al.*[59] concluded that,

under extreme climates, buildings would benefit from using low-energy mechanical systems, such as mechanically assisted ventilation, evaporative cooling, passive solar heating or occupants' adaptive responses such as clothing insulation, activities, opening controls and the use of fans.[59] The stack effect, which is a primary driver of natural ventilation, has also been found to be less prominent in short buildings such as residential buildings when compared to tall buildings.[61]

Deng[62], Li[63], Zhang[64], Dili *et al.*[65], Sadafi *et al.*[66], Reynolds[52] and Rajapaksha *et al.*[67] defended that natural ventilation can reduce cooling loads in courtyard houses. Deng[62], Li[63] and Zhang[64] studied buoyancy driven natural ventilation as a cooling strategy in high-rise residential atrium buildings. Dili *et al.*[65], Sadafi *et al.*[66], Reynolds[52] and Rajapaksha *et al.*[67] studied the use of natural ventilation in traditional low-rise courtyard houses as a cooling strategy and defended that passive cooling highly contributes to the comfort conditions in hot and humid climates. Bagneid[71] created a finite difference thermal network model for simulating a case study courtyard microclimate in a courtyard house in Cairo, Egypt. He then validated this model by calibrating it against the field data of the house. This courtyard microclimate model was then used in combination with DOE-2 to analyze the performance of the case study house.

2.6.2 Commercial Atrium Buildings

The studies on commercial atrium buildings can be summarized under four groups based on the four possible contributions of an atrium to a building according to Gordon.[72] These contributions are: 1)"daylight" into an otherwise deep-plan building, 2)"buffer space" that acts as insulation between the host building and the external climate, 3)"plenum atrium" integrated into the building's air-conditioning system, and 4)"natural ventilation" as a result of the stack effect.

The fenestration design of atrium buildings in warm climates is a challenge since it is a compromise between reducing direct solar gain and maximizing daylight. Several strategies have been recommended to meet this challenge. Using solar control and translucent glazing that reduce the transmitted solar gain by 20-80%[73,74] or the spectrally selective glazing

that reject nonvisible parts of the electromagnetic spectrum[74] or the photochromic[75] and electrochromic[76] films that alter the glazing transmittance depending on external stimuli (i.e. light levels or voltage signal) are a few examples. There are also fenestration materials alternative to glass such as ETFE[77], transparent refractive index matched microparticles (TRIMM)[74], polycarbonate[74] and aerogel[78], which have either better thermal/fire performance or lower weight when compared to glass. Despite the promising theoretical analysis of these new generation fenestration materials[79], there is little evidence on their performance in practice. Another solution suggested for atrium fenestration is a monopitched roof oriented north (assuming the vertical element of the roof was glazed and not part of the internal wall) which allows low altitude sunlight while blocking direct sunlight from higher angles.[80,81] The reflections off the internal sloped surface of this roof is claimed to further magnify the daylight entered into the building.[81] In order to further enhance the daylighting performance of the building, it also recommended using interior walls and light shelves that would produce diffuse and reflected light to the interior spaces from the atrium.[80] It is suggested to avoid east- and west-facing atria because they admit low-angle sunlight in summer and are hard to shade. Their heat loss in winter is also much higher than their equator-oriented equivalents.[80] These recommendations, however, contradict the statements of Givoni[82] and McCluney and Chandra[83] who claimed that sun blockage is equally effective in all directions in hot and humid climates due to the consistently cloudy sky in these regions.

An atrium acts as a "buffer space" and provides an obvious improvement in the overall building U-factor. Saxon[84] states that the energy economy of buffer spaces (i.e. atriums) is only fully achieved if no attempt is made to keep these spaces themselves comfortable all year. The buffer spaces are lightly constructed and are colder in winter and hotter in summer than the conditioned spaces they protect; therefore, the occupants of these spaces need to dress seasonably appropriate.[84] These buffer spaces, i.e. atriums, perform best when they are integrated into the building system as a 1) supply plenum, 2) exhaust plenum, and/or as a 3) heated buffer space.[29] Mills[29] stated that, when the atrium is used

as a supply plenum, fresh air is drawn through the atrium, where it is preheated by solar gains and the heat losses from the building before entering the air-handling plant. When the atrium acts as an exhaust plenum, the stale air from the building's air-handling system is exhausted into the atrium, where it provides a tempered buffer space that reduces heat flow from the adjacent occupied spaces.[29] Finally, in the heated buffer space mode of the atrium, the waste heat from the building is "moved" into the atrium to provide a tempered buffer space. This reduces building heat loss and gives added amenity value at no extra cost.[29]

Liu *et al.*[85] showed that, for the atrium buildings in hot and humid climates, the duration of the large temperature difference between indoor and outdoor is limited; therefore, the buoyancy-driven natural ventilation technique can be utilized in these climates only during the spring and winter seasons that have a bigger temperature difference. Lin and Chuah[86] and Wang *et al.*[87] agreed with this argument showing that natural ventilation is not beneficial all the time in these climates. Ayata and Yildiz[88] found that the effectiveness of natural ventilation is highly dependent on the orientation of the building with respect to the prevailing wind direction. Cheung and Liu[89] showed that the surrounding building interference is also a very important factor for the effectiveness of natural ventilation.

2.7 Integrated Modeling of Atrium Buildings

Atrium buildings include complex daylighting, airflow and thermal phenomenon; therefore, the energy simulation software packages for conventional buildings usually do not apply to atrium buildings.[90–92] The literature includes two groups of studies that looked into the combined use of simulation tools for improving modeling accuracy for atrium buildings i.e.: 1) integrated modeling of airflow and energy, and 2) integrated modeling of daylight and energy.

2.7.1 Integrated Modeling of Airflow and Thermal Performance

Building energy simulation (BES) programs such as EnergyPlus, TRNSYS and ESP-r have been shown to be both versatile and reliable.[93] These programs, however, do not typically solve for the fluid flow within a building directly.[94] The flow is usually determined by

experimental measurement or an additional program to generate estimates of flows between zones.[94] Literature includes studies that coupled two types of airflow calculator programs with BES programs. These airflow calculator programs are: 1) Multizone Airflow Network Modeling Programs (MAFN) and 2) Computational Fluid Dynamics (CFD) programs.

2.7.1.1 Integration of Multizone Airflow Network Modeling with Building Energy Simulation

Multizone airflow network (MAFN) modeling is a simplified airflow modeling method which consists of a set of nodes connected by airflow elements.[95] For each airflow element, a relationship is defined between airflow and pressure in this method.[95] Each thermal zone is represented with a single node (i.e. with a single pressure and velocity value) and there is no internal air circulation within zones.[95] The accuracy of this approach in MAFN models is similar to that of the well-mixed air assumption in BES programs, which represents each zone with uniform temperature and humidity.[95]

Several MAFN modeling programs have been developed over time. The National Institute of Standards developed the AIRNET program[96] and the Lawrence Berkeley National Laboratory (LBNL) developed the COMIS program.[97] AIRNET calculates airflow through envelope leakage and ducts and it uses height-independent air density to predict one- or two-way airflows through large vertical openings.[96] COMIS has a more enhanced airflow model than AIRNET, which takes the effect of temperature into account to predict airflows through envelope leakage.[95] COMIS can also model three-way airflows through large vertical openings by assuming that the air density varies linearly with height.[97] The AIRNET and COMIS programs cannot perform building load calculations directly; therefore, they need a BES program to predict loads and system performance.[95]

Gu and Swami[98], Hensen[99], Modera and Treidler[100], Huang *et al.*[101] and Gu[95] showed significant efforts to couple airflow network models with BES programs. Gu and Swami[98] integrated AIRNET was integrated with the FSEC 3.0 program in Florida Solar Energy Center. Hensen[99] developed an airflow network model at the University of Strathclyde and integrated it into ESPr.[102] Modera and Treidler[100] developed an energy loss model at the

Lawrence Berkeley National Laboratory and connected it to DOE-2 and COMIS programs, but did not fully integrate it. Huang *et al.*[101] integrated COMIS into EnergyPlus. In this integrated model, wind-driven multizone airflows were calculated through the building envelope using COMIS and this information was included in the EnergyPlus zone load calculation.[101] Later, Gu[95] implemented an Air Distribution System (ADS) model into EnergyPlus. This ADS model used equations derived from AIRNET to calculate airflows through an air distribution system including the energy losses due to duct heat conduction and air leaks (while lumping zone-level envelope leaks together).[95] A new model named AirflowNetwork model was subsequently implemented into EnergyPlus replacing COMIS and ADS with identical features except with one advantage of making the calculations at the HVAC time step instead of at the zone time step. This feature allowed the multizone airflow calculations to be synchronized with the HVAC system calculations in EnergyPlus and provided flexibility for the future development of hybrid ventilation system controls.[95] Finally, the hybrid ventilation modeling feature was added to EnergyPlus.[103]

The current integrated MAFN-BES modeling methods are not capable of simulating air stratification, which typically occurs in high spaces like atriums.[90,104,105] One effective solution approach to this problem has been to model high spaces as vertically stacked zones.[106] Laouadi and Atif[90] calculated stratification levels for a highly glazed office building in Ottawa using ESP-r by separating the air volume of high thermal zones with fictitious walls. They then entered the airflow values they obtained from measurements into their code as an input. This approach had two primary shortcomings. First, it required an actual atrium to perform measurements in and was only accurate for the conditions under which the measurements were taken.[94] Second, it caused erroneous interior radiative heat transfer calculations since ESP-r does not model long wave radiation heat exchanges between surfaces that belong to different thermal zones.[105] Voetzel *et al.*[105] then developed a model called AIRGLAZE for predicting the thermal and ventilation behavior of large highly-glazed spaces in transient conditions and validated it with field data. With this program, they discretized the air volume of the large spaces (i.e. atriums) in control volumes in which

pressure, air density and air temperature were assumed to be uniform.[105] These control volumes were connected to each other by airflows induced by the pressure difference between the control volumes.[105] The zonal model solved the mass balance equation, the enthalpy balance equation and the perfect gas law equation of each control volume of the computational domain.[105] The airflow from one control volume to the other was modeled as if the flow passes through a small opening with sharp edges.[105] The model of Voetzel *et al.*[105] furthermore achieved a correction for the radiative heat transfer between inside surfaces in large atriums. It calculated the longwave radiation absorbed by interior surfaces accounting for the fluxes emitted by the neighboring surfaces using the Gebhart[107] method. The internal shortwave radiation of the AIRGLAZE model was also detailed and took multiple reflections, direct transmission, reflection to the outside and transmission to other zones into account.[108] Later, Tan and Glicksman[109] developed a multizone model program for natural ventilation (MMPN) and integrated it with CFD in order to improve its accuracy. They provided either: 1) the velocity boundary condition, or 2) the pressure boundary conditions from the MMPN model to the CFD model and compared these two integration approaches with each other.[109] Their findings confirmed that the division of atriums into subzones has a strong impact on the result of the multizone model calculation.[109]

2.7.1.2 Integration of Computational Fluid Dynamics with Building Energy Simulation

CFD has been used to model the effects of fire[110], temperature, wind speed and CO_2 levels[111] and opening location[112,113] in atrium buildings and its results have been validated[94] with experimental data. CFD programs are steady state due to otherwise needed huge computational effort[114] and they are usually assumed with limited consideration for the thermal storage effects of the wall, external conditions, and interactions with building services systems.[115] The large highly glazed spaces like atriums are, however, subjected to rapid changes in insolation as the sun is viewed at different angles over the course of the day.[105] BES programs can model these transient conditions but they make energy predictions based on well-mixed zone air assumption, which cannot capture the dynamics of the flow near the surfaces.[115] BES programs use complex empirical models that make

unrealistic assumptions (i.e. isothermal surfaces) to calculate the surface heat transfer coefficients, which are not accurate for surfaces adjacent to stratified air.[105,116] CFD solves the governing equations for heat and fluid flow over discretized domain and provides detailed solutions including both temperature and velocity fields[94] and makes more accurate predictions of heat transfer coefficients than the empirical models.[115] CFD simulations, however, need detailed input data which is usually not consistent with the data available at the design stage of a building.[105]

For improving the accuracy of modeling results, researchers[115,117,118] coupled CFD programs with BES programs. In these coupled simulations, the BES program typically ran to determine the boundary conditions for the CFD simulation and for regions of the domain where the detail of CFD was not required. The CFD simulation then provided important inputs to the BES simulation, such as airflow and heat transfer coefficients. Zhai *et al.*[117] categorized coupling strategies of BES and CFD into two groups i.e. Static Coupling and Dynamic Coupling. Static coupling involved a one-step and two-step exchange of information between BES and CFD programs and it was applied when both BES and CFD were not sensitive to the exchanged variables. For instance, for an air-conditioned room with low velocity mixing ventilation, static coupling was considered an appropriate coupling method for CFD and BES programs. Dynamic coupling involved coupling between CFD and BES at every time-step and it was applied when both CFD and BES were sensitive to the transient boundary conditions. Zhai *et al.*[117] demonstrated these coupling strategies for an office under winter design conditions in Boston and an indoor auto-racing complex under summer design conditions in Pittsburgh. They showed that dynamic coupling can improve the heating/cooling load prediction by at least 10%, due to the improvement in predicted heat transfer coefficients. Later, Djunaedy *et al.*[115] suggested external coupling between BES and CFD rather than the traditional internal coupling for the purpose of eliminating the limitations of the CFD solver. Compared to internal coupling, external coupling showed a 2% improvement on the predicted energy consumption and a 96% (from 10.5 hours to 24 minutes) decrease in computing time. Pan *et al.*[118] coupled CFD with

BES to find out a simplified method of estimating cooling loads for various types of atria in hot and humid regions. They used the user-defined room air model of EnergyPlus with a nondimensional height temperature pattern entering the temperature gradient calculated by CFD. They then validated the modeling results with actual site measurements and proposed appropriate methods of modeling different types of atrium buildings. The studies of Pan *et al.*[118] showed that coupling CFD with BES improves the predicted energy consumption by at least 10%.

2.7.2 Integrated Modeling of Daylight and Thermal Performance

The first effort that allowed the users to determine the impact of daylight utilization on energy use in a widely-accepted, publicly available program was the implementation of a daylight model into the DOE-2 building energy use analysis program in the 1980s.[119] Later, a functional value input feature was added to this integrated model in order to allow the users to 1) input daylight factors obtained from scaled model photometric measurements, 2) model advanced glazing materials (i.e. angle-selective glazing and glazing whose transmittance is actively or passively controlled by environmental conditions), 3) control complex lighting control schemes including nonlinear dimming systems, and 4) modify algorithms used to calculate exterior daylight availability to conform to latest research results on luminous efficacy, partly-cloudy sky luminance distributions, etc.[120] Based on these improved DOE-2 daylighting algorithms, a new simulation engine, i.e. DElight Versions 1.x, was then developed by Hitchcock and Carroll.[121] The algorithms inherited from DOE-2 to DElight included precalculation of a set of daylight factors for each of a predefined series of sun positions, and then interpolating between these daylight factors at each timestep during the simulation run period.[121] A weighted combination of the interpolated values of these daylight factors at each timestep was used to simulate the actual mixed sky condition.[121] This calculation resulted in the interior illuminance level at each defined reference point.[121] A description of the installed electric lighting and control system was then used to determine the required electric light contribution to meet a defined illuminance set point.[121] Later, the DElight engine was enhanced with the radiosity interreflection calculations from

SUPERLITE[122], as well as with the newly developed algorithms for analyzing complex fenestration systems.[121] This enhanced version of the DElight engine was then integrated with the EnergyPlus building energy modeling program.[123]

Studies showed that the current EnergyPlus DElight model has fragility in calculating the internal illuminances.[124–126] Loutzenhiser *et al.*[124] found that EnergyPlus predicts internal illuminances within 119.2% when compared to the measured data. Loura *et al.*[125] found that in a simulation with nine reference points, the six points furthest from the window showed the same illuminance value in EnergyPlus; whereas the measured values for the same points were decreasing with increasing distance from the window. Similarly, Ramos and Ghisi[126] found that, for a deep room model with dimensions of 5m by 10m, EnergyPlus calculated a constant daylight factor value from the middle to the back of the room; whereas DAYSIM/RADIANCE and Troplux programs calculated decreasing illuminance values as the distance from the windows increases. The Radiance program has been validated by many researchers for a number of lighting environments[127–129]; therefore, there is currently a growing confidence in its accuracy for daylighting analysis.[130] The use of the Radiance program for daylighting modeling of an atrium building has also been validated very recently through comparisons with measured data.[129]

2.8 Slab-on-Grade Heat Transfer Modeling in Low-rise Residential Buildings

Ground coupled heat transfer (GCHT) through concrete floor slabs can be a significant component of the total load for heating or cooling in low-rise residential buildings. For a contemporary code or above code house, ground coupled heat losses may account for 30% to 50% of the total heat loss.[31] Ground coupling is still considered a hard-to-model phenomenon in building energy simulation since it involves three-dimensional thermal conduction, moisture transport, longtime constants and heat storage properties of the ground.[32] Over the years, many researchers worked on the development of slab-on-grade models. Some used simplified methods for slab-on-grade load calculations[131–133]; whereas others developed more detailed models.[134] For an uninsulated slab-on-grade building, the range of disagreement among simulation tools is estimated to be 25%-60% or higher for

simplified models versus detailed models.[32]

2.8.1 Slab-on-Grade models of DOE-2, EnergyPlus and TRNSYS

This section covers the common slab-on-grade models of the DOE-2, EnergyPlus and TRNSYS programs. The TRNSYS slab-on-grade model used in this study is currently the closest model to a "truth standard" in slab-on-grade heat transfer modeling.[32]

2.8.1.1 The Slab-on-Grade Model of DOE-2

In 1988, Huang *et al.*[135] calculated the perimeter conductance per perimeter foot for slab-on-grade floors, basements and crawl spaces using a two-dimensional finite-difference program. In 2002, Winkelmann[136] revised the work of Huang *et al.*[135] and described how to use their results in a DOE-2 model. The GCHT method referred to as "Winkelmann's method" in this study is based on the descriptions from Winkelmann.[136] In this method, it is assumed that the heat transfer occurs mainly in the exposed perimeter of the floor slab since this region has relatively short heat flow paths to the outside air. Instead of using the U-value of the floor, an effective U-value is entered for the floor construction that represents the heat flow through the exposed perimeter. A new construction is also assigned for the floor that will have an overall U-value equal to the entered effective U-value. This new construction accounts for the thermal mass of the floor construction when custom weighting factors are specified in DOE-2. From outside to inside, the new floor construction consists of three layers: 1) a fictitious insulation layer, 2) a 1 ft (0.3 m) layer of soil, and 3) the underground surface. Underneath the fictitious insulating layer, the system faces the ground temperatures (T_g) calculated by DOE-2 from the weather file using the Kasuda correlation.[137] Fig. 2.2 shows these layers.

2.8.1.2 The Slab Model of EnergyPlus

Slab is a preprocessor program of EnergyPlus that calculates monthly ground temperatures for single zone slab-on-grade buildings using a 3-D numerical analysis.[134,138] Slab was originally developed by Bahnfleth[134], and further modified by Clements.[138]

The current state of the Slab program is based on a calculation method that uses the

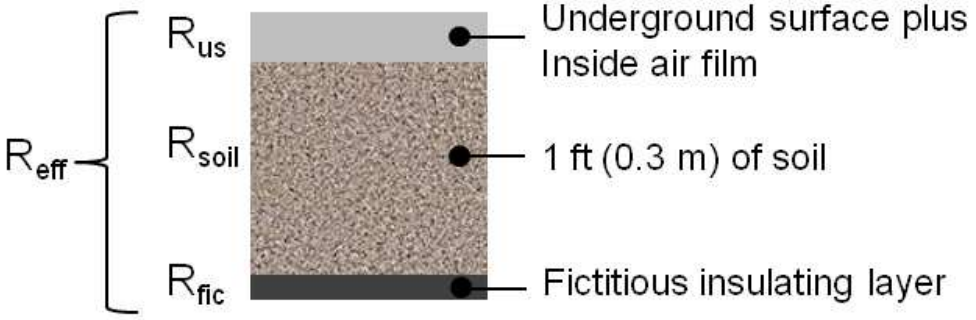

Figure 2.2: The layers of the Winkelmann's slab-on-grade heat transfer model.[136]

area to perimeter length (A/P) as the length scale to correlate the average heat flux for L-shaped and rectangular floors. The other significant parameters in this model are the thermal conductivity of the soil, ground surface boundary conditions and shading of adjacent soil. The mathematical basis of this model is a boundary value problem on the three-dimensional heat conduction equation. The boundaries of the system are interior slab surface, far-field soil, deep ground and ground surface. This boundary value problem is solved in Cartesian coordinates by a Fortran program that implements the Patankar-Spalding finite difference technique.[139] The three-dimensional domain of the model is discretized by an irregular grid into 10,000 cells. The minimum grid spacing is 4 in (0.1 m) near the ground level and slab boundaries. The user is expected to define the domain dimensions and grid spacings, weather data file (TMY), soil and slab properties, ground surface properties, slab shape and size, deep ground boundary condition, evaporative loss at the ground surface (evapotranspiration) and building height for shadowing calculations. Slab has an automated grid sizing function which sets the solution domain according to a modified Fibonacci sequence to provide grid flexibility. Slab also automatically calculates the undisturbed ground temperature profile for initialization purposes. The three-dimensional calculations of Slab are integrated with one-dimensional heat conduction calculations of EnergyPlus through iteration.

2.8.1.3 The TRNSYS Slab-on-Grade Model

The TRNSYS system simulation program has a commercially available ground coupling library.[140] The TRNSYS slab-on-grade models used for this study, the Type 49 and Type 1255 models, are parts of a larger suite of these ground coupling models that are identical in the core solution algorithm but differ in application. The Type 49 model calculates floor heat transfer by iterating with the Type 56 (Multizone Building) model of the TRNSYS program. In this coupled model, the Type 56 model calculates the aboveground building loads by assigning the slab/soil interface temperatures calculated by the Type 49 model. The Type 49 model calculates the slab/soil interface temperatures using the QCOMO output of the Type 56 model, which is the combined heat flux from the floor to outside. The Type 1255 model is the latest release of the TRNSYS slab-on-grade model and it allows for coupled use with other energy modeling tools by requiring only the zone air temperatures and the floor inside convection coefficients from the aboveground energy model.

According to the descriptions of McDowell *et al.*[141], the TRNSYS ground coupling models are multizone models and they rely on a three-dimensional finite difference representation of the soil. These models solve the resulting interdependent differential equations using an iterative analytical method. In these models, heat transfer is assumed to be conductive only and moisture effects are not accounted for. The solution is stable over all ranges of simulation steps and even for very high surface heat transfer coefficients. The soil nodes at the surface do not directly conduct to the zone air or ambient air. Instead, they conduct to a "local surface temperature" that is calculated on a massless, opaque plane located between the air and the soil node. This "local surface temperature" can be calculated from an energy balance, from a long-term average surface temperature correlation (Kasuda[137]), or provided to the model as an input.

In the TRNSYS slab-on-grade model, the soil volume surrounding the slab is divided into two parts: 1) the near-field and 2) the far-field. The far-field surrounds the near-field and it includes the soil beneath the near-field and below the deep earth boundary. The

deep earth boundary is defined by the deep earth temperatures, which are either calculated from the Kasuda[137] approach or entered by the user. The boundary between the near-field and the far-field can be defined as adiabatic or conductive. The near-field is affected by the heat transfer between the soil and the slab; whereas the far-field is not. The user defines the near-field entering the number of nodes and the field size/volume. The far-field is assumed as an infinite energy sink/source and its node temperatures are calculated either by using energy balance (between the surface and deep earth temperatures) or the Kasuda[137] correlation (temperature is a function of the time of year and distance below the surface).

2.8.2 Comparative Studies on Slab-on-Grade Models of DOE-2, EnergyPlus and TRNSYS

Comparative testing has long been used for validation and debugging of energy simulation tools.[32,142,143] The slab-on-grade models of EnergyPlus, DOE-2 and TRNSYS have been tested in comparison to multiple other models. This section summarizes the contents and the major conclusions of these studies.

2.8.2.1 Comparative Studies on Slab-on-Grade Models of DOE-2

DOE-2 uses simplified, steady state slab-on-grade GCHT models. The slab-on-grade GCHT models of DOE-2 have been compared with those of other tools by: 1) Judkoff and Neymark[144] and 2) McDowell *et al.*[141]

Judkoff and Neymark[144] compared the GCHT models of DOE-2 with those of BLAST-3.0 and SERIRES/ SUNCODE using the HERS* BESTEST♮ test suite. The HERS BESTEST test suite includes uninsulated and insulated slab-on-grade test cases.[144] Two GCHT calculation methods are used with DOE-2 to model these test cases: 1) Wang's[145] slab-on-grade perimeter heat loss method, and 2) a more detailed method that accounts for the effects of mass and solar radiation incident on soil[144], which eventually leads to lower loads when compared to Wang's method. In this more detailed method, "soil is modeled as a large amount of mass in contact with the ambient air" and "the soil thicknesses may be regarded as curved path lengths for one-dimensional heat conduction between the

a concrete surface/adjacent soil boundary and a soil/ambient air boundary."[144] For the slab-on-grade test cases of HERS BESTEST, these two GCHT methods lead to 18%-19% lower heating loads in DOE-2 than they did in BLAST and SERIRES.[144] The same slab-on-grade test cases of HERS BESTEST are currently used by RESNET[♭] to test energy simulation tools in comparison with DOE-2, BLAST and SERIRES for certification as a residential code compliance calculator.[146]

McDowell *et al.*[141] compared DOE-2's slab-on-grade model, Winkelmann's model, with three other slab-on-grade GCHT calculation methods. These methods were: 1) Wang's[145] slab-on-grade perimeter heat loss method, which was restricted to four construction types, 2) a modified form of Krarti and Chuangchid's[147] slab-on-grade floor design tool, which was based on a design value and an amplitude value, and 3) the TRNSYS slab-on-grade model. McDowell *et al.*[141] concluded that Wang's[145] method performed the worst in comparison to the detailed TRNSYS model. The method of Krarti and Chuangchid[147] showed similar results to the TRNSYS model in heating (within 8%) but exhibited significantly different results for cooling (up to 60%). Winkelmann's method showed good agreement in heating (within 13%) and high disagreement in cooling (up to 42%) with the detailed TRNSYS model.

2.8.2.2 Comparative Studies on Slab-on-Grade Models of EnergyPlus and TRNSYS

The slab-on-grade GCHT model of EnergyPlus, Slab, has been compared to other modeling tools by: 1) Deru *et al.*[148], 2) Neymark *et al.*[32], and 3) Henninger and Witte.[149]

Deru *et al.*[148] compared EnergyPlus with HOT3000, SUNREL and VA114 for various slab-on-grade constructions using the IEA* SHC[♮] Task 22 test cases. For these test cases, the annual ground coupling heating load results of HOT3000, SUNREL and VA114 showed up to ∼52% disagreement with the EnergyPlus results.[32,148] Since the test cases were not designed for diagnostic purposes, the source of this disagreement could not be identified. The study concluded that an in-depth diagnostics needs to be developed to identify the

* Home Energy Rating System
♮ Building Energy Simulation Test
♭ Residential Energy Services Network

reasons for this high variation.[32,148]

In 2001, Spitler *et al.*[150] presented a set of analytical solutions for the ground coupled heat transfer problem of slab-on-grade constructions. These solutions included a 3-D steady state analytical solution for rectangular buildings which was originally developed by CSIRO*, Australia.[151] Neymark *et al.*[32] then designed a set of in-depth diagnostic test cases for slab-on-grade GCHT based on the CSIRO♭ analytical solution. These test cases were improved in collaboration with the IEA SHC Task 34 and the ECBCS10 Annex 43 (IEA 34/43).[32] Using these diagnostic test cases, Neymark *et al.*[32] compared the slab-on-grade GCHT model of EnergyPlus with those of BASECALC, BASESIMP, EN ISO 13370, TRNSYS[152] and SUNREL-GC. Nakhi and Crowley developed two additional stand-alone models respectively using FLUENT[153,154] and MATLAB[155,156] to be tested in the study. With this study, the range of disagreement among the programs for the in-depth diagnostic test cases was reduced from a range of 9%-55% to a range of 1%-24%.[32] The IEA BESTEST building thermal fabric envelope tests were expanded to include these in-depth diagnostic analytical verification test cases for slab-on-grade GCHT. Neymark *et al.*[32] stated that they plan to expand ASHRAE Standard 140 by adding new GCHT test cases that will be used to test and compare the current simulation tools.

After the improvements of Neymark *et al.*[32], the TRNSYS steady state floor conduction compared well with the Delsante analytical solution case (within 0.5%) and to FLUENT (within 2.2%) and MATLAB (within -1.7%). Therefore, the TRNSYS ground coupling method currently appears to be the closest method to a "truth" standard (in the absence of empirical data) for the modeling of the ground coupling effect in a whole building energy simulation program. In the same study, the EnergyPlus steady state floor heat flow and steady-periodic annual floor heat conduction compared with those of TRNSYS within 4% to 9%, and within -11% to +16%, respectively.

Later, Henninger and Witte[149] compared EnergyPlus slab-on-grade GCHT with the

* The International Energy Agency.
♮ Solar Heating and Cooling Programme.
♭ The Commonwealth Scientific and Industrial Research Organization.

ASHRAE 1052-RP Toolkit along with other modes of heat transfer for the 16 different envelopes specified in the ASHRAE 1052-RP report. In this study, the EnergyPlus zone load for the ground coupling test case varied from the results of the ASHRAE 1052-RP Toolkit by 44%.

3. METHODOLOGY*

The goals of this methodology that are described in this chapter are:

1) to select a ground heat transfer modeling method for slab-on-grade low-rise residential buildings,

2) to model a baseline Habitat for Humanity house accounting for the effects of duct layout, thermostat location, building pressure and interzonal air flows,

3) to model an innovative HVAC design strategy, i.e. partial conditioning, that sends conditioned air to the occupied zones and then transfers the returning air to the unoccupied zones.

The following three sections describe the set of procedures followed to reach each of these goals. The first section includes the comparison of three well-known slab-on-grade heat transfer models (i.e. Winkelmann's, Slab and TRNSYS) and the selection of a reasonable ground heat transfer method for the for the following steps of the study through a comprehensive discussion. The second section describes the modeling of a Habitat for Humanity house using a detailed multi-zone approach. The third section describes the conversion of the Habitat for Humanity house modeled in the second section into a partially conditioned atrium house through a set of modeling steps.

3.1 EnergyPlus vs DOE-2: Slab-on-Grade Residential Buildings

DOE-2 has been used for more than three decades in design studies, analysis of retrofit opportunities and developing and testing standards.[157] In 1996, the U.S.D.O.E.[♮] initiated support for the development of EnergyPlus, which was a new program based on the best features of DOE-2 and BLAST.[158] The shift from DOE-2 to EnergyPlus raised questions in the simulation community on the differences between these two simulation programs.[159–161] Ground coupled heat transfer is an area that EnergyPlus differs significantly from DOE-2.

EnergyPlus calculates z-transfer function coefficients to compute the unsteady ground

* Partially reproduced from "EnergyPlus vs DOE-2.1e: The effect of ground coupling on cooling/heating energy requirements of slab-on-grade code houses in four climates of the U.S" by Simge Andolsun, Charles H. Culp, Jeff S. Haberl and Michael Witte, *Energy and Buildings*, 52(2012), 189-206, 2012. Copyright 2012, Elsevier B.V.

♮ The U.S. Department of Energy

coupled surface temperatures;[162] whereas DOE-2 sets the temperatures of the ground coupled surfaces as steady.[163] The slab-on-grade GCHT models of DOE-2 and EnergyPlus have been compared separately with other programs in order to maintain consistency among the results of current simulation tools for identical cases.[32,141,144,148,149] EnergyPlus and DOE-2 have been compared with each other based on thermal loads, HVAC systems and fuel-fired furnaces using the test cases defined in ANSI♯/ASHRAE Standard 140-20073, which were "effectively decoupled thermally from the ground."[149,164] This study extends the previous studies by comparing EnergyPlus and DOE-2 slab-on-grade heat transfer based on the results obtained from residential buildings in four climates of the U.S. In these comparisons, the TRNSYS slab-on-grade model is used as the truth standard for slab-on-grade heat transfer modeling. The reliabilities of the DOE-2 and EnergyPlus slab-on-grade models are then discussed and recommendations are made for the building energy modelers.

This study is divided into two sections. In Section I, empty, adiabatic, ground coupled sealed boxes were modeled using DOE-2, EnergyPlus and TRNSYS programs in order to isolate the slab-on-grade heat transfer from other building load components and compare it between these three programs. In these comparisons, the TRNSYS slab-on-grade model was assumed to be the truth standard for slab-on-grade heat transfer modeling. The results of the DOE-2 and EnergyPlus slab-on-grade models were then evaluated based on the closeness of their results to those of the TRNSYS slab-on-grade model.

In Section II, load components were added to the sealed boxes modeled in Section I to convert them into fully loaded residential buildings. The effect of slab-on-grade heat transfer on the thermal loads of these houses was then quantified and compared between the DOE-2, EnergyPlus and TRNSYS programs. The findings of this section will provide the code users an insight to estimate and understand the thermal load differences they will obtain if EnergyPlus replaces DOE-2 in energy code compliance calculations of low-rise slab-on-grade residential buildings.

♯ The American National Standards Institute

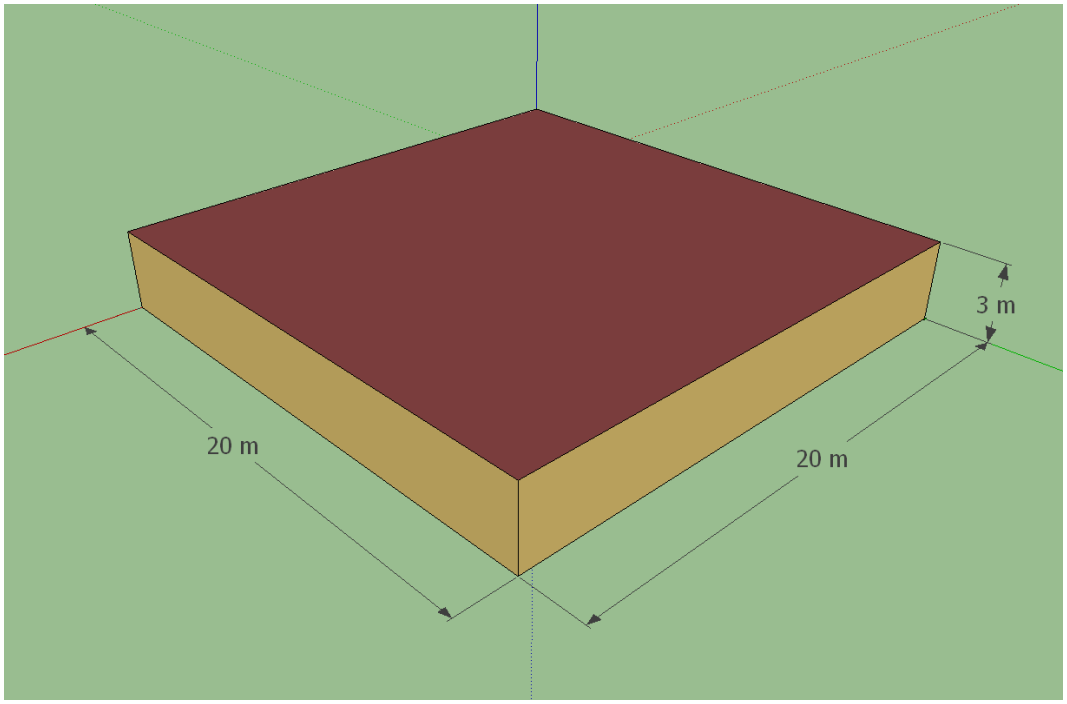

Figure 3.1: The slab-on-grade sealed box.

3.1.1 Section I - Sealed Boxes

In this section, an empty, ground coupled sealed box with dimensions of 20m×20m×3m was modeled with DOE-2, EnergyPlus and TRNSYS programs in hot-humid, hot-dry, temperate and cold climates of the U.S. with the building envelope features required by the International Energy Conservation Code (IECC) 2009 (see Fig. 3.1). These sealed boxes were located in Austin, TX; Phoenix, AZ; Chicago, IL; and Columbia Falls, MT to represent the hot-humid, the hot-dry, the temperate and the cold climates respectively.

Table 3.1 lists the envelope features and Table 3.2 describes the construction materials of these boxes. The zone air temperature was set to 23°C in these boxes throughout the year and their resulting ground coupling loads were compared between the results of the DOE-2, EnergyPlus and TRNSYS programs. The sealed boxes modeled in this section had neither infiltration nor ventilation. They had no windows, lights, equipment or occupants. The walls and the ceilings were assigned as adiabatic surfaces and conductive heat transfer was allowed only through the floor. The thermal storages of the sealed boxes were also

negligible when compared to the slab-on-grade heat transfer. Thus, the thermal loads of these boxes were driven exclusively by the slab-on-grade heat transfer. Thus, the total sensible thermal loads of these sealed boxes (Q_{sens}) were compared with each other in order to quantify the differences between the slab-on-grade models in this study. The corresponding monthly average floor heat fluxes in each model were also plotted.

Table 3.1: Features of the building envelope

	Austin/Phoenix	Chicago	Columbia Falls
Exterior Walls	U=0.082 Btu/hr.ft^2°F; Construction Layers: 0.25′ face brick (BK), 0.04′ plywood (PW), 0.33′ soft wood (WD) frame with 25% framing ratio filled with 0.37′ gypsum board (GP)	U=0.06 Btu/hr.ft^2°F; Construction Layers: Same as the Austin/Phoenix house except that the thickness of the mineral wool (IN) layer is 0.58′	U=0.06 Btu/hr.ft^2°F; Construction Layers: Same as the Chicago house
Ceiling	U=0.035 Btu/hr.ft^2°F; Construction Layers: 0.83′ soft wood (WD) frame with 25% framing ratio filled with 0.98′ mineral wool (IN), 0.04′ gypsum board (GP)	U=0.03 Btu/hr.ft^2°F; Construction Layers: Same as the Austin/Phoenix house except that the thickness of the mineral wool (IN) layer is 1.19′	U=0.027 Btu/hr.ft^2°F; Construction Layers: Same as the Austin/Phoenix house except that the thickness of the mineral wool (IN) layer is 1.42′.
Floor	Uninsulated slab with 1.97′ foundation depth; Construction Layers: 0.33′ heavyweight concrete (CC), massless carpet (CP)	Insulated Slab with 2′ of foundation depth; Construction Layers: Same as Austin/Phoenix house with vertical external insulation (R=10 hr.ft^2°F/Btu)	Insulated Slab with 4ft of foundation depth; Construction Layers: Same as Austin/Phoenix house with vertical external insulation(R=10 hr.ft^2°F/Btu)
Roof	Uninsulated roof; Construction Layers:massless shingle (AR), 0.83′ soft wood (WD) frame with 25% framing ratio, 0.04′ plywood (WD)	Same as the Austin/Phoenix house	Same as the Austin/Phoenix house

Continued on next page

Table 3.1 – *Continued from previous page*

	Austin/Phoenix	Chicago	Columbia Falls
Fenestration	U=0.75 Btu/hr.ft$^{2\circ}$F for the Austin house; U=0.65 Btu/hr.ft$^{2\circ}$F for the Phoenix house. For both houses, SHGC:0.4, total of four windows; one on each wall; each with dimensions of $4.92' \times 32.81'$; double-pane	U=0.35 Btu/hr.ft$^{2\circ}$F; SHGC: 0.7. Total of four windows; one on each wall; each with dimensions of $4.92' \times 32.81'$;double-pane	Same as the Chicago house
Door	R = 1.33 hr.ft$^{2\circ}$F/Btu for the Austin house, R = 1.54 hr.ft$^{2\circ}$F/Btu for the Phoenix house. Faces north; with dimensions of $5.91' \times 6.89'$; modeled as a massless opaque layer	R=2.857 hr.ft$^{2\circ}$F/Btu. Faces north; with dimensions of $5.91' \times 6.89'$; modeled as a massless opaque layer	Same as the Chicago house

Table 3.2: Properties of the materials used in the building envelope. Materials adopted from the DOE-2.1e Materials Library. $^{\flat}$: Mineral wool,$^{\sharp}$: Cellulose,§: Shingle and siding,†: Tile

	Conductivity		Density		Specific Heat		Resistance	
	$\frac{\text{W}}{\text{m.K}}$	$\frac{\text{Btu}}{\text{hr.ft}^{\circ}\text{F}}$	$\frac{\text{kg}}{\text{m}^3}$	$\frac{\text{lb}}{\text{ft}^3}$	$\frac{\text{J}}{\text{kg.K}}$	$\frac{\text{Btu}}{\text{lb.m.}^{\circ}\text{F}}$	$\frac{\text{m}^2\text{K}}{\text{W}}$	$\frac{\text{hr.ft}^2.^{\circ}\text{F}}{\text{Btu}}$
BK	1.31	0.757	2083	130	920	0.22	-	-
PW	0.115	0.066	545	34	1213	0.29	-	-
WD	0.115	0.066	513	32	1381	0.33	-	-
IN$^{\flat}$	0.043	0.025	96	6	837	0.2	-	-
IN$^{\sharp}$	0.039	0.023	48	3	1381	0.33	-	-
GP	0.16	0.093	801	50	837	0.2	-	-
CC	1.310	0.757	2243	140	837	0.2	-	-
AR§	-	-	1121	70	1464	0.35	0.078	0.440
AR†	-	-	-	-	1255	0.3	0.0088	0.05
CP	-	-	-	-	-	-	0.3	1.704
SL	1.73	1	1842	115	418	0.1	-	-
VBR	0.24	0.139	1370	86	1370	0.33	-	-
HP	0.298	0.173	1415	89	2100	0.51	-	-
TV	-	-	-	-	-	-	0.194	1.102
FE	-	-	-	-	-	-	0.021	0.119

The following three models were compared in this section:

1. DOE-2 with Winkelmann's slab-on-grade model (D2-GCW).
2. EnergyPlus with the Slab model (EP-GCS).
3. TRNSYS with the TRNSYS slab-on-grade model (TR-GCT).

There were two major reasons why the ground coupled heat transfer (GCHT) (Q_{floor}) differred between the above mentioned three models. First, the DOE-2, EnergyPlus and TRNSYS programs calculated the heat transfer between the slab and the zone air ($Q_{slab/zair}$) differently. Second, Winkelmann's model, the Slab model and the TRNSYS slab-on-grade model calculated the heat transfer between the soil and the slab ($Q_{soil/slab}$) differently. In order to isolate the effects of the $Q_{soil/slab}$ and $Q_{slab/zair}$ calculation differences and to examine them separately, two intermediate models were introduced to the study. These models were EnergyPlus with Winkelmann's slab-on-grade model (EP-GCW) and EnergyPlus with the TRNSYS slab-on-grade model (EP-GCT). Using these two intermediate models, the comparison process was then divided into two steps. These steps were:

Step 1- The same slab-on-grade model was used with different aboveground energy modeling programs and then the resulting Q_{sens} were compared. Thus, the effect of the $Q_{slab/zair}$ calculation differences between programs was isolated and quantified with the following two comparisons:

(1) The EP-GCW model vs the D2-GCW model: This step quantified the $Q_{slab/zair}$ calculation differences between EnergyPlus and DOE-2.

(2) The EP-GCT model vs the TR-GCT model: This step quantified the $Q_{slab/zair}$ calculation differences between EnergyPlus and TRNSYS.

Step 2- The same aboveground energy modeling program (EnergyPlus) was used with different slab-on-grade models(Winkelmann's, Slab and TRNSYS slab-on-grade models) and the resulting Q_{sens} were compared. Thus, the $Q_{soil/slab}$ calculation differences between programs were isolated and quantified. This step included the following two comparisons:

(1) The EP-GCW model vs the EP-GCT model: This step quantified the $Q_{soil/slab}$ cal-

culation differences between Winkelmann's model and the TRNSYS slab-on-grade model.

(2) The EP-GCS model vs the EP-GCT model: This step quantified the $Q_{soil/slab}$ calculation differences between the Slab model and the TRNSYS slab-on-grade model.

3.1.1.1 Winkelmann's Slab-on-Grade Model

In this study, Winkelmann's slab-on-grade model was used in DOE-2 (D2-GCW) and in EnergyPlus (EP-GCW). In order to apply this model in both programs, the perimeter conduction factors (F2) were selected from the list of Huang *et al.*[135] for the sealed boxes based on their floor insulation configuration and foundation depth. These values were determined to be 1.33 W/m.K (0.77 Btu/h°F.ft) for the Austin, TX and Phoenix, AZ boxes, 0.64 W/m.K (0.37 Btu/h°F.ft) for the Columbia Falls, MT box and 0.85 W/m.K (0.49 Btu/h°F.ft) for the Chicago, IL box. Using these F2 values, the effective resistance (R_{eff}) values for the floors of these boxes were then calculated using Eq. 3.1.

$$R_{eff} = \frac{A_s}{F2 \times P_{exp}} \tag{3.1}$$

Then, the effective U-values of the floors (U_{eff}) were calculated using the Eq. 3.2.

$$U_{eff} = \frac{1}{R_{eff}} \tag{3.2}$$

Assuming that the air film resistance is 0.136 m^2.K/W (0.77 h.ft^2°F/Btu), the actual slab resistance (R_{us}) was then calculated as 0.213 m^2.K/W (1.21 h.ft^2°F/Btu) from the Eq. 3.3.

$$R_{us} = R_{slab} + R_{carpet} + R_{film} \tag{3.3}$$

The resistance of the 12 in soil layer (R_{soil}) was assumed as 0.176 m^2.K/W (1 h.ft^2°F/Btu). The resistances of the fictitious layers (R_{fic}) under the soil layers were then calculated using the Eq. 3.4.

$$R_{fic} = R_{eff} + R_{us} + R_{soil} \tag{3.4}$$

The calculated R_{fic} values were directly entered into DOE-2 and EnergyPlus as inputs. The U_{eff} values were, however, entered only into DOE-2. The underground floor constructions were then modeled with three layers both in DOE-2 and EnergyPlus. These layers were: (1) the massless fictitious insulation layer with the R_{fic} resistance, (2) the 1 ft (0.3 m) soil layer, and (3) the 4 in 0.1 m concrete slab (see Fig. 2.2).

3.1.1.2 The Slab Model of EnergyPlus

In this part of the study, the Slab preprocessor of EnergyPlus was used with EnergyPlus version 5.0.0.031 (EP-GCS). In this version, the EnergyPlus program is integrated with the Slab program. EnergyPlus does a single internal automatic iteration with the Slab program (EP-GCSiit) for slab-on-grade buildings. EnergyPlus documentation, however, does not provide information on whether there are any internal adjustments in this combined model for quick convergence.

In this study, in order to have full control over the iteration process, EnergyPlus was iterated with the Slab program externally by writing a code in Python (EP-GCSeit). In these external iterations, first, the main EnergyPlus input file was run to obtain monthly average zone air temperatures. The zone air temperatures were then entered into the Slab input file and the Slab program was run. The monthly average ground temperatures calculated by Slab were then reentered into the main EnergyPlus input file and EnergyPlus was rerun with the new ground temperatures. EnergyPlus was iterated with Slab until the difference between the monthly average zone air temperatures calculated by the last two EnergyPlus runs was 0.0001°C or lower.

The course material for EnergyPlus[165] describes three different methods for iterating EnergyPlus with the Slab program (EP-GCSeit). These methods differ only in the initial EnergyPlus run. The first method recommended assigning 18°C for the monthly average ground temperatures in the initial run. The second method recommended assigning a high

insulation layer underneath the slab in the initial run. The third method recommended simulating the slab as an interior surface in the initial run. In this study, test runs were made using all of these three methods. The second method, where a high insulation layer is added underneath the slab in the first EnergyPlus run, was found to need fewer iterations to achieve a convergence of 0.0001°C. Therefore, it was selected and used in the study. A high resistance (500 m^2.K/W) insulation layer was placed underneath the slab in the initial EnergyPlus run. The insulation layer was then removed in the later runs and the iteration was continued until the convergence (within 0.0001°C) was achieved.

For each climate, both the internally iterated and the externally iterated EP-GCS models were used in this study. Each of these models was run with and without evaporative transpiration (evapotranspiration). Thus, the following four runs were done for each location.

-iitwtEv: EnergyPlus iterated with the Slab program internally considering evapotranspiration

-eitwtEv: EnergyPlus iterated with the Slab program externally considering evapotranspiration

-iitwotEv: EnergyPlus iterated with the Slab program internally disregarding evapotranspiration

-eitwotEv: EnergyPlus iterated with the Slab program externally disregarding evapotranspiration

In all of these runs, the floor model required two construction layers: (1) a 0.1 m 4 in concrete slab with a thermal resistance value of 0.0716 m^2.K/W (0.433 h.ft^2°F), and (2) a massless carpet with a resistance of 0.3 m^2.K/W (1.702 h.ft^2°F). The physical properties of the slab and soil (SL) used in the Slab model are listed in Table 3.2.

In order to reflect the typical user behavior, the default values of the Slab program were used for multiple parameters. The surface albedo was assumed to be 0.379 with snow and 0.158 without snow. The surface emissivity with/without snow was 0.9. The surface roughness was assumed to be 0.03 with snow and 0.75 without snow. The indoor

convection coefficient was 9.26 upward and 6.13 downward. The slab convergence was 0.1. The distance from the edge of the slab to the domain edge and the depth of the region below the slab were assigned to be 15 m. The annual average outside air temperature of each city was then entered as the deep ground temperature (TDEEPin) of that city. These values were 20.1°C, 22.5°C, 9.8°C and 12.1°C for Austin, Phoenix, Chicago and Columbia Falls respectively. The ground surface heat transfer coefficient was automatically calculated by the program.

3.1.1.3 The TRNSYS Slab-on-Grade Model

The ground coupled test cases were modeled in TRNSYS version 17-00-0019 (TR-GCT) by using the Type 49 slab-on-grade model with the Type 56 multizone building model. In order to compare the results of the TRNSYS slab-on-grade model with the other slab-on-grade models, the hourly (EP-GCTh) and the monthly average(EP-GCTm) slab/soil interface temperatures of the TR-GCT model were also entered into EnergyPlus.

The TRNSYS slab-on-grade model is a finite difference model; therefore, the initial temperatures of the various soil nodes make a significant difference on the calculated heat transfer. For this reason, it is necessary to run the model for multiple years until the ground temperature profiles of the last two years are within an acceptable convergence tolerance. The IEA Task work[32] showed that, in TRNSYS runs, less than 0.2% change occurs after 5 years. Based on this finding, all TRNSYS simulations were run for 5 years and the results of the 5^{th} run were presented.

The node sizes of the TRNSYS slab-on-grade model have been determined for the horizontal and vertical directions through a set of initial test runs. The smallest node size along the perimeter of the slab was finally set to 0.1 m. The distance between the nodes was multiplied by a factor of 2 as the nodes expanded away from the slab perimeter. The near-field far-field boundary was defined as "conductive" in all x, y and z axes. In TRNSYS, the deep ground temperature is assumed to be very close to the yearly average outside air temperature. Therefore, the yearly average outside air temperatures were calculated for all four climates and entered into the Type 49 models as the deep ground (average surface

soil) temperatures. In TRNSYS, the amplitude of the annual surface temperature profile of the soil is assumed to be equal to the half of the maximum monthly average outside air temperature minus one half of the minimum monthly average outside air temperature. These values were calculated to be 9.3 delta°C, 11.0 delta°C, 14.1 delta°C and 14.1 delta°C for Austin, Phoenix, Chicago and Columbia Falls respectively and entered into the Type 49 models. The soil temperature was also assumed to be unaffected by the building at a distance of 15 m beneath from the bottom of the footer in the vertical direction and 15 m from the edge of the building in the horizontal direction.

3.1.2 Section II - Fully Loaded Test House

The sealed boxes modeled in Section I were added the following features to obtain fully loaded test houses located in Austin, TX; Phoenix, AZ; Chicago, IL and Columbia Falls, MT. The resulting houses are shown in Fig. 3.2

(1) An unconditioned attic

(2) Standard ceiling and exterior walls

(3) Windows, doors and shades

(4) Lights and equipment

(5) Infiltration

A 3 m high unconditioned attic with a gable roof was added to the top of the sealed box turning the ceiling of the sealed box into an interior surface. The features of the roof construction are listed in Table 3.1. The adiabatic ceiling and the exterior walls were turned into standard heat transfer surfaces that allow conduction heat transfer. Four windows and a door were added to the exterior walls as described in Table 3.1. The windows were designed in Window 5.2.17a (Window 5) and imported into DOE-2, EnergyPlus and TRNSYS separately. To do this, DOE-2 and EnergyPlus reports were generated from Window 5 program and then copied into the window dataset files of the DOE-2, EnergyPlus and TRNSYS programs. DOE-2, EnergyPlus and TRNSYS read the window information from their window dataset files to model the required windows. All windows had interior shades. As per required by IECC 2009,[166] from 30 April until 31 October, the shading

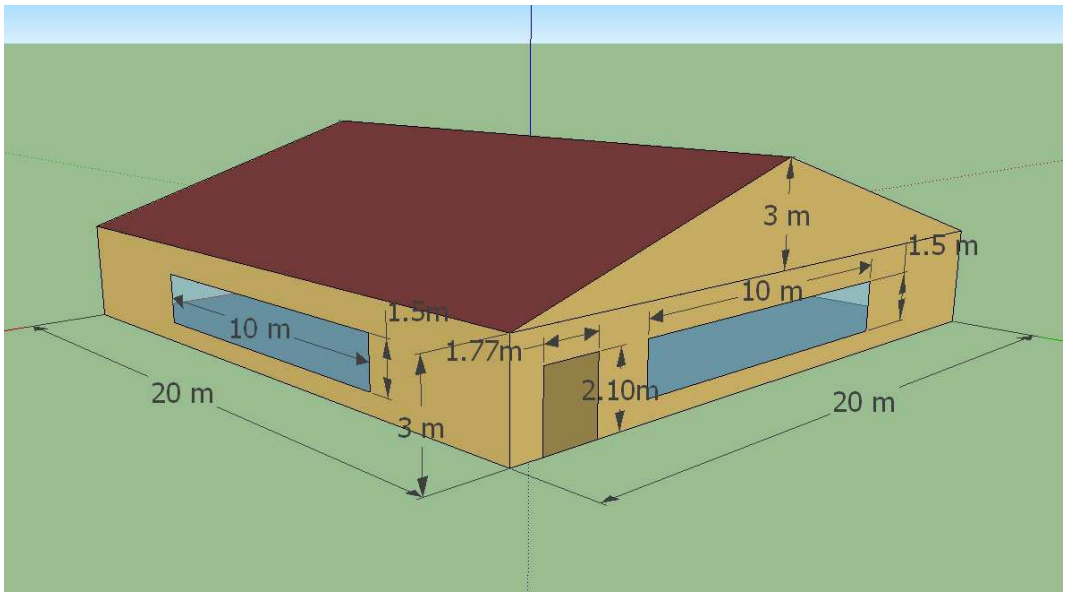

Figure 3.2: The slab-on-grade fully loaded test house.

ratio was set to 70%, while at all other times it was set to 85%.

In the IECC,[166] the overall daily average internal gain of a residential building is calculated by the Eq. 3.5.

$$IGain = 17,900 + 23.8 \times CFA + 4104 \times N_{br}(\frac{Btu}{day}) \tag{3.5}$$

The fully loaded houses were assumed to have five bedrooms. In Eq. 3.5, the N_{br} value was, therefore, taken as "5." The total conditioned floor areas (CFA) of the houses were 400 m^2 (4305.6 ft^2). When these CFA and Nbr values were substituted into the Eq. 3.5, the internal gains of the houses were calculated to be 140,893.6 Btu/day which corresponded to 5870.5 Btu/h (1720.5 Watts). This value was then divided into two and assigned for the lights (860.2 W) and the equipment (860.2 W) equally. The radiant fraction of the heat generated by the lights was set to 0.71. The remaining 0.29 was then assigned as the fraction of the heat convected to the zone air. The radiant fraction of the heat generated by the equipment was 0.7. The lights and the equipment were always on all through the year to provide an average constant internal load.

According to the IECC 2009, the infiltration requirement of a residential building is defined in terms of Specific Leakage Area (SLA) and the SLA value is required to be 0.00036 assuming no energy recovery. The SLA value is calculated by the Eq. 3.6.

$$SLA = \frac{L(\text{ft}^2)}{CFA} \tag{3.6}$$

Substituting the overall conditioned floor areas of the modeled houses (4305.6 ft^2) into the Eq. 3.6, 1.55 ft^2 (1440 cm^2) was obtained for the effective leakage area (L) of the main living space of the houses. The IECC also requires a vented aperture of 1 ft^2 surface area per 300 ft^2 of the roof area. Since the roof areas of the modeled houses were 4305.6 ft^2, the effective leakage area (L) of their attics was calculated to be 14.35 ft^2 (13,333 cm^2). The final "L" values obtained for the main living space and the attic were then directly entered into EnergyPlus and TRNSYS as inputs using the Sherman Grimsrud Infiltration Model. In DOE-2, the "L" values were entered relative to total floor area using the Sherman Grimsrud Infiltration Model in order to model the same infiltration condition.

3.2 Modeling of the Baseline Affordable House in a Hot and Humid Climate

For a reasonable estimation of the energy saving potential of a residential energy efficiency measure, it is significant to have a realistic baseline energy model that represents an IECC 2012 complaint house. The energy requirements of residential buildings in hot and humid climates have been studied extensively using energy modeling tools.[45,47,167,168] In these studies, residential buildings were modeled as single zone volumes with well-mixed inside air and they were represented by a single air temperature and humidity value at each time-step. This section of the study combines multiple simulation tools (including EnergyPlus, TRNSYS and DAYSIM) and resources, and describes an integrated multizone modeling method for the modeling of a baseline affordable house in a hot-humid climate. This method extends the earlier single zone modeling approaches by considering the effects of thermostat location, duct layout, and the interzonal variations in air infiltration, ground heat transfer and zone air temperatures.

During this modeling process, the following important points were observed:

* The AirflowNetwork model required every room of the house to be modeled as a separate zone in order to define a supply duct for that room. This multizone system was assigned a single control zone (the corridor and the living room, i.e. CR-LR) and the cooling/heating was supplied to the six other zones based on the readings of the thermostat in the control zone.

*The infiltration air changes, the number of hours that the set points were not met varied significantly between the rooms of the modeled baseline Habitat for Humanity house, which highlighted the benefits of using a multi-zone energy model for the modeling of residential buildings.

* In weather zone 2 in Texas, the 5 ACH at 50 Pa pressure difference resulted in less than 0.3 ACH annual average air exchange rate in cities (0.07 ACH), urban environments (0.14 ACH), suburbs (0.14 ACH) and open country (0.25 ACH). This finding showed that an outside air system is required in weather zone 2 in Texas in all environments.

* The IECC 2012 requires residential buildings to have mechanical ventilation. The IECC 2012 also requires this ventilation rate to be in addition to the air leakage rate required by the code (5 ACH at 50 Pa pressure difference). This study showed that mechanical ventilation positively pressurized the baseline affordable house modeled in Texas which made the building envelope leakages cause exfiltration rather than infiltration.

In literature, it is advised to model most buildings as multizone structures even when no internal partitions are present in order to account for the effect of interzonal airflows.[95,169] Airflows in buildings can have a significant effect on building loads, indoor air quality and energy use. Gu[95] divides airflow in buildings into two types: 1) controlled, and 2) uncontrolled. He defines the controlled airflows as the ones driven by fans. Uncontrolled airflows are then defined as the those driven by a combination of wind and forced airflow through the building envelope, leaky air distribution system ducts, and unbalanced return and exhaust airflows.[95] Fan flow rates are also affected by the uncontrolled airflows since they are functions of external pressures.[95] The EnergyPlus energy modeling program has an

airflow network model (i.e. the AirflowNetwork model) which is based on the calculations of the AIRNET and the COMIS programs (see Sec. 2.7.1.1). This model provides the ability to calculate multizone airflows due to forced air, wind and surface leakage, including adjacent zones and outdoors during both the on and off hours of the system.[104] In this study, this model was used for the modeling of the aboveground section of the multizone baseline Habitat for Humanity house.

For low-rise residential buildings, slab-on-grade heat transfer calculations are critical for reasonable estimation of building energy use (see Sec. 3.1). Most simulation tools currently assume single zone ground heat transfer calculations for simplification purposes. The current slab-on-grade heat transfer model of EnergyPlus (i.e. Slab) is also a single zone model and it assumes a single air temperature at each timestep for all buildings regardless of the zoning condition. The slab-on-grade heat transfer model of TRNSYS is a multizone model and is superior to Slab. It relies on a three-dimensional finite difference representation of the soil,[141] which makes it the closest model to a "truth standard" for the calculation of slab-on-grade heat transfer (as can be deducted from the works of Neymark *et al.*[32]) The new release of the TRNSYS slab-on-grade model (i.e. the Type 1255) allows for coupled use with other energy modeling tools. In this study, this new Type 1255 slab-on-grade heat transfer model was coupled with the above-ground AirflowNetwork model of EnergyPlus for the modeling of the baseline affordable house in Bryan, Texas.

For this study, the Habitat for Humanity houses in Bryan, Texas were examined and a typical house type (Type 310) was selected. Fig. 3.3 presents the selected Bryan Habitat for Humanity house. This house had 994 ft^2 floor area (excluding the interior and exterior walls), a $6' 9\frac{3}{4}''$ high unconditioned attic space under a pitched roof, an entrance porch on the south side and a total of two entrance doors (one from the south and the other from the west side). The conditioned space consisted of a living room (436 ft^2) that included the kitchen and the dining area, 3 bedrooms (127 ft^2, 129 ft^2 and 140 ft^2), one main bathroom (54 ft^2), one WC for the master bedroom (23 ft^2) and a utility room (47 ft^2) where the washer and the dryer of the house were located.

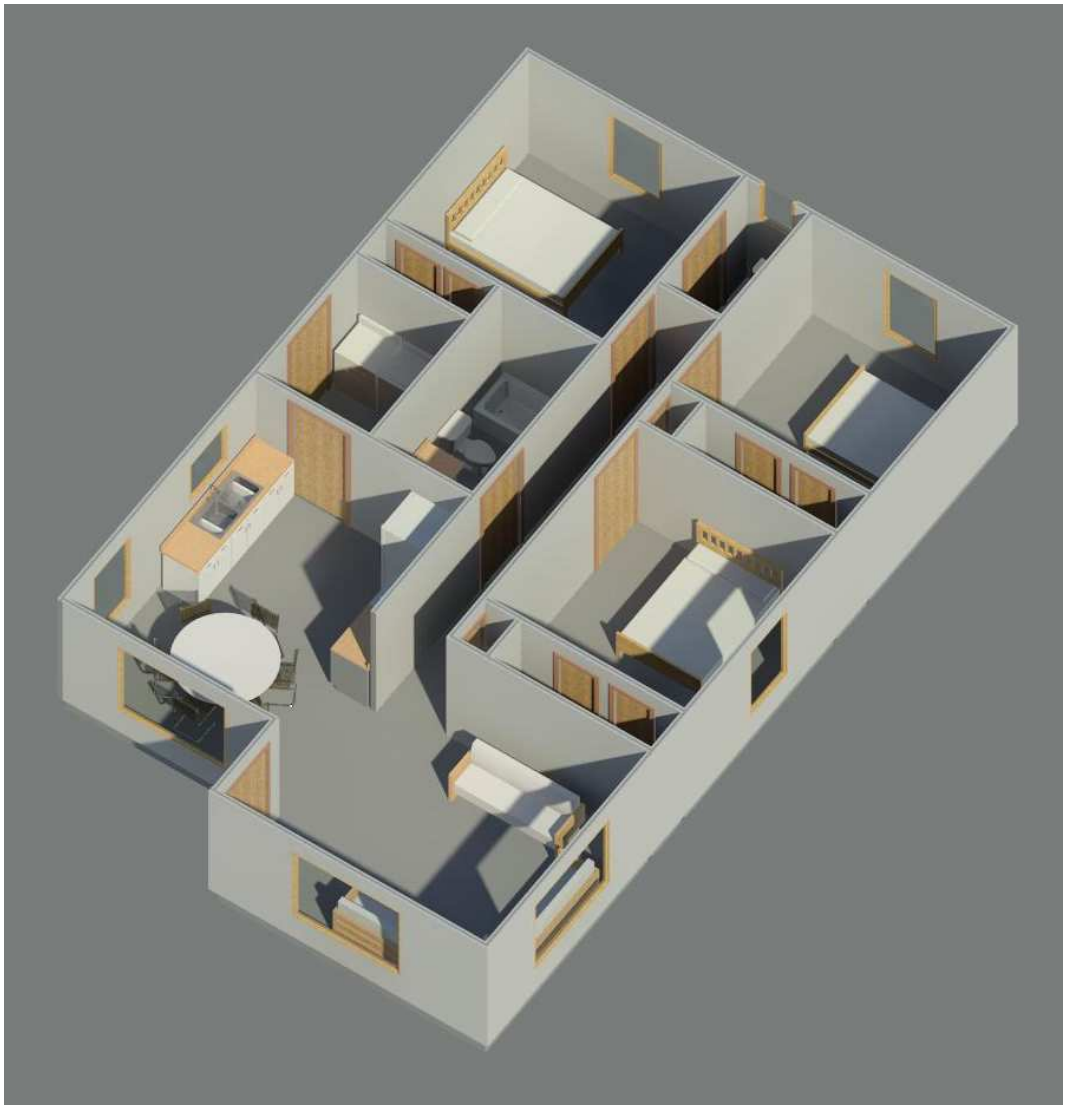

Figure 3.3: A Typical Habitat for Humanity house (Type 310) in Bryan, Texas.

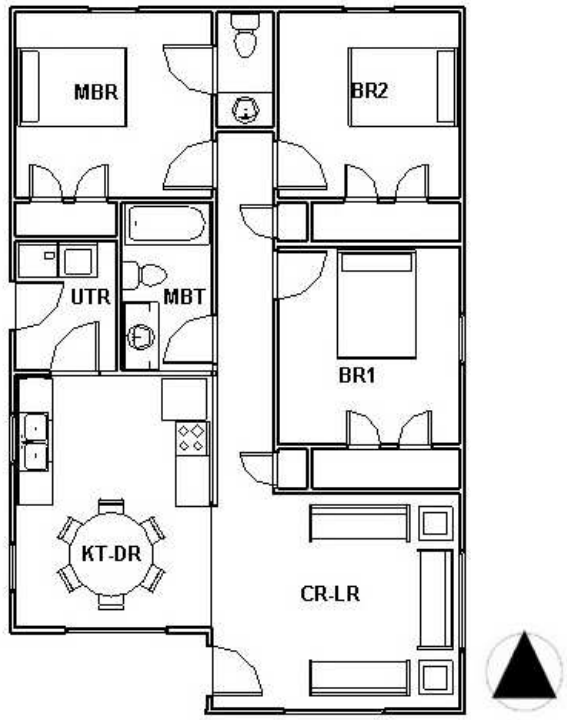

Figure 3.4: The zones of the multizone Bryan Habitat for Humanity house (Type 310) model. BR1: Bedroom 1, BR2: Bedroom 2, MBR: Master bedroom, UTR: Utility room, MBT: Main bathroom, KT-DR: Kitchen and dining room, CR-LR: Corridor and the living room.

This house was modeled as a multizone building with six zones, i.e. the kitchen and the dining room sections of the living area (KT-DR), the corridor and the living room sections of the living area (CR-LR), the master bedroom (MBR), the bedroom 1 (BR1), the bedroom 2 (BR2), the main bathroom (MBT) and the utility room (UTR) (see Fig. 3.4). This multizone baseline model was prepared in two primary steps. First, the aboveground portion of the building was modeled with an adiabatic floor in EnergyPlus. Second, the aboveground EnergyPlus model was iterated with the TRNSYS slab-on-grade model until the HVAC energy consumption outputs converged between two consecutive EnergyPlus runs. Fig. 3.5 shows the EnergyPlus model of the baseline Habitat for Humanity house as it looks in the Open Studio Plug-in for SketchUp.

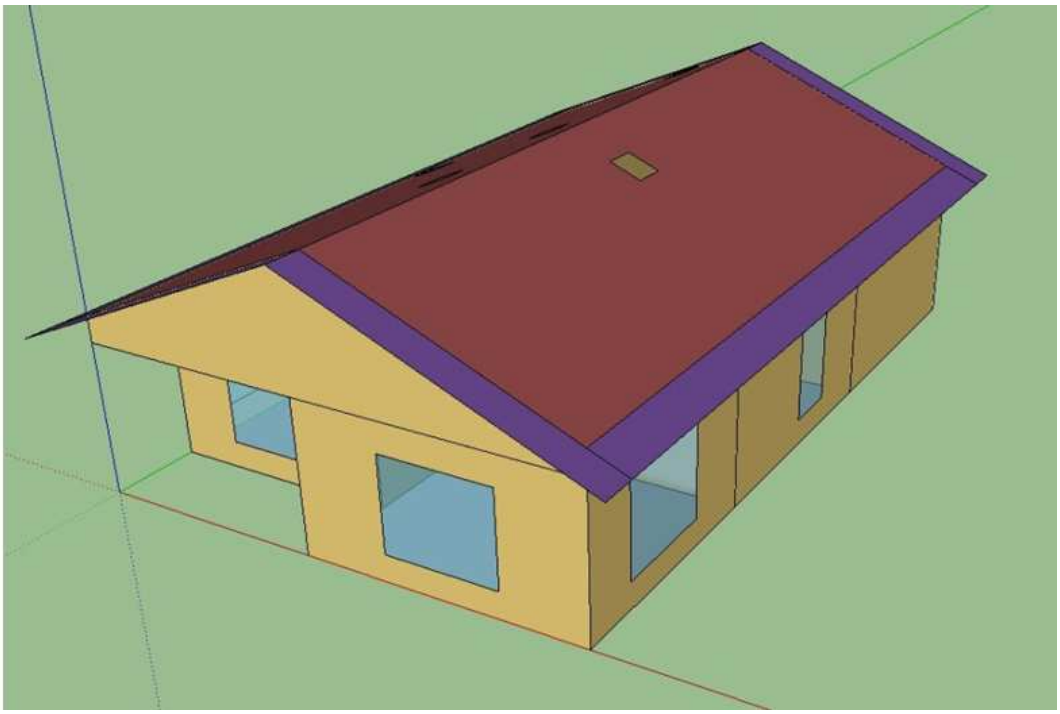

Figure 3.5: The EnergyPlus model of the baseline house.

3.2.1 Modeling of the Aboveground Building Envelope

The typical building envelope features of the Bryan Habitat for Humanity houses were obtained from the Bryan Habitat for Humanity office. These features were compared with the building envelope requirements of the IECC 2012.[34] When necessary, modifications were done on the typical building envelopes of the Bryan Habitat for Humanity houses in order to improve their performance. Table 3.3 and Table 3.2 list the resulting features of the building envelope in the baseline house.

3.2.2 Modeling of the Internal Gains

In IECC 2012,[34] it is stated that the annual total internal load of a residential building can be calculated using Eq. 3.5. This total value includes people, lights and the equipment of the building. The quantity and the hourly schedule of each individual internal load are, however, not clear in the code. This study was aimed at modeling an affordable baseline house that represents the typical residential lifestyle in the U.S. Thus, the assumptions and the calculation methods of Building America House Simulation Protocols[35] were adopted

Table 3.3: Construction materials of the Bryan Habitat for Humanity house from outside towards inside.

Construction	Material
Exterior Walls	Hardie Plank (HP), Tyvek (TV), $\frac{7}{16}''$ OSB (PW), 3 $\frac{1}{2}''$ studs (WD) on 24″ centers filled with cellulose insulation (IN), $\frac{1}{2}''$ sheetrock (GP)
Interior Walls	$\frac{1}{2}''$ sheetrock (GP), 3 $\frac{1}{2}''$ wood frame (WD) on 24″ centers, $\frac{1}{2}''$ sheetrock (GP)
Ceiling	3 $\frac{1}{2}''$ ceiling joists (WD) on 24″ centers with R38 cellulose insulation (IN), $\frac{1}{2}''$ sheet rock (GP)
Roof	Asphalt shingles (AR), 30 felt (FE), $\frac{7}{16}''$ radiant barrier OSB (PW), 3 $\frac{1}{2}''$ rafters (WD) on 24″ centers, no insulation
Windows	U= 2.27 W/m^2.K, Solar Heat Gain Coefficient: 0.25, Visible Transmittance:0.7
Floor	6 mil polyethelene moisture barrier (VBR), 4″ concrete (CC) with beams which are 14″ wide at 12′ intervals, vinyl tile (AR†)

to determine the daily totals and schedules for the people and equipment in the baseline house. The lighting requirement of the house was, however, calculated using the DAYSIM program. The resulting total internal load of the baseline affordable house was found to be 56,364 Btu/day. This value was close (within 4.6%) to the *IGain* value calculated by Eq. 3.5 (53,869 Btu/day) as per the IECC 2012.[34]

For the simulation of the equipment heat gain in the baseline house using EnergyPlus, four parameters were required for each equipment type. These parameters were daily totals, sensible and latent fractions of the equipment heat gain, the convective and radiative fractions of the sensible heat gain, and the daily schedule of each equipment type. The Building America House Simulation Protocols[35] examine each equipment type individually and recommend Eq. 3.7 to calculate the annual total heat gain from each equipment type. In this study, it was assumed that the baseline affordable house had six types of equipment. This equipment included a refrigerator, a 3.2 ft^3 drum clothes washer, an electric clothes dryer, a dishwasher with 8 place settings, an electric range (assuming 74% EF cooktop and 11% EF oven) and miscellaneous other equipment loads of a gas/electric house.

$$EGain = a + b \times N_{br} + FFA(\frac{kWh}{year}) \tag{3.7}$$

The daily total heat gain from each equipment type was calculated by dividing the annual total heat gain calculated with Eq. 3.7 by 365 days (see Table 3.4). The sensible and latent fractions and the hourly schedules of each equipment type were also adopted from Building America House Simulation Protocols[35] (see Table 3.4). Fig. 3.6 and Fig. 3.7 show the hourly equipment schedules used for the modeling of the baseline affordable house. Of the total sensible energy generated by all equipment, 77% was assumed to be radiant while the remaining 23% was convective.

Table 3.4: Total heat gains from the equipment in the Bryan Habitat for Humanity house.

	a	b	c	Annual $\frac{kWh}{yr}$	Daily $\frac{Wh}{day}$	Sensible Fraction	Latent Fraction
Refrigerator	434	-	-	434	1189	1	0
Clothes Washer	38.8	12.9	-	77.5	212.33	0.8	0
Clothes Dryer	538.2	179.4	-	1076.4	2949.04	0.15	0.05
Dishwasher	87.6	29.2	-	175.2	480	0.6	0.15
Range	250	83	-	499	1367.12	0.4	0.3
Miscellaneous Loads	1595	248	0.426	2762.5	7568.53	0.734	0.2

For the modeling of heat gain from the people in the baseline affordable house in EnergyPlus, four input parameters were required. The first required parameter was the number of people. According to Building America House Simulation Protocols,[35] the number of occupants in a single family house is calculated with Eq. 3.8. Using this equation, the total number of people in the baseline house was calculated to be 2.64. This number was then rounded up to 3. Each room of the house was then assigned a maximum number occupant (see Table 3.5).

$$Number\ of\ occupants = 0.59 \times N_{br} + 0.87 \tag{3.8}$$

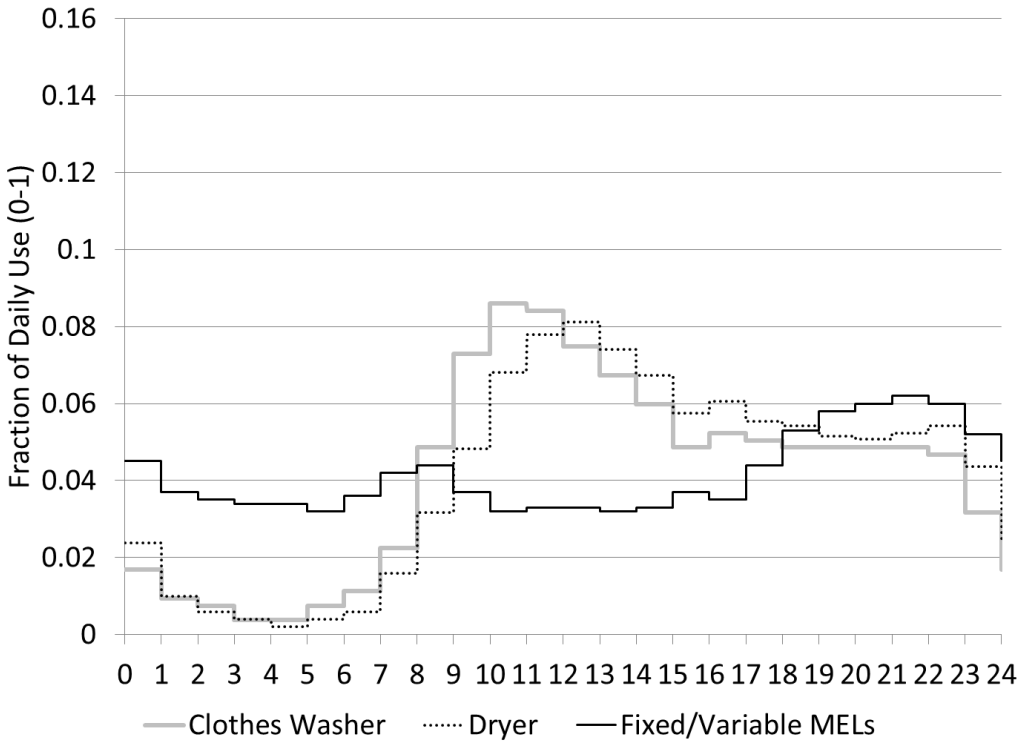

Figure 3.6: The utility room equipment and the fixed/variable miscellaneous equipment of the baseline affordable house. Adapted from Hendron.[35]

Table 3.5: Total heat gains generated by people in each room in the baseline affordable house.

		Sensible		Latent	
Room Type	Maximum # of people	Heat (Btu/ person/hr)	Fraction (0-1)	Heat (Btu/ person/hr)	Fraction (0-1)
Bedroom 1	0	210	0.6	140	0.4
Bedroom 2	1	210	0.6	140	0.4
Master Bedroom	2	210	0.6	140	0.4
Living Room	3	230	0.5476	190	0.4524
Utility Room	1	250	0.5555	200	0.4444
Bathroom	1	245	0.6125	155	0.3875

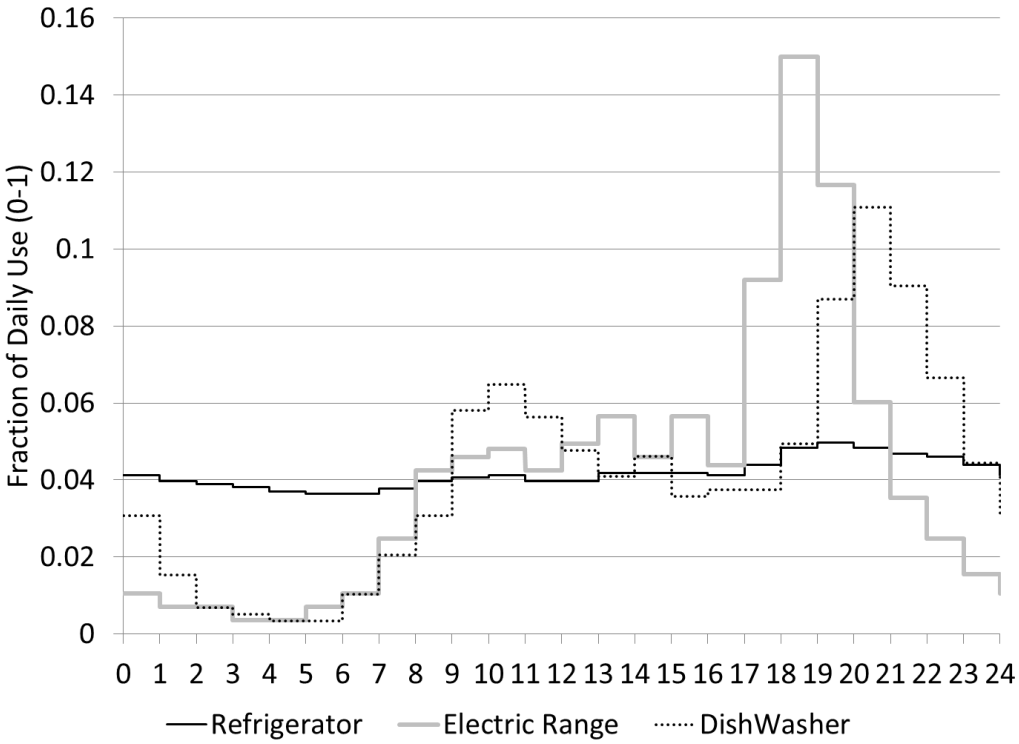

Figure 3.7: The kitchen equipment of the baseline affordable house. Adapted from Hendron.[35]

The second input parameter required to model the people in the baseline house was the occupancy schedule of each room. Building America House Simulation Protocols[35] provided occupancy schedules for typical residential buildings in the U.S. These protocols divided a typical single family U.S. house into two primary areas (i.e. the living area and the bedroom area) and presented their schedules separately. They also presented the typical whole-house occupancy schedule for these houses which was equal to the sum of the living area and bedroom area schedules. This indicated that the occupancy schedules of the subspaces like the utility room or the bathrooms were included in the schedules of the living area and bedroom area. Thus, the occupancy schedules of the baseline house were produced from Hendron's[35] schedules in three steps. First, the bathroom schedules of Hendron[35] for multi-family houses were assigned to the bathrooms of the baseline house based on the fact that bathroom occupancy depended more on need rather than preference. Second, it was realized that Hendron's[35] occupancy schedule for the utility rooms in multi-family houses was the same as the washer's operation schedule. The same logic was followed in the baseline house and the schedule of the washer was assigned as the occupancy schedule of the utility room. Third, the occupancies of the bathrooms and the utility room were subtracted from Hendron's[35] schedules for the living area and bedroom area to obtain the exact schedules of the living room and bedrooms. The resulting occupancy schedules are given in Fig. 3.8 and Fig. 3.9. The occupancy schedule of the living room was then further broken down into three subschedules, i.e. kitchen, dining room and living room (see Fig. 3.10 and Fig. 3.11).

The remaining two parameters required to model people in EnergyPlus were the radiant fraction and the sensible fraction of the heat generated by the people. These fractions are listed in Table 3.5.

The hourly electric lighting requirement of the baseline house was calculated in EnergyPlus with Eq. 3.9. The O_f value in this equation showed the occupied fraction of the hour for each room. This value was equal to the occupancy schedule of each room as presented in Fig. 3.8, Fig. 3.9, Fig. 3.10 and Fig. 3.11. As per Eq. 3.9, the lights of the rooms in

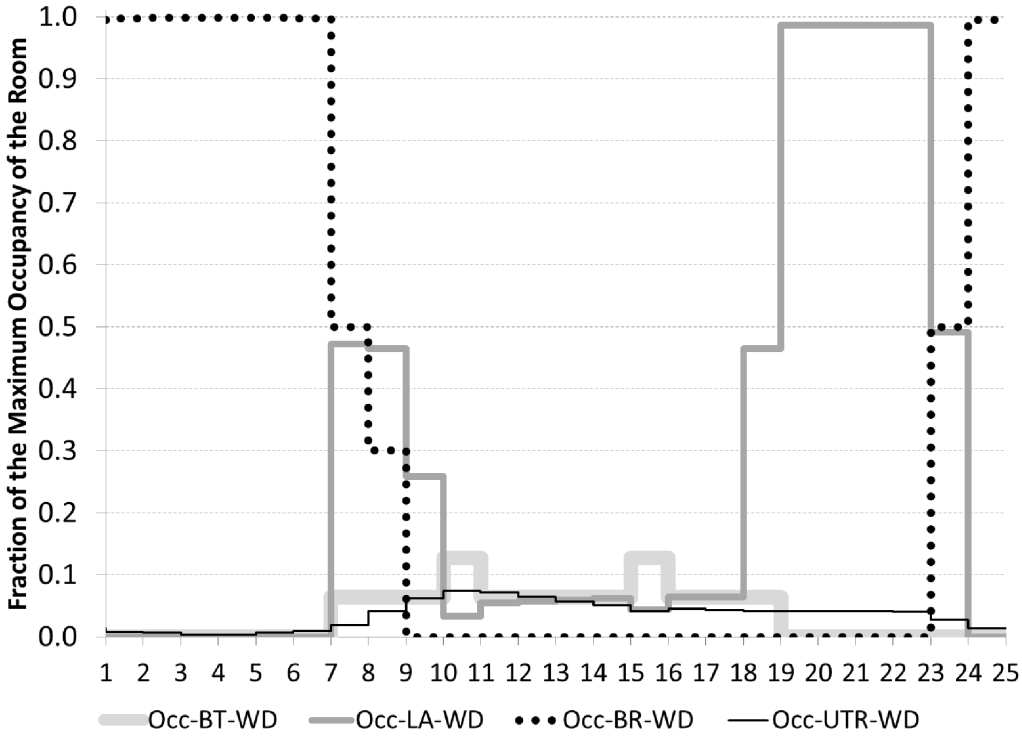

Figure 3.8: The occupancy (Occ) schedules of the baseline house on weekdays. Adapted from Hendron.[35] BT: Bathroom, LA: Living area, BR: Bedroom, UTR: Utility room, WD: Weekday, WE: Weekend.

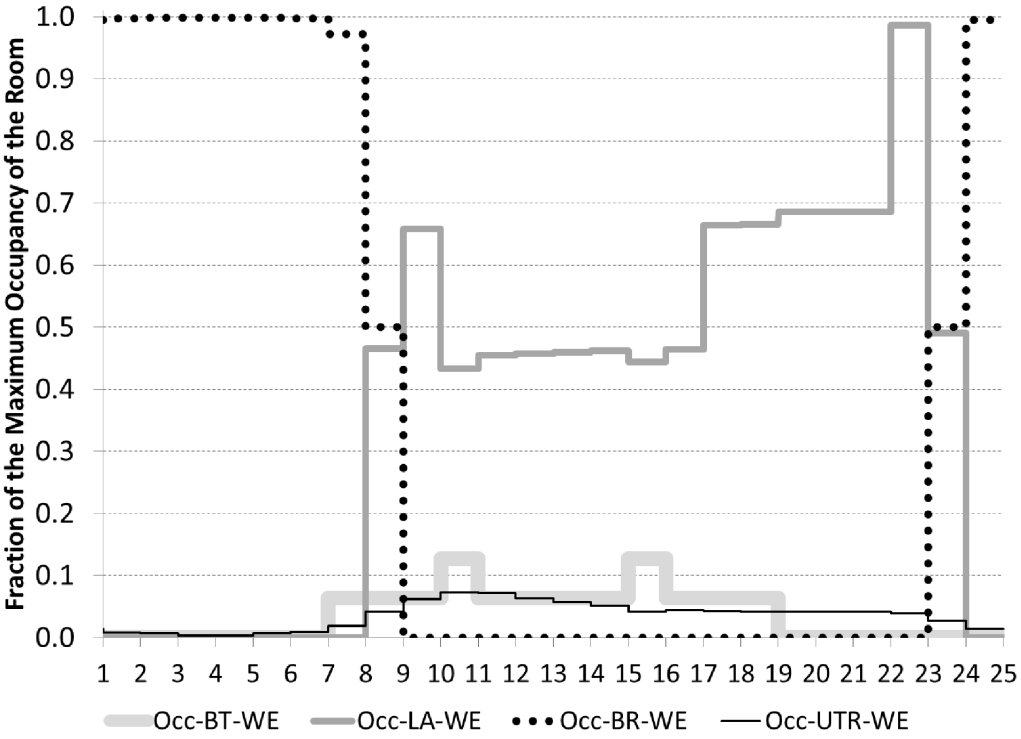

Figure 3.9: The occupancy (Occ) schedules of the baseline house on weekends. Adapted from Hendron.[35] BT: Bathroom, LA: Living area, BR: Bedroom, UTR: Utility room, WD: Weekday, WE: Weekend.

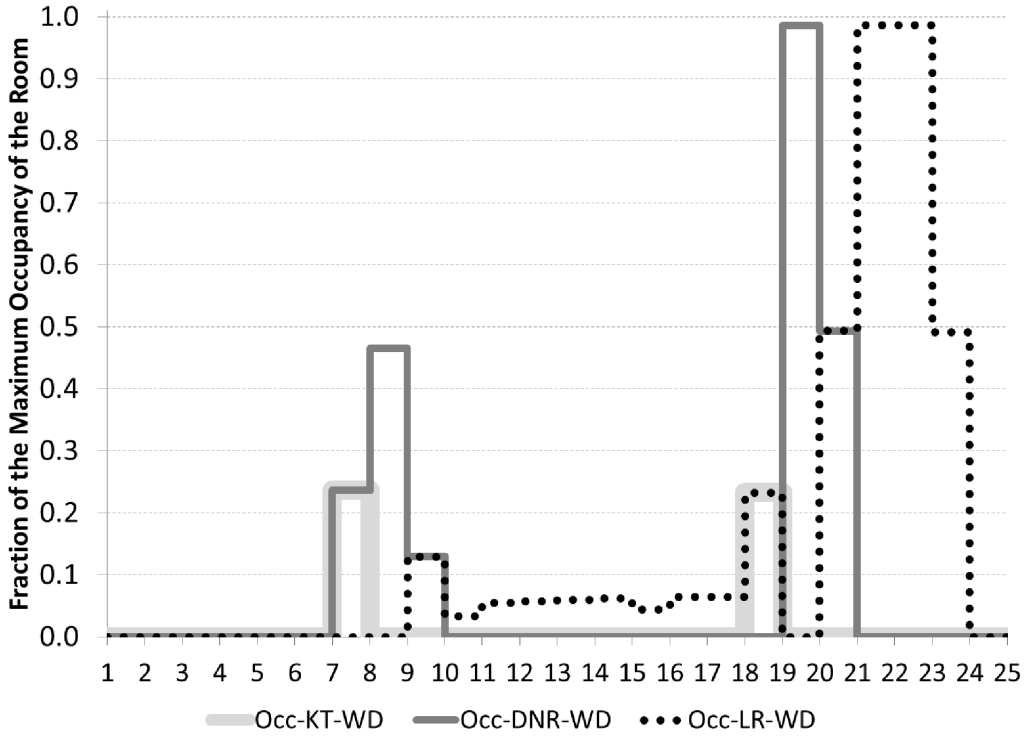

Figure 3.10: Living area occupancy (Occ) schedule on weekdays broken down into the schedules of subspaces. Adapted from Hendron.[35] KT: Kitchen, DNR: Dining room, LR: Living room, WD: Weekday.

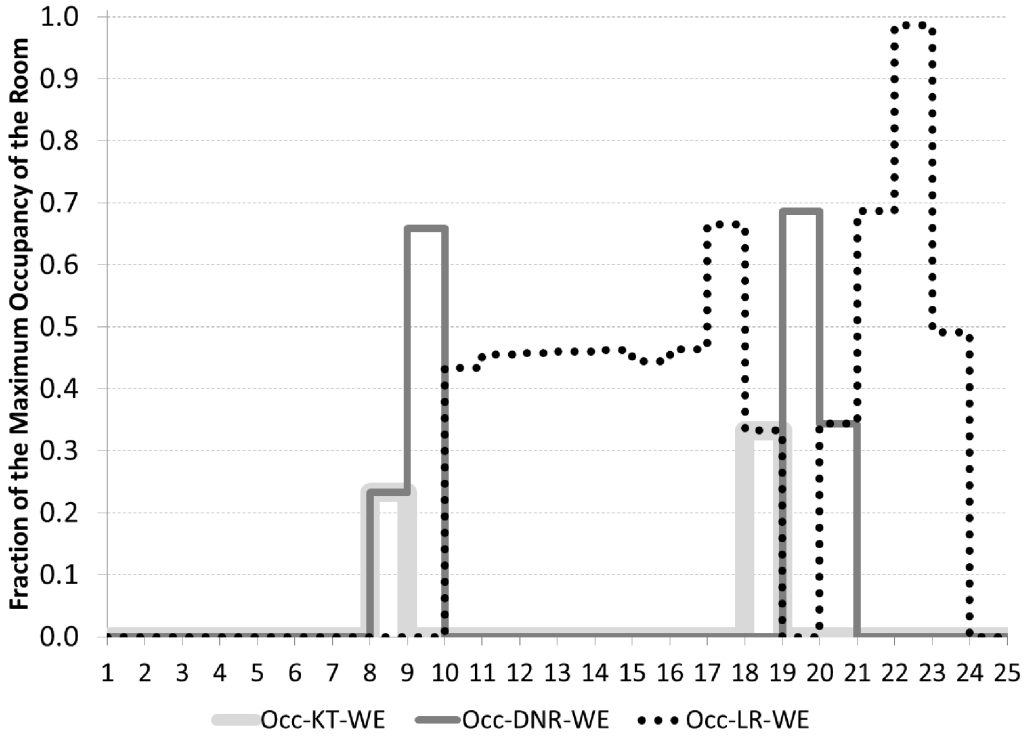

Figure 3.11: Living area occupancy (Occ) schedule on weekends broken down into the schedules of subspaces. Adapted from Hendron.[35] KT: Kitchen, DNR: Dining room, LR: Living room, WE: Weekend.

the baseline house were assumed to be off during the unoccupied hours. The L_f value in Eq. 3.9 then showed the fractional use of the electric lights in a room. For instance, a room with a L_f value of 1 showed that all of the electric lights in the room were on whereas the room with a L_f value of 0 showed that the lights in the room were all off.

$$LR = O_f \times L_f \times L_L \tag{3.9}$$

For determining the L_f value of each room, a yearly daylight analysis tool was required. The EnergyPlus program has a daylight calculation model which originates from that of DOE-2. Earlier studies showed that this model calculates ±20% illuminance values when compared to the DAYSIM/RADIANCE program at distances up to 3.75m from the window in 5m×5m×3m and 5m×10m×3m rooms.[126] This difference reached +50% at 7.50 m distance from the external window in a 5m×10m×3m room.[126] These high deviations in EnergyPlus results from those of DAYSIM/RADIANCE were explained by the fact that the DAYSIM/RADIANCE program uses a more advanced ray tracing method for the calculation of interior illuminances whereas EnergyPlus uses Daylight Factors (DF). EnergyPlus calculates the internal illuminances through the integration between the DF relating to the sky vault portion and the DF of the sunlight, multiplied by their corresponding external illuminance.[103] The depths of the rooms of the baseline house modeled in this study ranged between 3.3m and 7.9m from the exterior windows (see Fig. 3.3). Thus, the DAYSIM/RADIANCE program was used in this study to calculate the L_f values of the baseline house.

According to the IES Lighting Handbook,[36] whether or not a room requires electric lighting depends on two important parameters. These parameters are the activity typically performed in the room and the age of the occupant. Table 3.6 lists the threshold lighting levels (E_{thres}) recommended for different rooms of a residential building for the occupants between the ages of 25 and 65.[36] Assuming that the occupants of the baseline house were between the ages of 25 and 65, the threshold levels given in Table 3.6 were

entered into DAYSIM for calculation of the L_f value for each room of the baseline model. In these calculations, it was assumed that the rooms of the baseline house were always occupied throughout the daytime. Thus, the hours that required electric lighting according to DAYSIM calculations (the hours with L_f >0) were further checked for room occupancy and for the occupants' awake hours to determine the final L_f values of the rooms. In these final checks, it was assumed that the occupants were awake as long as they were outside of their bedrooms and/or it was between 7 a.m. and 12 a.m. any day of the week. The final average hourly electric lighting schedules for the four seasons of the year are presented in Fig. 3.12. These results showed that lighting electricity use made a three separate peaks. The first peak occurred in the morning when the occupants were in the kitchen (7 a.m.-8 a.m.) since there was not sufficient daylight in the kitchen during these hours and the lighting level of the kitchen was significantly high (see Table 3.6). The second peak occurred in the evening when the occupants were in the dining room (7 p.m.-8 p.m.), because it was after the sunset and because the maximum lighting level of the dining area was higher than the living room (see Table 3.6). The third peak occurred between 11 p.m. and 12 a.m. which was a transitional time when the occupants were leaving the living room to go to their bedrooms causing the lights of these two primary spaces partially on (see Table 3.6).

The L_L value in Eq. 3.9 refers to the nighttime lighting level of the room, which is the lighting level when all lights of the room are on. In order to determine a reasonable L_L value for each room of the baseline house, the typical electric lighting design of the Bryan Habitat for Humanity houses was examined. The typical number and types of the lightbulbs used in the Bryan Habitat for Humanity houses are listed in Table 3.6. These lights were fluorescent lights. According to Grondzik *et al.*,[170] the maintained illuminance (E) of a room can be calculated using Eq. 3.10. Using this equation, the E values of each room of the baseline house were calculated using the typical light bulbs of the Bryan Habitat for Humanity houses. The resulting illuminance values (E_{typ}) are listed in Table 3.6.

$$E(fc) = (Lumen/lamp) \times N_{La} \times COU \times \frac{LLF}{FFA(ft^2)} \tag{3.10}$$

Table 3.6: The electric lighting design of the baseline Habitat for Humanity house in accordance with the IES Lighting Requirements.[36] LR: Living room, BR1: Bedroom 1, BR2: Bedroom 2, MBR: Master bedroom, MBT: Main bathroom, UTR: Utility room, DNR: Dining room, KT: Kitchen, HLL: Hallway, [a]: General, [b]: Toilets and bidets, [c]: Laundry, [d]: Study use, [e]: Preparation counters, [f]: Cooktops, [g]: Independent passageways.

IES			Typical*					Modified				
Rm	E_{thres}	FFA♯	N_{La}	$\frac{W}{bulb}$	$\frac{lm}{bulb}$	COU	E_{typ}	N_{La}	$\frac{W}{bulb}$	$\frac{lm}{bulb}$	E_{mod}	L_L
LR	30[a]	17.5	4	15	700	0.44	56.3	2	13	900	36	26
BR1	50[a]	11.8	4	15	700	0.23	43.7	4	13	900	56	52
BR2	50[a]	11.0	4	15	700	0.23	46.7	4	13	900	60	52
MBR	50[a]	12.0	4	15	700	0.23	43.1	4	13	900	55	52
	100[b]	2.1	3	15	700	0.42	333.4	1	13	900	143	13
MBT	100[b]	5.0	3	15	700	0.42	141.3	2	13	900	121	26
UTR	200[c]	4.3	1	19	1200	0.46	102.1	2	19	1200	204	38
DNR	200[d]	7.9	4	15	700	0.4	114.0	6	13	900	220	78
KT	500[e]	8.5	2	40	2650	0.46	230.8	7	13	900	549	91
	300[f]	8.5	1	15	700	0.29	19.2	7	13	900	346	91
HLL	30[g]	6.7	2	13	900	0.23	49.8	1	19	1200	33	19

*The typical N_{La} and $\frac{W}{bulb}$ values were provided by Mr. Jim Davis, the Property Director of the Bryan/College Station Habitat for Humanity.

♯: m^2

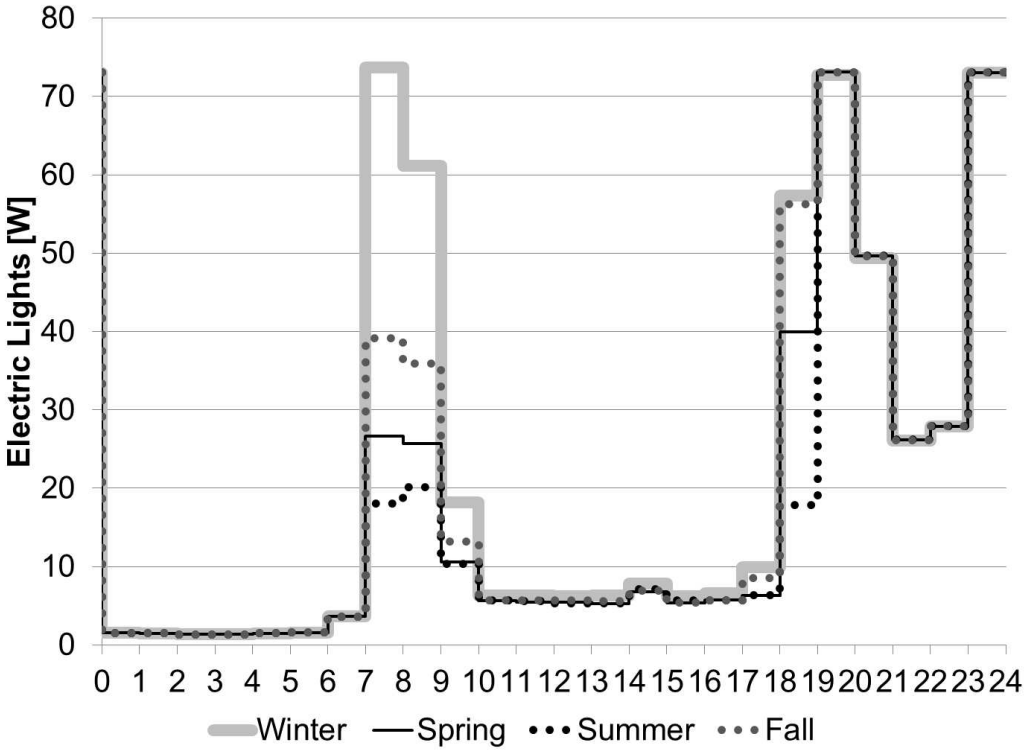

Figure 3.12: The average hourly lighting power schedule of the baseline house for each season.

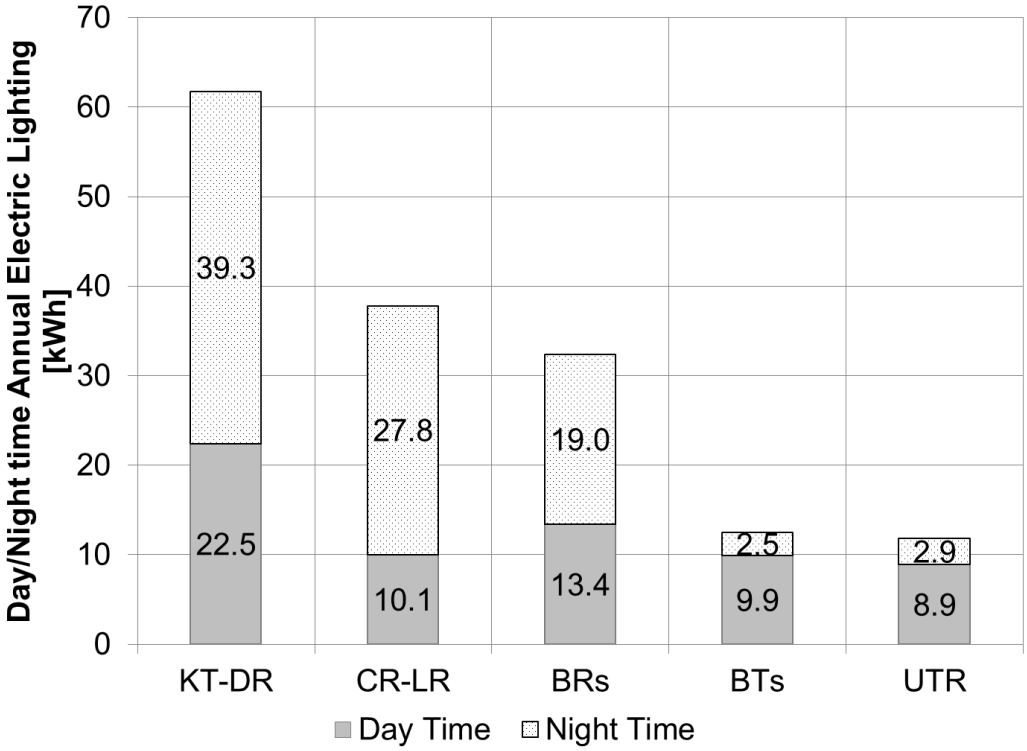

Figure 3.13: The annual day/nighttime lighting electric consumption for the primary living areas of the baseline house, KT-DR: Kitchen and dining Room, CR-LR: Corridor and living Room, BRs: Bedrooms, BTs: Bathrooms, UTR: Utility room

Comparing these typical values (E_{typ}) with the IES lighting requirements[36] (E_{thres}), it was found that the bedrooms, utility room, dining room and kitchen of the typical Bryan Habitat for Humanity houses did not have sufficient lighting at nights. The living room, bathrooms and hallway of these houses, however, had more than required lighting. Thus, modifications were made on the typical lighting designs of these houses in order to meet the IES lighting requirements.[36] The elements of the final lighting design of the baseline house are given in Table 3.6 along with the resulting L_L values. These lights were assumed to be suspended fluorescent lights that had 0.42 radiant, 0.18 visible and 0.42 convected fractions. The resulting lighting electric consumption of the baseline house is shown in Fig. 3.13.

3.2.3 Modeling of the Infiltration/Ventilation

The International Energy Conservation Code[34] requires all dwellings to be tested to 5 ACH50 (5 air changes per hour of infiltration at 50 Pa pressure differential) or tighter in climate zone 2, where Bryan, Texas is located. A dwelling in this zone tested tighter than 5 ACH50 requires mechanical ventilation with a rate not to exceed that calculated with Eq. 3.11. This limiting ventilation rate was found to be 0.3 ACH for the baseline house. The IECC 2012 also requires this ventilation rate to be in addition to the infiltration provided with the 5 ACH50 air tightness. Before modeling of infiltration/ventilation in the baseline house, the validity of these requirements of IECC 2012 was discussed. In this discussion, the AirflowNetwork model of EnergyPlus provided the capability to observe the impact of mechanical ventilation on infiltration rates.

$$Q = 0.01 \times CFA + 7.5(N_{br} + 1) \tag{3.11}$$

The data required for this discussion was provided in three steps. First, the effective leakage area (L) of a house with 5 ACH50 air tightness was calculated using Eq. 3.12[70] and was found to be 568.56 cm^2 at 50 Pa pressure differential for the baseline house. Second, this total effective leakage area (L) was equally distributed along the perimeter of the baseline building and assigned to the exterior walls in proportion to their surface areas. Third, the baseline house was modeled with these leakages in different shielding conditions with and without the code required mechanical ventilation system. The resulting infiltration rates were compared. The resulting air changes in these models were also compared with the total ventilation requirement of ASHRAE 62.2[171](see Eq. 3.13). The modeled cases and the resulting annual average infiltration rates of the baseline models are shown in Table 3.7.

$$L(\mathrm{cm}^2) = 10,000 \times Q_r \frac{\sqrt{\frac{\rho}{2\Delta P_r}}}{C_d} \tag{3.12}$$

The results showed that the shielding condition of a house is effective on the resulting infiltration rates. Considering that the total (infiltration + mechanical) ventilation

Table 3.7: The annual average air infiltration in the baseline building with 5 ACH50 air tightness in different shielding conditions with and without the code required mechanical ventilation system.

	Without Mechanical Ventilation (ach)	With Mechanical Ventilation (ach)
City	0.067	1.2×10^{-6}
Urban	0.137	4.8×10^{-3}
Suburbs	0.137	4.8×10^{-3}
Country	0.249	3.4×10^{-2}
Ocean	0.335	6.3×10^{-2}

requirement for the baseline house was 0.45 ACH as per ASHRAE 62.2[171] (see Eq. 3.13), it was concluded that the Bryan houses with 5 ACH50 air tightness will definitely require mechanical ventilation no matter what the shielding condition is.

$$Q = 0.03 \times CFA + 7.5(N_{br} + 1) \tag{3.13}$$

When the IECC 2012 required mechanical ventilation system was introduced into these models with a constant ventilation rate calculated with Eq. 3.11 (i.e. 39.9 cfm), they became positively pressurized and their infiltration rates decreased drastically (see Table 3.7). This finding showed that the item in the IECC 2012 that requires having both infiltration and ventilation at the same time in the house did not seem possible for the baseline model. Thus, the baseline model was prepared in the following three ways:

1) *NEG0.45ACH*: a leaky negatively pressurized house with an annual average infiltration rate equal to the total ventilation requirement of ASHRAE 62.2 (see Eq. 3.13).

2) *NEG0.30ACH*: a tight negatively pressurized house with an annual average infiltration rate equal to the mechanical ventilation requirement of ASHRAE 62.2 (see Eq. 3.11).

3) *POS0.30ACH*: a positively pressurized house with the mechanical ventilation rate required by ASHRAE 62.2. (see Eq. 3.11)

The *NEG0.45ACH* house met the total ventilation requirement of ASHRAE 62.2[171]

through infiltration only and represented the common infiltration condition of Texas houses more closely.[172] Various leakage components were modeled on the exterior building envelope of this baseline house with a total leakage area of 0.146 m^2 at 50Pa pressure differential in order to provide the required 0.45 ACH in the AirflowNetwork model of EnergyPlus.

The *NEG0.30ACH* house represented an air tight house which had an annual average air change equal to that would be provided through mechanical ventilation in a code compliant house (see Eq. 3.11). This model required a total surface leakage area of 0.0976 m^2 at 50 Pa pressure differential in the AirflowNetwork model which resulted in an annual average air changes of 0.3 ACH. This case provided the chance to compare the effectiveness of infiltration and ventilation in providing the outside air requirement of a residential building given the same annual average air changes.

The *POS0.30ACH* house represented the IECC 2012 compliant ventilation condition where all the outside air requirement of the house was provided through the mechanical system with a rate calculated using Eq. 3.11. This ventilation rate was 39.9 cfm (0.0188 m^3/s) and it resulted in a 0.3 ACH annual average infiltration in the house positively pressurizing the building. The leakages of this house were compliant with the IECC 2012 (i.e. 5ACH at 50 Pa pressure differential converted into L as per Eq. 3.12) which corresponded to 0.05686 m^2 total leakage area at 50 Pa pressure differential. As the house was positively pressurized, these leakages served mostly for exfiltration rather than infiltration.

All other openings (i.e. windows, doors, roof aperture) of these baseline houses were modeled in accordance with the IECC 2012 using the AirflowNetwork (AFN) model of EnergyPlus. The AFN model required modeling of the airflows through each opening of the house individually. In this modeling process, it was assumed that the baseline houses did not have natural ventilation through the windows or doors. Thus, the exterior openings of the house (i.e. doors and windows) were simulated in closed condition all year with the maximum air leakages allowed by IECC 2012.[34] The interior doors of the multizone baseline model, however, were set to be always open to allow air mixing between the zones as per IECC 2012.[34] The code required leakage rates were calculated and assigned to the window

frames, door frames, roof apertures and ceiling luminaires as follows.

The baseline houses had four types of windows and a single type of door. Table 3.8 lists the characteristics of these openings. Eq. 3.14 was the primary equation of the AFN model that calculated the airflows through these openings. The IECC 2012 requires windows and doors to have an air infiltration rate no more than 0.3 cfm per ft^2 of opening area (1.5 L/s per m^2 of opening area) when tested according to NFRC 400 or AAMA/WDMA/CSA 101/I.S.2/A440. Both the NFRC 400 and the AAMA/WDMA/CSA 101/I.S.2/A440 standards measure this maximum allowable air leakage rate at 75 Pa pressure differential. Table 3.8 shows the corresponding maximum allowed volume flow rate of air leakage ($\dot{v}_{max}$) for each opening type. Assuming 1.204 kg/m^3 for the air density, the maximum allowed mass flow rate ($\dot{m}_{max}$) of air leakage for these openings was also calculated and presented in Table 3.8. Entering these $\dot{m}_{max}$ values, the 75 Pa reference pressure differential (ΔP) and the perimeter length (P) of each opening into Eq. 3.14, the air mass coefficient (C) of each opening was calculated. The resulting C values are listed in Table 3.8. These C values were entered into the EnergyPlus AFN model by creating a "SimpleOpening" object for each opening type. In the AFN model, the "Discharge Coefficient" was assumed to be 0.55 and the "Air Mass Flow Exponent (n)" was set to be 0.65.

Table 3.8: The features of the openings on the building envelope of the Bryan Habitat for Humanity house.

Opening Type	P(m)	A (m^2)	$\dot{v}_{max}$ (m^3/s)	$\dot{m}^*_{max}(\frac{kg}{s})$	C ($\frac{kg}{s.m}$)
Window	4.86	1.38	2.11×10^{-3}	2.54×10^{-3}	3.16×10^{-5}
Window	3.04	0.56	8.44×10^{-4}	1.02×10^{-3}	2.03×10^{-5}
Window	3.64	0.83	1.26×10^{-3}	1.52×10^{-3}	2.52×10^{-5}
Window	6.70	2.78	4.24×10^{-3}	5.10×10^{-3}	4.60×10^{-5}
Door	6.04	1.90	2.89×10^{-3}	3.48×10^{-3}	3.48×10^{-5}

* Density of air is assumed to be 1.204 m^3/s.

$$\dot{m} = C \times P \times (\triangle P)^n \tag{3.14}$$

The IECC 2012 requires the roof aperture to be 1 ft^2 per 300 ft^2 ceiling area. For the baseline houses, this corresponded to a 3,388 cm^2 roof aperture. Assuming a square shaped aperture, an opening with the dimensions of 0.582m $\times$ 0.582m was modeled on the roof and defined as a door which was always open. For the modeling of the air leakages through the luminaries on the ceilings, the "Surface:EffectiveLeakageArea" class of the AFN model was used. Since all the electric lights in the house were suspended fluorescent lights, no leakage actually occurred at these points. A very low "Effective Leakage Area" value higher than zero (1×10^{-18}) was, however, assigned to the ceilings in order to connect the infiltration calculations of the rooms to those of the attic while assuming minimal ceiling leakages.

The baseline houses had three exhaust fans: 1) one in the main bathroom, 2) one in the bathroom of the master bedroom, and 3) one in the kitchen above the cooktop unit as per ASHRAE 62.2.[171] These fans operated intermittently and were connected to the electric light switches of the areas they were serving. Thus, the lighting schedules also became the availability schedules of the exhaust fans in these areas. The maximum airflow rates of these fans were set to be 100 cfm for the kitchen, and 50 cfm for the bathroom in accordance with ASHRAE 62.2.[171] The WC of the master bedroom was then assigned a 24 cfm exhaust fan rate using Eq. 3.15.[173] For the modeling of these fans in EnergyPlus, additional surfaces with very low thermal resistance (0.001 m^2.K/W) and thermal absorptance (0.001) were simulated on the roof. These surfaces were assigned to the zones that require these fans and were defined as the surfaces that these exhaust fans were attached to under the "AirflowNetwork:Multizone:Surface" object of EnergyPlus.

$$\dot{v} = CFA \times 1.07 \tag{3.15}$$

3.2.4 Modeling of the HVAC System

The HVAC system of the baseline house was a split system that included a blow-through supply air fan, direct expansion air conditioner, a gas furnace and an evaporator coil. As the baseline house was modeled as a multizone building, the furnace was configured to serve multiple zones but the system operation was controlled by a thermostat located in the corridor section of the living area. The system was sized to keep the temperature of this control zone between the 22°C (72°F) heating and 24°C (75°F) cooling set points all year as per IECC 2012.[34] In this configuration, one of the key parameters for the furnace component was the fraction of the total system airflow that went through the control zone. This fraction was calculated to be the ratio of the maximum mass flow rate ($\dot{m}_{max}$) supplied to the control zone to the $\dot{m}_{max}$ of the whole system. "The furnace module of EnergyPlus scaled the calculated load for the control zone upward based on this fraction to determine the total load to be met by the furnace. The module then proceeded to calculate the required part-load ratio for the system coil and the supply air fan to meet this total load."[103]

Building America House Simulation Protocols require a 13 SEER air conditioner for the residential benchmark for a split system central air conditioner.[35] This corresponded to 11.18 EER as per Eq. 3.16[174] and to a COP value of 3.23 as per Eq. 3.17.[35] The COP value of 3.23 was entered into EnergyPlus for the cooling coil of the baseline house. For the burner efficiency of the gas furnace, the steady state efficiency of 80% was assumed in this model. The resulting cooling and heating capacities and the system airflow rates calculated for the ground isolated multizone baseline house for the three outdoor air exchange conditions are given in Table 3.9.

$$EER = -0.02 \times SEER^2 + 1.12 \times SEER \tag{3.16}$$

$$COP = \frac{EER}{3.412} \tag{3.17}$$

Table 3.9: The sizes of the heating/cooling coils and the maximum system airflow rate of the ground isolated baseline house models as determined by EnergyPlus.

	Cooling System	Heating System	$\dot{v}_{max}$
NEG0.45ACH	5,942 W (1.7 tons)	4,624 W (15,778 Btu/hr)	0.308 m^3/s (651 cfm)
NEG0.30ACH	4,711 W (1.3 tons)	3,525 W (12,028 Btu/hr)	0.251 m^3/s (531 cfm)
POS0.30ACH	3,979 W (1.1 tons)	2,904 W (9,909 Btu/hr)	0.197 m^3/s (417 cfm)

The duct layout of the negatively pressurized baseline houses is shown in Fig. 3.14 as an example. This duct layout was designed based on the descriptions of the EPA[175,176] for standard air distribution systems in unconditioned spaces. In this duct layout, the main supply/return ducts were connected to the air handling unit. The zone branches which supplied air to the rooms or returned air from the zones were connected to these main ducts. The air handling system of the baseline house was assumed to be located in the attic based on the information provided in Kim's[47] Ph.D. dissertation on Bryan Habitat for Humanity houses. Thus, the air ducts of the baseline house were exposed to the air temperature of the attic space. The IECC 2012 requires all ducts in the attic to be insulated to a minimum of R-8 (8 hr.ft^2.°F/Btu, 1.4098 m^2-K/W). In EnergyPlus, air ducts were assumed to have an outside film coefficient of 5 W/m^2-K and an inside film coefficient of 25 W/m^2-K. Subtracting the thermal resistances of these air films from the required heat resistance of the air ducts, the U-value of the air ducts was calculated to be 0.606428 W/m^2-K.

The air distribution system of the baseline house was modeled with the AiflowNetwork:Distribution model of EnergyPlus. The AiflowNetwork:Distribution model of the duct layout shown in Fig. 3.14 is shown in Fig. 3.15. Note that, in this figure, the outdoor air system (OA) is shown with dotted lines as it was used only for the *POS0.30ACH* case of the baseline house.

The AiflowNetwork:Distribution model is attached to the AirloopHVAC model and interacts with it to simulate: 1) the airflow through the air ducts, 2) the heat flows across the air ducts, and 3) the resulting variations on the zone air temperatures and interzonal

Figure 3.14: The air duct layout of the negatively pressurized, multizone baseline Habitat for Humanity house.

airflows. The AirflowNetwork:Distribution model has a very similar nodal structure to that of the AirloopHVAC model. Fig. 3.15 shows the nodal structures of both models for the baseline house. Table 3.10 presents concise descriptions for the nodes in the AirloopHVAC model of the baseline house. The AirloopHVAC nodes are categorized in two groups, i.e. the supply side nodes and the demand side nodes. The supply side nodes include the nodes used for the modeling of the air handling unit including the outdoor air system. This part of the system is also called the "main air loop side." The demand side nodes include the nodes used to model the equipment that delivers air to the zones, collects it and returns it back to the air handling unit. This part of the system is also called the "equipment side" of the system.

Table 3.10: The supply and demand side nodes of the AirloopHVAC model of EnergyPlus for the baseline house.

Supply Side Nodes		Demand Side Nodes	
Node # in Fig. 3.15	Description	Node # in Fig. 3.15	Description
26	Supply Side Inlet Node	1	Demand Side Inlet Node
28	Outside Air Inlet Node	8-14	Zone Air Inlet Nodes
29	Relief Air Outlet Node	15-21	Zone Air Nodes
30	Supply Fan Inlet Node	22x	Zone Air Outlet Nodes
31	Heating Coil Air Inlet Node	25	Demand Side Outlet Node
32	Cooling Coil Air Inlet Node		
33	Supply Side Outlet Node		

As shown in Fig. 3.15, the AirflowNetwork:Distribution model included all air nodes of the AirloopHVAC model listed in Table 3.10 and required additional nodes. These additional nodes in the AirflowNetwork:Distribution model included the zone splitter node

(node 2 in Fig. 3.15), the zone mixer node (node 23 in Fig. 3.15, the connection points of the branch ducts to the main ducts (nodes 3, 4, 5, 6 and 7 in Fig. 3.15), the leakage points which were not AirloopHVAC nodes (node 24 in Fig. 3.15) and the outdoor air system node (node 27 in Fig. 3.15).

Every line between two nodes in Fig. 3.15 represented an air duct of the baseline house. The supply and return diffusers of the house were also modeled as separate air ducts in the AirflowNetwork:Distribution model of EnergyPlus. The 10-17, 11-18, 12-19, 13-20, 14-21, 8-15, and 9-16 ducts shown in Fig. 3.15 were the zone supply diffusers. The 15-22, 16-22, 17-22, 18-22, 19-22, 20-22 and 21-22 ducts in the same figure were the zone return diffusers. The modeling order of the air ducts shown in Fig. 3.15 was important in order to avoid errors in the EnergyPlus runs. There were two primary rules that were followed in order to ensure a correct order in the modeling of these ducts. First, the direction of the airflow was followed in the listing of the ducts. Second, the listing of the parallel branches of the same type were completed before proceeding further in the air loop. For instance, 1-2, 2-3, 2-4, 3-8, 3-9, 4-14, 4-5... etc. was how the listing of these ducts started in EnergyPlus.

EnergyPlus AirflowNetwork: Distribution model had limitations that restricted the modeling of the original duct layout of the multizone baseline house as is. For instance, a single return duct (which is typical for a residential system) was not allowed in the AirflowNetwork:Distribution model. One return duct was required for each zone of the house in order to run the EnergyPlus simulation without an error. Thus, the actual zone return duct of the system (22-23 duct in Fig. 3.15) was converted into seven equivalent return ducts (the 22CR-LR-23, 22KT-DR-23, 22BR1-23, 22BR2-23, 22MBR-23, 22UTR-23 and the 22MBT-23 ducts in Fig. 3.15) by keeping the pressure loss identical to that of the original duct. This adjustment was achieved by taking the duct pressure loss equation of EnergyPlus (see Eq. 3.18) as the basis. First, the hydraulic diameter (D_h) of the original return duct was assigned to all of the seven equivalent ducts. Second, The cross-section area of the original duct was divided between the equivalent ducts in proportion to their mass flow rates. This resulted in the same pressure loss in all of the seven equivalent ducts

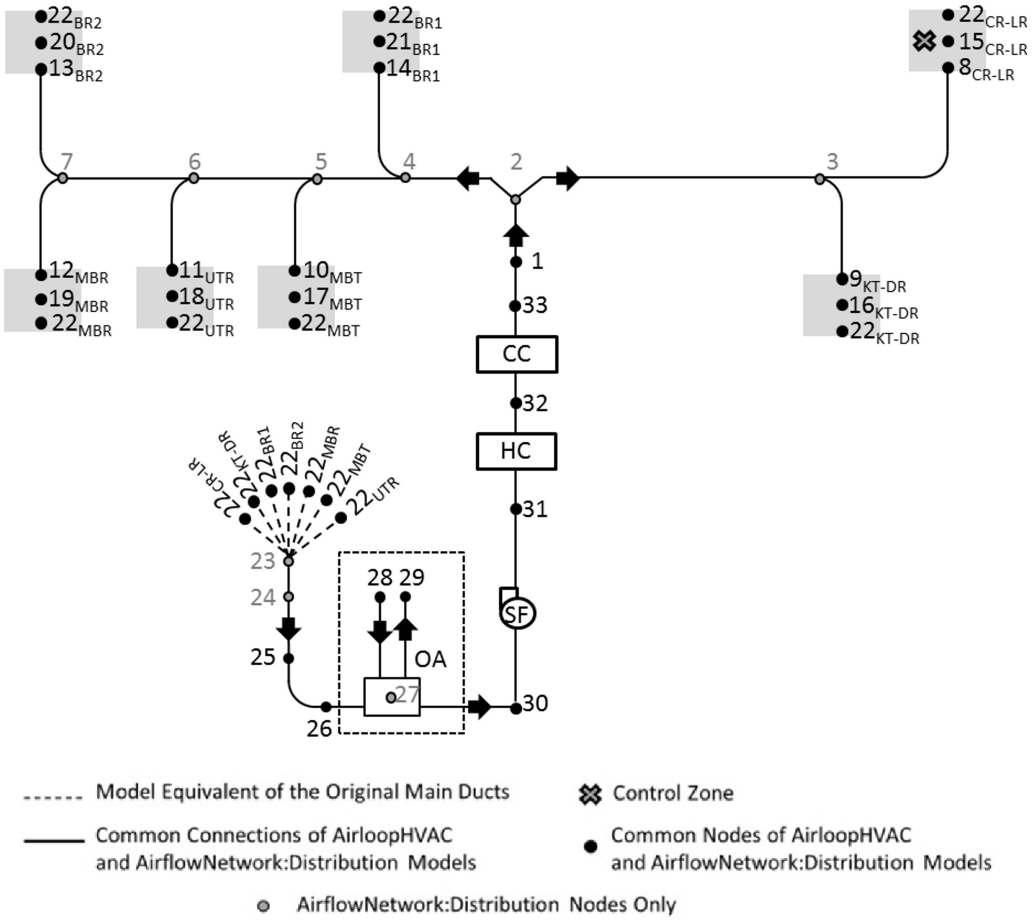

Figure 3.15: The duct layout of the multizone baseline building as modeled in the AirflowNetwork:Distribution model. CR-LR: Corridor and living room, KT-DR: Kitchen and dining room, BR1: Bedroom 1, BR2: Bedroom 2, MBR: Master bedroom, MBT: Main bathroom, UTR: Utility room, SF: Supply fan, HC: Heating coil, CC: Cooling coil, OA: Outdoor air system.

which was also identical to that in the original return duct. EnergyPlus calculated the duct surface area (SA_{duct}) using Eq. 3.19. As the D_h value of the equivalent ducts was equal to that of the original duct, this resulted in 7 times larger duct surface area in the adjusted duct layout when compared to that in the original layout. In order to correct this problem, the conduction heat transfer coefficient of the original return duct (0.606428 W/m^2-K) was divided by 7 and assigned as the U-value of the equivalent ducts.

$$\Delta P = \frac{\dot{m}^2(\frac{fL_d}{D_h} + \sum C_d)}{2\rho {A_d}^2} \tag{3.18}$$

$$SA_{duct} = D_h \times L_d \tag{3.19}$$

The air distribution system of the baseline house was sized using the equal friction method.[177] The basic idea of this method was to use the same friction rate for the sizing of all of the air ducts in the system. For this process, the design friction rate (h) was assumed to be 0.12 in.wg./100 ft (0.98 Pa/m).[177] Trial iterations between EnergyPlus and the TRNSYS Type 1255 slab-on-grade heat transfer model showed that ground coupling causes a different variation on the supply airflow rate of each zone. The maximum airflow rates occurred in the cooling season and the cooling energy use was found to differ less than 1% after the second EnergyPlus run in the EnergyPlus-TRNSYS iterations (see Fig. 3.16). The variations of the zone airflow rates of the second EnergyPlus run from those of the first run (i.e. the ground isolated condition) are shown in Table 3.11 for all baseline models. Using these percentage variations, the zone airflow rates calculated for the ground isolated models were modified. Based on these modified zone airflow rates, the air ducts of the system were sized.

The friction chart of ASHRAE[70] was used for the sizing of the ducts. On this chart, the intersection point of the 0.12 in.wg./100ft (0.98 Pa/m) friction loss line and the maximum airflow rate ($\dot{v}_{max}$) determined for each zone by EnergyPlus indicated the initial duct size. If this duct size corresponded to an air velocity higher than the maximum allowed velocities

Table 3.11: The variations observed in zone design airflow rates between the first and the second EnergyPlus runs of the EnergyPlus-TRNSYS ground coupling iterations.

Zone	NEG0.45ACH (%)	NEG0.30ACH (%)	POS0.30ACH (%)
KT-DR	-24	-26	-32
CR-LR	-10	-15	-17
MBT	-31	-31	-35
BR1	-7	+24	-24
BR2	-3	-4	-5
MBR	+11	+15	+1
UTR	-5	-6	-14

listed in Table 3.12, then the intersection point of the maximum allowed air velocity and the $\dot{v}_{max}$ value was accepted to be the final size of the duct.

Table 3.12: The air velocities recommended for different parts of a residential air system.[177,178]

	Velocity- fpm (m/s)			
	Supply Side		Return Side	
Duct Type	Recommended	Maximum	Recommended	Maximum
Main Ducts	700 (3.6)	900 (4.6)	600 (3)	700 (3.6)
Branch Ducts	600 (3)	900 (4.6)	400 (2)	600 (3)
Supply Outlet Face	Size for throw	700 (3.6)	-	-
Return Grille Face	-	-	-	500 (2.5)
Branch Risers	-	-	-	-

The friction chart of ASHRAE[70] was valid for standard air flowing through round galvanized ducts with beaded slip couplings on 1220 mm centers, which is equivalent to an absolute roughness of 0.09 mm. According to ASHRAE,[70] no corrections to this chart were needed for duct materials with a medium smooth roughness factor. Thus, all ducts

of the system were sized as round galvanized ducts and were assumed to have a roughness factor of 0.09 mm in this study. The main ducts of the baseline house were assumed to be rectangular and the zone branches were round galvanized ducts. The rectangular main ducts were first sized as round galvanized ducts using the friction chart of ASHRAE.[70] Then, the sides of their rectangular equivalents were determined using Huebscher's[179] equation given in Eq. 3.20.

$$D_e = \frac{1.30 \times (ab)^{0.625}}{(a+b)^{0.250}} \tag{3.20}$$

The IECC 2012 allowed for a total duct leakage of 4 cfm (113.3 L/min) per 100 ft^2 (9.29 m^2) of conditioned floor area when tested at a pressure differential of 0.1 in. w.g. (25 Pa) across the entire system. For the 994 ft^2 (92.36 m^2) baseline house, this corresponded to a total duct leakage of 0.110389 m^3/s. According to Hendron,[35] the supply duct leakage in residential buildings is approximately 9 times of the return duct leakage. Using these ratios, the supply and return leakages of the system were calculated to be 0.09935 m^3/s and 0.011039 m^3/s respectively both at 25 Pa pressure differential. EnergyPlus allowed for the modeling of only the equipment side duct leakages. In this study, for simplicity, it was assumed that all supply ducts on the equipment side had an equal amount of air leakage. These leakages occurred at 9 air nodes. Seven of these nodes were at the points right after the supply branches made a 90° turn with an elbow towards the zone supply diffusers (nodes 8, 9, 10, 11, 12, 13 and 14 in Fig. 3.15). The last supply leakage point was at the zone air splitter (node 2 in Fig. 3.15) and the only return leakage point was at around halfway through the main return duct (node 24 in Fig. 3.15).

The supply fan of the system was sized to provide sufficient pressure rise (P_{furn}) that could overcome the sum of the pressure losses caused by: 1) the air ducts (P_{ducts}), and 2) the air handling unit (P_{sys})(see Eq. 3.21).

$$P_{furn} = P_{ducts} + P_{sys} \tag{3.21}$$

The calculation of the pressure loss across the air ducts (P_{ducts}) required the calculation of the TEL value of the system. The TEL value was an equivalent duct length that corresponded to the total pressure loss caused by the ducts and fittings of the air distribution system. For calculation of this TEL value, first, the actual duct lengths (L_{actual}) were determined for each zone through a detailed duct design. Then, virtual lengths ($L_{fitting}$) were added to these actual lengths for each zone in order to represent the pressure losses through the fittings (see Eq. 3.22 and Eq. 3.23). Finally, the TEL values of each zone were compared to each other. The maximum was selected and accepted as the TEL value of the system. Entering this maximum TEL value into Eq. 3.24[178] then provided the maximum pressure loss of the air ducts (P_{ducts}).

$$TEL = L_{actual} + L_{fitting} \tag{3.22}$$

$$L_{fitting} = \frac{D_h \times C_d}{f} \tag{3.23}$$

$$P_{ducts} = \frac{h \times TEL}{100} \tag{3.24}$$

The total pressure loss through the air handling unit (P_{sys}) included the pressure losses through the evaporative coil and the air filter. Stein[177] listed a set of typical pressure loss values for these system components. The average of these values (0.25 in. w.g. for the evaporative coil, 0.15 in. w.g. for the filter) were selected for each component and added to each other. This calculation resulted in a total system pressure loss (P_{sys}) of 0.4 in. w.g. (99.6 Pa). The sum of the P_{sys} and P_{ducts} values then resulted in a total P_{furn} value of 0.7 in. w.g. (169 Pa) as per Eq. 3.21. The 169 Pa P_{furn} value was entered into the EnergyPlus model of the baseline house.

3.2.5 Modeling of the Slab-on-Grade Heat Transfer

In Section 3.1, the slab-on-grade heat transfer model of EnergyPlus (i.e. Slab) was found to have convergence problems besides being limited to modeling of single zone buildings. Thus, in this part of the study, one of the TRNSYS ground heat transfer models (i.e. Type 1255) was used coupled with EnergyPlus for the modeling of the ground heat transfer in the multizone baseline house (see Section 2.8.1.3). Fig. 3.16 shows the schematic representation of this coupled model. The modeling process started with an initial EnergyPlus run with an adiabatic floor. The zone air temperatures (T_{zair}) and the floor inside surface convection coefficient values (h_{fi}) obtained from this run were then entered into the TRNSYS Type 1255 model. The Type 1255 model used these values to calculate the inside surface temperatures (T_{fi}) of each floor surface in the multizone baseline house. These temperatures were then entered into the EnergyPlus model as the outside surface temperatures of the floor using the "SurfaceProperty:OtherSideCoefficients." This iterative process continued until a convergence of 1% was achieved between two successive EnergyPlus runs for the cooling, heating and fan energy consumption outputs.

In the TRNSYS Type 1255 model, the floor construction was modeled as $4''$ concrete (CC) with beams which are $14''$ wide at $12'$ intervals with vinyl tile (AR†) (see Table 3.3). The materials used in this floor construction are given in Table 3.2. The properties of the soil (SL) modeled in Type 1255 are also given in Table 3.2. The heat transfer/storage through the floor construction was already taken into account in the Type 1255 simulations. In order to avoid the repetition of this factor in the aboveground energy calculations, the floor was simulated as a low resistance (0.001 m^2.K/W) and massless construction in the EnergyPlus model.

The Type 1255 model was a multizone model that relied on a three dimensional representation of the soil (see Sec. 2.8.1.3). In this model, the nodes at the surface conducted to a "local surface temperature" that was calculated on a massless, opaque plane located between the air and the soil node. In this study, this "local surface temperature" was calculated with an energy balance. The node temperatures of the far-field were also calculated

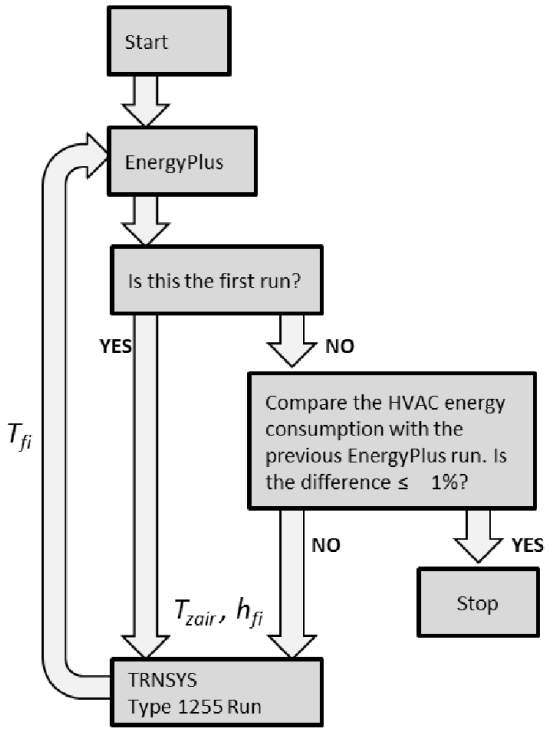

Figure 3.16: The schematic diagram of the coupled EnergyPlus-TRNSYS model. T_{zair}= Zone air temperatures [°C], h_{fi}= Interior convection coefficient of the floor [kJ/hr.m^2.K], T_{fi}= Inside surface temperature of the floor [°C]

by an energy balance.

The TRNSYS slab-on-grade model was a finite difference model; therefore, the initial temperatures of the various soil nodes made a significant difference on the calculated heat transfer. For this reason, it was necessary to run the model for multiple years until the ground temperature profiles of the last two years were within an acceptable convergence tolerance. The IEA Task work[32] showed that, in TRNSYS runs, less than 0.2% change occurs after 5 years. Thus, for each TRNSYS run shown in Fig. 3.16, TRNSYS was actually run 5 times to ensure internal convergence.

The node sizes of the Type 1255 model for the horizontal and vertical directions have been determined through a set of initial test runs. Finally, the smallest node size along the perimeter of the slab was set to 0.1 m. The distance between the nodes was multiplied by a factor of 2 as the nodes expanded away from the slab perimeter. The boundary between the

near-field and the far-field was defined as "conductive" in all x, y and z axes. In TRNSYS, the deep ground temperature is assumed to be very close to the yearly average outside air temperature. Thus, the yearly average outside air temperature for Bryan was calculated (19.65°C) and entered into the Type 1255 model as the deep earth temperature of the site. In TRNSYS, the amplitude of the annual surface temperature profile of the soil is also assumed to be equal to half of the maximum monthly average outside air temperature minus one half of the minimum monthly average outside air temperature. This value was calculated to be 21.35°C for Bryan, Texas and entered into the Type 1255 model. The soil temperature was assumed to be unaffected by the building at a distance of 15 m beneath from the bottom of the footer in the vertical direction and 15 m from the edge of the building in the horizontal direction.

3.3 Modeling of the Partially Conditioned Atrium House

In this section, a new HVAC design strategy i.e. partial conditioning is introduced into the multizone Bryan Habitat for Humanity (HFH) house simulated in Section 3.2 in order to improve its energy performance. This strategy is simulated step by step by producing the following models:

Case 1: The baseline atrium house - In this case, an unconditioned atrium was added to the baseline Habitat for Humanity house to convert it into an atrium house.

Case 2: Atrium as the return plenum - In this case, the air returning from the conditioned zones were sent into the atrium before it returned to the system.

Case 3: The atrium house with occupancy-based heating and cooling - In this case, the occupied zones of the Case 2 house were conditioned leaving the unoccupied zones unconditioned. As the occupied zones change during the day, this resulted in two separate duct layouts and the system switched between them depending on the hour of the day. These duct layouts were designed 1) to supply air to the occupied living area and return it back to the system, and 2) to supply air to the occupied bedrooms and return it back to the system.

Case 4: The atrium house with multiple reuse of air - In this case, the conditioned air

was sent to the occupied zones and then was rerouted to the unoccupied zones. This case also resulted in two duct layouts and the system switched between them depending on the hour of the day. These duct layouts were designed 1) to supply air to the occupied living area, reroute it into the bedrooms, move it into the atrium and return it to the system, and 2) to supply air to the occupied bedrooms, reroute it into the unoccupied living area, move it into the atrium and return it to the system.

These cases were modeled isolated from the ground and compared with each other to identify the individual effects of each step of the partial conditioning strategy. The final case (i.e. Case 4) was then coupled with the ground with a slab-on-grade floor and its results were compared with those of the slab-on-grade baseline Habitat for Humanity houses modeled in Section 3.2 in order to quantify the overall energy savings obtained with this strategy.

3.3.1 The Design and Modeling of the Baseline Atrium Houses (Case 1)

At the first step of this study, two primary facts were considered in order to improve the energy performance of the baseline Habitat for Humanity house. The first fact was that transitional areas of a house such as corridors, hallways and entrance areas are occupied for a very short time during the day; therefore, they do not require heating/cooling as much as the primary spaces (living rooms, bedrooms and kitchen) do.[35] The second fact was that using courtyards and atriums in residential buildings provides an obvious U-factor improvement in hot-humid climates while providing adequate amount of daylight.[52,57,68,72] Saxon[84] stated that the energy economy of buffer spaces such as atriums is fully achieved only if no attempt is made to keep these spaces themselves comfortable all year round. The buffer spaces are lightly constructed and are colder in winter and hotter in summer when compared to the conditioned spaces they protect. The occupants in the buffer zones, therefore, need to dress seasonably appropriate.[84] Following these facts and suggestions, the initially dark corridor space and the utility room of the baseline HFH house were converted into an unconditioned central atrium as shown in Fig. 3.17 and Fig. 3.18 in order to improve the thermal and the daylighting performance of the house. This central atrium space was

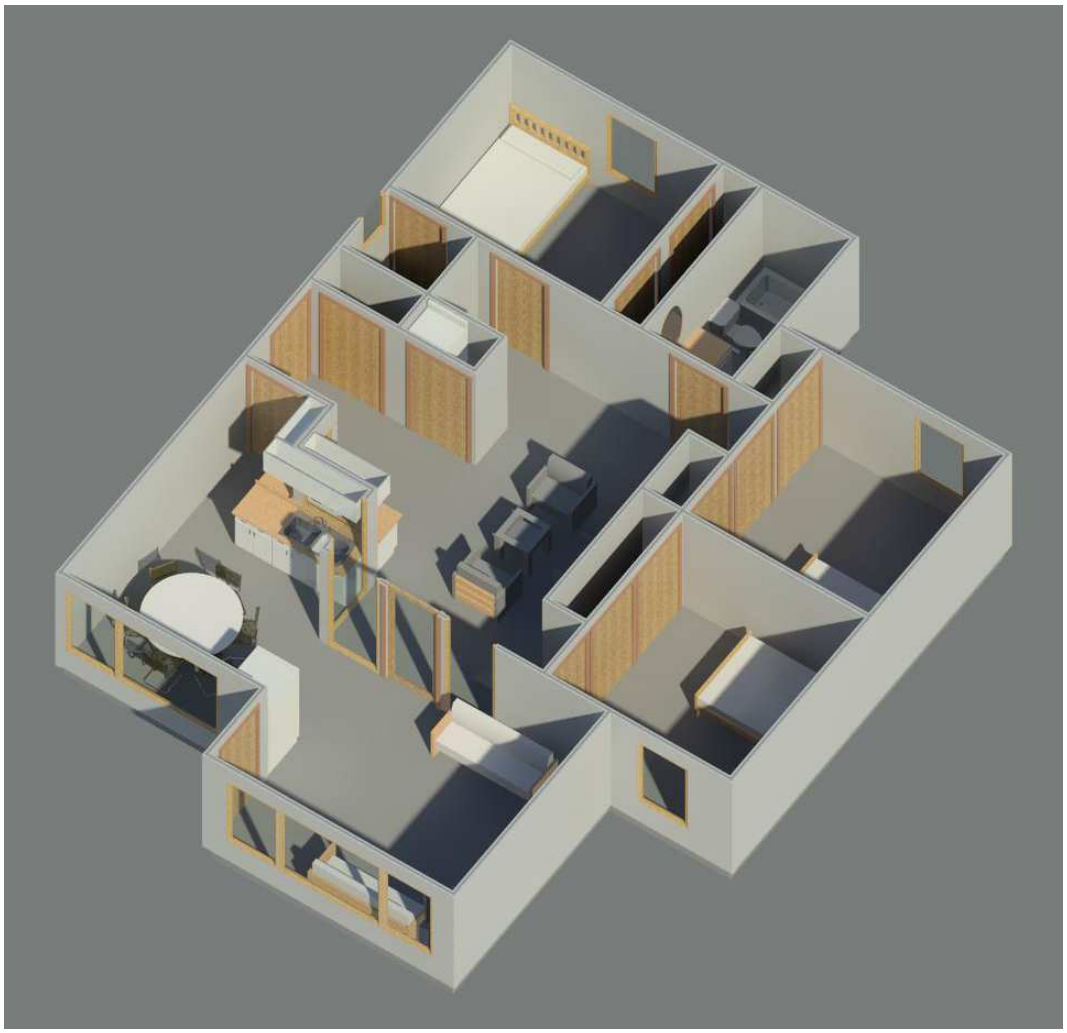

Figure 3.17: The 3D Revit drawing of the baseline atrium house.

modeled as an unconditioned zone which was ventilated via the infiltration through the clerestory windows. Fig. 3.19 shows an interior perspective view of this unconditioned central atrium space and Fig. 3.20 shows the resulting EnergyPlus model.

The total conditioned area of this final atrium house was 809 ft^2 (75 m^2) and the atrium was 280 ft^2 (26 m^2) resulting in a total floor area of 1,089 ft^2 (101 m^2). Each room of this house was modeled as a thermal zone in EnergyPlus resulting in 7 zones, i.e. LR: Living room (17.22 m^2), KT-DR: Kitchen and dining room (12.22 m^2), BR1: Bedroom 1 (12.97 m^2), BR2: Bedroom 2 (12.9 m^2), MBR: Master bedroom (15.08 m^2), MBT: Main

Figure 3.18: The 3D Cross section of the baseline atrium house.

bathroom (4.77 m^2), and ATR: atrium (26.03 m^2) (see Fig. 3.21).

The building envelope of the atrium house was identical to that of the baseline HFH house modeled in Section 3.2 (see Table 3.3 and Table 3.2). The walls between the conditioned rooms and the atrium were modeled with the "Interior Wall" construction shown in Table 3.3 by filling the wall frame with cellulose insulation (IN$^\sharp$). The windows and doors on these walls were modeled to be always closed with the IECC 2012 required fenestration leakages. The windows (both the interior and exterior) were all the same type and were as described in Table 3.3. Modifications were done on the orientation of the windows by removing the east and west facing windows and locating them on the north and south facades. The energy code (IECC 2012) is unclear about the window-to-wall ratio for the exterior windows of unconditioned atriums and for windows facing the unconditioned atriums. Thus, windows were designed freed from the window to floor area limitations of the code in this study to maximize daylighting in the house.

Exterior shades were designed for the clerestory windows of the atrium space using the

Figure 3.19: The perspective view from the inside of the baseline atrium house.

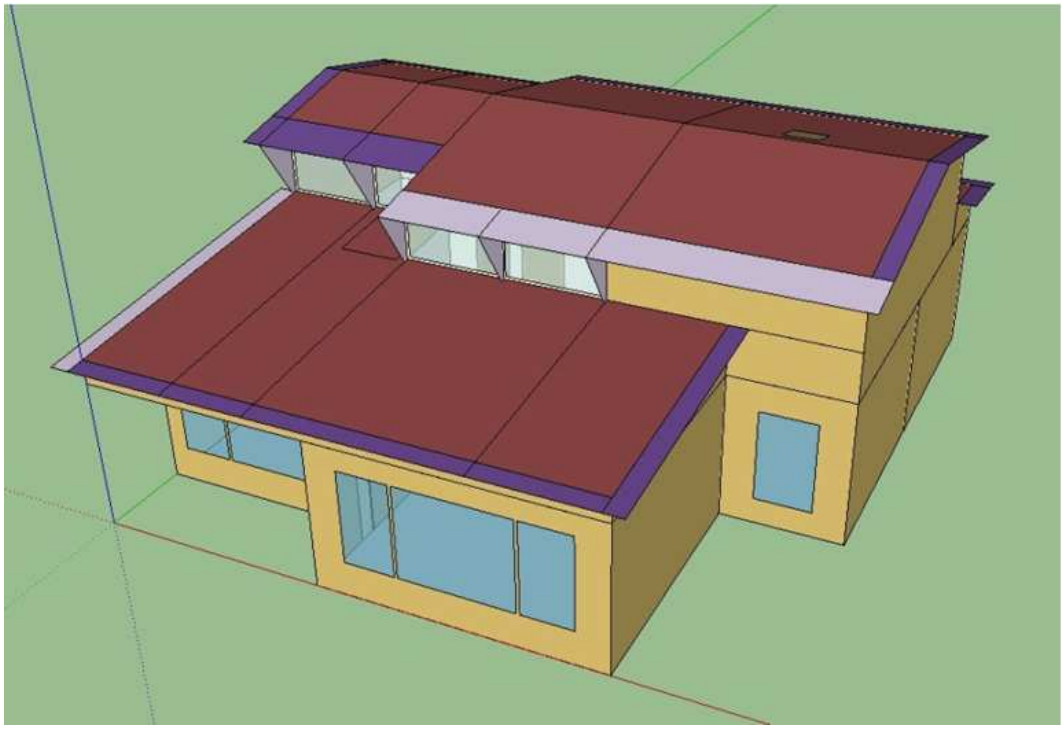

Figure 3.20: The EnergyPlus model of the atrium house.

Solar tool of Ecotect Analysis programs. These shades blocked the direct sun throughout the whole summer on the north facade. Fig. 3.22 shows the stereographic diagram obtained from the Solar tool for the north facade when the depths of the horizontal and vertical shades were assumed to be equal all around the window. The north facing windows of the atrium required a 0.35 m horizontal shade above the window (see points b and c in Fig. 3.22) and 1 m vertical shade at the bottom level of the windows (see points a and d in Fig. 3.22). In order to minimize the reduction in daylight levels while providing sufficient sun blockage, the points a, b, c and d in Fig. 3.22 were connected and the shapes of the exterior shades of the north facing clerestory windows were determined. These resulting shades are shown in Fig. 3.23 as they appear in Ecotect.

The south facing clerestory windows of the atrium were also assigned exterior shades. These shades were designed to block the direct sun between mid March (15^{th}) and late September (26^{th}). During the remainder of the year, direct sun was allowed into the atrium in order to heat the atrium space and to reduce the heat losses from the surrounding zones.

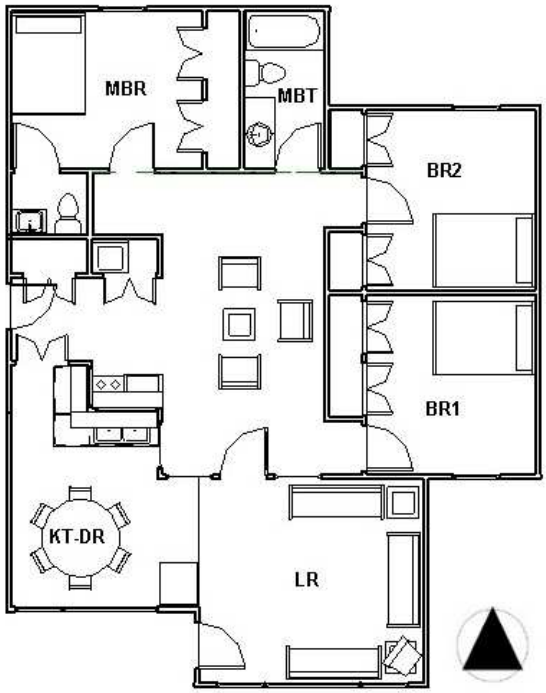

Figure 3.21: The zones of the baseline atrium house. BR1: Bedroom 1, BR2: Bedroom 2, MBR: Master bedroom, ATR: Atrium, MBT: Main bathroom, KT-DR: Kitchen and dining room, LR: Living room.

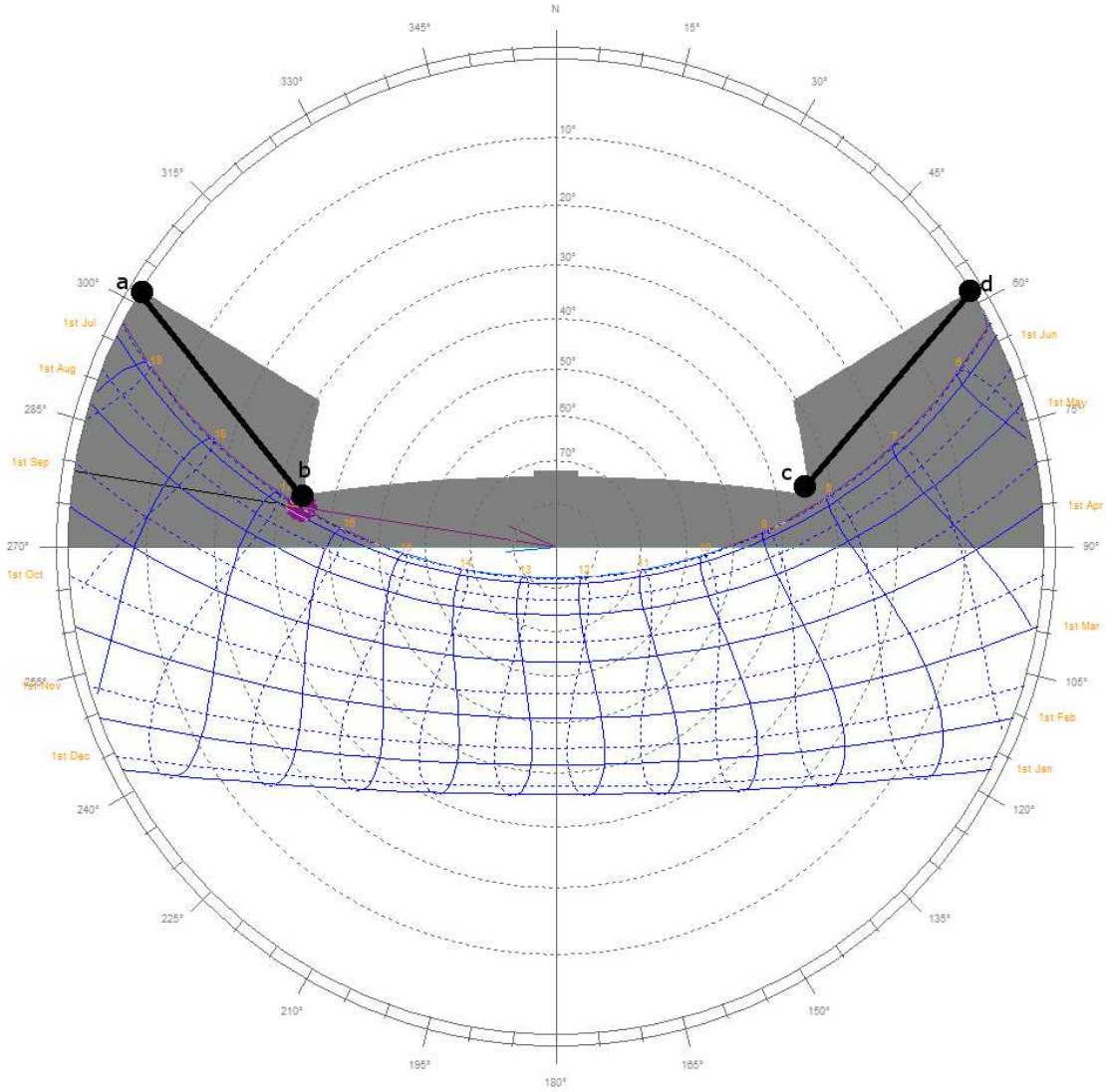

Figure 3.22: The stereographic diagram for the shades of the north facing clerestory windows.

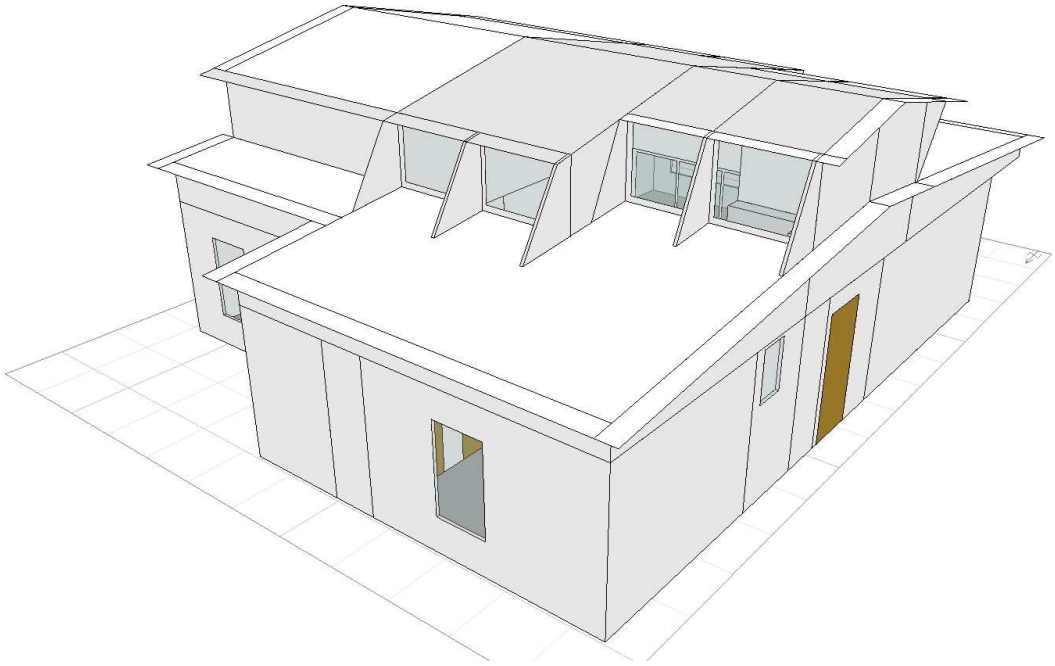

Figure 3.23: The shading design of the north facing clerestory windows.

This configuration also improved the daylighting performance of the house by providing reflected daylight into the atrium during the very hot summer days of Bryan, Texas. The south facing clerestory windows required 0.85 m horizontal shade above the window (see points b and c in Fig. 3.24) and 0.1 m vertical shade at the bottom level of the windows (see points a and d in Fig. 3.24). When the points a, b, c and d were connected, the exterior shades shown in Fig. 3.25 were obtained.

The number and type of home equipment in the atrium house were identical to those in the baseline house, but the locations of some of these items were modified in order to reduce the cooling load of the building. For instance, the oven, the cooktop unit, the washer and the dryer were moved into the atrium in order to avoid the heat generated by this equipment during the warm days. This equipment also heated up the unconditioned atrium during the cold days of winter reducing the heat loss from the surrounding zones to the atrium. The miscellaneous electric loads of the utility room of the baseline house were also assigned to the atrium. The resulting average hourly heat energy generated by

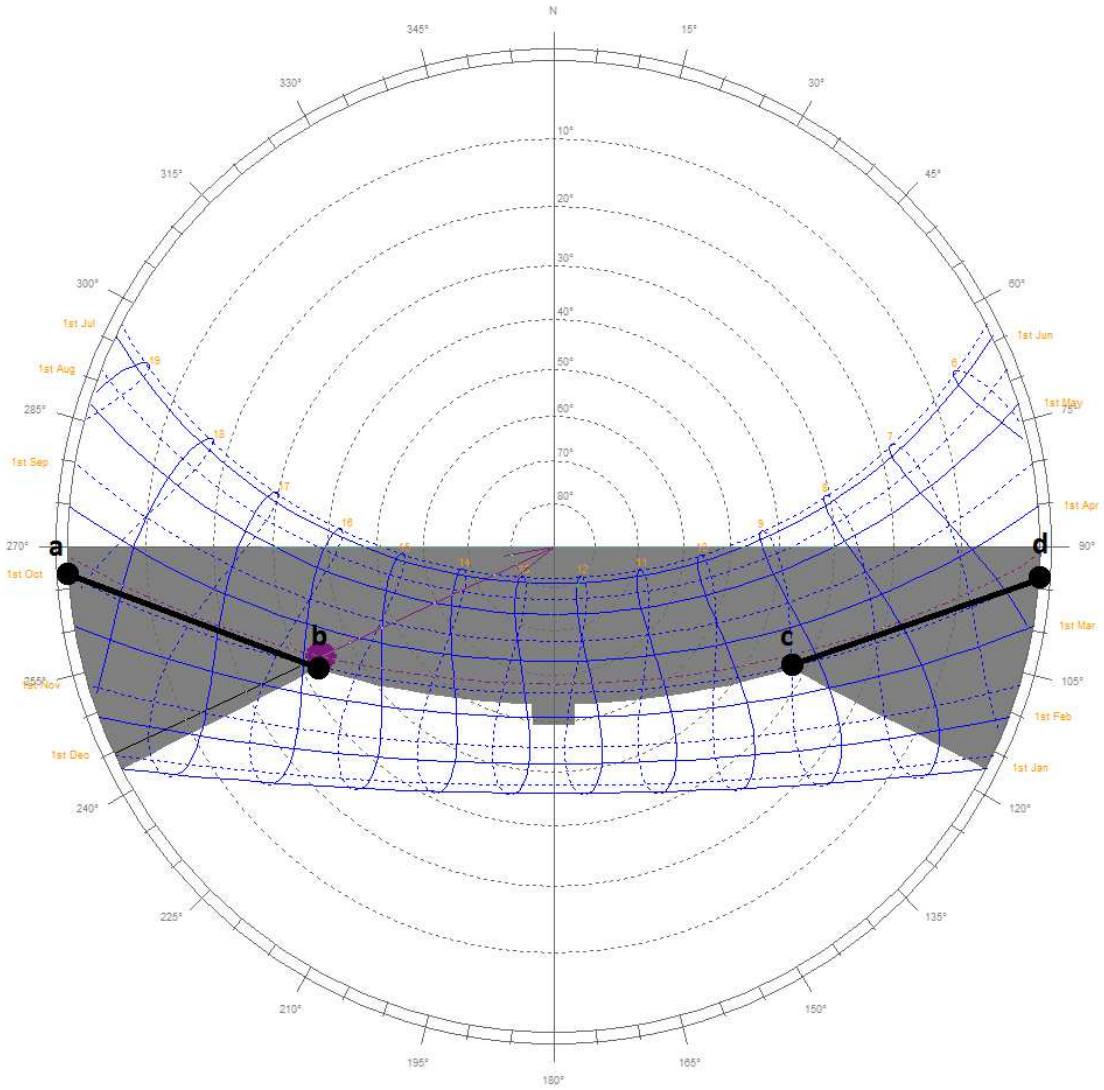

Figure 3.24: The stereographic diagram for the shades of the south facing clerestory windows.

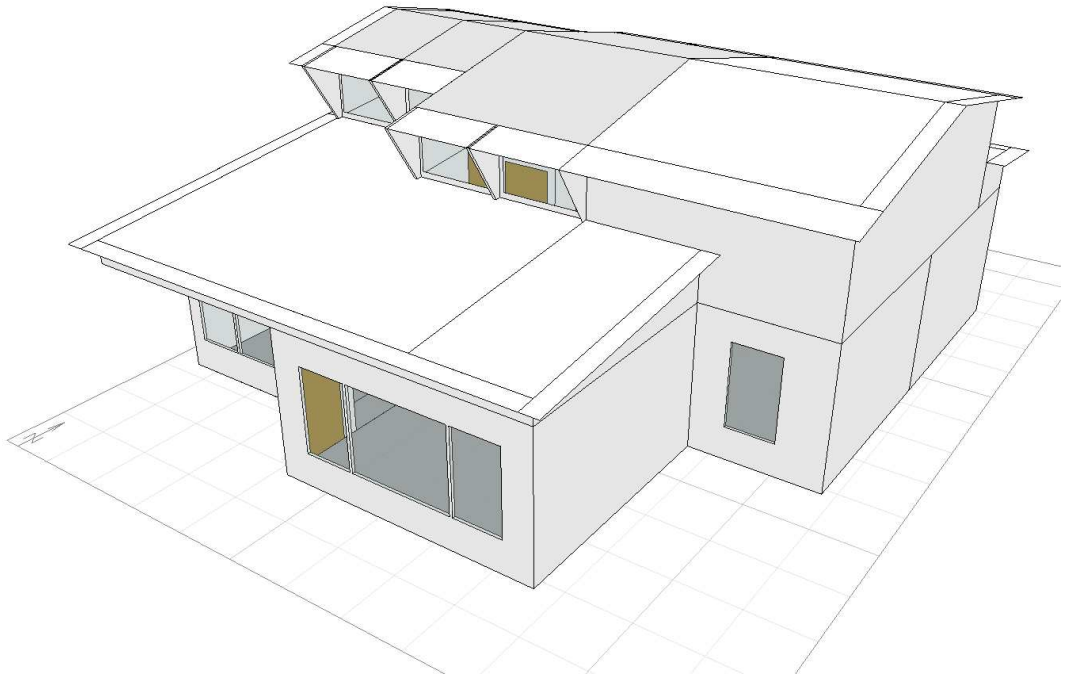

Figure 3.25: The shading design of the south facing clerestory windows.

the equipment of the atrium house in comparison to that of the baseline house is shown in Fig. 3.26.

The occupancy of the atrium house was also identical to that of the baseline house with a few exceptions. For instance, the atrium house did not have a separate utility room. Since the equipment of the utility room was located in the atrium, the occupants of this room in the baseline house were assigned to the atrium. As the cooktop unit was also in the atrium, the kitchen occupancy of the baseline house was divided equally between the unconditioned atrium and the conditioned kitchen of the atrium house assuming that the occupants spend half of their time for food preparation and the other half for cooking during the time they spend in the kitchen. The resulting average hourly heating energy generated by the people in the conditioned zones of the atrium house versus that generated by the people in the baseline house is given in Fig. 3.27.

The floor areas of the primary living areas in the atrium house (i.e. bedrooms, living room, dining area, kitchen, bathroom) were very similar to those in the baseline house.

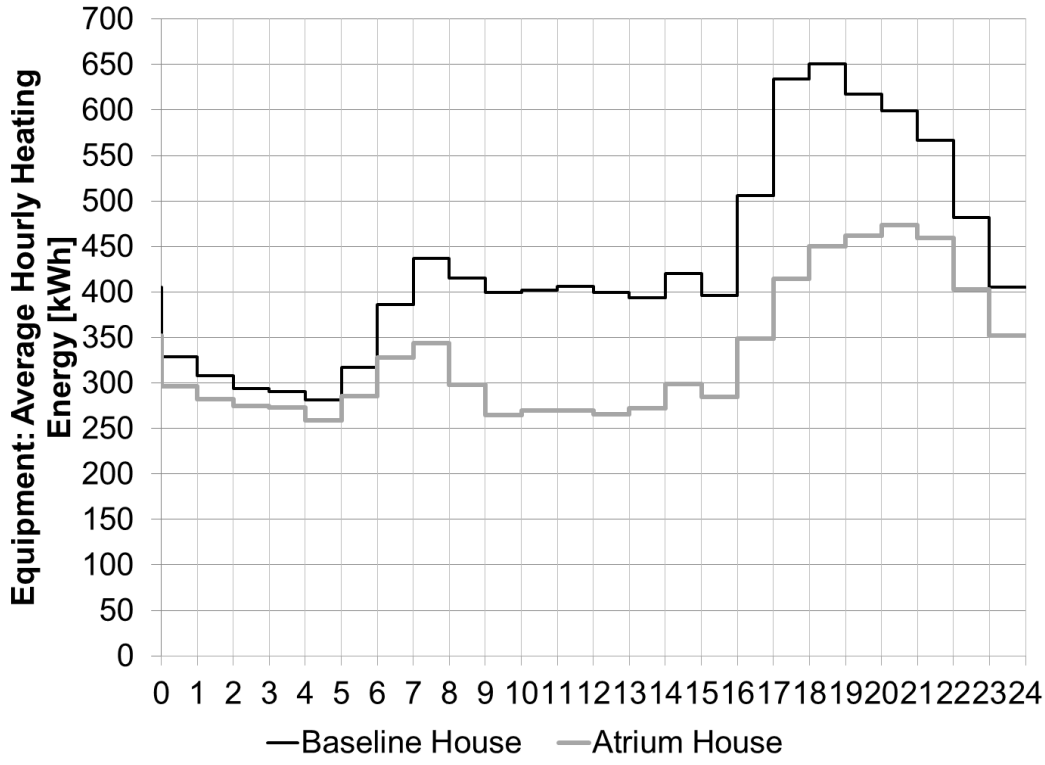

Figure 3.26: The baseline Habitat for Humanity house vs the atrium house: The average hourly heat generated by the equipment in the conditioned zones.

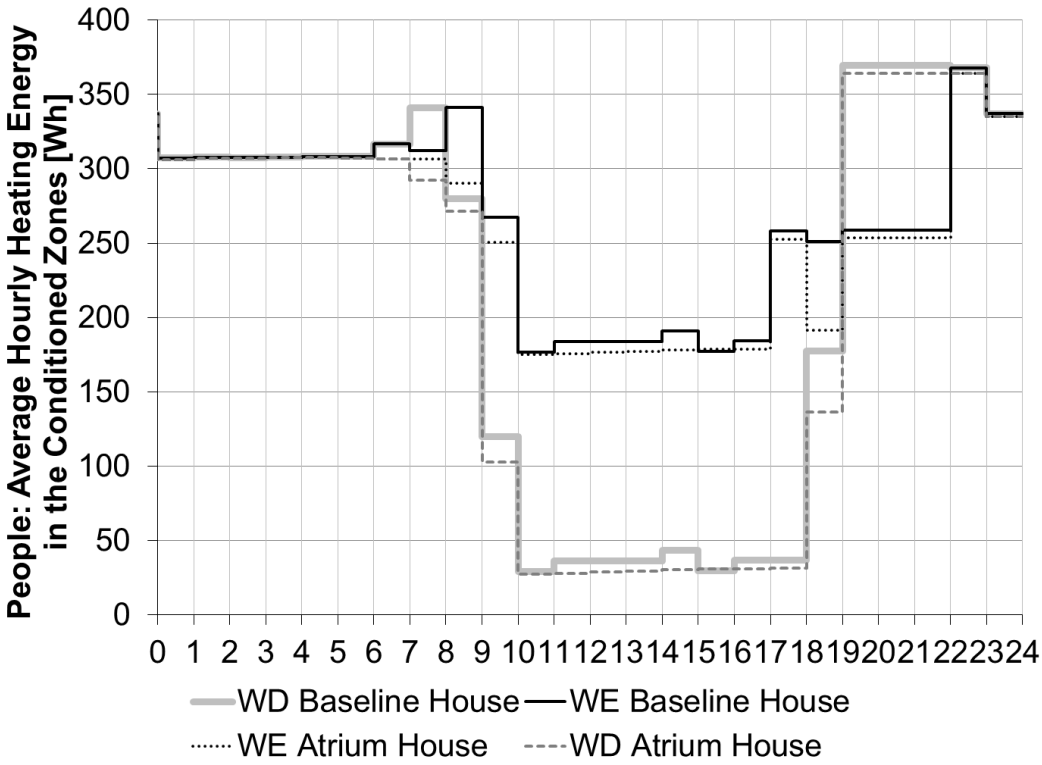

Figure 3.27: The baseline Habitat for Humanity house vs the atrium house: The average hourly heat generated by the people in the conditioned zones. WD: Weekday, WE: Weekend.

Thus, the electric lighting design of the atrium house was also very similar to that of the baseline house. Table 3.13 shows the electric lighting elements and the resulting lighting levels of the atrium house. For the calculation of the hourly electric lighting schedules, DAYSIM was used as described in Section 3.2.2. After the consideration of room occupancies and the occupants' awake hours, the average hourly lighting requirement of the atrium house was found to be as shown in Fig. 3.28. The resulting annual total electric lighting consumptions of the primary living areas of the atrium house are given in Fig. 3.29. These results showed that a significant part (13%) of the annual lighting consumption occurred in the unconditioned atrium since it had the lights of the hallway, the utility room and the cooktop unit of the baseline house. The heat generated by these lights were thereby avoided from the conditioned zones of the house. As a result, the monthly total heating energies generated by the electric lights in the conditioned areas of the atrium house were 11%-16% lower than those in the baseline house (see Fig. 3.30). The corresponding average hourly heat energy generated by the electric lights of the baseline and atrium houses is given in Fig. 3.31.

The infiltration in the atrium house was modeled in two steps following the process similar to that followed in Sec. 3.2.3. First, the openings of the house was modeled using the "SimpleOpening" object of the AirflowNetwork model of EnergyPlus in compliance with the IECC 2012. Second, leakages were added to the exterior walls of the house in order to provide the three leakage conditions that the baseline HFH house was modeled with. (see the descriptions of the *NEG0.45ACH*, *NEG0.30ACH* and *POS0.30ACH* models in Section 3.2.3)

The atrium house had 15 types of fenestration units. These units and their calculated C values are listed in Table 3.14. The atrium house also had a roof aperture which was modeled as an always open $2' \times 2'$ door on the roof.

After the modeling of the fenestration leakages, the exterior wall leakages of the atrium house were determined through a set of test runs. It was found that a total effective leakage area of 1,172 cm^2 at 50 Pa pressure differential was required to model the *NEG0.45ACH*

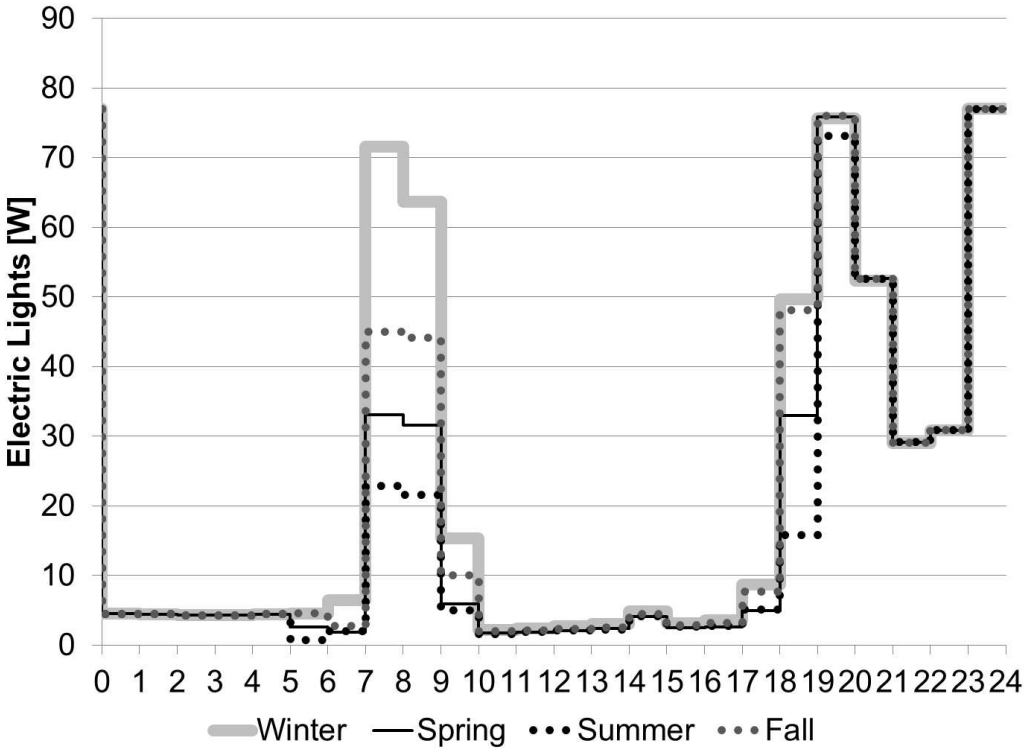

Figure 3.28: The average hourly lighting power schedule of the atrium house for each season.

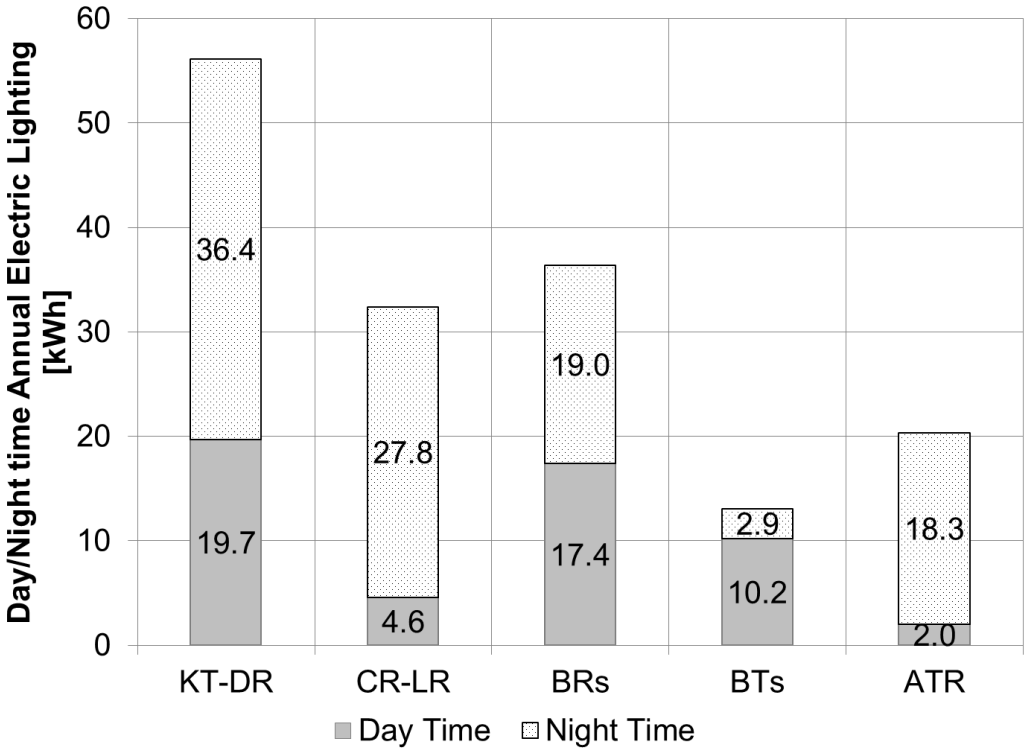

Figure 3.29: The annual total electric lighting consumption of the atrium house.

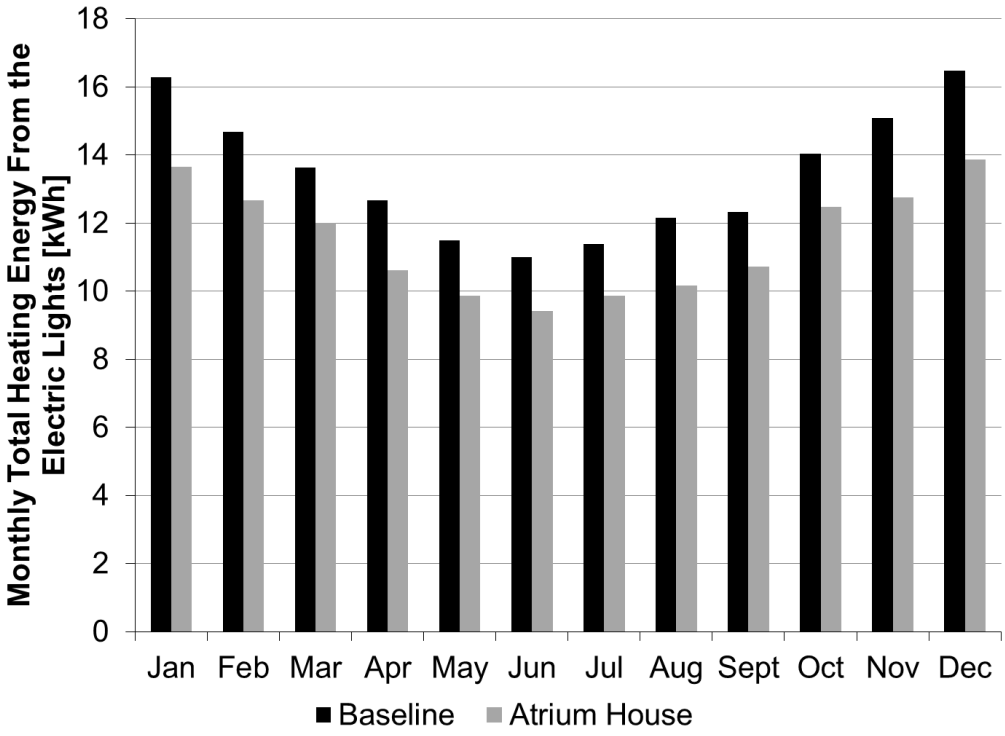

Figure 3.30: The baseline Habitat for Humanity house vs the baseline atrium house: The monthly total heating energy generated by the electric lights in the conditioned zones.

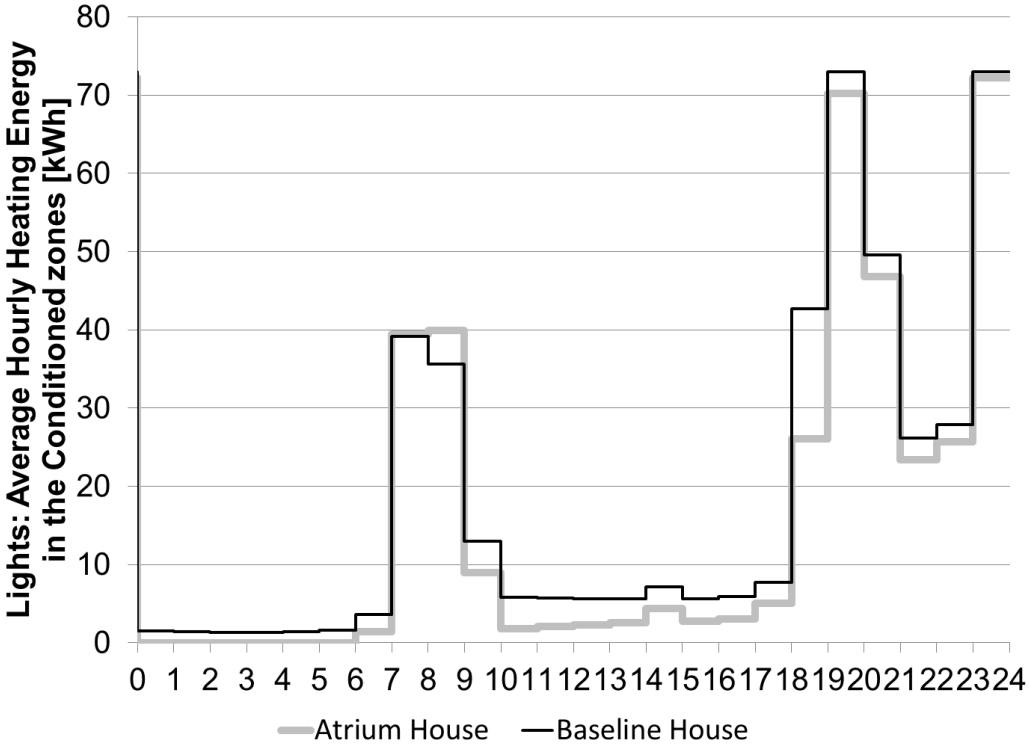

Figure 3.31: The baseline Habitat for Humanity house vs the baseline atrium house: The average hourly heating energy generated by the electric lights in the conditioned zones.

Table 3.13: The electric lighting design of the atrium house in accordance with the IES Lighting Requirements.[36] LR: Living room, BR1: Bedroom 1, BR2: Bedroom 2, MBR: Master bedroom, MBT: Main bathroom, MBRBT: Master bedroom bath, UTR: Utility room, DNR: Dining room, KT: Kitchen, ATR: Atrium, [a]: General, [b]: Toilets and bidets, [c]: Laundry, [d]: Study use, [e]: Preparation counters, [f]: Cooktops, [g]: Independent passageways

Room Type	E_{thres} (Lux)	FFA (m^2)	COU	N_{La}	$\frac{W}{bulb}$	$\frac{Lumen}{bulb}$	E (Lux)	L_L (W)
LR	30[a]	17.22	0.44	2	13	900	36.79	26
BR1	50[a]	11.45	0.23	4	13	900	57.85	52
BR2	50[a]	11.45	0.23	4	13	900	57.85	52
MBR	50[a]	11.37	0.23	4	13	900	58.26	52
MBT	100[b]	4.77	0.42	2	13	900	126.75	26
MBRBT	100[b]	1.79	0.42	1	15	700	131.31	15
UTR	200[c]	4.33	0.46	2	19	1200	204.00	38
DNR	200[d]	7.86	0.4	6	13	900	220.00	78
KT	500[e]	5.13	0.46	8	13	900	516.20	104
ATR	300[f]	1.73	0.29	2	19	1200	322.74	38
	30[g]	26.16	0.23	5	13	900	31.65	65

condition for the baseline atrium house. By the same method, it was also found that a total effective leakage area of 543 cm^2 at 50 Pa pressure differential was required for the *NEG0.30ACH* condition. Finally, for the *POS0.30ACH* case, the IECC 2012 required leakage condition (5 ACH at 50 Pa pressure differential) was found to correspond to 466 cm^2 at 50Pa as per Eq. 3.12. The mechanical ventilation rate required for the *POS0.30ACH* case was calculated to be 38 cfm (0.0179768 m^3/s) using Eq. 3.11. The *POS0.30ACH* case was then further improved by adding an economizer to the outside air system and setting it to be available at outside air temperatures under the cooling set point (24°C). In this new case (POS0.30ACHECON), the economizer was also set to keep the outside air at the minimum required rate (38 cfm) when the heating system was on using the "LockoutWithHeating" function of the "Controller:OutdoorAir" class in EnergyPlus.

The atrium house had the same type of air handling unit as of the baseline HFH house and it was modeled as described in Section 3.2.4. The duct layout of the atrium house

Table 3.14: The features of the openings on the building envelope of the atrium house. [a]: Bedroom and small south windows, [b]: Bathroom window, [c]: Large south windows, [d]: Clerestory window, [e]: Kitchen to atrium windows/doors, [f]: Dining room to atrium windows, [g]: Living room to atrium windows, [h]: Interior/exterior doors.

Opening Type	P (m)	A (m^2)	$\dot{v}_{max}$ (m^3/s)	$\dot{m}^*_{max}$ ($\frac{kg}{s}$)	C ($\frac{kg}{s.m}$)
Window[a]	4.86	1.38	2.11×10^{-3}	2.54×10^{-3}	3.16×10^{-5}
Window[b]	3.04	0.56	8.45×10^{-4}	1.02×10^{-3}	2.03×10^{-5}
Window[c]	6.7	2.78	4.24×10^{-3}	5.10×10^{-3}	4.60×10^{-5}
Window[d]	5.38	1.79	2.73×10^{-3}	3.29×10^{-3}	3.69×10^{-5}
Window[d]	4.96	1.54	2.34×10^{-3}	2.82×10^{-3}	3.44×10^{-5}
Window[d]	5.44	1.78	2.71×10^{-3}	3.27×10^{-3}	3.63×10^{-5}
Window[e]	7.96	3.78	5.75×10^{-3}	6.93×10^{-3}	5.26×10^{-5}
Window[e]	3.54	0.78	1.19×10^{-3}	1.44×10^{-3}	2.45×10^{-5}
Window[e]	3.34	0.69	1.05×10^{-3}	1.27×10^{-3}	2.30×10^{-5}
Window[e]	6.79	2.62	6.66×10^{-3}	8.02×10^{-3}	7.13×10^{-5}
Window[f]	4.36	1.16	1.76×10^{-3}	2.12×10^{-3}	2.94×10^{-5}
Window[f]	6.66	2.20	3.36×10^{-3}	4.04×10^{-3}	3.67×10^{-5}
Window[f]	5.82	1.19	1.81×10^{-3}	2.18×10^{-3}	2.26×10^{-5}
Window[g]	9.54	5.69	8.66×10^{-3}	1.04×10^{-2}	6.61×10^{-5}
Door[h]	6.04	1.90	2.89×10^{-3}	3.48×10^{-3}	3.48×10^{-5}

* Density of air is assumed to be 1.204 m^3/s.

Figure 3.32: The 3-D northeast view of the duct layout of the atrium house with an outdoor air system before the implementation of the partial conditioning strategy.

Figure 3.33: The 3-D southeast view of the duct layout of the atrium house with an outdoor air system before the implementation of the partial conditioning strategy.

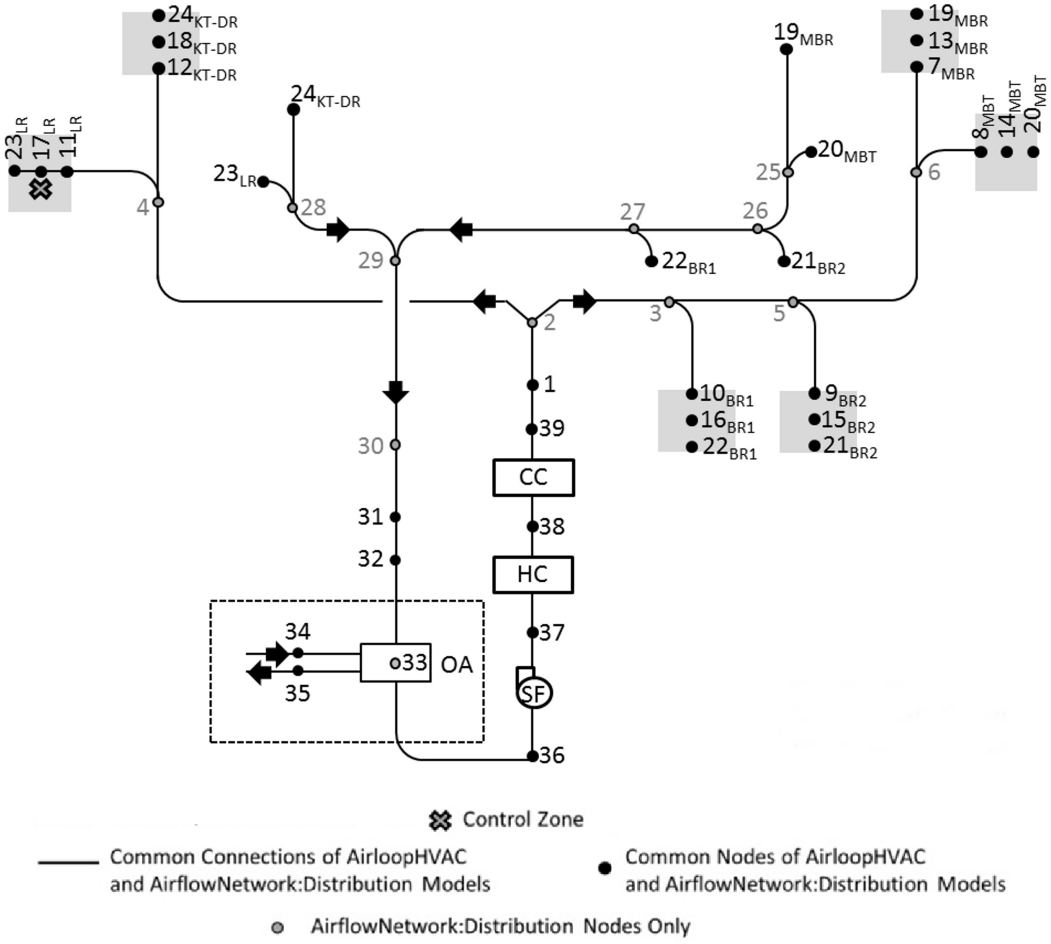

Figure 3.34: The AirflowNetwork:Distribution model of the duct layout of the atrium house with an outdoor air system before the implementation of the partial conditioning strategy. LR: Living room, KT-DR: Kitchen and dining room, BR1: Bedroom 1, BR2: Bedroom 2, MBR: Master bedroom, MBT: Main bathroom, SF: Supply fan, HC: Heating coil, CC: Cooling coil, OA: Outdoor air system.

before the implementation of the partial conditioning strategy is shown in Fig. 3.32 and Fig. 3.33. The AirflowNetwork:Distribution model of this duct layout is also given in Fig. 3.34. The highest TEL value was determined to be 114 m (373 ft) for this duct layout which resulted in a total pressure loss of 211 Pa (0.848 in. w.g.) considering the average pressure losses in the evaporator (62.3 Pa) and the filter (37.4 Pa). This total pressure loss value was then entered into the EnergyPlus models as the pressure rise of the supply fan at the design airflow rate of the system. The air ducts of the atrium house were covered with the ceiling insulation such that the half of the insulation depth was above the ducts and the other half was below the ducts resulting in a duct heat transmittance coefficient value of 0.2 W/m^2-K.

3.3.2 Atrium as the Return Plenum (Case 2)

This case (PLPOS0.30ACH) was designed to quantify the energy savings that can be obtained through the use of a central atrium space as a return plenum in a residential building. This new design was obtained through a set of modifications on the equipment (demand) side of the duct layout of the atrium house described in Sec. 3.3.1. For instance, in this case, it was assumed that the air supplied to the rooms was returned to the atrium through the openings on the atrium walls attached to those rooms. This required the exit nodes of the conditioned zones (19_{MBR}, 20_{MBT}, 21_{BR2}, 22_{BR1}, 23_{LR} and $24_{\mathrm{KT-DR}}$) to be connected to the supply air inlet node (25_{ATR}) of the atrium zone in the AirflowNetwork:Distribution model as shown in Fig. 3.35. The atrium zone was then defined as the return plenum of the system in the AirloopHVAC model, thus it never received supply air directly from the air handling unit. The air returning from the surrounding rooms partly conditioned the atrium and avoided extreme temperatures. The atrium zone was then connected to the zone mixer node (node 28 Fig. 3.35) which then connected to the demand side outlet node of the air loop (node 30 Fig. 3.35). The maximum TEL value of the resulting duct layout was calculated to be 88.7 m (291 ft) which corresponded to 87 Pa (0.349 in. w.g.). Considering the pressure losses of the evaporator (62.3 Pa) and the filter (37.4 Pa), the total pressure loss of the system was found to be 186.7 Pa (0.749

in. w.g.). This total pressure loss value was entered as the pressure rise of the supply fan at the system design airflow rate into the EnergyPlus model of this case. The resulting house was then further improved to obtain a new case (PLPOS0.30ACHECON). This case included an economizer in the outside air system and was used to quantify the combined effect of an atrium plenum and an economizer on the energy performance of the atrium house.

3.3.3 The Atrium House with Occupancy-based Heating and Cooling (Case 3)

Residential buildings use excessive amounts of energy by making cooling/heating available to all rooms all the time including the unoccupied hours. In this case (OCPOS0.30-ACH), energy savings were obtained in the atrium house modeled in Section 3.3.1 by conditioning the rooms only when they were in use. Based on Hendron's[35] occupancy schedules, the atrium house was first divided into two main spaces, i.e. the living area and the bedrooms. The living room (LR), the kitchen, the dining room (KT-DR) and the main bathroom (MBT) were included in the living area. All bedrooms (BR1, BR2 and MBR) and the bathroom of the master bedroom (MBRBT) were considered in the bedrooms space. It was assumed that the occupants of the house were in the living area between 7 a.m. and 11 p.m. on weekdays and between 8 a.m. and 11 p.m. on weekends.[35] During these hours, only the living area was cooled/heated. For the rest of the week, the occupants were assumed to be in their bedrooms; therefore, only the bedrooms were cooled/heated.

This new system required a duct layout which is partly cancelled to exclude the unoccupied zones. The EnergyPlus AirflowNetwork:Distribution model would not allow for such a duct layout in a single EnergyPlus input file. A typical constant volume residential system modeled in EnergyPlus also would not allow for airflow rate variations between summer and winter. Thus, the modeling of this case required multiple steps. First, two separate duct layouts were modeled for this occupancy based system, i.e. one for the living area and one for the bedrooms. Fig. 3.36 and Fig. 3.37 show these duct layouts. Second, each of these duct layouts were used both for the cooling and the heating of the space they were serving. In order to differentiate the heating and cooling design airflow rates for

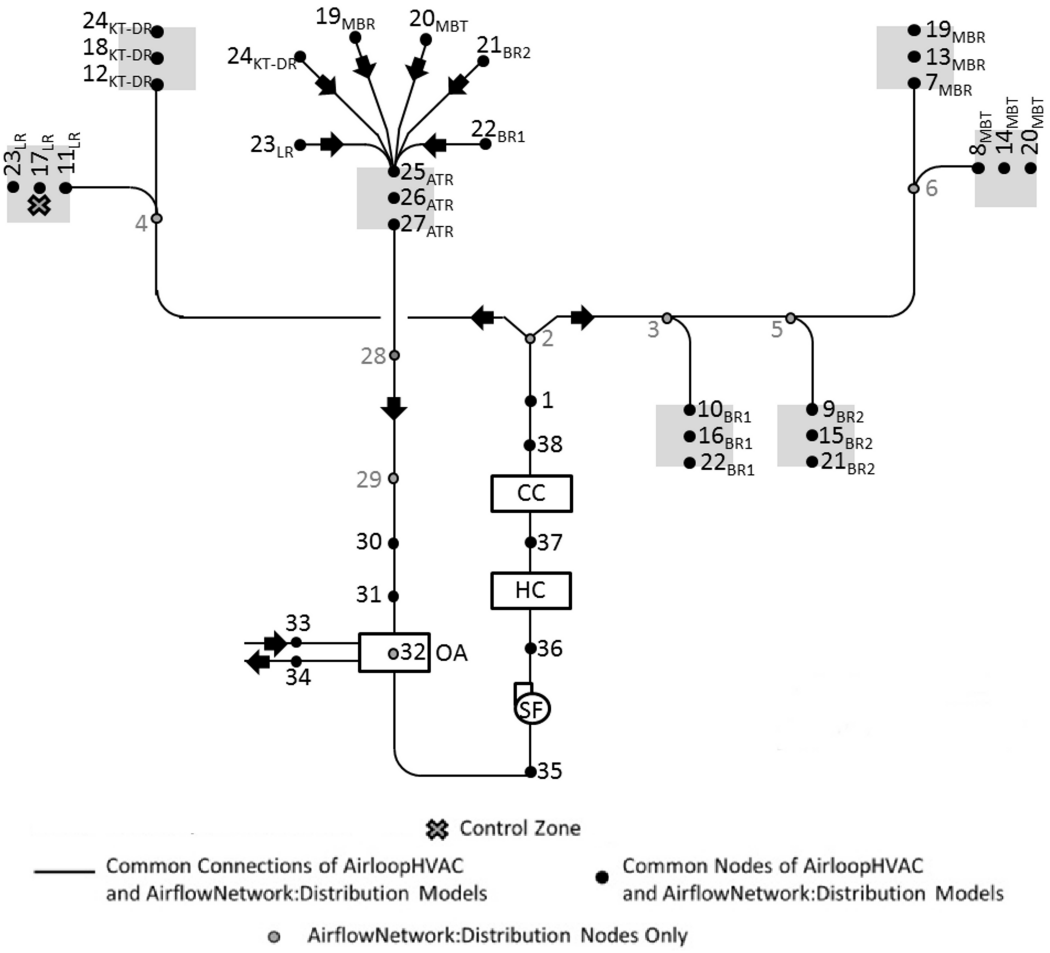

Figure 3.35: The duct layout of the test house with an atrium as a return plenum in the AirflowNetwork:Distribution model. LR: Living room, KT-DR: Kitchen and dining Room, BR1: Bedroom 1, BR2: Bedroom 2, MBR: Master bedroom, MBT: Main bathroom, SF: Supply fan, HC: Heating coil, CC: Cooling coil, OA: Outdoor air system.

these duct layouts, separate EnergyPlus files were required for heating and cooling. As a result, four EnergyPlus input files were produced for the modeling of this case. These files include:

1) the cooling scenario of the living area (LA),

2) the heating scenario of the living area (LA),

3) the cooling scenario of the bedrooms (BRs),

4) the heating scenario of the bedrooms (BRs).

Each of these scenarios required a different design airflow rate. Thus, the system operated with four airflow rates. The calculated cooling design airflow rates were found to be always higher than the heating design airflow rates; therefore, all air ducts of the system were designed for the cooling airflow rates. This resulted in lower air velocities in these ducts during the heating season than in the cooling season. When the air velocity decreased below a certain limit (not given in the manuals) in the AirflowNetwork:Distribution model, EnergyPlus reported errors for the air ducts. Adjustments were made on the designed air ducts when necessary in order to avoid these errors.

In the living area scenarios, the control zone was set to be the living room (LR). In the bedrooms scenarios, Master Bedroom (MBR) was assigned as the control zone of the system. Every day, the system needed to switch between the living area (see Fig. 3.36) and the bedrooms scenarios (see Fig. 3.37) depending on the hour of the day. This was achieved by combining the results of the occupied hours of each scenario in a single sheet. The resulting model represented a system that had control dampers at the splitter (node 2 in Fig. 3.36 and Fig. 3.37) and mixer (node 16 in Fig. 3.36 and Fig. 3.37) points of the duct layouts of the living area and bedrooms. Each of these two duct layouts also switched between the heating and cooling design airflow rates depending on the season. The results of the on hours of the cooling and heating were then combined in a single sheet to obtain the full year.

In the resulting occupancy based system, the minimum outdoor air requirement of each of the two main spaces of the house (i.e. the living area and the bedrooms) was calculated

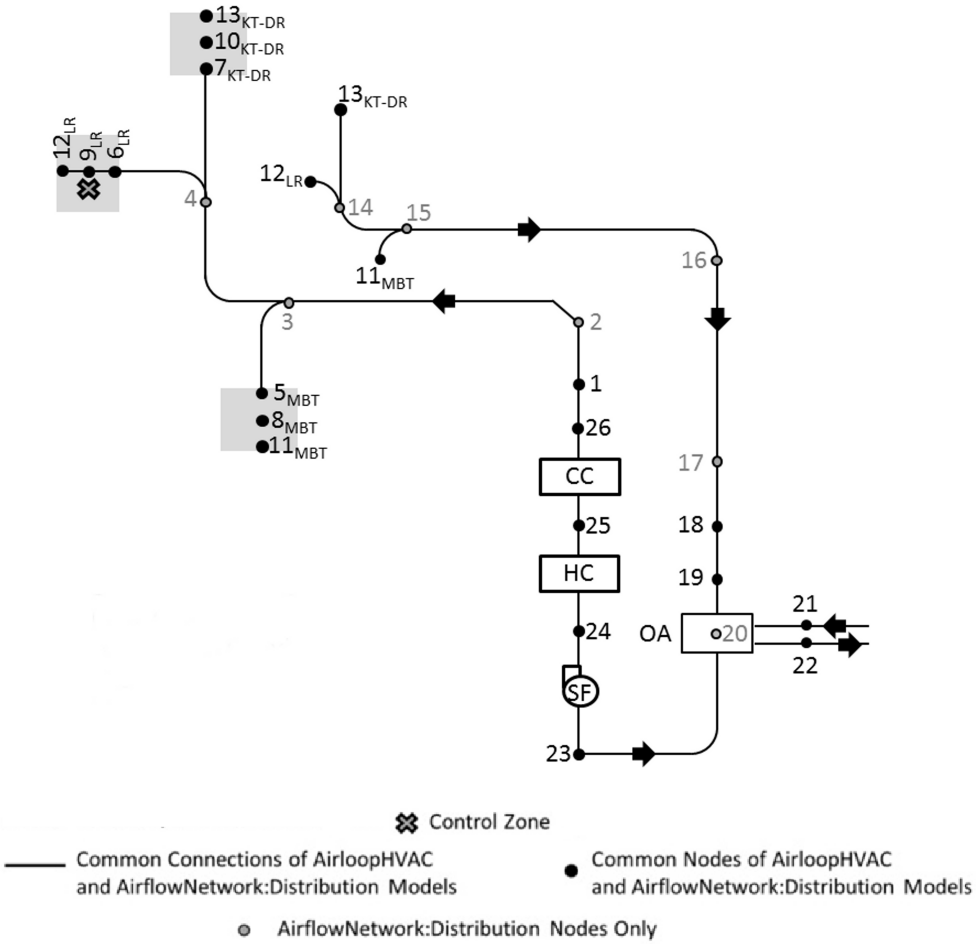

Figure 3.36: The AirflowNetwork:Distribution model of the duct layout of the atrium house with occupancy based heating/cooling for the living area scenario. LR: Living room, KT-DR: Kitchen and dining Room, MBT: Main bathroom, SF: Supply fan, HC: Heating coil, CC: Cooling coil, OA: Outdoor air system.

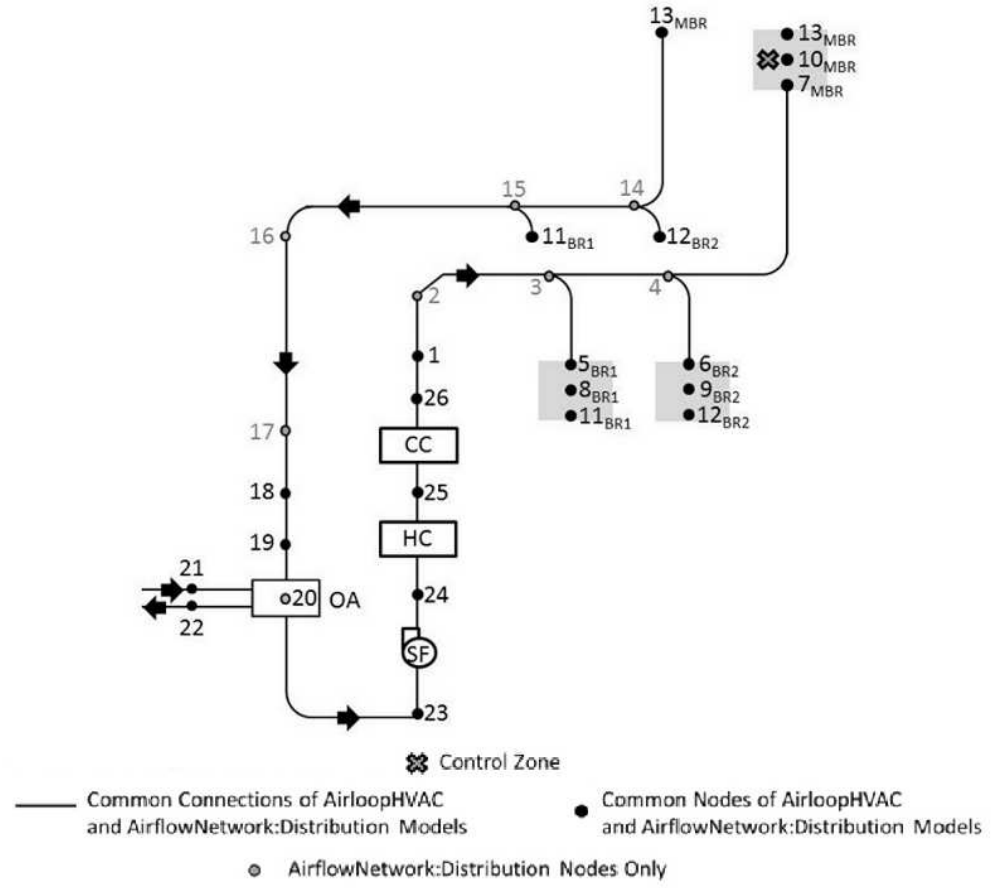

Figure 3.37: The AirflowNetwork:Distribution model of the duct layout of the atrium house with occupancy based heating/cooling for the bedrooms scenario. BR1: Bedroom 1, BR2: Bedroom 2, MBR: Master bedroom, SF: Supply fan, HC: Heating coil, CC: Cooling coil, OA: Outdoor air system.

in proportion to their total conditioned floor areas. Thus, Eq. 3.11 was multiplied by a coefficient to calculate the minimum outdoor airflow rate required for each of these spaces (see Eq. 3.25). These rates were found to be 0.00818 m^3/s (17 cfm) for the living area and 0.00979 m^3/s (21 cfm) for the bedrooms.

$$Q = \frac{CFA_{scenario}}{CFA}(0.01 \times CFA + 7.5(N_{br} + 1)) \tag{3.25}$$

The sizing of the heating and cooling coils was also handled differently when compared to a typical residential system. The capacities were autosized for the living area and the bedrooms in separate EnergyPlus files. The sizes were then compared with each other. The largest of the two sizes was selected and accepted as the final coil capacity. The scenario that actually required a lower capacity was then rerun with this final coil capacity. The highest design airflow rate of the four scenarios of the system was accepted as the maximum airflow rate of the system at which the calculated fan pressure rise occurred. EnergyPlus then adjusted the fan pressure rise for the lower airflow rates of the system. The maximum TEL value for this atrium house with occupancy based heating/cooling was calculated to be 97.5 m (319.9 ft) which corresponded to 0.38 in. w.g. (95.6 Pa) pressure rise at the maximum system airflow rate. Considering the pressure drops in the evaporator and the filter, the total pressure rise in the supply fan needed to be 0.78 in. w.g. (195.3 Pa).

3.3.4 The Atrium House with Multiple Reuse of Air (Case 4)

In the system described in Section 3.3.3, the exit ducts of the occupied zones were connected to the return ducts (see 11-15, 12-14, 13-14, 14-15 and 15-20 ducts in Fig. 3.36 and Fig. 3.37) which carried the air used in these zones back to the air handling unit. The unoccupied zones were unconditioned and never received air from the system directly or indirectly. This resulted in three primary disadvantageous conditions. First, the zones reached extreme (very high or very low) temperatures during their unoccupied hours which took more energy to reheat/recool them when they were occupied again. Second, the extreme temperatures in the uncontrolled rooms led to higher heat transfer through the

interior walls between the controlled and uncontrolled rooms making it harder to maintain the set points in the controlled zones. Third, the zones became favorable for mold and mildew growth during their unoccupied hours due to the high temperature and humidity in these areas.

As a means to avoid these conditions, a new design case (MRSPOS0.30ACH) was developed by improving the occupancy based atrium house described in Sec. 3.3.3. In this new case, the air exiting the occupied zones was sent to the unoccupied zones instead of being returned to the air handling unit. The air reused in the unoccupied zones was then moved into the atrium through the openings on the walls between the atrium and the neighboring rooms. Finally, the air in the atrium was returned to the air handling unit through a single return duct. Fig. 3.38 schematically describes the airflow design in this new atrium house.

For reasonable estimation of the energy savings that can be achieved with this system, it was critical to correctly model the air temperatures of the unoccupied zones before the system started to supply air to them. Fig. 3.38 shows how the final temperatures of the unoccupied rooms are carried between the Living Area and Bedrooms files to be used as the starting temperatures of the occupied hours in order to connect the two scenarios. This interaction between the Living Area and Bedrooms scenarios was achieved through an iterative modeling process (see Fig. 3.39).

The process was initiated by running the model of the Living Area scenario. With this run, the capacity of the heating ($W_{heating}$) or the cooling ($W_{cooling}$) coil and the maximum airflow rate of the system ($\dot{v}_{max}$) were determined and the zone air temperatures of the unoccupied bedrooms ($T_{z-unocBRs}$) were reported. The capacity of the cooling/heating (depending on the season) coil was then entered into the model of the Bedrooms scenario. The $\dot{v}_{max}$ value was also entered into the bedrooms model as the maximum airflow rate of the supply fan at which the calculated pressure rise (155.7 Pa) occurred. EnergyPlus did not allow zone air temperatures to be entered as inputs.

Thus, the zone air temperatures of the unoccupied bedrooms right before the system

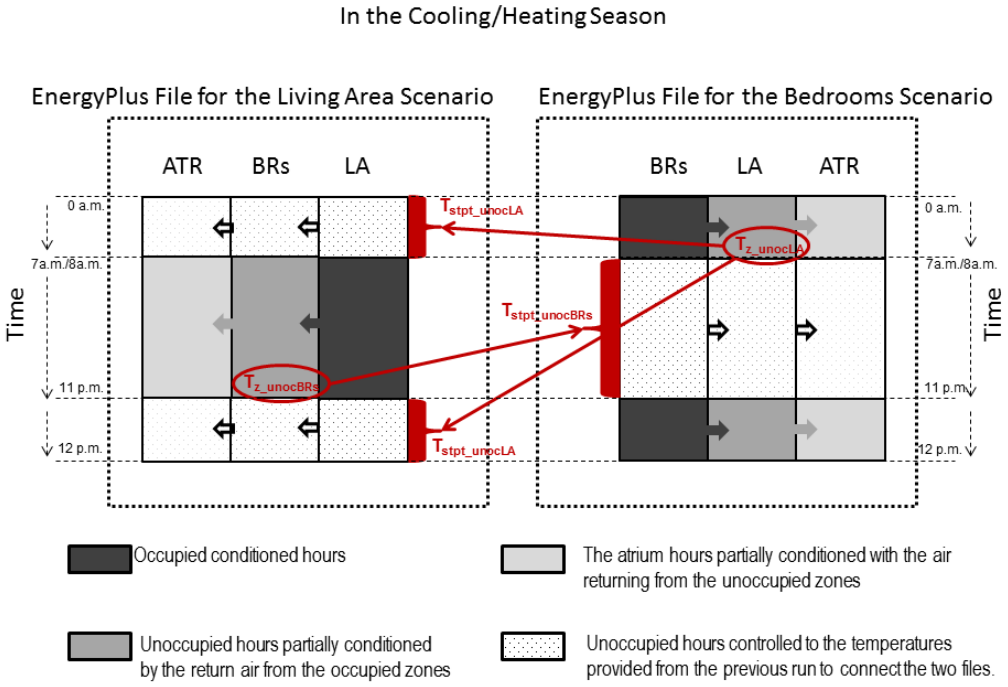

Figure 3.38: The schematic representation of the airflow in the atrium house with multiple reuse of air. $T_{z-unocBRs}$: the zone air temperature of the unoccupied Bedrooms at the end of the Living Area scenario, $T_{z-unocLA}$: the zone air temperature of the unoccupied Living Area at the end of the Bedrooms scenario, $T_{stpt-unocLA}$: the cooling/heating set points assigned to the unoccupied hours of the Living Area in the EnergyPlus file for the Living Area scenario, $T_{stpt-unocBRs}$: the cooling/heating set points assigned to the unoccupied hours of the Bedrooms in the EnergyPlus file for the Bedrooms scenario.

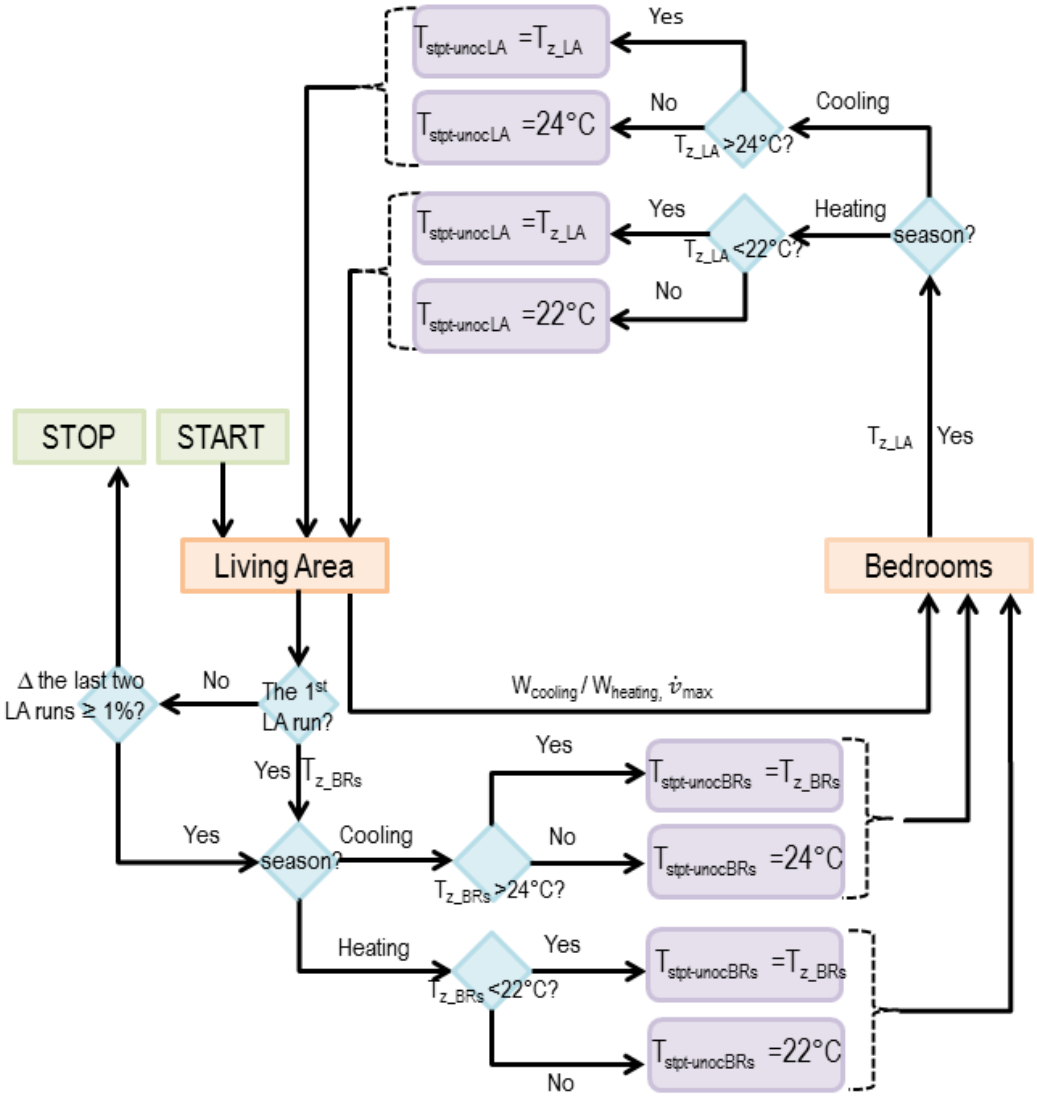

Figure 3.39: The iterative modeling process between the EnergyPlus files of the living area (LA) and the bedrooms (BRs) scenarios when the living area is the determining scenario for the coil capacity. $T_{stpt-unocLA}$: set point assigned to the unoccupied hours of the living area, $T_{stpt-unocBRs}$: set point assigned to the unoccupied hours of the bedrooms, $W_{cooling}$: capacity of the cooling coil, $W_{heating}$: capacity of the heating coil, $\dot{v}_{max}$: maximum airflow rate of the system, T_{z-BRs}: the zone air temperatures of the bedrooms during the unoccupied hours, T_{z-LA}: the zone air temperatures of the living area during the unoccupied hours.

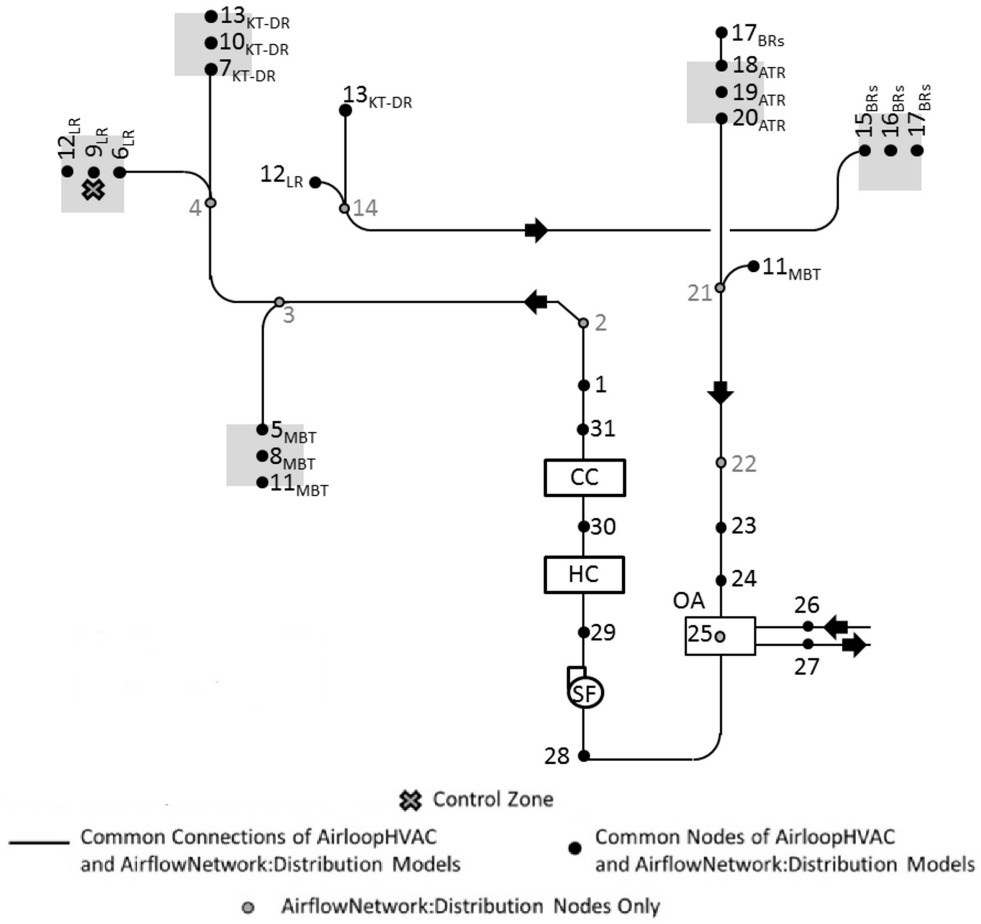

Figure 3.40: The AirflowNetwork:Distribution model of the duct layout of the atrium house with multiple reuse of air during the occupied hours of the living area. LR: Living room, KT-DR: Kitchen and dining Room, MBT: Main bathroom, ATR: Atrium, BRs: Bedroom 1, Bedroom 2, Master bedroom, SF: Supply fan, HC: Heating coil, CC: Cooling coil, OA: Outdoor air system.

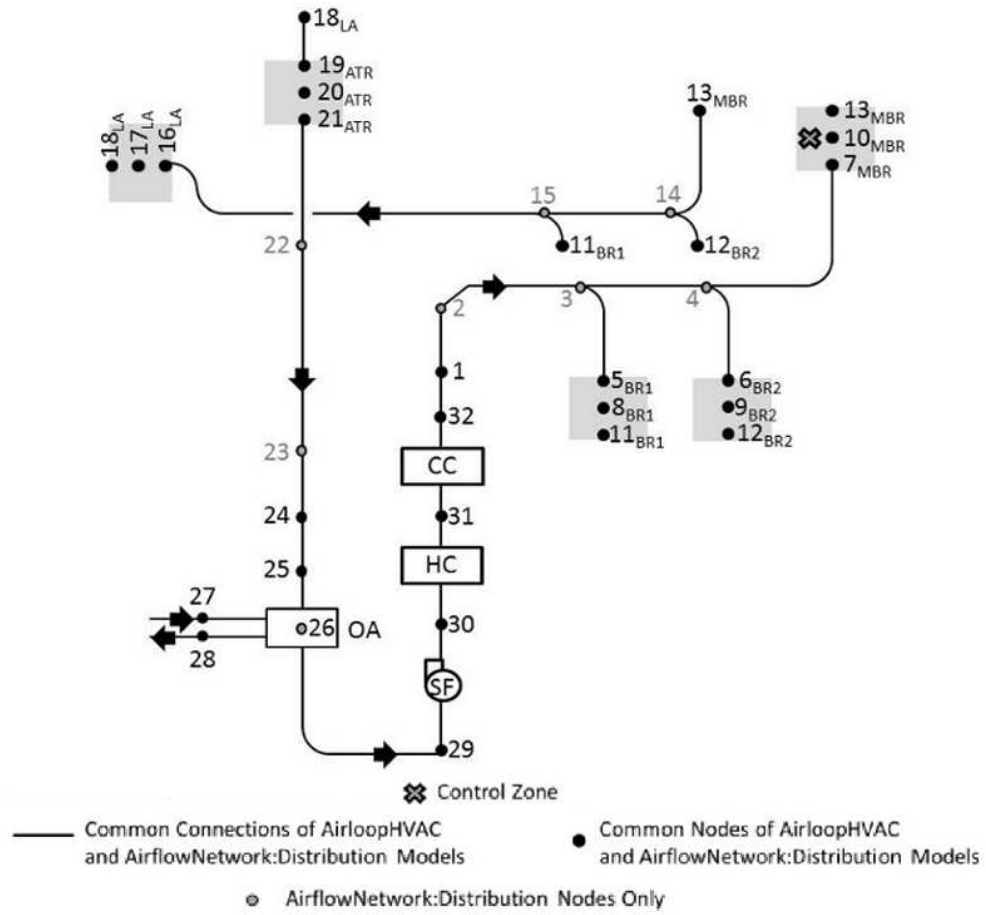

Figure 3.41: The AirflowNetwork:Distribution model of the duct layout of the atrium house with multiple reuse of air during the occupied hours of the bedrooms. BR1: Bedroom 1, BR2: Bedroom 2, MBR: Master bedroom, LA: Living room, Kitchen and dining room, Main bathroom, ATR: Atrium, SF: Supply fan, HC: Heating coil, CC: Cooling coil, OA: Outdoor air system.

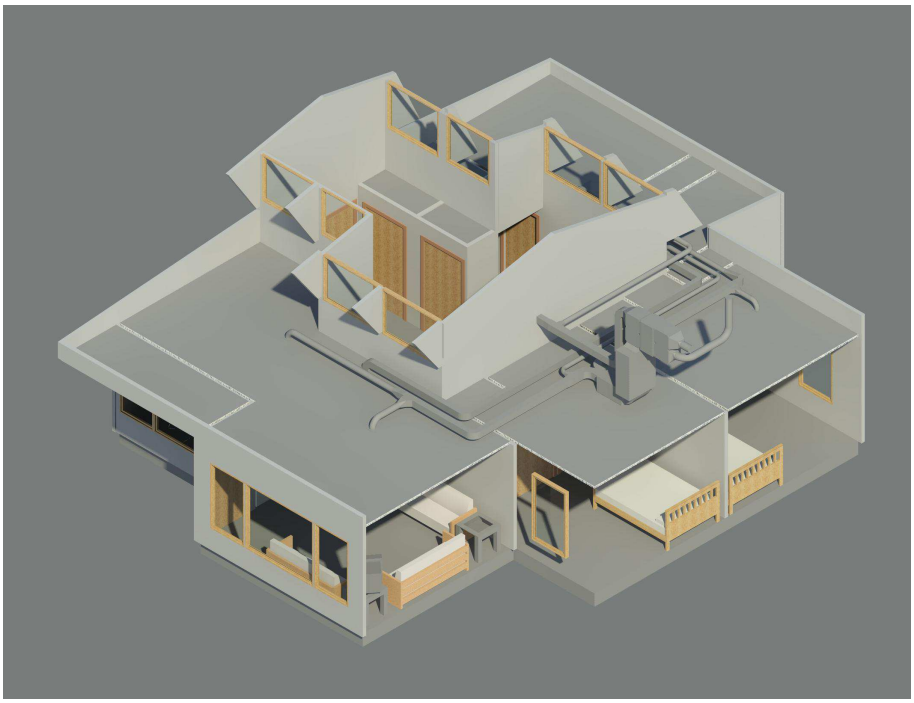

Figure 3.42: The southeast 3-D view of the duct layout of the atrium house with multiple reuse of air.

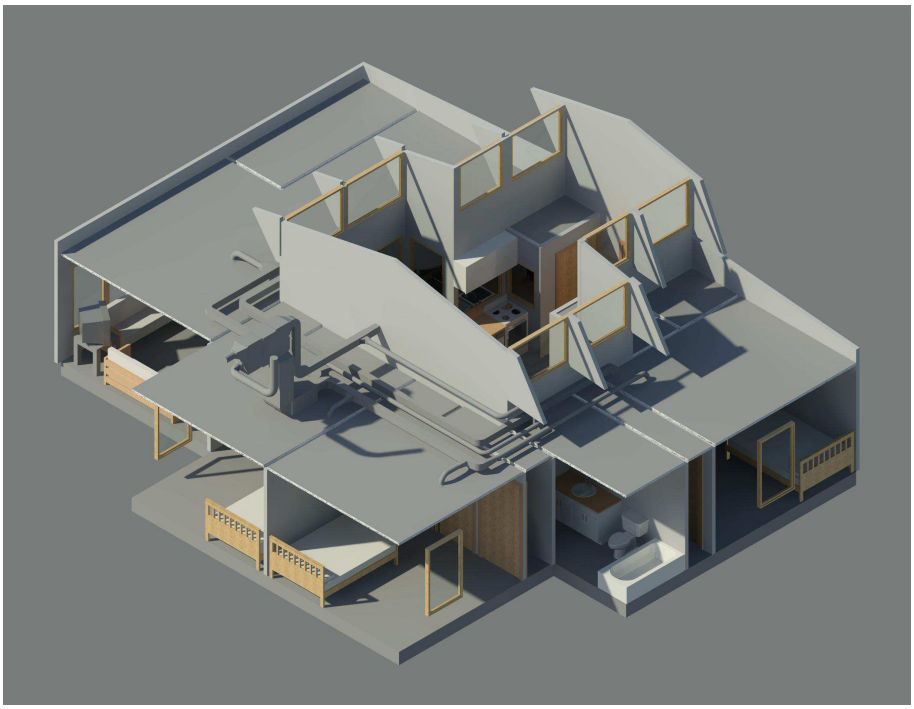

Figure 3.43: The northeast 3-D view of the duct layout of the atrium house with multiple reuse of air.

started to heat/cool them ($T_{z-unocBRs}$) were modified through a decision process shown in Fig. 3.39 and the resulting temperatures were entered as set points of the bedrooms during the unoccupied hours. This way, the system kept the zone air temperatures of the unoccupied bedrooms at these set points throughout the unoccupied term and started to heat/cool them from this temperature. For the estimation of the final HVAC energy use in the building, only the occupied hours were considered for each part of the building. Thus, the additional cooling/heating that occurred in the EnergyPlus files during the unoccupied hours was disregarded. The same process was repeated after running the bedrooms scenario. This time, the temperatures of the unoccupied living area (T_{z-LA}) were put through the same decision process and were entered as the set points of the living area during the unoccupied hours. This process continued until the difference between the results of the two successive living area runs were less then 1% for all HVAC categories.

For the modeling of this high performance atrium house in the AirflowNetwork:Distribution model of EnergyPlus, the duct layouts presented in Fig. 3.36 and Fig. 3.37 were improved to include the reuse of air idea. The resulting duct layouts are presented in Fig. 3.40 and Fig. 3.41. The 3-D view of this duct layout is shown in Fig. 3.42 and Fig. 3.43. In this new model, the unoccupied zones and the atrium were represented as return plenums in the AirloopHVAC classes in order to simulate the airflows between the zones. As EnergyPlus did not allow for multiple return plenums between two successive AirloopHVAC nodes, all unoccupied rooms had to be combined and modeled as a single return plenum zone (see the BRs zone in Fig. 3.40 and the LA zone in Fig. 3.41). These unoccupied plenum zones were then connected to the atrium plenum which collected the whole air of the system and returned it to the air handling unit. In this system, in order to avoid possible odor problems, the return air of the main bathroom zone (MBT) was isolated from the reuse of air scenario during its occupied hours and was directly connected to the zone mixer (see node 21 in Fig. 3.40). During the nighttime, the main bathroom zone was unoccupied. Thus, the air of this zone was mixed with those of the living room (LR) and the kitchen and dining room (KT-DR) zones and moved into the atrium before it was sent

back to the system (see the LA zone in Fig. 3.41).

For the sizing of the air ducts in this system, initial test runs were conducted by iterating the EnergyPlus files of all four scenarios with the TRNSYS Type 1255 slab-on-grade model separately. The variations in the zone airflow rates with ground coupling were determined and the ducts were sized for the estimated rates of the slab-on-grade condition. Finally, the longest TEL value of this duct layout was determined to be 57 m (188 ft) which corresponded to a maximum pressure drop of 56 Pa (0.225 in. w.g) at the maximum airflow rate of the system. Considering the pressure drops of the evaporator and the filter, the total pressure drop reached 155.7 Pa (0.625 in. w.g.). This final pressure loss value was then entered as the pressure rise of the supply fan at the maximum airflow rate of the system in all EnergyPlus files.

Among the test cases modeled in Section 3.3, this final atrium house with multiple reuse of air was the only one that was coupled with the ground to model a slab-on-grade house. The results obtained for this high performance house was then compared with the baseline slab-on-grade Habitat for Humanity houses modeled in Section 3.2 and the obtained performance improvements were discussed. Fig. 3.44 describes the iterative ground coupling process for this partially conditioned atrium house with multiple reuse of air. This process was similar to that of the baseline Habitat for Humanity houses shown in Fig. 3.16 with three primary differences. First, the iteration of the living area and bedrooms of the building were conducted separately. Second, three input parameters were carried between the living area and bedrooms runs at each iteration. These parameters were the capacities of the cooling ($W_{cooling}$) and heating ($W_{heating}$) coils, the maximum supply airflow rate of the system ($\dot{v}_{max}$) and the pressure rise of the supply fan at this rate (P_{furn}). Third, after the iterations were completed, the EnergyPlus files for the living area and bedrooms were iterated with each other until convergence following the procedure described in Fig. 3.39.

The modeling process shown in Fig. 3.44 showed variations between the heating and cooling seasons. Through a series of test runs, it was found that, the Living Area scenario was the determinative scenario for the capacity of the heating coil and the maximum system

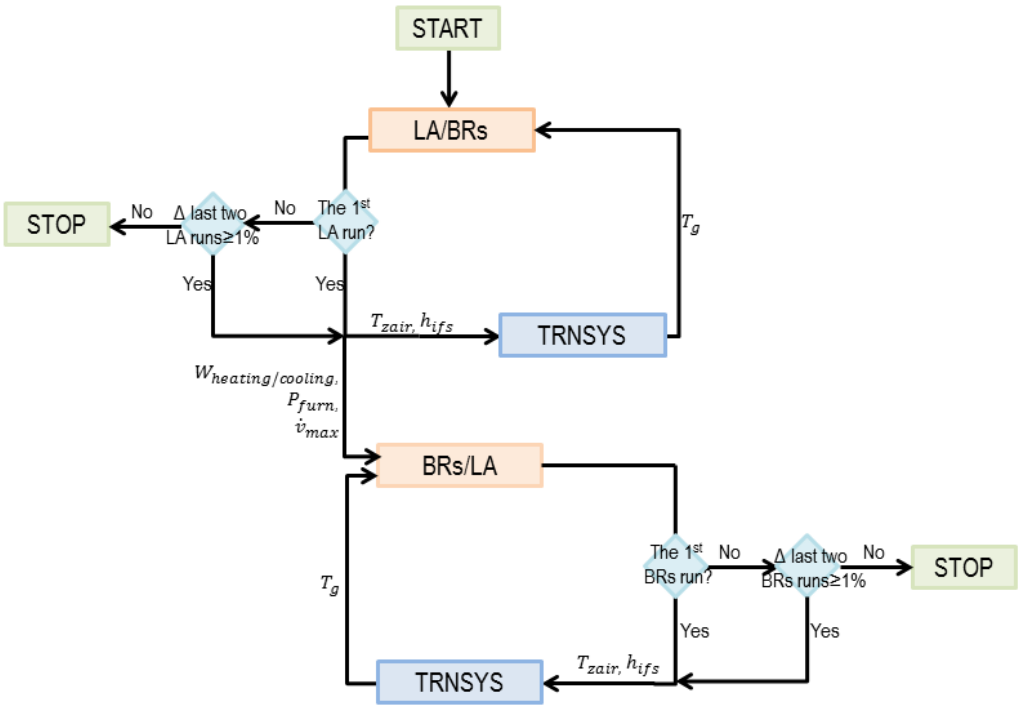

Figure 3.44: The iterative modeling process between the EnergyPlus and TRNSYS Type 1255 model for the living area (LA) and the bedrooms (BRs) scenarios to model the slab-on-grade atrium house with multiple reuse of air. $W_{cooling}$: capacity of the cooling coil, $W_{heating}$: capacity of the heating coil, $\dot{v}_{max}$: maximum airflow rate of the system, T_{zair}: the zone air temperatures, h_{ifs}: convection coefficient of the inside surface of the floor, P_{furn}: pressure rise of the supply fan at the maximum airflow rate, T_g: inside surface temperature of the floor.

airflow rate in the heating season. Thus, the $W_{heating}$ and $\dot{v}_{max}$ values were carried from the Living Area scenario file to the Bedrooms scenario file in this season. It was also found that the Bedrooms scenario was the determinative scenario for the capacity of the cooling coil and the maximum system airflow rate in the cooling season. Thus, during the cooling season, the $W_{cooling}$ and $\dot{v}_{max}$ values were carried from the Bedrooms scenario file to the Living Area scenario file.

The unique airflow design of this atrium house provided multiple benefits to the building. First, it provided partial conditioning for the unoccupied zones without requiring any additional heating/cooling. This reduced the risk of mold and mildew growth in these

zones and reduced the energy required to recool/reheat these spaces when they became occupied again. Second, it maintained a healthier indoor environment for the occupants by supplying the outdoor air directly into the occupied zones first and then circulating it in the whole house. Third, it kept the building positively pressurized which reduced the uncontrolled airflow into the building (i.e. infiltration). Consequently, a healthier and energy efficient residential building was obtained.

4. RESULTS AND DISCUSSION

This chapter presents the results of the study in two primary sections. The first section presents the comparisons of the DOE-2 and EnergyPlus slab-on-grade heat transfer models with that of TRNSYS and a ground coupling method was selected for the study. The second section presents the energy performances of the test cases modeled in this study during the conversion of the baseline Habitat for Humanity houses to the partially conditioned atrium house.

4.1 EnergyPlus vs DOE-2: Slab-on-grade Heat Transfer*

The results of this part of the study are discussed in two sections: (1) the sealed boxes and (2) the fully loaded test houses. The first section presents the results obtained for the empty, ground coupled sealed boxes with adiabatic walls and ceiling, and compares the three slab-on-grade models by isolating the ground coupling effect. The second section presents the results obtained for the fully loaded code-compliant houses and quantifies the significance of the discrepancies in slab-on-grade heat transfer modeling relative to the total building energy requirement.

The primary findings of this section can be summarized as follows:

* The current Slab model of EnergyPlus (EP-GCSiitwotEv) has convergence problems and needs urgent improvement. It is also a single zone model which can only differentiate periphery and core areas.

* When the Slab model of EnergyPlus is manually converged with the aboveground model (EP-GCSeitwotEv), it shows closer results to those calculated with the detailed TRNSYS slab-on-grade model (EP-GCTh) than Winkelmann's model (EP-GCW) (see Table 4.1). Using Slab as directed in EnergyPlus documentation results in one iteration. Manual convergence was achieved in 4-5 iterations.

* Coupling of the multizone TRNSYS slab-on-grade model (Type 1255 model) with an aboveground multizone EnergyPlus model has been selected for the modeling of the

* Partially reproduced from "EnergyPlus vs DOE-2.1e: The effect of ground coupling on cooling/heating energy requirements of slab-on-grade code houses in four climates of the U.S" by Simge Andolsun, Charles H. Culp, Jeff S. Haberl and Michael Witte, *Energy and Buildings*, 52(2012), 189-206, 2012. Copyright 2012, Elsevier B.V.

baseline Habitat for Humanity houses and the partially conditioned atrium house.

Table 4.1: Total building loads (heating and cooling) calculated using Slab (EP-GCS), Winkelmann's method (EP-GCW) and the TRNSYS slab-on-grade model (EP-GCT) in EnergyPlus.

Model	Austin (GJ)	Phoenix (GJ)	Chicago (GJ)	Columbia Falls (GJ)
EP-GCW	78.74	106.05	129.67	115.70
EP-GCSiitwotEv	48.74	65.52	*	85.99
EP-GCSeitwotEv	65.16	88.58	*	101.41
EP-GCT	71.25	93.96	117.25	104.79

* Slab crashed.

The results were generated from the program outputs in various ways. The DOE-2 thermal loads presented in this study were obtained from the System Monthly Loads Summary (SS-A) reports of DOE-2 after "SUM" was assigned to the test houses as the "system-type." Similarly, the thermal loads of the EnergyPlus houses were obtained from the "Zone/Sys Sensible Heating Energy" and "Zone/Sys Sensible Cooling Energy" reports of EnergyPlus after the "Ideal Loads Air System" was assigned to the test houses. The DOE-2 monthly average floor heat fluxes were obtained by modifying the "underground floor conduction gain" values reported by DOE-2. This modification was necessary due to the load calculation and reporting differences between DOE-2 and EnergyPlus. In DOE-2, thermal loads are calculated in the LOADS subroutine based on a constant zone air temperature throughout the year.[180] The thermal loads calculated in the LOADS subroutine are then transferred into the SYSTEMS subroutine of DOE-2 where the variations in the zone air temperatures are taken into account.[180] The output for floor conduction heat gain is available only from the LOADS subroutine of DOE-2. The values obtained from the LOADS subroutine of DOE-2, therefore, had to be multiplied by correction factors (C_c) to obtain floor heat gain/loss values for the varying zone air temperatures. The resulting

DOE-2 values then became comparable with EnergyPlus values. The EnergyPlus results were generated by subtracting the "Opaque Surface Inside Face Conduction Loss" values from the "Opaque Surface Inside Face Conduction Gain" values for the ground coupled floor.

$$C_c = \frac{(T_g - T_{zair})}{(T_g - 23°C)} \tag{4.1}$$

4.1.1 Sealed Boxes

For slab-on-grade floors, DOE-2, EnergyPlus and TRNSYS programs solve a heat balance on the inside surface of the floor.[103,140,180] In this heat balance, the heat transferred from the soil to the inside surface of the floor ($Q_{slab/soil}$) is assumed to be equal to the heat transferred from the zone to the inside surface of the floor ($Q_{slab/zair}$). In all three programs, the heat is transferred between the soil and the slab ($Q_{slab/soil}$) by conduction. The heat transfer between slab and the zone air ($Q_{slab/soil}$) then occurred by convection and radiation.[103,140,180] The methods and assumptions used to calculate the conduction, convection and radiation components of the slab-on-grade heat transfer, however, differed between programs. In this section, the ground coupling loads of the slab-on-grade empty sealed boxes were compared between DOE-2, EnergyPlus and TRNSYS in order to isolate and quantify the slab-on-grade heat transfer calculation differences between these programs. First the $Q_{slab/zair}$ (Step 1) and then the $Q_{soil/slab}$ (Step 2) of the sealed boxes were compared between these programs.

4.1.1.1 Step 1: Heat Transfer Between the Slab and the Zone

At this step, the $Q_{slab/zair}$ calculation differences between the EnergyPlus, DOE-2 and TRNSYS programs are quantified. In order to explain these $Q_{slab/zair}$ differences, the inside convection and radiation models of these programs are compared (see Table 4.2).

Table 4.2: Differences between the calculations of DOE-2, EnergyPlus (EPlus) and TRNSYS programs for interior surface convection and radiation

	Convection	Radiation
DOE-2	Provides a single option; uses user-defined constant convective heat resistance (RC). Convective heat resistance is entered within the Inside-Film-Resistance(I-F-R) input of DOE-2 along with the radiative heat resistance (RR).[180] Eq. 4.2 shows the relationship between the radiative heat resistance (RR), convective heat resistance (RC) and the I-F-R input of DOE-2: $$\frac{1}{I-F-R} = \frac{1}{RC} + \frac{1}{RR} \qquad (4.2)$$	Provides a single option; uses user-defined constant radiative resistance (RR). The radiative resistance (RR) is entered within the I-F-R input of DOE-2 along with the convective resistance (RC) as described on the left in DOE-2/Convection section.[180]
EPlus	Provides four options:[103] (1) The user defined option allows the user to input constant convection coefficients for interior and exterior surfaces. The simple algorithm is based on using constant coefficients for different heat transfer configurations to determine reduced and enhanced convection. The coefficients are taken directly from Walton[181] and they are not user-defined. (2) The detailed algorithm is based on Walton's[181] algorithm that correlates the convective heat transfer coefficient to the surface orientation and the temperature difference between the interior surface and the zone air. (3) The ceiling diffuser algorithm is based on empirical correlations of Fisher and Pedersen[182] between the supply air changes per hour (ACH) and the convective heat transfer coefficient (h_{con}). These correlations were reformulated in EnergyPlus to use the room outlet temperature as the reference temperature. (4) The trombe wall algorithm is used to model convection in a "trombe wall zone", i.e. the air space between the storage wall surface and the exterior glazing. In this study, the default interior convection algorithm of EnergyPlus i.e. the *detailed algorithm* was used.	Provides a single option and includes three heat components:[103] (1) For long wave radiation heat exchange among zone surfaces: uses a grey interchange model based on the "ScriptF" concept developed by Hottel and Sarofim.[183] This procedure relies on a matrix of exchange coefficients between pairs of surfaces that include all exchange paths between the surfaces. In other words, all reflections, absorptions and reemissions from other surfaces in the enclosure are included in the exchange coefficient, which is called ScriptF. The major assumptions are that all surfaces are grey and the radiation from these surfaces is diffuse. (2) For long wave radiation from internal sources: a radiative/convective split is entered for the heat introduced into the zone from equipment. The radiative part is distributed over the surfaces in a prescribed manner.[183] (3) For short wave radiation: the short wave radiation from lights and the transmitted solar radiation is distributed over the surfaces in the zone in a prescribed manner.[183]

Continued on next page

Table 4.2 – *Continued from previous page*

	Convection	Radiation
TRNSYS	Provides two options:[140] (1) The user defined option allows the user to input constant convective heat transfer coefficients for interior and exterior surfaces. The default convective heat transfer coefficient is 11 kJ/h.m^2.K for the interior surfaces and 64 kJ/h.m^2.K for the exterior surfaces. (2) Internal calculation of convective heat transfer calculation option calculates the convective heat transfer coefficient based on the temperature difference between the surface and the air near the surface. In this study, since the internal calculation option was available only for interior surfaces, the user-defined option was selected for the exterior walls. The default convective heat transfer coefficient for interior surfaces (11 kJ/h.m^2.K) was assigned for the inside surface of the floor.	Provides three options: (1) the standard model, (2) the simple model and (3) the detailed model. (1) The standard model is based on Seem's[184] star network which uses an artificial temperature node i.e. the star node. The star node is connected to the zone air node by convection and to the other wall and window elements by a combined radiative and convective heat component. (2) The simple model is a single node model that uses combined radiative and convective heat transfer coefficients. (3) The detailed model does not use an artificial star node. It calculates long wave radiative heat transfer separate from convection using view factors. In this study, the standard (Starnet) model was used.

In DOE-2, the heat transfer between the interior surfaces and the zone air is modeled by assigning a single massless fictitious air layer to the inside surface of each building envelope construction.[180] This fictitious air layer is then assigned an invariant thermal resistance that accounts for the combined effect of the inside radiation and convection on the surface.[180] The combined radiation and convection heat transfer on each inside surface is then calculated as part of the building envelope conduction heat transfer calculations with a single 1-D conduction heat transfer equation. For the inside film resistances (I-F-R) of the floors in the DOE-2 sealed boxes, the average of the cooling (0.92) and heating (0.61) mode air film resistances recommended by ASHRAE Handbook of Fundamentals were used.

In TRNSYS, the standard Starnet model was used in this study. In this model, each zone is represented with two nodes: (1) the Starnet node, and (2) the zone air node.[140] The heat transfer between the inside surfaces and the zone air then occurs in two steps: (1) between the inside surfaces and the Starnet node, and (2) between the Starnet node

and the zone air node. The heat transfer between the inside surfaces and the Starnet node includes: (1) the solar radiation and the long wave radiation generated from the internal objects such as people or furniture, (2) a combined convective and radiative heat flux, and (3) a user defined floor energy flow to the surface. The "combined convective and radiative heat flux" component corresponds to the equivalent sum of: (1) the radiative heat transfer between the inside surfaces, and (2) the convective heat transfer between the inside surfaces and the zone air. The heat transfer between the Starnet node and the zone air node occurs only by convection. This convection heat transfer represents the sum of the heat transfer to the zone air by (1) infiltration from outside, (2) ventilation from the outside, (3) convection from the internal gains (people, lights, equipment, etc.), and (4) connective airflow from the neighboring air nodes.

In the TRNSYS sealed boxes, there was no infiltration, no ventilation, no neighboring zone air node, no heat generating internal objects and no additional energy flow defined towards the floor. Thus, the heat transfer between the slab and the zone air ($Q_{slab/zair}$) included only the combined radiative and convective heat flux component between the slab and the Starnet node in these boxes. The convective part of this combined heat flux was defined by entering the default TRNSYS convection heat transfer coefficient for interior surfaces (11 kJ/h.m^2.K) for the floor. Using this input, TRNSYS calculated a combined radiative and convective heat resistance as described by Seem.[184]

In the EnergyPlus inside heat balance equation, the heat transfer between the inside surfaces and the zone air includes four heat transfer components. These are: (1) the shortwave radiation from solar and internal sources, (2) the long wave radiation exchange with other surfaces in the zone, (3) the long wave radiation from internal sources, and (4) the convective heat exchange with the zone air.[103] In the EnergyPlus sealed boxes modeled in this study, there were no windows (no solar gains) and no internal sources. Thus, the $Q_{slab/zair}$ included only two components: (1) the long wave radiation heat exchange between the floor and the other surfaces, and (2) the convective heat exchange between the floor and the zone air. For the radiation component of the $Q_{slab/zair}$, EnergyPlus

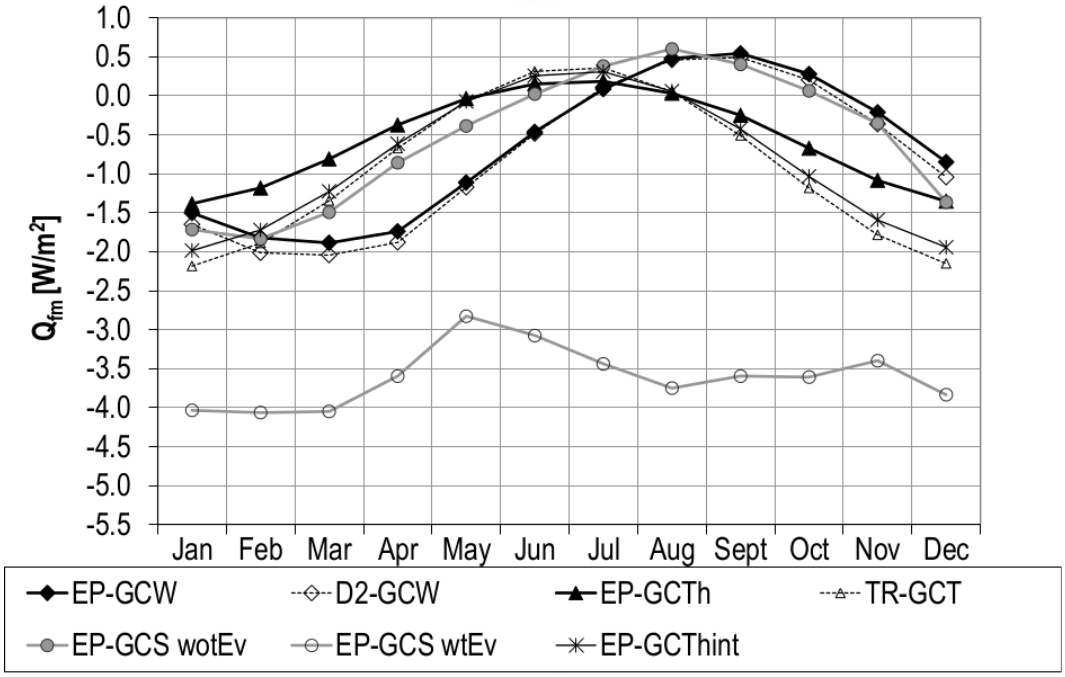

Figure 4.1: Monthly average floor heat fluxes of the Austin sealed box.

used a matrix of exchange coefficients between pairs of surfaces, which was developed by Hottel and Sarofim.[183] For the convection component, the default "detailed" inside convection model of EnergyPlus was selected. This model recalculated the convective heat transfer coefficients (h) at each time step based on the orientation of the surface and the temperature difference between the surface and the zone air, which resulted in varying convection coefficient (h) values during the simulation.[103]

In this study, Winkelmann's ground temperatures and underground construction were entered into DOE-2 (D2-GCW) and EnergyPlus (EP-GCW), and the resulting ground coupling loads in these two models were compared. The results showed that the EP-GCW model calculated slightly (0.1-0.3 W/m^2) lower floor heat fluxes than the D2-GCW model throughout the year (see Figs. 4.1-4.4). This variation resulted in slightly (0.2-0.4 GJ) lower annual ground coupling loads in the EP-GCW models than in the D2-GCW models (see the I-a arrows in Fig. 4.5).

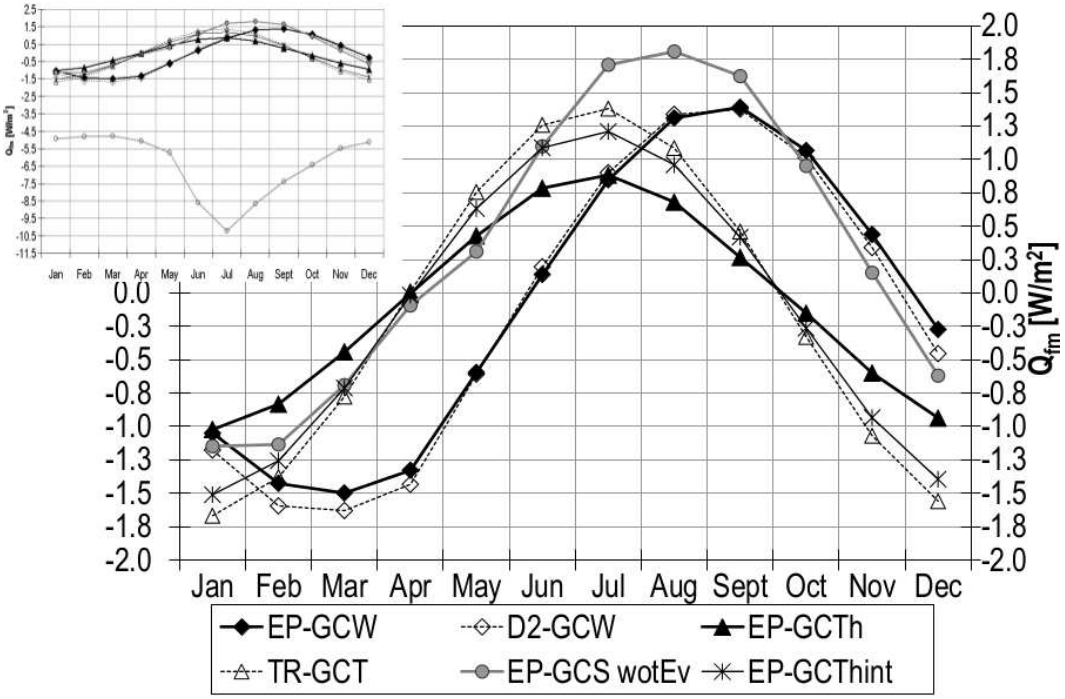

Figure 4.2: Monthly average floor heat fluxes of the Phoenix sealed box.

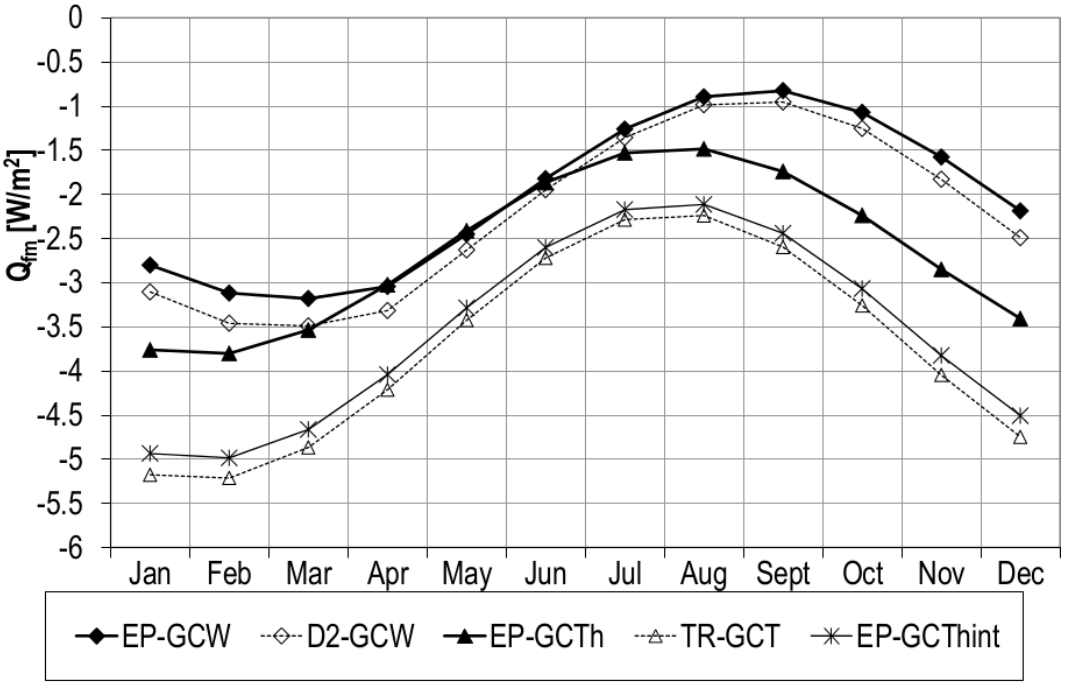

Figure 4.3: Monthly average floor heat fluxes of the Chicago sealed box.

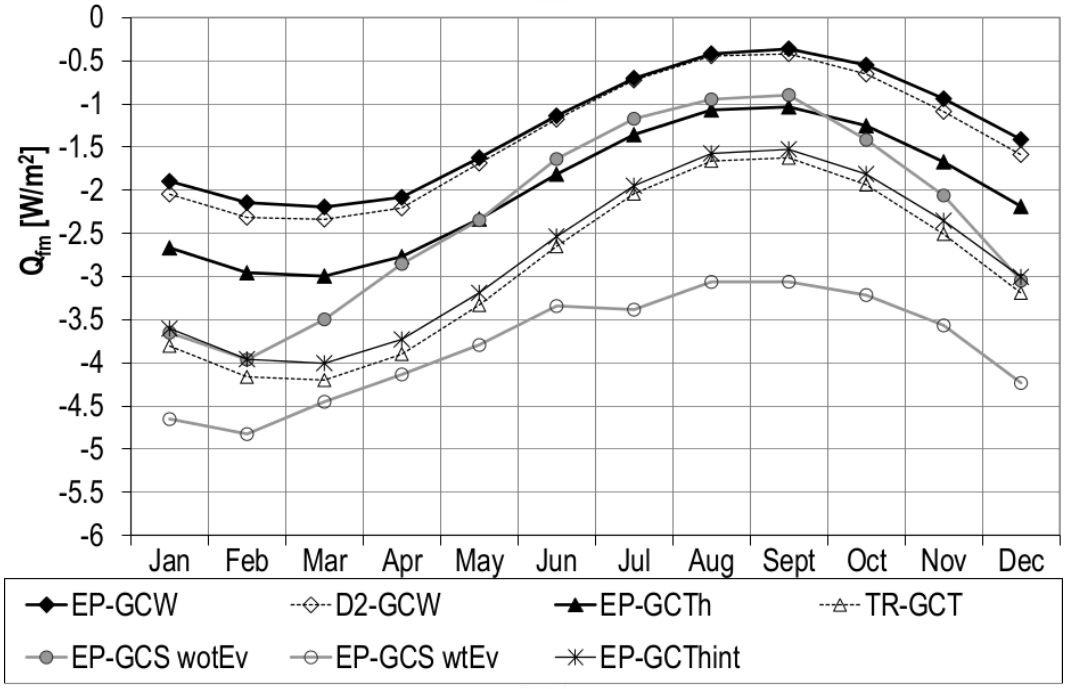

Figure 4.4: Monthly average floor heat fluxes of the Columbia Falls sealed box.

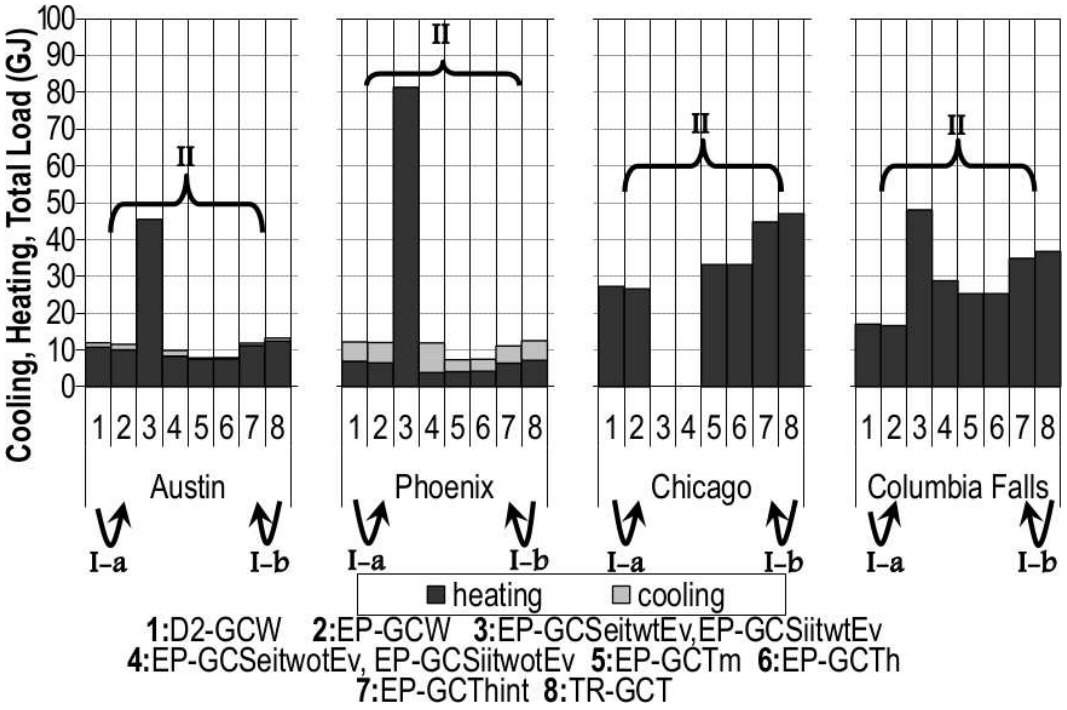

Figure 4.5: Cooling, heating and total thermal loads of the sealed boxes.

Among the radiation and convection models used in this study, those of EnergyPlus were the most detailed models. The D2-GCW models showing close floor heat fluxes to those of the EP-GCW models, therefore, indicated that the simple combined radiation and convection model of DOE-2 makes good estimations for $Q_{slab/zair}$ when the inside air film resistance (I-F-R) of 0.136 m^2.K/W(0.77 h.ft^2.°F/Btu) is used for the floor. Besides the differences between the inside radiation and convection models of DOE-2 and EnergyPlus programs, there were two other factors that caused the 0-0.2 W/m^2 heat flux variation between the D2-GCW and EP-GCW models. First, the zone air temperatures (T_{zair}) fluctuated in DOE-2 throughout the year; whereas they were constant at 23°C in EnergyPlus all year (Fig. 4.6). Second, DOE-2 assumed that the inside surface temperatures of the floor (T_{is}) are equal to the zone air temperatures[180]; whereas EnergyPlus calculated the T_{is} at each time step as part of its inside heat balance calculations.[103] These differences in interior boundary conditions between the D2-GCW and EP-GCW models caused these two models to have different slab-soil interface temperatures ($T_{slab/soil}$). Fig. 4.7 shows the $T_{slab/soil}$ of the D2-GCW and EP-GCW models for the sealed boxes.

The $Q_{slab/zair}$ calculation differences between the EnergyPlus and TRNSYS programs were also quantified in this study. The $T_{slab/soil}$s of the TR-GCT models were entered into EnergyPlus (EP-GCT) and the variation in the ground coupling load was quantified. The results showed that the EP-GCT models calculated 5-14 GJ lower ground coupling loads than the TR-GCT models with a 0-1.2 W/m^2 monthly average variation (see Figs. 4.1-4.4 and I-b arrows in Fig. 4.5). The monthly average differences between the EP-GCT and TR-GCT fluxes were particularly higher in the cold (0.6-1.2 W/m^2) and temperate (0.8-1.4 W/m^2) climates than in the hot-humid (0-0.8 W/m^2) and hot-dry (0-0.6 W/m^2) climates. Thus, the annual ground coupling load difference between the EP-GCT and the TR-GCT models ended up being higher in the cold (11 GJ) and temperate (14 GJ) climates than in the hot-humid (5 GJ) and hot-dry (5 GJ) climates.

An intermediary model was introduced between the EP-GCT and TR-GCT models, the EP-GCTint, in order to further analyze the high ground coupling load variation between

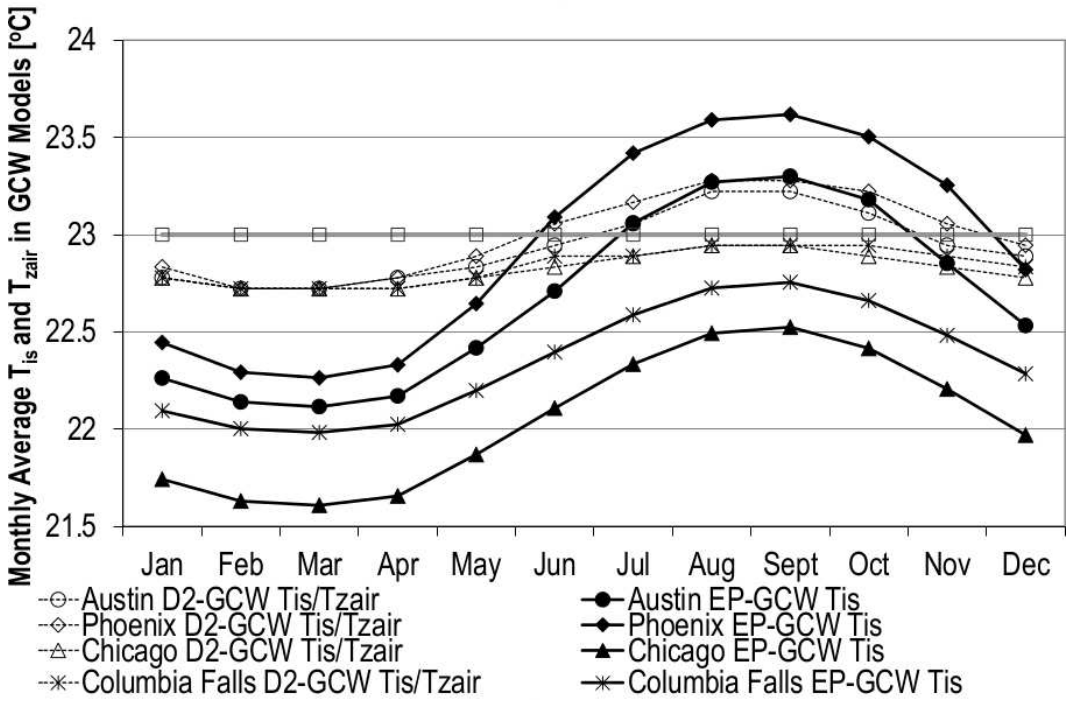

Figure 4.6: Monthly average inside surface temperatures (T_{is}) and zone air temperatures (T_{zair}) of the Winkelmann floors of the sealed boxes.

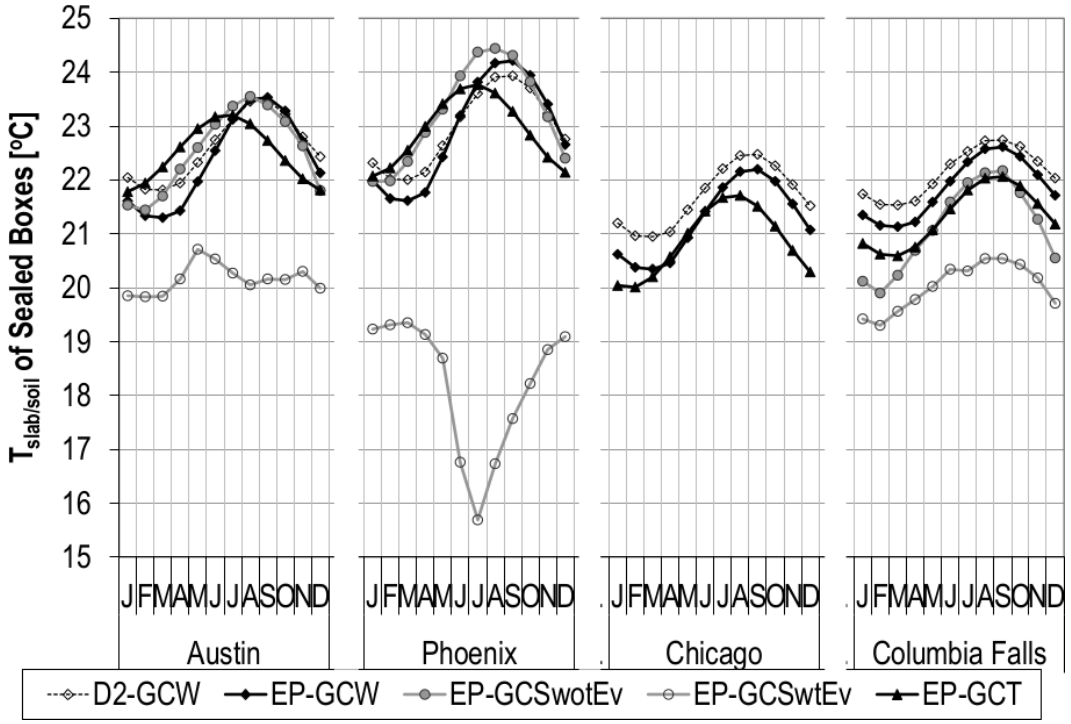

Figure 4.7: The slab-soil interface temperatures ($T_{slab/soil}$) of the sealed boxes.

these two models(see Fig. 4.5). This intermediary model had the same interior convection coefficients with the TRNSYS (TR-GCT) model, but it did the interior radiation heat transfer calculations using the detailed interior radiation algorithm of the EnergyPlus (EP-GCT) model. Thus, it allowed us to isolate and compare the radiation and convection heat transfer components of the ground coupling load difference between the EP-GCT and the TR-GCT models. The EP-GCTint models showed closer ground coupling loads to the TR-GCT models (within -12%) than to the EP-GCT models (within +50%) in all four climates. This result showed that the high variation between the ground coupling loads of the EP-GCT and TR-GCT models was caused primarily by the differences in the inside convection heat transfer calculations of the EnergyPlus and TRNSYS programs. This difference was explained by the 63-88% higher convective heat transfer coefficients used in TRNSYS than those calculated by EnergyPlus. Fig. 4.8 presents the monthly averages of the inside convection heat transfer coefficients of the EP-GCT models in comparison with those of the TR-GCT models. These findings revealed that the surface convection properties (particularly the h value) of the floor can have a significant effect on the calculated ground coupling load in low-load conditions.

4.1.1.2 Step 2: Heat Transfer between the Soil and the Slab

At this step, the conductive heat transfer between the soil and the slab ($Q_{soil/slab}$) is compared between Winkelmann's model, the Slab model and the TRNSYS slab-on-grade model for the sealed boxes modeled in EnergyPlus. The following are the compared models:

1) The TRNSYS slab-on-grade model with EnergyPlus (EP-GCT)

2) The Slab model with EnergyPlus (EP-GCS)

3) Winkelmann's slab-on-grade model with EnergyPlus (EP-GCW)

The ground coupling load differences between these three models were quantified and explained for the sealed boxes by referring to their primary assumptions and the calculation methods. The results are shown in Fig. 4.5 with column 2. This analysis was started by examining the parameters that affected the conductive heat transfer between the soil and the slab ($Q_{soil/slab}$). These parameters were: (1) the inside surface temperatures of the

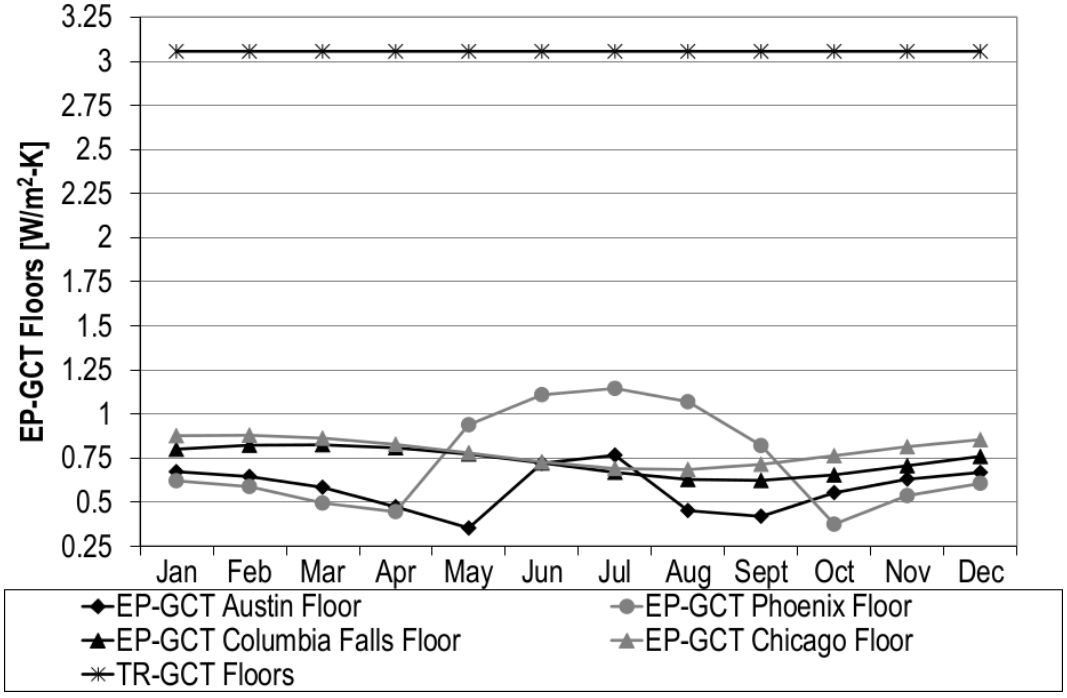

Figure 4.8: The convection coefficients of the TRNSYS floors.

floor (T_{is}), (2) the ground temperatures that the slab was exposed to ($T_{slab/soil}$), and (3) the overall heat transfer coefficient of the floor without the air film (U_{floor}). The U_{floor} was assigned as 2.647 W/m^2.K in all of the three slab-on-grade models. The calculated inside (T_{is}) and outside($T_{slab/soil}$) temperatures of the slab, however, differed significantly between these models.

The inside temperatures (T_{is}) of the EP-GCT, EP-GCS and EP-GCW floors depended on the assumptions and calculation methods of the aboveground heat transfer calculator program (which in this case is EnergyPlus) for inside convection and radiation (see Step 1). Since the aboveground heat transfer calculator program was the same in all of the three models compared at Step 2, the differences in the T_{is} of these models were triggered primarily by the ground temperatures ($T_{slab/soil}$) that the slabs were exposed to. The soil-slab interface temperatures ($T_{slab/soil}$) of these floors then depended on the assumptions and the calculation methods of the slab-on-grade models used to simulate the floor, the soil and the heat transfer between them. Table 4.3 presents these assumptions and calculation

methods in comparison with each other and Fig. 4.7 shows the resulting $T_{slab/soil}$ in these models.

Table 4.3: Comparison of Winkelmann's, Slab and TRNSYS slab-on-grade models

	Winkelmann's Slab-on-grade Model (...-GCW)	Slab Model of EnergyPlus (...-GCS)	TRNSYS Multizone Slab-on-grade Model i.e. Type 49 (...-GCT)
Calculation Method	1-D conduction heat transfer calculations are made by the energy simulation program. The inputs of the program are derived from the findings of an early two-dimensional finite difference study conducted by Huang *et al.*[135]	Uses a numerical method[138] to solve a boundary value problem on the 3-D heat conduction equation. The boundaries were interior slab surface, far-field soil, deep ground, and ground surface. The ground heat transfer calculation is partially decoupled from the thermal zone calculation. The outside face temperature of the floor is the "separation plane" between the 1-D aboveground and 3-D belowground heat transfer calculations	Uses a simple iterative analytical method to solve the resulting interdependent differential equations of a 3-D finite difference soil model at each time step.[103] In this method, the subroutine solves its own mathematical problem and does not rely on nonstandard numerical recipes that must be attached to the subroutine. This method is time-step independent; therefore, it converges in multizone simulations.
Primary Assumptions	Primary ground coupled heat flux occurs from the exposed perimeter of the underground construction. The heat flux is correlated with the perimeter length (P). It is a two-dimensional approximation of three-dimensional foundation heat flux. Ignores lateral heat flow at the building corners.	The heat flux is correlated with the area over perimeter ratio (A/P). Floor heat transfer rates depend on the shape and the size of the slab. Thermal conductivity of the soil and ground surface conditions affect floor heat transfer rates, whereas thermal diffusivity, far-field boundaries and deep ground conditions do not. The time scales of ground heat transfer processes are much longer than the other building heat transfer processes.	The system (including the soil and the slab) consists of cubic nodes which have six unique heat transfers to analyze. The edge of the floor surface is adiabatic i.e. no heat transfer occurs between the edges of the slab and the surroundings
Floor Model	An effective U-value (U_{eff}) is assigned to the underground construction to adjust the floor heat fluxes to a constant zone air temperature. This U_{eff} value is calculated from the perimeter conductance values Huang *et al.*[135] listed.	The original U-value of the underground construction is used.	The original U-value of the underground construction is used.

Continued on next page

Table 4.3 – *Continued from previous page*

	Winkelmann's Slab-on-grade Model (...-GCW)	Slab Model of EnergyPlus (...-GCS)	TRNSYS Multizone Slab-on-grade Model i.e. Type 49 (...-GCT)
	Fictitious underground layers are modeled including a 0.3 m soil layer, a massless insulation layer and a concrete slab. This new construction has a U-value equal to the calculated U_{eff}. Limited to the foundation depths and insulation configurations that Huang *et al.*[135] studied.	The original layers of the underground constructions are used. The slab properties (density, conductivity and specific heat), the slab shape (rectangle or L) and size are the important inputs of the model. Applies to any floor construction; however, shows convergence problems for certain configurations.	The original layers of the underground constructions are used. Resistance of footer insulation is the only floor input parameter. The floor construction is defined in the aboveground Multizone Building Model of TRNSYS i.e.Type 56.
Soil Model	The thermal conductivity, specific heat and the density of the soil up to 0.3 m depth and the weather data file (TMY) are the input parameters.	Domain dimensions and grid spacings, weather data file (TMY), the density, conductivity and specific heat of the soil, ground surface properties, deep ground boundary condition, evaporative loss at ground surface, shadowing and building height are the input parameters.	The number of nodes and the size/volume of the near-field (2-dimensional map of the soil surface), the node temperature calculation method for the far-field, the density, conductivity and specific heat of the soil, average surface soil temperature, amplitude of soil surface temperature, the day of minimum surface temperature are the input parameters.
	Ground temperatures are calculated by DOE-2 using the Kasuda correlation.[136]	Ground temperatures are the outputs of the Slab model. These temperatures are then entered into EnergyPlus as inputs.	Ground temperatures are the outputs of the Type 49 model. These temperatures are then used by the aboveground multizone building model of TRNSYS i.e.Type 56.
	The fictitious insulation layer faces the entered ground temperatures. Ground temperatures are location specific but same for all underground surfaces in a certain location.	The actual concrete floor faces the calculated ground temperatures. Slab calculates separate, case-specific ground temperatures for each underground surface.	The actual concrete floor faces the calculated ground temperatures. Type 49 calculates separate, case-specific ground temperatures for each underground surface.

Among the studied slab-on-grade models, the TRNSYS slab-on-grade model was the most detailed one (see Table 4.3). This model assumes that the slab and the soil consist of cubic nodes which have six unique heat transfers to analyze. A simple iterative analytical method then solves the interdependent differential equations of a 3-D finite difference soil model at each time step. In this study, the soil-slab interface temperatures ($T_{slab/soil}$) of the test houses modeled in TRNSYS (TR-GCT) were entered into EnergyPlus hourly

(EP-GCTh) and monthly (EP-GCTm). The ground coupling loads obtained with these two coupling methods were found to be very similar (within 6%) in all studied climates (see Fig. 4.5). This finding showed that ground temperatures do not show significant hourly variation and; therefore, monthly coupling of aboveground and belowground heat transfer calculations are reasonable. This finding was in agreement with an important assumption of the Slab model, which states that the time scales of the ground heat transfer processes are much longer than those of the building heat transfer processes (see Table 4.3). Thus, the monthly average floor heat fluxes(Q_{fm}s) were used to compare the slab-on-grade models with each other in this step of the study.

In the EP-GCT models, it was observed that there is a clear relationship between the Q_{fm}s and the monthly average outside air temperatures (T_{am}s) (see Figs. 4.1-4.4 and 4.9). This relationship, however, varied depending on the insulation configuration of the floor. For the uninsulated floors in the hot-humid and hot-dry climates, for instance, the peak Q_{fm}s and the peak T_{am}s occurred in the same month in the EP-GCT models (see Figs. 4.1-4.4). The maximum floor heat gains occurred in the hottest month (July) and the maximum floor heat losses occurred in the coldest month (January) (see Figs. 4.1 and 4.2). This was explained with the two assumptions of the TRNSYS slab-on-grade model. First, the average surface soil temperature was assumed to be equal to the annual average air temperature in TRNSYS. Second, the amplitude of the soil surface temperature was assumed to be equal to the one half of the maximum monthly average air temperature minus one half of the minimum monthly average air temperature. The vertical floor insulation used for the temperate and cold climates delayed the peaks of the Q_{fm}s in the EP-GCT models and the time delay between the peaks of the Q_{fm}s and T_{am}s in this model increased with increasing insulation depth in these climates (see Figs. 4.3 and 4.4). For instance, in the EP-GCT models that had 2 ft deep insulation in Chicago, the maximum Q_{fm} to the ground occurred one month later than the minimum T_{am} (see Fig. 4.3). In the EP-GCT models that had 4 ft deep insulation in Columbia Falls, however, the maximum Q_{fm} to the ground occurred two months later than the minimum T_{am} (see Fig. 4.4).

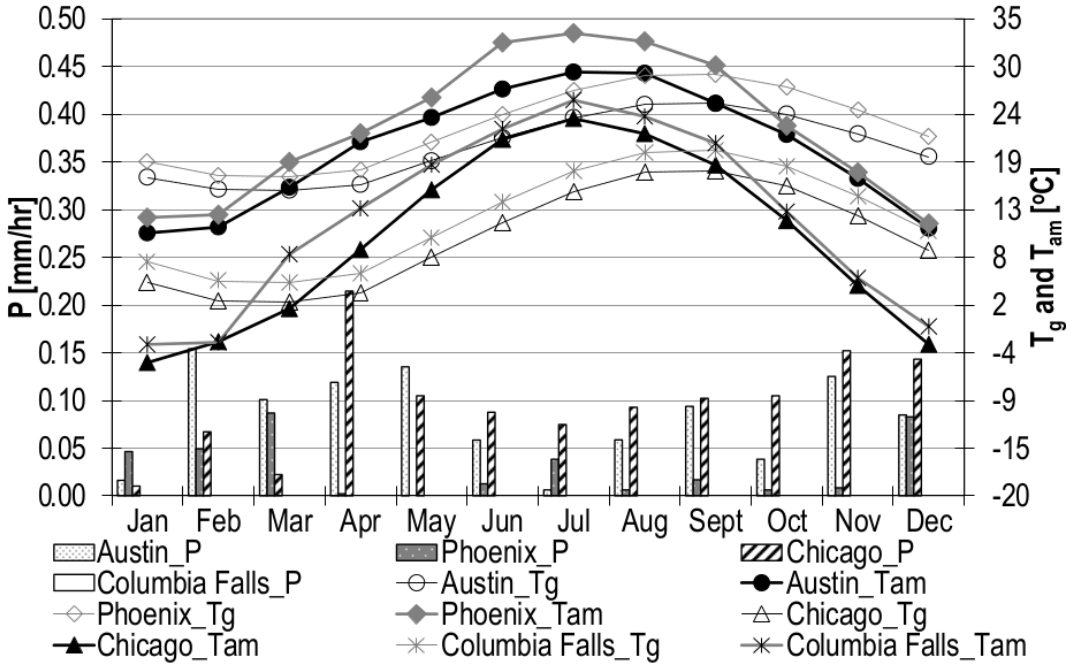

Figure 4.9: The monthly average precipitation (P), ground temperatures (T_g) and outside air temperatures (T_{am}) in Austin, Phoenix, Chicago and Columbia Falls.

The Slab model of EnergyPlus was the second most detailed slab-on-grade heat transfer model discussed in this study and it used a numerical method to solve a boundary value problem on the 3-D heat conduction equation and produced monthly slab-soil interface temperatures. These temperatures were then entered into EnergyPlus as the exterior boundary temperatures of the floor and were used in the aboveground 1-D heat conduction calculations of EnergyPlus. This coupled EnergyPlus-Slab model was represented with "EP-GCS" in this study.

Our results showed that, for the sealed boxes at 23°C constant zone air temperature, the internal (EP-GCSiit) and external (EPGCSeit) iterations of EnergyPlus and Slab programs showed exactly the same ground coupling loads in all climates (see Fig. 4.5). The Slab program gave an error for the required insulation configuration for temperate climates (0.6 m deep R-10 vertical insulation) by reporting a contradictory error note (see Fig. 4.3). The error note indicated that an invalid insulation depth was entered for the slab, whereas the entered insulation depth (0.6 m) was one of the values suggested by the program. When

all available insulation depths were tried for this climate (0.2, 0.4, 0.6, 0.8, 1, 1.5, 2, 2.5, 3), it was found that the Slab model could not model the R-10 vertical insulation with depths less than 1 m. This error was attributed to an internal limitation of the Slab model for providing convergence. It was determined that it is necessary to overcome this limitation before the EP-GCS model is used for residential code compliance in temperate climates.

When the evapotranspiration flag was off, the EP-GCS models (EP-GCSwotEv) exhibited 0.3-1 W/m^2 higher Q_{fm} peaks to the ground and 0.2-1.4 W/m^2 higher Q_{fm} peaks into the space when compared to the EP-GCT models (see Figs. 4.1-4.4). This was primarily because the EP-GCSwotEv models showed lower minimum ground temperatures in winter and higher maximum ground temperatures in summer by 0.1-0.7°C when compared to the EP-GCT models (see Fig. 4.7). Consequently, the EP-GCSwotEv models showed 2.0-4.4 GJ higher annual ground coupling loads than the EP-GCT models for identical sealed boxes (see Fig. 4.5).

It was observed that, for the uninsulated floors in the hot climates, the peaks of the Q_{fm}s in the EP-GCSwotEv model were a month delayed when compared to the peaks of the T_{am}s. Since the peak Q_{fm}s of the EP-GCT models occurred at the peak outside air temperatures in these climates, the Q_{fm}s of the GCSwotEv models was also a month late when compared to those of the EP-GCT models. This was because the Slab model of EnergyPlus shifted the ground temperatures by a phase lag to account for the effect of the soil thermal mass.[134] For the insulated floor in the cold climate, however, the peak Q_{fm}s of the EP-GCSwotEv and the EP-GCT models occurred in the same months (see Fig. 4.4).

In the finite difference calculations of the Slab model, insulation is represented by an additional surface resistance on the exterior of the floor cells.[134] This additional resistance reduces the peak heat gains and losses through the floor resulting in smaller peak to peak amplitudes in the insulated conditions of the same floors. Our results showed that the peak to peak amplitudes of the Q_{fm}s in the EP-GCSwotEv models were 1.5 times higher than those in the EP-GCT models for both the insulated and uninsulated floors (see Figs. 4.1, 4.2 and 4.4).

According to Bahnfleth[134], the ground surface condition is the most significant boundary condition for the floor heat transfer and evaporative transpiration (evapotranspiration) is a significant parameter for this boundary. The Slab program models a potential evapotranspiration case which accounts for a number of naturally occurring situations, most often through the action of vegetation.[134] In this case, grasses and other similar ground covers, when well watered, are assumed to transpire moisture into the atmosphere at near the potential rate even when the ground surface is relatively dry.[134] According to Bahnfleth,[134] the evapotranspiration model of Slab takes these processes into account and brackets the range of boundary evapotranspiration effects. He claims that this model is, therefore, a useful asymptotic model that does not require specification of moisture conditions at the surface.[134] Fig. 4.9 shows the annual total precipitation of the four cities studied in this paper. It was realized that although the weather file showed zero annual precipitation for Columbia Falls, the Slab model identified a difference in ground coupling load with the use of the evapotranspiration model (see Fig. 4.5). This result supported Bahnfleth's statement by showing that the evaporative transpiration case modeled by the Slab model is independent from the precipitation level.

In our runs for the sealed boxes, evapotranspiration decreased the mean ground temperature several degrees below the mean zone air temperatures resulting in higher heat losses from the floor (see Figs. 4.1, 4.2, 4.4 and 4.7). For the floors located in Austin, Phoenix and Columbia Falls, a drastic decrease occurred in the $T_{slab/soil}$ values in July and August, which happened to be the hottest months (see Figs. 4.7 and 4.9). This result showed that the peak floor heat losses observed in the EP-GCSwtEv models (see Figs. 4.1, 4.2 and 4.4) in summer were triggered by the high outside air temperatures. This finding also explained the peak basement heat losses that Andolsun *et al.*[161] obtained in summer using the Basement preprocessor of EnergyPlus in an earlier study.

The EP-GCSwtEv models showed significantly higher Q_{fm}s when compared to the EP-GCT models (see Figs. 4.1, 4.2 and 4.4). In earlier test runs, it was also observed that the Slab program often resets the slab thickness to a higher value to achieve the

user-defined internal convergence. This problem resulted in inconsistent slab thicknesses between the aboveground and belowground models of EnergyPlus. These findings showed that the Slab model of EnergyPlus needs urgent improvements. Particularly the evapotranspiration model of Slab needs to be validated through experimental studies. Thus, it was determined that it is important to avoid using the Slab model in residential code compliance calculations until the necessary validations and improvements are made on this model.

When the slab-soil interface temperatures ($T_{slab/soil}$) shown in Fig. 4.7 for Austin were compared with those measured by Kim[47] for Bryan, Texas, two primary points were observed. First, the model that showed the closest peak $T_{slab/soil}$ month to that in the measured data was the Slab model with EnergyPlus (EP-GCS). Second, the Slab model with evapotranspiration flag on (EP-GCSwtEv) showed a quick drop in $T_{slab/soil}$ values right after May similar to that was observed with the measured data. The $T_{slab/soil}$ values then stayed almost constant in the EP-GCSwtEv model through September and October which was also similar to that occurred in the measured data. These findings showed the EP-GCS model has significant potential in estimating the monthly variation of ground temperatures close to reality. It was concluded that further studies are required to improve this potential by improving the magnitudes produced by this model particularly with the evapotranspiration flag on.

Winkelmann's method was a simplified slab-on-grade heat transfer modeling method based on the earlier findings of Huang *et al.*[135] Huang *et al.*[135] did 2-D finite difference calculations in the 1980s to calculate the daily heat fluxes at each interior node point of a representative one-foot vertical section of the foundation and surrounding soil. They then derived the total heat fluxes through the 28 ft$\times$55 ft foundation of the prototypical house by multiplying the fluxes at each node point of the vertical section by the length of that nodal condition. The resultant foundation fluxes for the 65 different below grade configurations in the 13 cities were stored in utility files.[135] These fluxes were stored for 123 three-day periods of the year to fit the memory limitations of the Function feature in

the LOADS subprogram of DOE-2.1C. Linear interpolations were then done between the sequential three-day average fluxes in DOE-2 in order to produce smoothly varying fluxes for each hour.[135]

Huang *et al.*[135] determined the daily floor heat fluxes for each foundation configuration by assuming 70°F constant zone air temperature all year. The 70°F was the default indoor air temperature that DOE-2 LOADS uses(T_{LOADS}). Huang *et al.*[135] also found that there is a linear relationship between the variation in the underground heat flux ($\triangle Q = Q_{mod} - Q_{LOADS}$) and the variation in the constant zone air temperature ($\triangle T = T_{mod} - T_{LOADS}$). They defined this relationship as a linear function the slope of which equaled to the effective conductivity of the slab (U_{eff}). They then calculated the U_{eff} value of each slab configuration using Eq. 4.3.

$$U_{eff} = \frac{Q_{mod} - Q_{LOADS}}{(T_{mod} - T_{LOADS})X_A} \tag{4.3}$$

In Winkelmann's method, these U_{eff} values are currently entered into DOE-2 as an input and used in the SYSTEM subprogram in DOE-2. In SYSTEMS, the U_{eff} values correct the floor heat fluxes calculated in DOE-2 LOADS to account for the constant zone air temperatures different than 70°F. For slabs, the floor heat transfer calculations of Winkelmann's model are complete after this correction, and no further correction is made to take the varying indoor temperatures into consideration. In the sealed boxes modeled in this study, the zone air temperatures were set to 23°C (73.4°F) all year. Thus, the possible errors of Winkelmann's slab-on-grade model for varying zone air temperatures were avoided for these boxes. There was, however, another limitation of Winkelmann's slab-on-grade model, which was still valid for the sealed boxes. The 2-D finite difference calculation of Huang *et al.*[135] was made on a rectangular prototype building with unequal sides; therefore, the obtained U_{eff} values were expected to be somewhat off for the square slabs of the sealed boxes modeled in this study. When Winkelmann's slab-on-grade model was used in EnergyPlus (EP-GCW), the same underground construction layers used in the

D2-GCW model were assigned to the floor. Thus, the resistances of the fictitious layer, soil, slab and carpet were identical to those in the D2-GCW model. Only the air film resistances of the EP-GCW models were different than those of the D2-GCW models due to the varying inside convection coefficients in EnergyPlus.

For the uninsulated sealed boxes in Austin and Phoenix, the EP-GCW models showed 3.6 GJ and 4.5 GJ higher ground coupling loads when compared to the EP-GCT models respectively (Fig. 4.5). For the insulated floors in Chicago and Columbia Falls, however, the ground coupling loads of the EP-GCW boxes were 6.6 GJ and 8.7 GJ lower than those of the EP-GCT models respectively (Fig. 4.5).

It was observed that, for the uninsulated floors in the hot climates, the EP-GCW models showed very similar (with a maximum of 0.5°C difference) soil-slab interface temperatures ($T_{slab/soil}$) to those of the EP-GCT models with a two month time delay (Fig. 4.7). This then caused the Q_{fm}s of the EP-GCW models to be similar (with a maximum of 0.6 W/m^2 difference) but two month delayed when compared to those of the EP-GCT models (see Figs. 4.1 and 4.2). These delayed $T_{slab/soil}$s and Q_{fm}s in the EP-GCW models were attributed to the deep ground temperatures (T_gs) calculated by DOE-2 using the Kasuda correlation.[137] Fig. 4.9 shows that these deep ground temperatures (T_gs) were two months delayed when compared to the monthly average outside air temperatures (T_{am}s). These findings indicated that if an internal back shifting is done on the floor heat fluxes of Huang *et al.*,[135] significant improvement can be obtained in annual ground coupling loads under constant zone air temperatures. It was also observed that, for the insulated floors, the EP-GCW models made close estimates for the peak months (with a maximum of 1 month shift) to those of the EP-GCT models (see Figs. 4.3 and 4.4). The peak months of the EP-GCW models approached those of the EP-GCT models with increasing insulation depth.

The peak-to-peak amplitudes of the EP-GCW and EP-GCT heat fluxes were closer for the insulated floors than for the uninsulated floors (see Figs. 4.1-4.4). For the uninsulated floors in hot-humid and hot-dry climates, the peak-to-peak amplitudes of the EP-GCW fluxes were 1.4 times higher than those of the EP-GCT fluxes (see Figs. 4.1 and 4.2). For

the insulated floors in temperate and cold climates, however, the EP-GCW models showed identical peak to peak amplitudes with the EP-GCT models (see Figs. 4.3 and 4.4). This finding showed that, the peak-to-peak amplitudes of the heat fluxes calculated by Huang *et al.*[135] for uninsulated floors need to be reduced by ~1.4 times for better ground coupling load estimations under constant zone air temperatures.

4.1.2 Fully Loaded Test Houses

Building thermal load is an important parameter that affects both the magnitude and the direction of the estimated heat flux through the floor. Building load affects the zone air temperatures (T_{zair}s). The zone air temperatures (T_{zair}s) then affect the inside surface temperatures of the floor (T_{is}), which is one of the primary parameters of conductive heat transfer through the floor. DOE-2, EnergyPlus and TRNSYS programs are known to have calculation differences for both aboveground and belowground load components, which result in different annual thermal load estimations for identical conditions.[149,157]

In this part of the study, an unconditioned attic, wall and ceiling heat transfer, windows, doors and shades, lights and equipment and infiltration were added to the sealed boxes. As a result, four fully loaded houses located in hot-humid (Austin), hot-dry (Phoenix), temperate (Chicago) and cold (Columbia Falls) climates were obtained. First, these houses were modeled with an adiabatic floor that did not allow conductive heat transfer through the floor and the differences in the thermal load estimates of DOE-2, EnergyPlus and TRNSYS programs were quantified excluding the effect of ground coupling. Second, the adiabatic floors of these houses were converted into standard heat transfer surfaces exposed to the ground and the differences between the results of these programs were quantified including the effect of slab-on-grade heat transfer.

Fig. 4.10 shows the thermal loads of the fully loaded houses modeled in DOE-2, EnergyPlus and TRNSYS programs in the ground isolated condition. For these houses, the EnergyPlus results differed from the DOE-2 results by 0-31% in cooling load and 3-15% in heating load (Fig. 4.10). The magnitude of the difference between the load estimates of the DOE-2 and EnergyPlus programs was not proportional to the magnitude of the load.

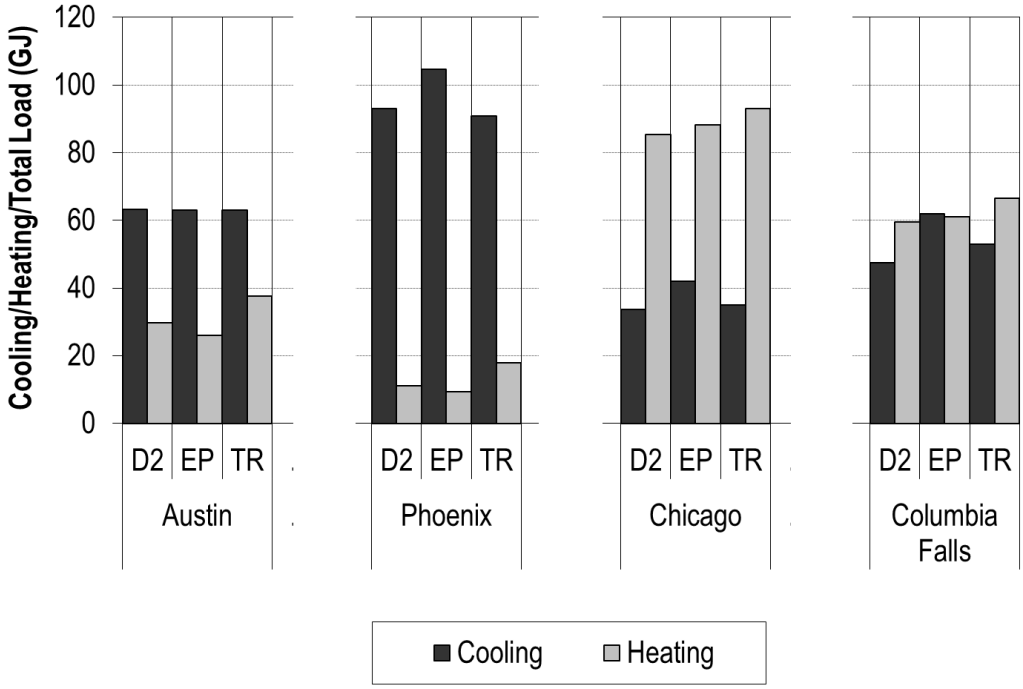

Figure 4.10: The cooling and heating loads of the ground isolated fully loaded test houses.

Thus, the percentage difference between the results of the programs varied from climate to climate. For instance, the heating load estimates of EnergyPlus differed from those of DOE-2 more in hot climates (13-15%) than in temperate and cold climates (3%). Similarly, the cooling load estimates of EnergyPlus program differed from those of DOE-2 more in temperate and cold climates (25-31%) than in hot climates (0-13%).

Based on this fact, our findings were compared with the findings of the studies conducted in similar climates. In an earlier study, Henninger and Witte[149] had compared the results of DOE-2 and EnergyPlus programs in "cold clear winters and hot dry summers" using the 13 ground isolated test cases of ASHRAE Standard 140. They had found that EnergyPlus results varied from those of DOE-2 by 7-32% in cooling load and by 4-13% in heating load. Our findings for the cooling load variation in hot-dry summers (13%) and the heating load variation in cold winters (3%) were within the range presented by Henninger and Witte.[149]

In the ground isolated condition, one of the primary reasons for the differences in

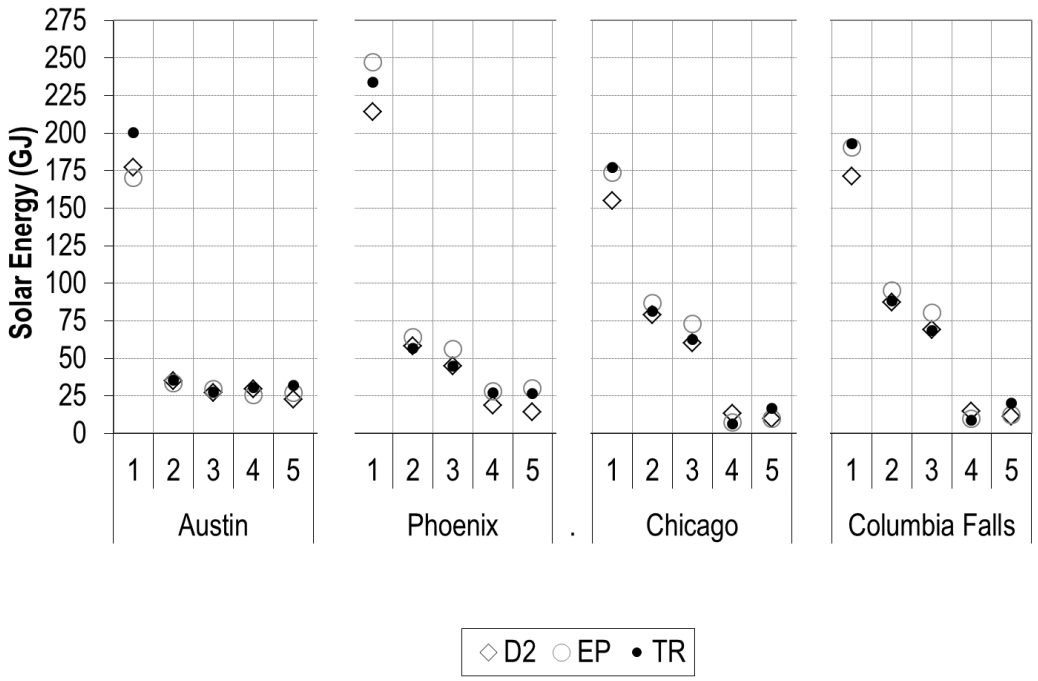

Figure 4.11: The total incident, transmitted and absorbed solar gains of the fully loaded test houses. 1: Total incident solar, 2: transmitted solar without the shades, 3: transmitted solar with the shades, 4: absorbed solar without the shades, and 5: absorbed solar with the shades.

thermal load estimates of DOE-2 and EnergyPlus programs was the different window solar heat gains calculated by these programs from identical Window 5 inputs. EnergyPlus showed generally higher (11-15%) total solar incidents on windows than DOE-2 did with the exception of the Austin house, which was under an overcast sky most of the year (see the 1^{st} columns in Fig. 4.11). These total solar incidents included direct and diffuse solar incidents. The direct solar incidents on windows were very similar (within 1%) in the DOE-2 and EnergyPlus programs (see Fig. 4.12). The diffuse solar incident on windows, however, showed 6-33% variation from DOE-2 to EnergyPlus (see Fig. 4.12).

For the calculation of the solar incidents on windows, DOE-2 read both the direct and the diffuse horizontal solar radiation values from the weather file and modified them considering the tilt of the surface, the sun's position, cloud cover and the fraction of the hour that the sun was up.[180] EnergyPlus, however, calculated each of the direct and

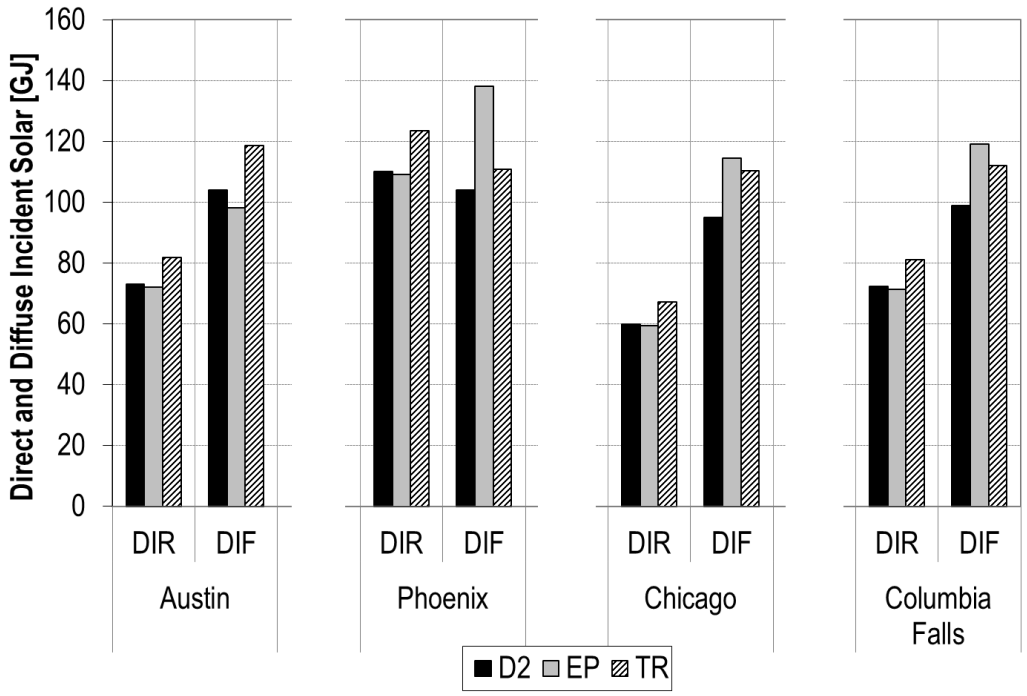

Figure 4.12: The direct and diffuse incident solar on windows in the fully loaded test houses.

diffuse horizontal solar incidents rather than importing them from the weather file. For the calculation of direct horizontal solar incident, EnergyPlus used ASHRAE's Clear Sky model which uses the extraterrestrial radiant flux values and the relative mass of the atmosphere.[70] For the calculation of the diffuse horizontal solar incident, EnergyPlus then used an anisotropic sky radiance distribution model based on the measurements of Perez *et al.*[185]. This model included three superimposed distributions: (1) an isotropic distribution that covers the entire sky dome, (2) a circumsolar brightening centered at the position of the sun, and (3) a horizon brightening.

The transmitted solar gains through the glazing layers were 9-11% higher in EnergyPlus than in DOE-2 in all climates except in the hot-humid climate in Austin (see the 2nd columns in Fig. 4.11). The solar energy absorbed by the glazing layers and transferred to the zone were 12-50% higher in EnergyPlus than in DOE-2 (see the 4th columns in Fig. 4.11). The introduction of interior shades to these windows further increased the

discrepancies between the solar gains calculated by these programs in all climates. For instance, the EnergyPlus interior shades absorbed a user-defined percentage (in this case 1% to minimize difference between programs) of the solar energy transmitted through the glazing. They then transferred this heat by convection into the zone air and into the air gap between the shade and the adjacent glass. These shades also transferred heat back into the zone air by IR radiation and reflected some of the IR radiation back onto the adjacent glazing layers. The introduction of these shades with 80% transmittance finally resulted in a 12-16% decrease in annual transmitted solar gains and 5-28% increase in annual absorbed solar gains in EnergyPlus (see the 3rd and the 5th columns in Fig. 4.11). In DOE-2, however, the interior shades with 80% transmittance reduced both the transmitted and the absorbed annual solar gains by 20% (see the 3rd and the 5th columns in Fig. 4.11). These findings explained the generally higher cooling loads in EnergyPlus when compared to those in DOE-2 in the ground isolated condition (Fig. 4.10).

The solar incidents on windows calculated by TRNSYS were similar to those calculated by EnergyPlus within 5% except in the Austin house (see the 1st columns in Fig. 4.11). The absorbed solar gains in TRNSYS were also within 19% of those in EnergyPlus and showed very high (up to 51%) differences from those in DOE-2 (see the 4th columns in Fig. 4.11). The transmitted solar gains in TRNSYS were, however, generally lower (6-12%) than those in EnergyPlus and were within 3% of those DOE-2 (see the 3rd columns in Fig. 4.11). Since the magnitudes of the transmitted solar gains were higher than the absorbed solar gains in all three programs, TRNSYS showed closer overall window heat gains to DOE-2 than to EnergyPlus in all houses. This explained the close cooling loads of the DOE-2 and TRNSYS models in all climates. These discrepancies between the DOE-2, EnergyPlus and TRNSYS programs in window heat gains showed that the simulation community needs a validated and standardized window heat transfer model in order to provide consistency in residential code compliance calculations.

TRNSYS calculated 1-5°C lower zone air temperatures than EnergyPlus did all year for the unconditioned empty houses before load components were introduced. This suggested

that the opaque building envelopes of the TRNSYS houses gained less heat in summer and lost more heat in winter when compared to those of the EnergyPlus houses. Thus, the introduction of identical heat gains into these building envelopes resulted in lower cooling loads and higher heat gains in TRNSYS than it did in EnergyPlus. This finding further explained the 5-12 GJ higher heating loads and 7-14 GJ lower cooling loads of the TRNSYS houses when compared to the EnergyPlus houses.

Another important discrepancy between the DOE-2 and EnergyPlus programs occurred in the modeling of air infiltration. Fig. 4.13 presents the annual average air changes per hour and the resulting sensible heat gains and losses in the four fully loaded houses modeled in this study. These values showed that infiltration primarily caused heat losses in the fully loaded houses and these heat losses were higher in temperate and cold climates than they were in hot climates. In temperate and cold climates, identical infiltration inputs resulted in 4% higher annual average air changes in EnergyPlus than in DOE-2. These higher air changes then resulted in 9-10 GJ higher sensible heat losses in temperate and cold climates (see Fig. 4.13), which became an important factor that explained the 3% higher heating loads in EnergyPlus than in DOE-2 in these climates (see Fig. 4.10). The different air changes obtained from DOE-2 and EnergyPlus with identical infiltration inputs were attributed to the different local wind speeds and zone air temperatures calculated by these programs.

Fig. 4.14 shows the heating and cooling loads of the fully loaded DOE-2, EnergyPlus and TRNSYS houses after they were coupled with the ground. The load calculation discrepancies identified between DOE-2, EnergyPlus and TRNSYS programs for the ground isolated houses were also the primary reasons for the thermal load variations between the D2-GCW and EP-GCW models (the 1^{st} and the 2^{nd} columns in Fig. 4.14) and between the TR-GCT and EP-GCT models (the 8^{th} and 9^{th} columns in Fig. 4.14). Our comparisons were then isolated from these discrepancies by inserting the slab-soil interface temperatures calculated by each slab-on-grade model into EnergyPlus and comparing them in EnergyPlus (see columns 2-8 in Fig. 4.14). It was found that the EnergyPlus total ther-

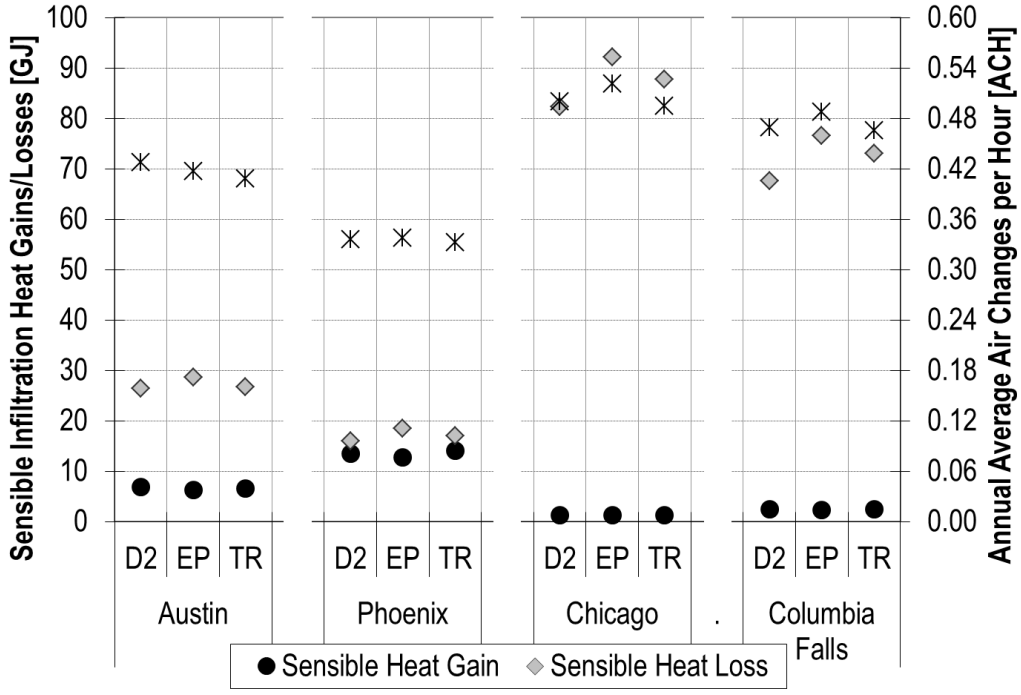

Figure 4.13: The sensible infiltration heat gains and losses in the fully loaded test houses.

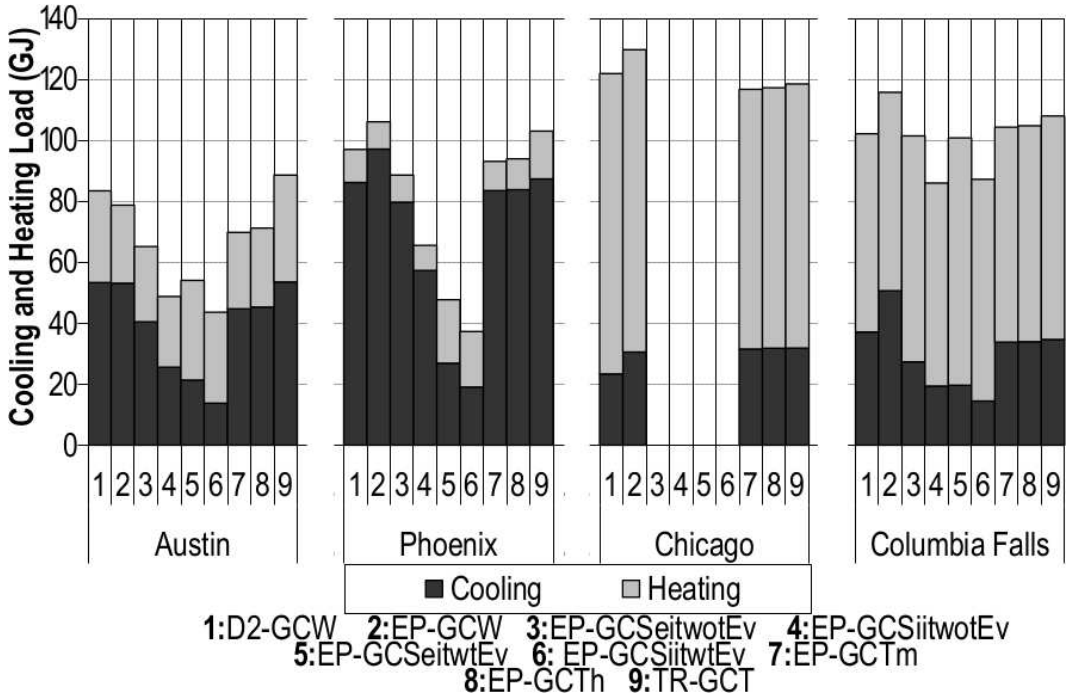

Figure 4.14: The cooling and heating loads of the slab-on-grade fully loaded test houses.

mal loads for the fully loaded code compliant houses varied by 14-51% when compared to the averages depending on the selected slab-on-grade model. Among these slab-on-grade models, the EnergyPlus model with the hourly TRNSYS slab-soil interface temperatures (EP-GCTh) represented the most detailed slab-on-grade heat transfer calculations. Using the TRNSYS slab-soil interface temperatures in EnergyPlus monthly (EP-GCTm) instead of hourly (EP-GCTh) caused 0-2% variation in total building load (see the 7^{th} and 8^{th} columns in Fig. 4.14). This finding showed that the slab-soil interface temperatures did not show significant hourly variations in fully loaded houses with zone air temperatures varying between 20°C (68°F) and 25.55°C (78°F). Monthly coupling of aboveground and belowground heat transfer calculations can; therefore, make reasonable enough building load estimates.

Among the studied slab-on-grade models, the EP-GCS models without evapotranspiration that iterated externally until the zone air temperatures converged to 0.0001°C (EP-GCSeitwotEv) exhibited the closest results to those calculated by the detailed EP-GCTh models. These models exhibited only 3-9% lower total building loads than the EP-GCTh models did (see the 3^{rd} and the 8^{th} columns in Fig. 4.14). They also showed cooling and heating loads within 19% and 13% of those of the EP-GCTh models respectively. When the EP-GCS models iterated internally for once (EP-GCSiitwotEv) as recommended in EnergyPlus manuals, however, the zone air temperatures did not converge and the estimated total building load became significantly (18-32%) lower than those calculated by the EP-GCTh models for the same houses. This convergence problem was attributed to the zone air temperatures of the fully loaded houses that varied between 20°C (68°F) and 25.55°C (78°F) throughout the year. These findings showed that the current internally iterated EP-GCS model needs to be improved before it is used for the modeling of low-rise slab-on-grade houses. The improved model needs to allow for multiple iterations between the EnergyPlus and Slab programs until the zone air temperatures converge. The cooling and heating loads of all studied houses showed only 1% variation between the convergence tolerances of 0.0001°C and 0.1°C for zone air temperatures. It was also found that assigning

a high resistance insulation layer under the concrete slab in the first EnergyPlus run and removing it in the later runs decreased the number of iterations needed for convergence. With this method, a 0.1°C convergence tolerance that resulted in load estimates within 1% of the fully converged (within 0.0001°C) values was met at the end of the 4^{th} iteration, the latest.

Evaporative transpiration (evapotranspiration) increased the difference between the total thermal load estimates of the EP-GCS and EP-GCTh models. By considering the evapotranspiration from the soil around the building, the externally iterated EP-GCS models(EP-GCSeitwtEv) showed 4-49% lower thermal loads and the internally iterated EP-GCS models (EP-GCSiitwtEv) showed 17-60% lower total thermal loads when compared to the EP-GCTh models. Evapotranspiration affected both the cooling and heating loads of the fully loaded houses dramatically with a higher impact in hot climates. It decreased the cooling loads by 25-67% and increased the heating loads by 9-135% in the fully loaded houses in all studied U.S. climates.

The EnergyPlus models with Winkelmann's slab-soil interface temperatures (EP-GCW) calculated 10-13% higher total building loads than the EP-GCTh models. The EP-GCW models appeared to make better estimates for heating loads (within 16%) than they did for the cooling loads (within 49%) of the slab-on-grade fully loaded houses. The overestimation of cooling loads in the EP-GCW model was attributed partly to the fact that Winkelmann's slab-on-grade model was based on earlier calculations of Huang *et al.*[135] that assumed constant zone air temperatures all year.

4.2 The Baseline Habitat for Humanity House vs the Partially Conditioned Atrium House

In this section, the results obtained for the energy performances of the test cases from the baseline Habitat for Humanity house models to the final partially conditioned atrium house are discussed. These discussions are categorized into the following five groups:

1) The baseline Habitat for Humanity house models: EnergyPlus currently has a multizone air flow network model (AirflowNetwork) which is based on COMIS in calculation of

air leakages through the building envelope. This model also uses the equations of AIRNET in calculation of airflows through the air distribution system and the energy losses due to duct heat conduction.[95] The COMIS link and ADS models focus on different aspects, but the multizone airflow calculations are somewhat overlapped and two airflow network solvers are used for them.[95] In this study, the AirflowNetwork model of EnergyPlus was used and further extended by combining it with the multizone TRNSYS Type 1255 slab-on-grade heat transfer model. With this combined modeling method for the baseline Habitat for Humanity house, the temperature variations between the rooms were determined, the effects of infiltration and mechanical ventilation on energy consumption were discussed and the different ground heat transfers in different rooms were accounted for,

2) the baseline atrium house models (Case 1): These models were obtained by adding an unconditioned central atrium to the baseline Habitat for Humanity house models. In this case, the internal heat gains were reduced in the house by improving daylighting and moving the primary house equipment into the atrium,

3) the atrium as a return plenum (Case 2): In this case, the conditioned air returning from the occupied zones was moved into the atrium to partially condition the atrium space. This improved the energy performance of the house by reducing $\triangle$T between the atrium and the surrounding conditioned zones,

4) the atrium house with occupancy-based heating and cooling (Case 3): In this case, the energy consumption of the baseline atrium house models (Case 1) were reduced by saving the energy used by the unoccupied rooms,

5) the atrium house with multiple reuse of air (Case 4): This case was obtained by partially conditioning the unoccupied zones of the Case 3 house by sending the return air of the occupied zones to them. Finally, the air was moved into the atrium and returned to the system. The reuse air helped heat/cool the unoccupied zones which reduced the energy required to bring them from unoccupied temperatures to occupied temperatures. This case also reduced the $\triangle$T between the occupied and the unoccupied rooms which limited the heat transfer through the interzonal walls.

4.2.1 The Baseline Habitat for Humanity House Models

The annual HVAC energy consumption of the three baseline Habitat for Humanity house models are presented in Fig. 4.15. The monthly total HVAC energy consumption determined for these models are also given in Fig. 4.16, Fig. 4.17 and Fig. 4.18. These results showed that the flow rate and the supply method of outside air is a critical factor in the energy requirement of the low-rise affordable residential buildings in Texas. The cooling energy consumption of the Habitat for Humanity houses modeled with three different outdoor air exchange conditions differed by -43% to +27% from the average of the results (1,145 kWh). The heating energy consumption of these houses differed by -22% to +25% from the average of the results (3,177 kWh).

All baseline houses were found to have higher heating energy consumption than cooling in a hot-humid climate. This was caused by a combination of factors. First, these houses were very lightly occupied during the day time when the highest outside temperatures were observed (see Fig. 3.26). Second, the electric lights were assumed to be used only when they were required due to the insufficient illuminance values. In a real house, the use of electric lights is far from this ideal behavior. Third, the baseline houses modeled in this study were IECC 2012 compliant houses which required a fenestration U-value (0.4 Btu/hr.ft^2°F) for climate zone 2 which was 38% lower than that required by the IECC 2009 (0.65 Btu/hr.ft^2°F). The IECC 2012 also required a SHGC value (0.25) which was 17% lower than that required by the IECC 2009 (0.3). Finally, ground coupling affected the building energy consumption significantly by decreasing the cooling energy consumption by 19%-30% and increasing the heating energy consumption by 28%-45% (see in Fig. 4.21, Fig. 4.22 and Fig. 4.23). Among the modeled houses, the negatively pressurized house with 0.45 ACH annual average air exchange rate (NEG0.45ACH) showed close (within 14%) total HVAC energy consumption to that calculated by Kim *et al.*[186] for an IECC 2012 compliant house with 0.4 ACH total air exchange rate in Harris, Texas.

Given the same annual average air exchange rate (i.e. 0.3 ACH), mechanical ventilation resulted in 60% higher heating energy consumption and 50% lower cooling energy consump-

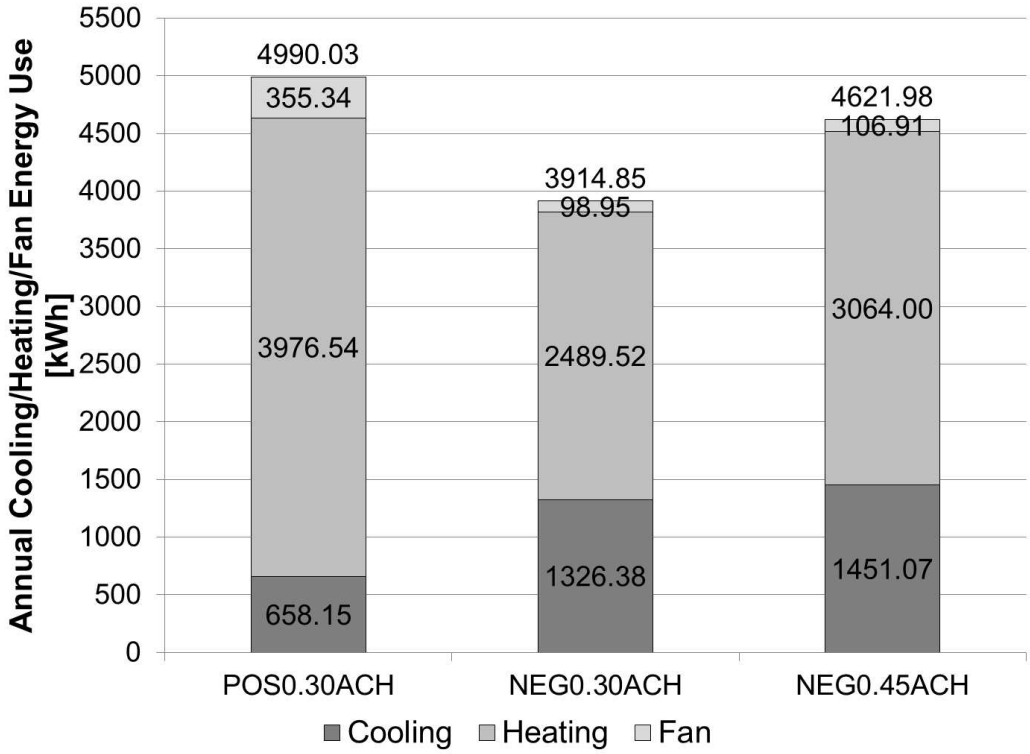

Figure 4.15: The annual HVAC energy consumption of the baseline Habitat for Humanity house models.

tion than infiltration did (see POS0.30ACH and NEG0.30ACH models in Fig. 4.15). The fan energy consumption of the mechanically ventilated case was also 3.6 times higher than the case with infiltration since it worked in continuous fan operation mode to provide continuous outside air to the house. Consequently, the total HVAC energy consumption of the mechanically ventilated case was found to be 27% higher.

These results were explained by drawing the hourly infiltration rate plots of these cases together with the outside air temperatures in the coldest and warmest months. (see Fig. 4.19 and Fig. 4.20). In these plots, it was observed that at the local minima of the outside air temperatures, the infiltration rates of the negatively pressurized models (NEG0.30ACH and NEG0.45ACH) dropped below 0.3 ACH, whereas the ventilation rate in the positively pressurized model stayed constant at 0.3 ACH. This finding was identified as the reason of the higher heating energy consumption of the mechanically ventilated

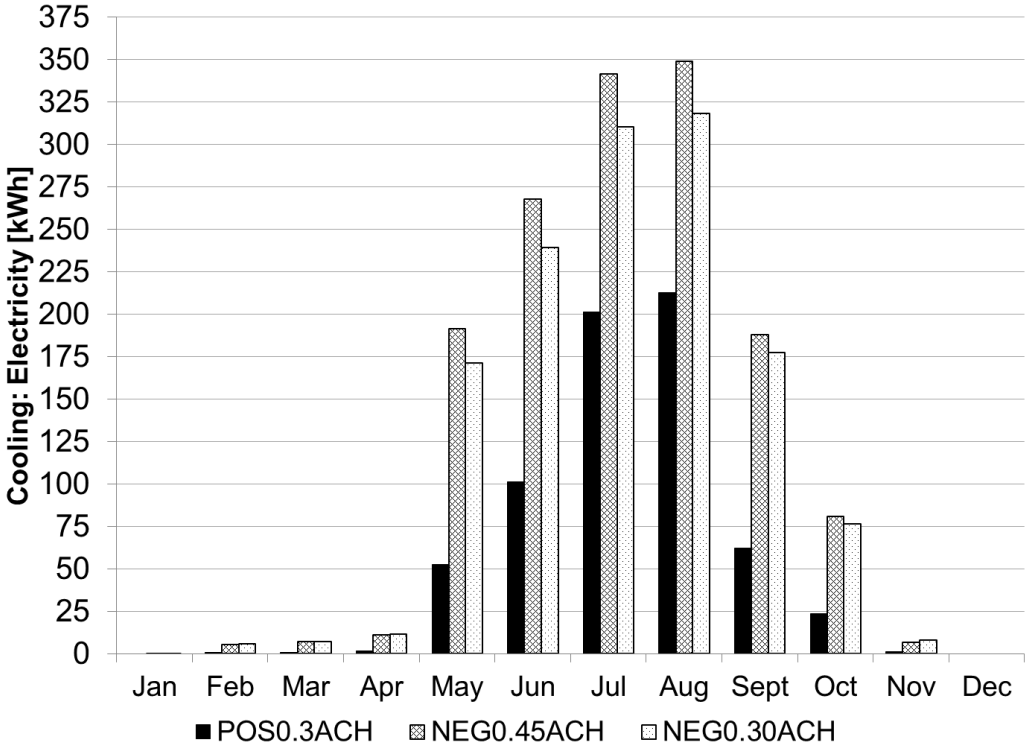

Figure 4.16: The monthly total cooling electricity use of the baseline Habitat for Humanity house models.

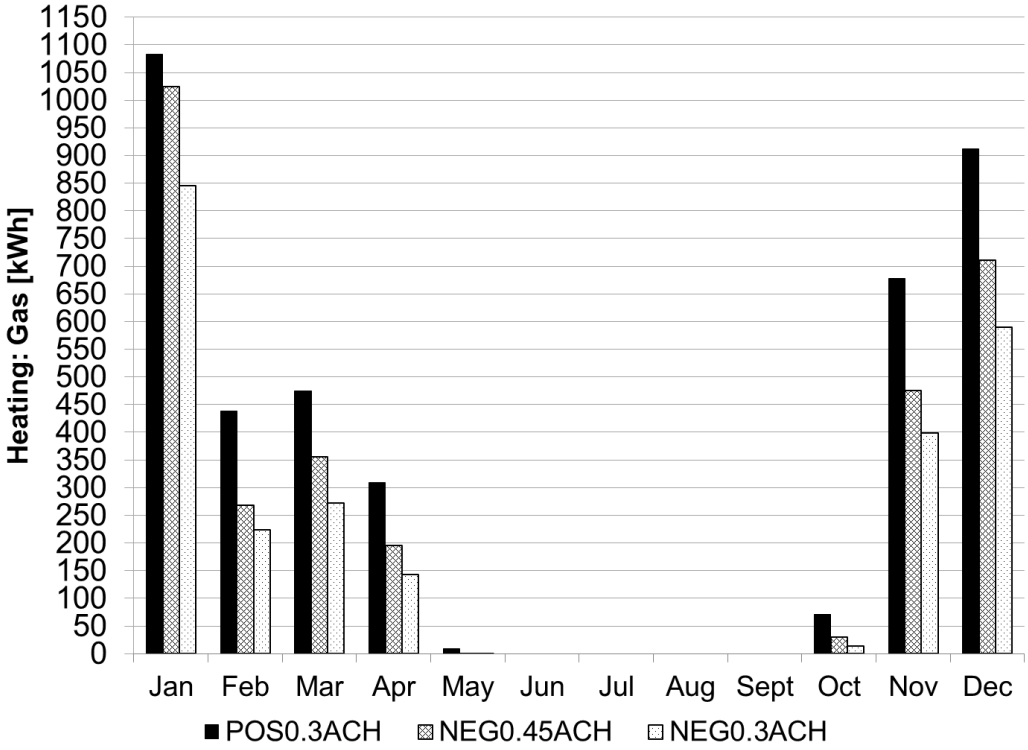

Figure 4.17: The monthly total gas consumption of the heating system of the baseline Habitat for Humanity house models.

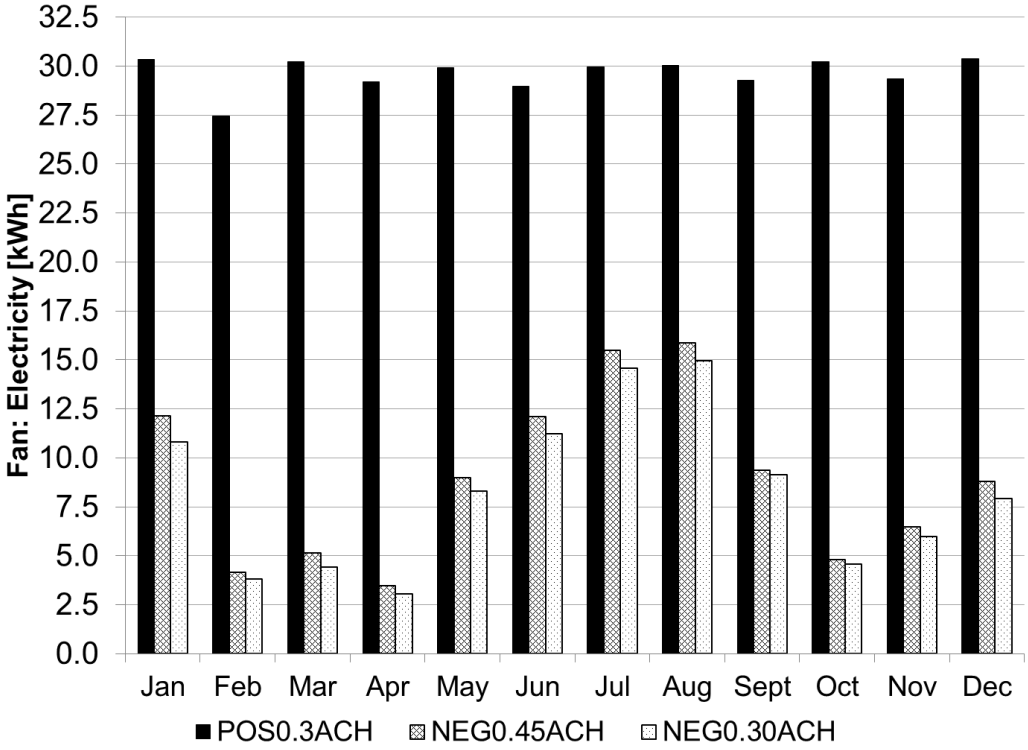

Figure 4.18: The monthly total fan electricity consumption of the baseline Habitat for Humanity house models.

case (POS0.30ACH) (see Fig. 4.19). This finding also explained the lower cooling energy consumption of the mechanically ventilated case (see Fig. 4.20). During the cooling season, mechanical ventilation provided the opportunity to benefit from the lower nighttime temperatures of the outside air. The infiltration in the negatively pressurized houses was lower during these hours limiting the cooling effect that can be provided with the outside air.

Increasing the annual average infiltration rate from 0.3ACH to 0.45ACH increased the heating energy consumption by 23% and cooling energy consumption by 9% in the negatively pressurized baseline models (see NEG0.30ACH and NEG0.45ACH models in Fig. 4.15). In order to explain this variation, the peak cooling and heating hours of the control zone (CR-LR) were examined. It was found that, at the peak cooling hour of the control zone (3^{rd} of August at 6 p.m.) when it was 39.4°C outside, the infiltration rate in the NEG0.45ACH model (1.27 ACH) was 1.5 times higher than that in the NEG0.3ACH model (0.85 ACH). This resulted in a 1.46 times higher infiltration heat gain in the NEG0.45ACH model (4.96 MJ) than in the NEG0.30ACH model (3.40 MJ) leading to a 1.25 times higher cooling capacity. At the peak heating hour of the control zone (7^{th} of January at 10 a.m.) when it was -2°C outside, the infiltration rate of the NEG0.45ACH model (1.37 ACH) was also 1.5 times higher than that in the NEG0.30ACH model (0.93 ACH). This resulted in 1.46 times higher infiltration heat loss in the NEG0.45ACH model (8.66 MJ) than in the NEG0.30ACH model (5.94 MJ) leading to a 1.3 times higher heating capacity.

Besides the quantity of outside air at peak hours, the daily variation of outside air also played part in the difference between the annual energy consumption of the NEG0.30ACH and NEG0.45ACH models. In the cooling season, the cooler air that occurred at nights leaked into the building more in the NEG0.45ACH model than in the NEG0.30ACH, which reduced the cooling energy consumption of the NEG0.45ACH model approaching the results of the two models to each other (see Fig. 4.20). In the heating season, the colder nighttime outside air also infiltrated into the building more in the NEG0.45ACH model. This time, however, infiltration increased heating energy consumption more in the

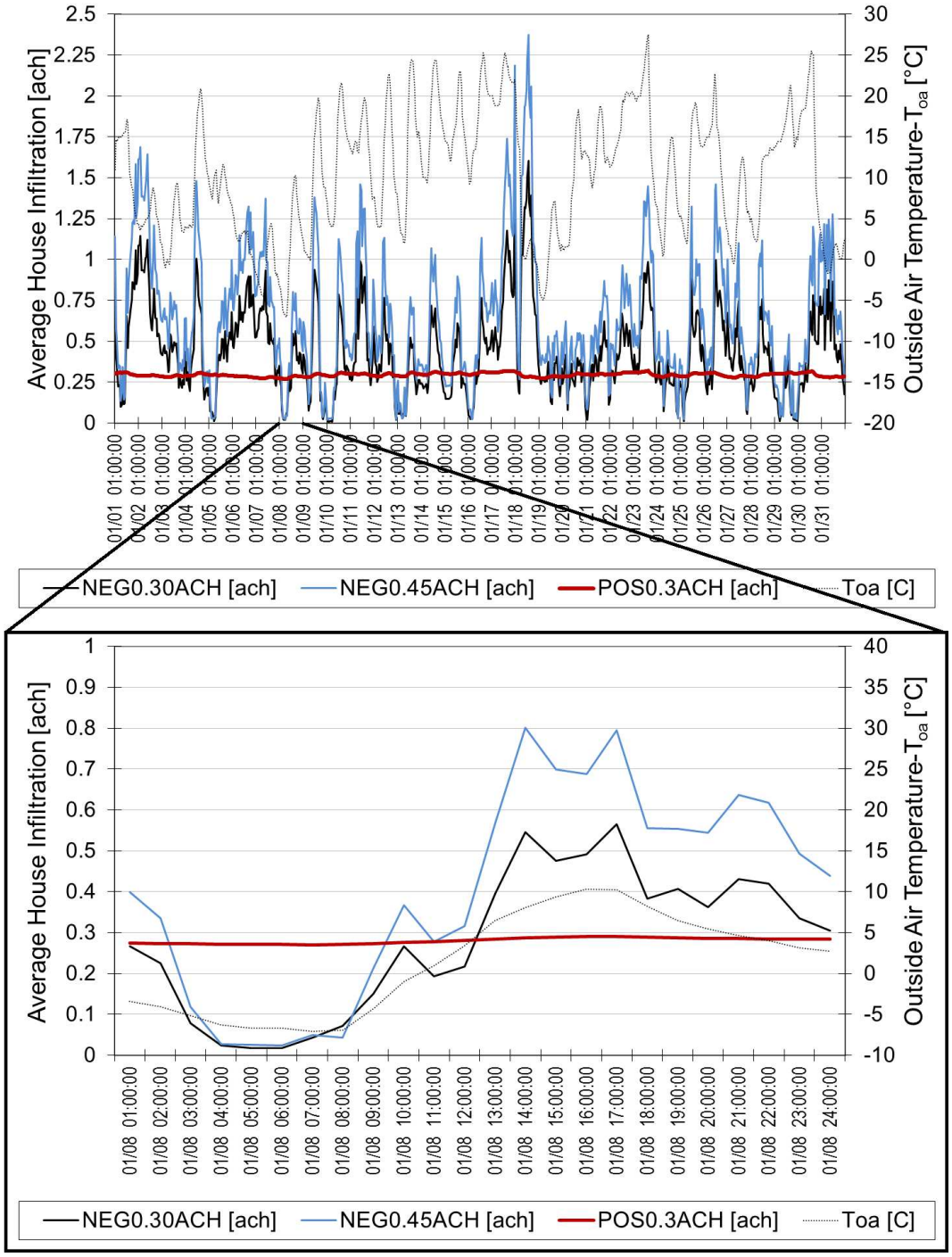

Figure 4.19: The hourly variation of outside air exchange rate in the baseline houses in the coldest month, i.e. January.

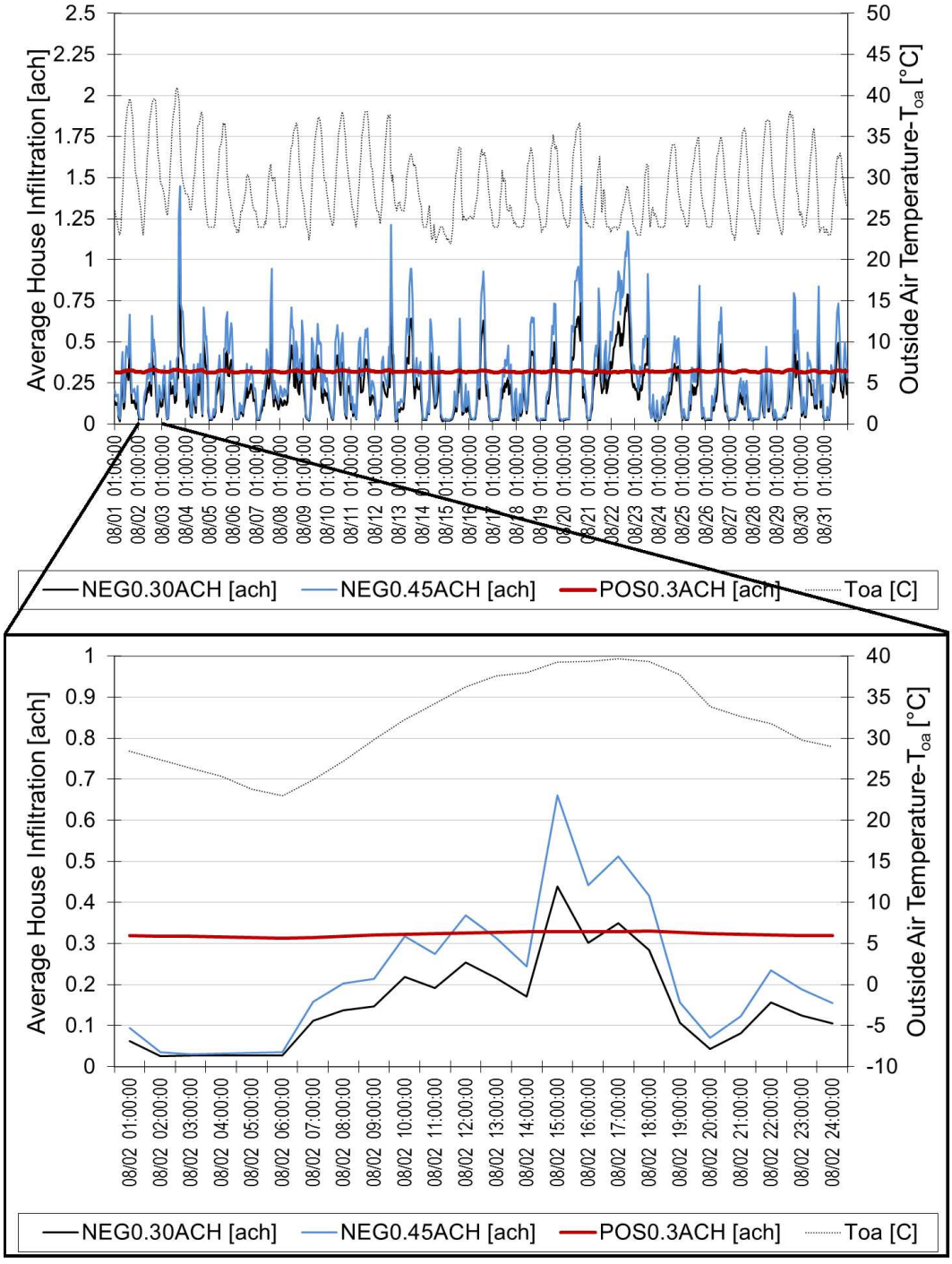

Figure 4.20: The hourly variation of outside air exchange rate in the baseline houses in the warmest month, i.e. August.

NEG0.45ACH model than it did in the NEG0.30ACH model. Consequently, primarily an increase in heating energy consumption was observed from the NEG0.30ACH model to the NEG0.45ACH model (see Fig. 4.15).

The energy requirements presented in Fig. 4.15 belonged to the slab-on-grade conditions of the baseline models. In fact, these results were obtained through an iteration process between the aboveground EnergyPlus models and the TRNSYS Type 1255 slab-on-grade heat transfer models. The variation in cooling, heating and fan energy consumption during this iteration process is given in Fig. 4.21, Fig. 4.22 and Fig. 4.23 for each of the three baseline Habitat for Humanity house models. These results showed that cooling energy consumption converged within 1% after the 3rd EnergyPlus run in the negatively pressurized models whereas it converged only after the 5th EnergyPlus run in the positively pressurized model. Similarly, heating energy consumption converged within 1% after the 5th EnergyPlus run in the negatively pressurized models whereas it took 6 EnergyPlus runs to converge in the positively pressurized model. These findings showed that the length of the ground coupling iteration process used in this study is affected by the pressurization of the house. It was also concluded that convergence within 1% takes more iterations for heating than it does for cooling.

Using the AirflowNetwork:Multizone model of EnergyPlus for the simulations in this study provided the opportunity to observe the variation in infiltration rates of the rooms in the modeled houses. Fig. 4.24 and Fig. 4.25 show the monthly average infiltration rates of each room in the NEG0.45ACH and NEG0.30ACH models. It was found that infiltration generally decreased in late summer (July, August) and early fall (September) in all rooms in both models. This condition was explained with the decrease in wind speed (V_{wind}) in these months in all directions.

The maximum infiltration occurred in the rooms in different times of the year depending on the orientation of the room with respect to the prevailing wind direction and on the number and sizes of the openings facing toward that direction (see Fig. 4.24 and Fig. 4.25). For instance, the highest monthly average infiltration rates were observed in the corridor

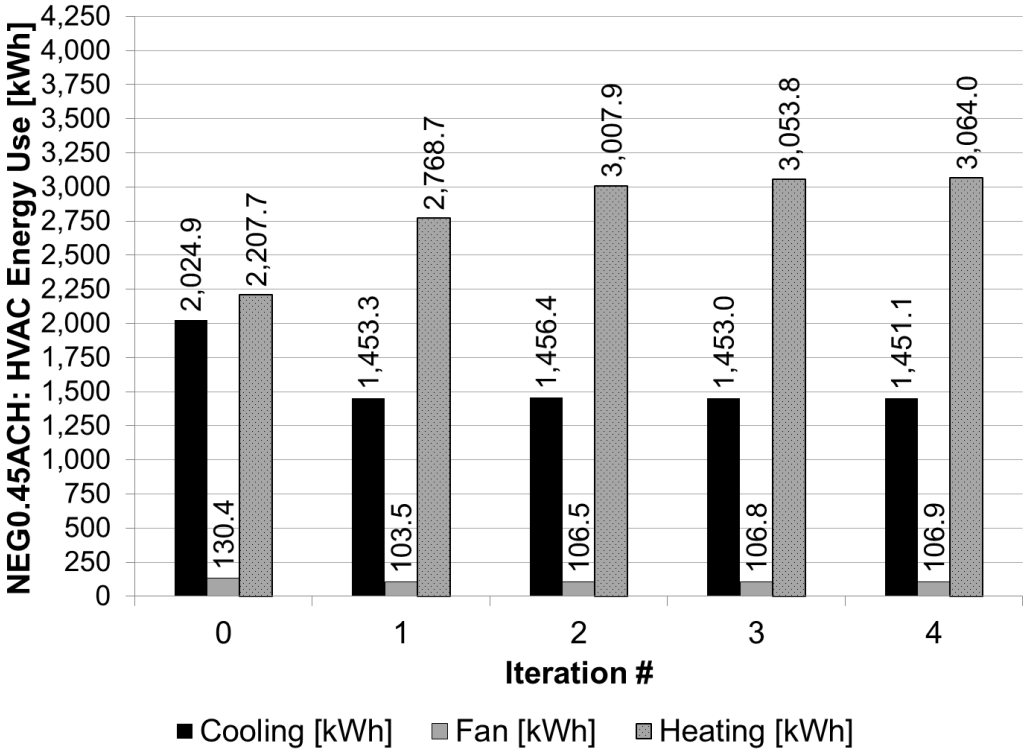

Figure 4.21: The heating, cooling and fan energy use of the negatively pressurized leaky baseline house with 0.45 ACH during the iterations between EnergyPlus and TRNSYS Type 1255.

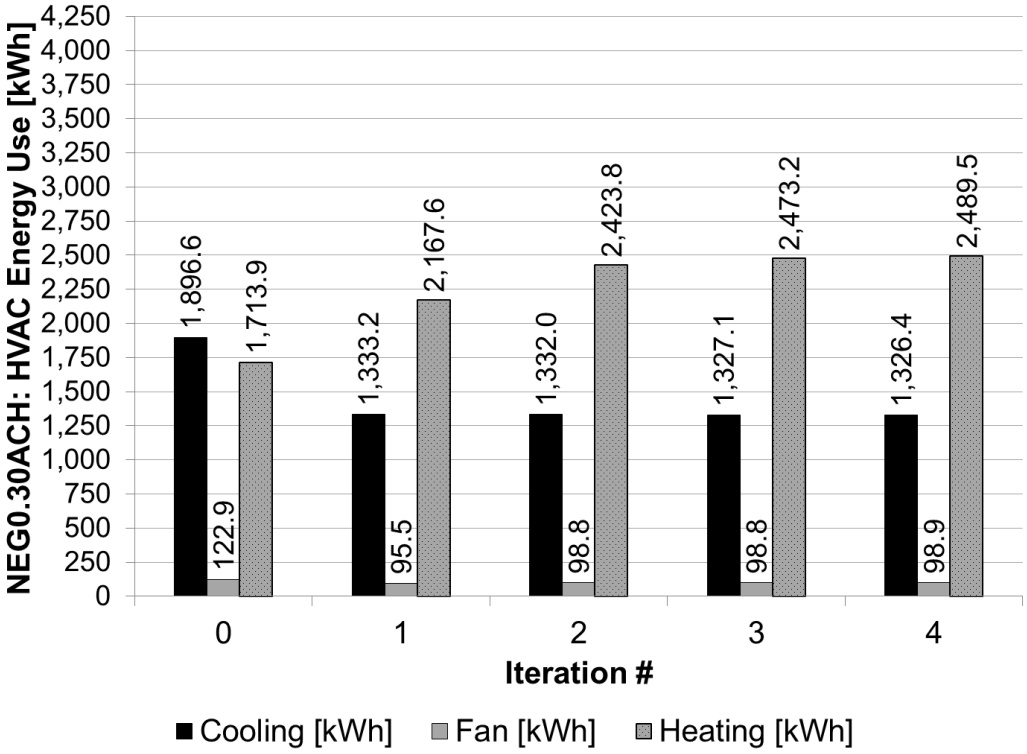

Figure 4.22: The heating, cooling and fan energy use of the negatively pressurized air tight baseline Habitat for Humanity house with 0.3 ACH during the iterations between EnergyPlus and TRNSYS Type 1255.

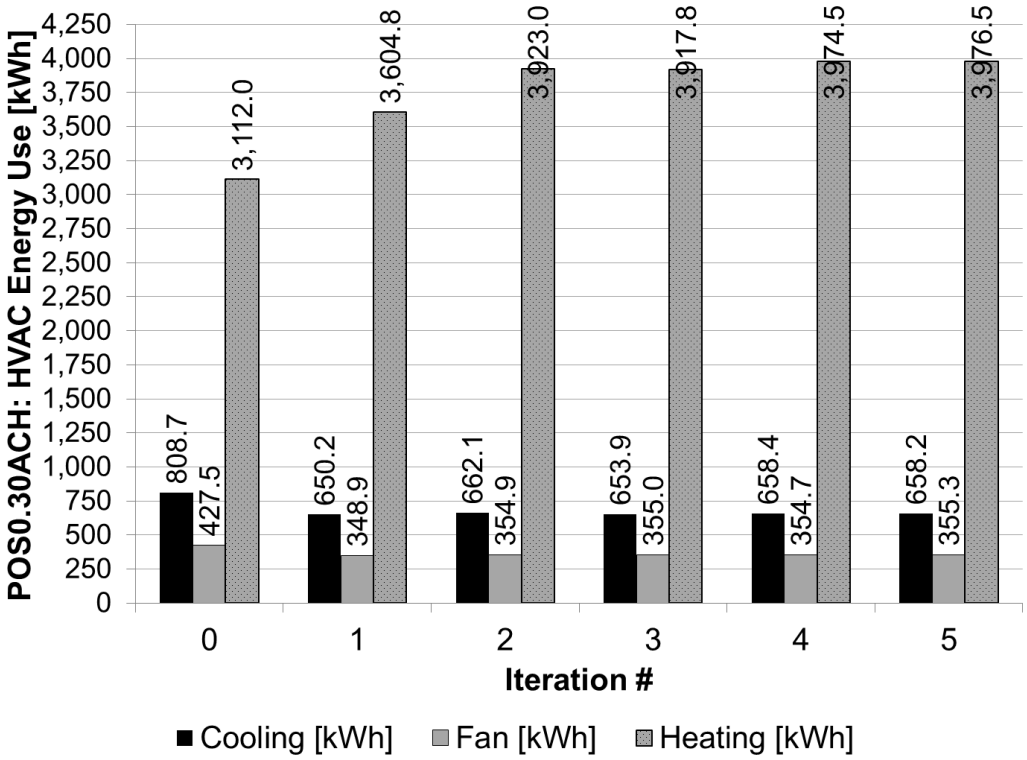

Figure 4.23: The heating, cooling and fan energy use of the positively pressurized baseline Habitat for Humanity house with 0.3 ACH mechanical ventilation rate during the iterations between EnergyPlus and TRNSYS Type 1255.

and living room sections (CR-LR) of the living area in these models and these rates were observed in May. This condition was explained with two facts. First, the prevailing wind direction in this month was from south-east which the CR-LR zone was facing (Fig. 4.26). Second, the CR-LR zone had large windows on both the east and the west facing walls which increased the total leaky exterior surface facing the prevailing wind direction.

The rooms that showed the lowest air exchange rates were the main bathroom (MBT) and the utility room (UTR) in both the NEG0.30ACH and NEG0.45ACH models (see Fig. 4.24 and Fig. 4.25) The main bathroom exhibited zero infiltration rate at all times throughout the year as it was an interior zone and had no direct connection to outside air. The utility room had a single relatively small exterior wall facing west and there was the side entrance of the house on this wall. This room received insufficient infiltration (around 0.1 ACH) during the cooling season which was foreseen to cause poor indoor air quality resulting in an unfavorable laundry room.

Mechanical ventilation in the positively pressurized baseline Habitat for Humanity house (POS0.30ACH) provided a better solution by providing a more even distribution of outdoor air in the house. Fig. 4.27 shows the annual average mechanical ventilation rate of each zone in the POS0.30ACH house. These rates were maintained almost constant all year. Three primary benefits were obtained with the use of mechanical ventilation instead of infiltration. First, the outside air requirements of the occupants were provided at all times as it depended less on the availability of sufficient wind speed. Second, all zones received outside air including the interior zones since having a direct connection to outdoors was no longer a requirement for receiving outside air. Third, mechanical ventilation provided better control of zone air temperatures in the rooms. The number of occupied cooling and heating hours that the set points were not met are presented in Fig. 4.28, 4.29 and 4.30 for the Habitat for Humanity house models. The positively pressurized POS0.30ACH model showed an improvement of 47% fewer hours than the NEG0.30ACH model and 54% fewer hours than the NEG0.45ACH model that the set points were not met.

Besides these advantageous features, this mechanically ventilated case also had a few

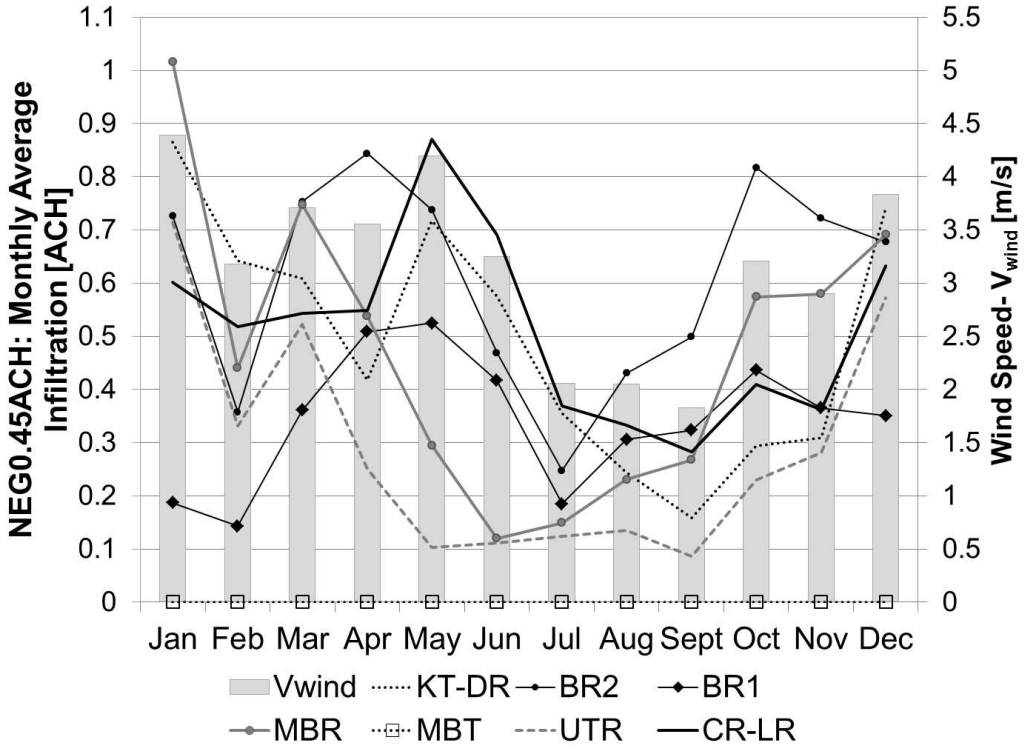

Figure 4.24: The monthly average infiltration in the negatively pressurized Habitat for Humanity house with 0.45 ACH.

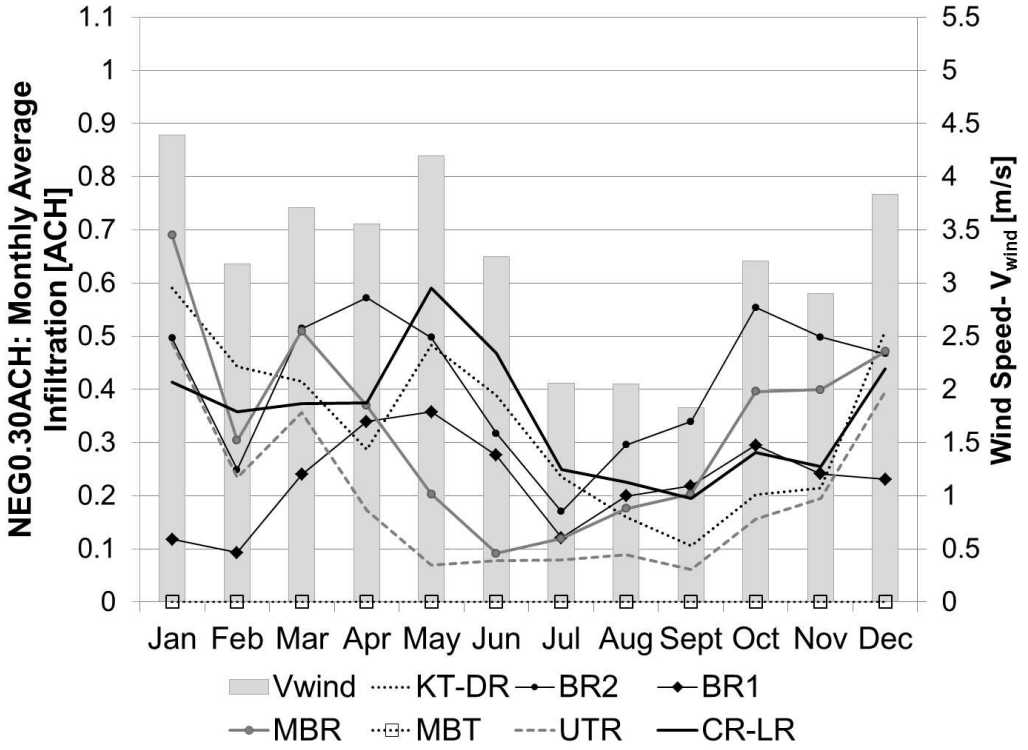

Figure 4.25: The monthly average infiltration in the negatively pressurized Habitat for Humanity house with 0.3 ACH.

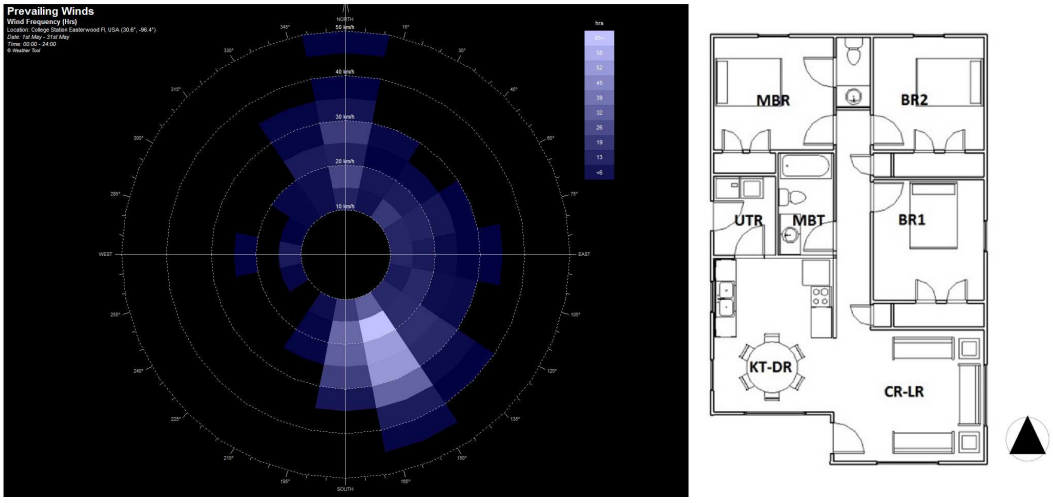

Figure 4.26: The prevailing wind direction chart for College Station, Texas in May.

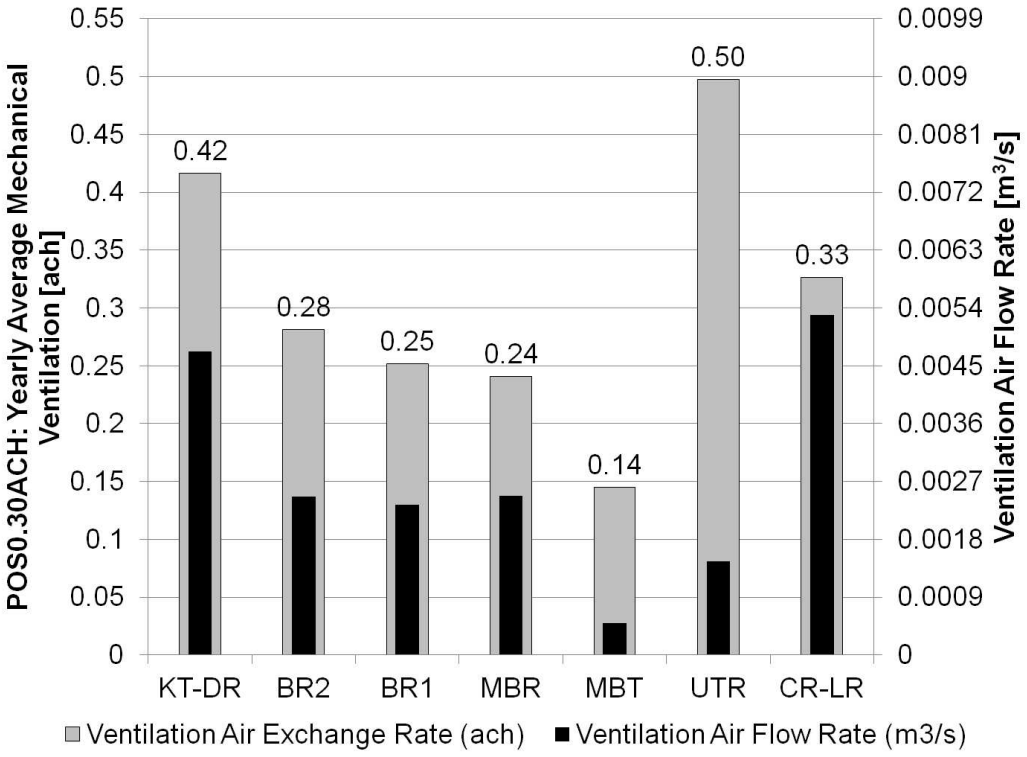

Figure 4.27: The yearly average ventilation rate in each zone of the positively pressurized Habitat for Humanity house with 0.3 ACH, i.e. POS0.30ACH.

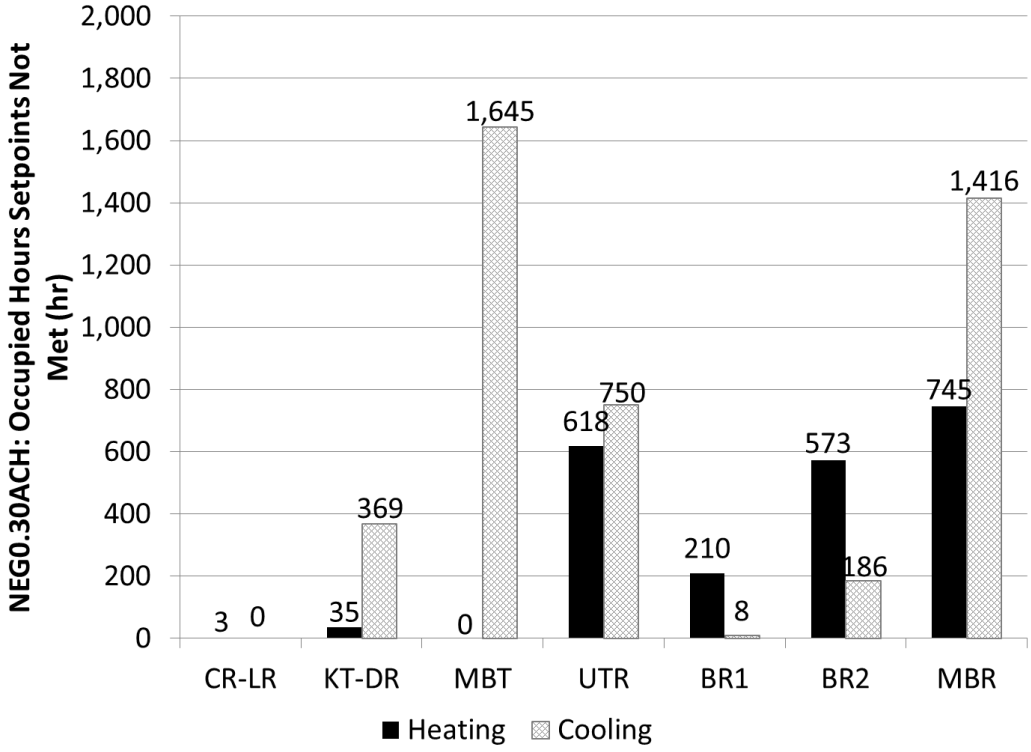

Figure 4.28: The baseline Habitat for Humanity House: NEG0.30ACH: The number of occupied heating and cooling hours that the set points were not met.

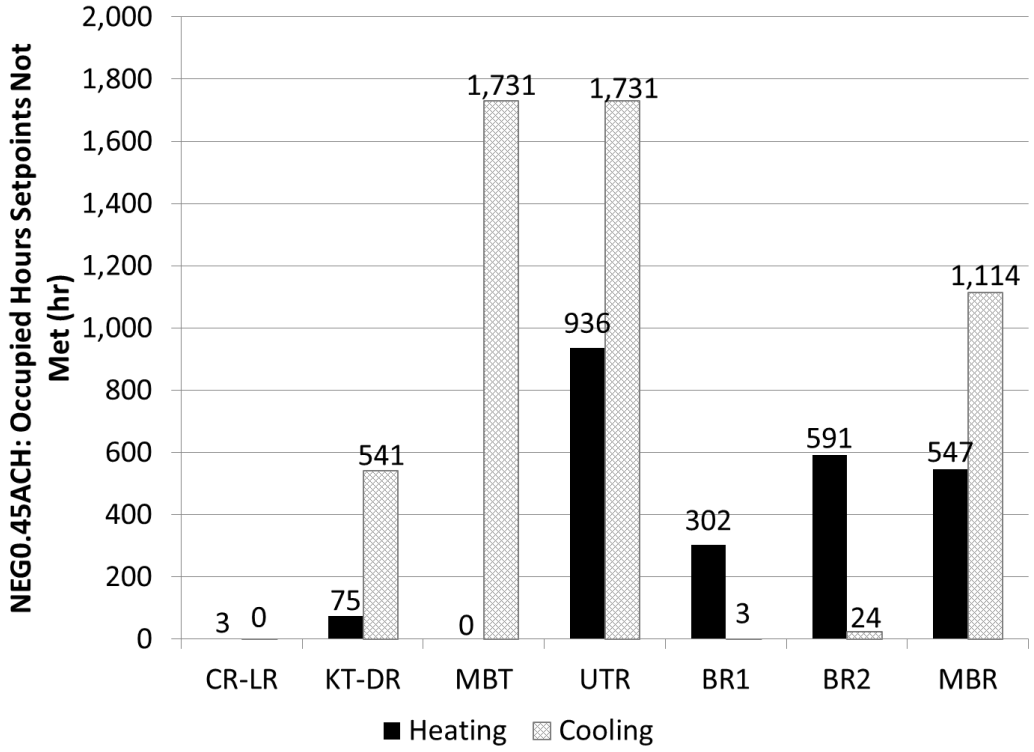

Figure 4.29: The baseline Habitat for Humanity House: NEG0.45ACH: The number of occupied heating and cooling hours that the set points were not met.

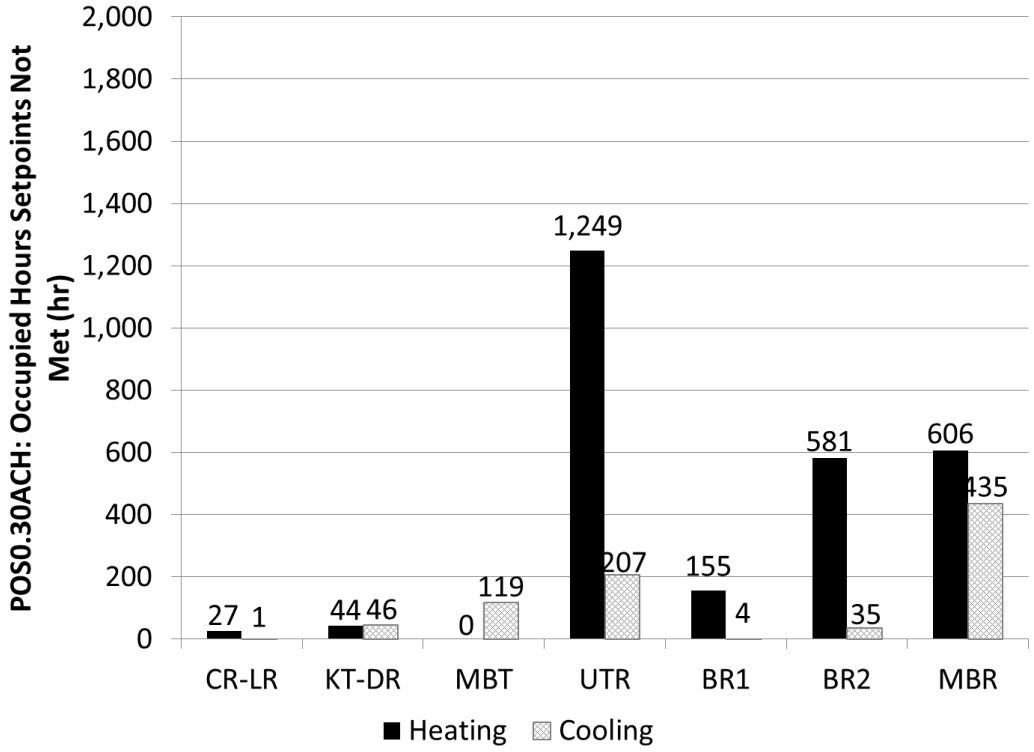

Figure 4.30: The baseline Habitat for Humanity House: POS0.30ACH: The number of occupied heating and cooling hours that the set points were not met.

drawbacks. For instance, it supplied a constant outdoor airflow rate set to the minimum outdoor air requirement at all times including the hours that the outdoor air was favorable for free cooling. This system also distributed the outdoor air to the zones based on their peak loads since the zone supply air ducts were sized based on the peak airflow rates of the zones. This caused the unoccupied rooms to receive outdoor air as well resulting in excessive energy consumption.

4.2.2 The Baseline Atrium House Models (Case 1)

Atrium house models were produced in this study by making modifications on the baseline Habitat for Humanity house models discussed in Section 4.2.1. This was considered as the first step of the modeling of the partial conditioning strategy. Fig. 4.31 presents a comparison between the annual energy consumptions of the baseline Habitat for Humanity (HFH) and the baseline atrium (ATR) houses in ground isolated condition. It was found that for both cases of the negatively pressurized models (i.e. NEG0.30ACH and NEG0.45ACH), the baseline atrium houses showed lower (6%-11%) cooling energy consumption and higher (24%-35%) heating energy consumption when compared to the baseline Habitat for Humanity houses. In the positively pressurized condition (POS0.30ACH), the atrium house also showed 23% higher heating energy consumption than the Habitat for Humanity house.

The differences in energy performances of the atrium and the Habitat for Humanity house models were attributed to the fact that the internal heat gains of the atrium house models were significantly lower than those of the Habitat for Humanity house models particularly during the warmest hours of the day (see Fig. 4.31). This factor worked for the advantage of the cooling system during the cooling season and decreased the cooling requirement of the house. In the heating season, however, it acted the opposite way and increased the heating requirement.

The lower internal heat gains of the atrium house models were caused by two primary factors. First, the atrium house used 31.68 Wh less electric lighting energy during the day time (between 9 a.m. and 7 p.m.) which included the warmest hours of the day. This

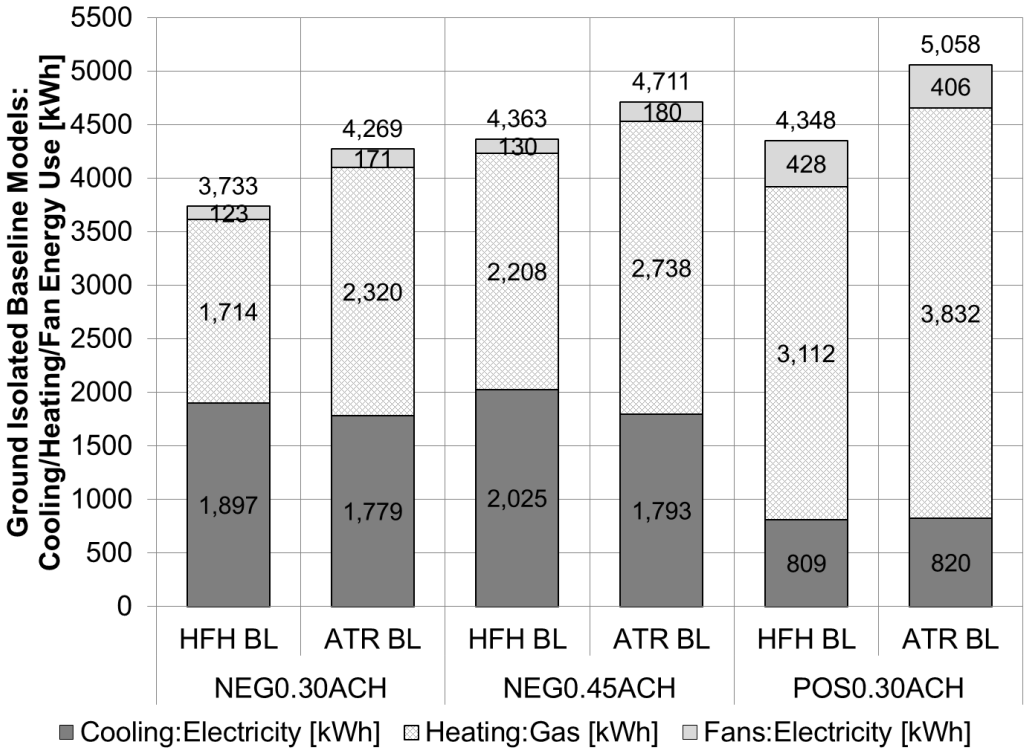

Figure 4.31: The annual heating, cooling and fan energy consumption of the baseline (BL) Habitat for Humanity (HFH) and atrium (ATR) houses. The atrium house models presented are Case 1 atrium houses (see Section 3.3 for definitions)

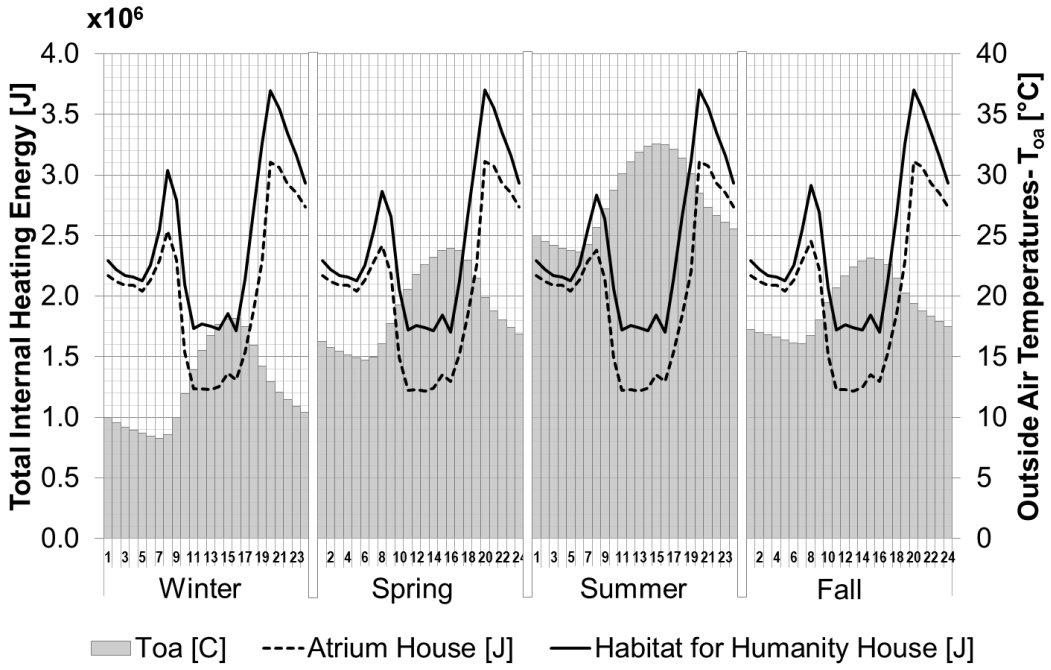

Figure 4.32: The total internal heating energy of the baseline (BL) Habitat for Humanity (HFH) and atrium (ATR) houses in an average day in each season.

resulted in 9.8 kJ - 59.9 kJ less hourly heat gain from the lights during these hours and the maximum difference between the two houses occurred between 6 p.m. and 7 p.m. (see Fig. 3.30). Second, many primary heat generating equipment of the house (i.e. the cooktop unit, the washer, dryer and the dish washer) were in the unconditioned atrium in the atrium house, whereas they were included in the conditioned zones in the Habitat for Humanity house. This resulted in 8.76 MJ less daily total heat gain from the equipment in the atrium house than in the Habitat for Humanity house (see Fig. 3.26). The hourly difference between these two houses varied between 70 kJ and 789 kJ and the maximum difference (789 kJ) occurred between 5 p.m. and 6 p.m.

When an economizer was added to the positively pressurized baseline atrium house (POS0.30ACH), a new case was obtained (POS0.30ACHECON). The HVAC energy consumption of this case is presented in Fig. 4.33. It was found that, with the introduction of the economizer, the cooling energy consumption decreased by 7% and the heating energy consumption decreased by 26%. In order to discuss the reasons for the high variation in

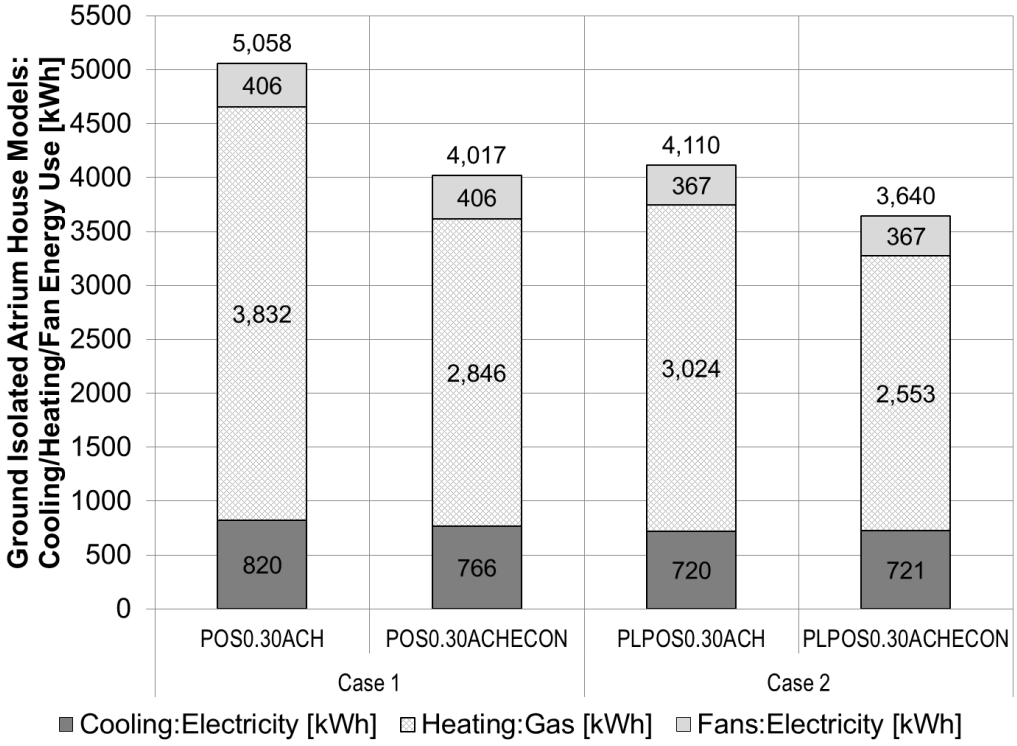

Figure 4.33: The Case 2 vs Case 1: The annual heating, cooling and fan energy consumption of the positively pressurized atrium houses.

heating energy consumption, the mixed air temperatures (T_{mix}) and the supply air temperatures (T_{sup}) of the POS0.30ACHECON and POS0.30ACH cases were compared for the coldest month, i.e. January (see Fig. 4.34 and Fig. 4.35).

It was found that, the AirflowNetwork model calculated lower supply air temperatures (T_{sup}) and higher mixed air temperatures (T_{mix}) for the case with an economizer (POS0.30ACHECON) when compared to the one without (POS0.30ACH). This resulted in lower temperature differences between the inlet and outlet points of the heating coil which caused the lower annual heating energy consumption shown in Fig. 4.33. The POS0.30ACHECON house was also found to perform better than the POS0.30ACH model in meeting the heating set points in winter (see Fig. 4.36) As of June 6th 2013, these findings were under discussion with the EnergyPlus development team for further improvement of the program code.

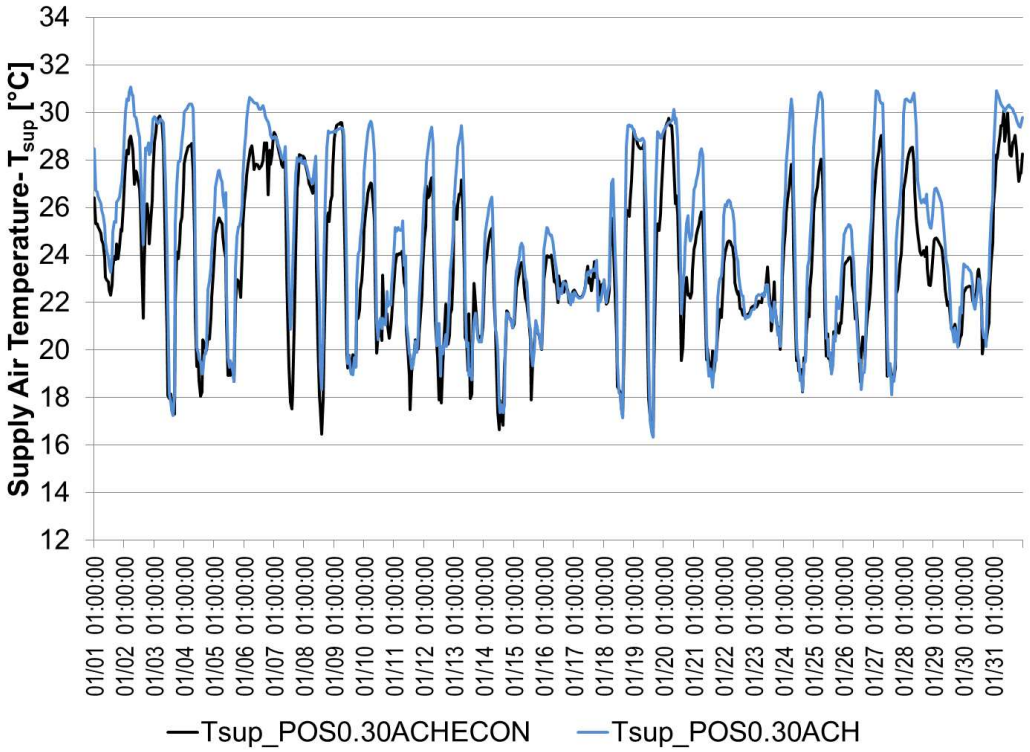

Figure 4.34: The supply air temperatures of the positively pressurized Case 1 houses in January with and without an economizer.

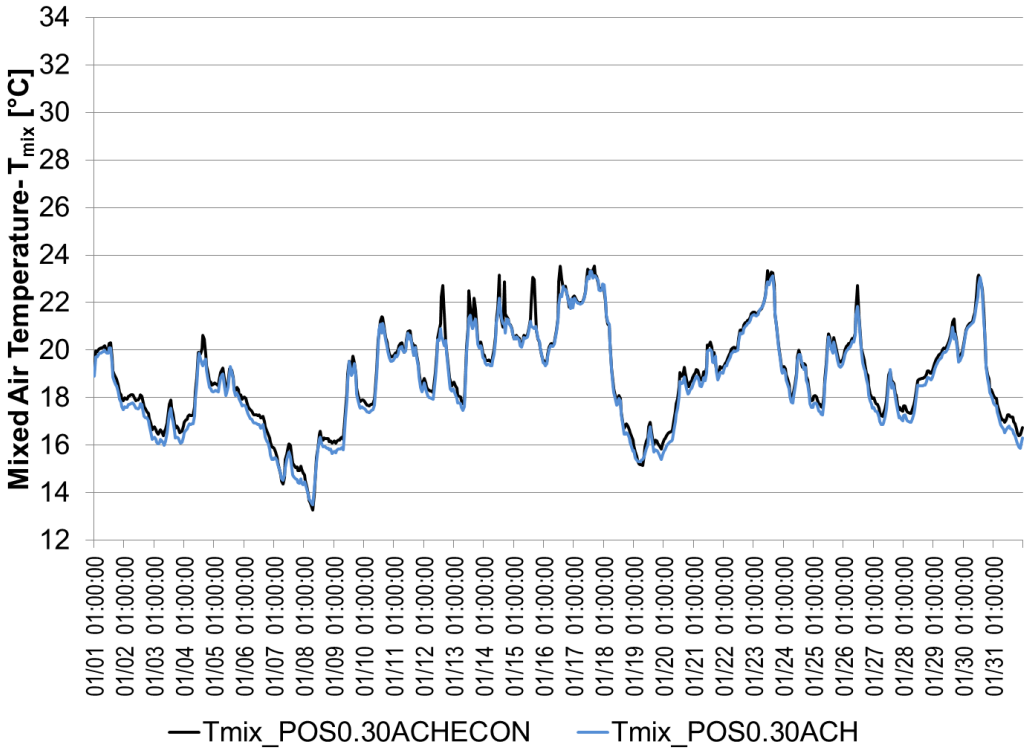

Figure 4.35: The mixed temperatures of the positively pressurized Case 1 houses in January with and without an economizer.

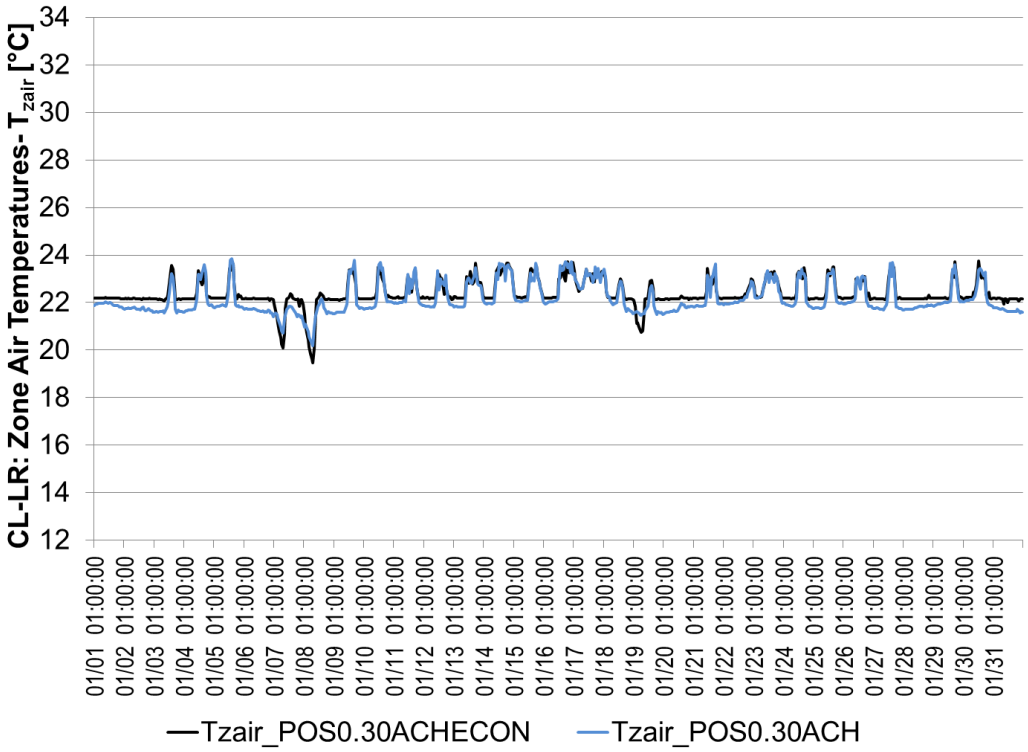

Figure 4.36: The air temperatures of the control zone (i.e. LR) of the positively pressurized Case 1 houses in January with and without an economizer.

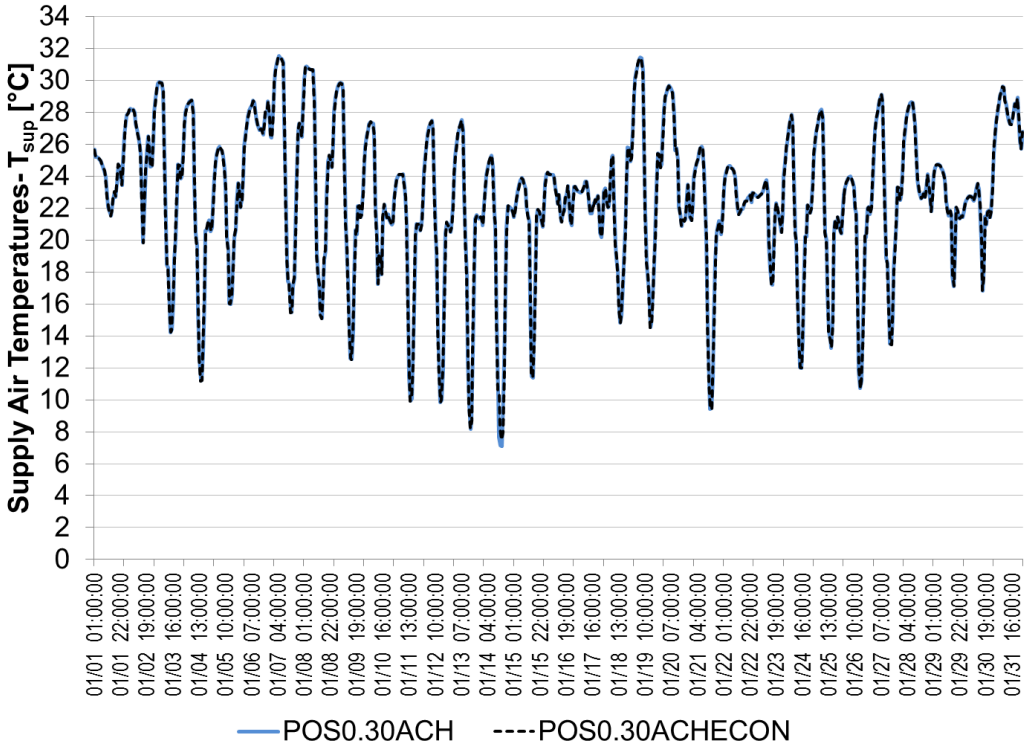

Figure 4.37: The supply air temperatures of the positively pressurized Case 1 houses in January with and without an economizer when the AirflowNetwork model was off.

In order to explain the lower supply air and zone air temperatures of the POS0.30 ACHECON model, the AirflowNetwork model was turned off and these two cases were run again. In these new runs, the supply air temperatures (T_{sup}) of the two models became identical to each other in winter when the AirflowNetwork model was off (see Fig. 4.37). This finding ensured that the lower supply air temperatures of the POS0.30ACHECON case were caused by the current limitations of the AirflowNetwork model in EnergyPlus v.8.0.0.007. The EnergyPlus development team was updated on these points accordingly for the improvement of the code.

In the cooling season, the reason for the lower HVAC energy consumption of the POS0.30ACHECON model was the lower mixed air temperatures (T_{mix}) provided through air mixing with outdoor air. The highest savings in cooling energy with the use of the economizer occurred in September (see Fig. 4.38). The comparison of the T_{mix} values of

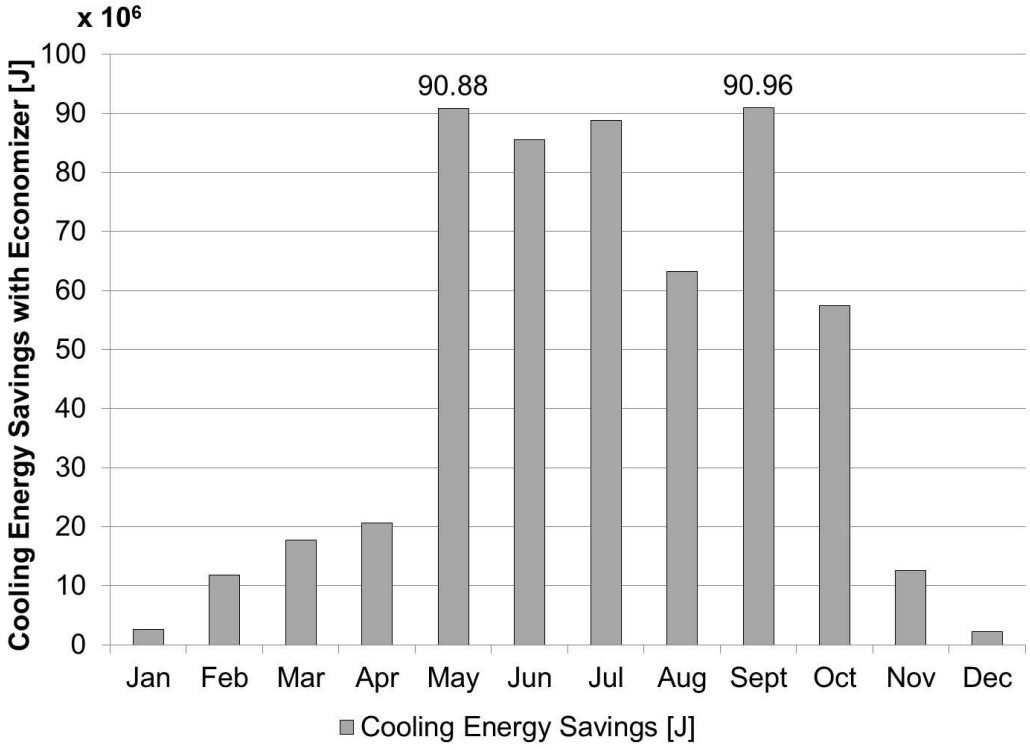

Figure 4.38: The monthly total cooling energy savings obtained with the use of the economizer.

the POS0.30ACHECON and POS0.30ACH models for September is presented in Fig. 4.39. These lower T_{mix} values of the POS0.30ACHECON model resulted in lower temperature differences between the inlet and the outlet points of the cooling coil which then reduced the cooling energy consumption of the corresponding hours. This fact was identified as the primary reason for the lower annual cooling energy consumption of the POS0.30ACHECON model when compared to the POS0.30ACH model in Fig. 4.33.

4.2.3 Atrium as a Return Plenum (Case 2)

Using the central atrium as the return plenum of the building provided multiple benefits to the atrium houses discussed in Section 4.2.2. First, it maintained the central circulation area of the house at moderate temperatures which turned this space into an additional room of the building without spending additional heating/cooling energy. The air returning from the surrounding zones managed to keep the atrium between 16°C and 28°C (see Fig. 4.40).

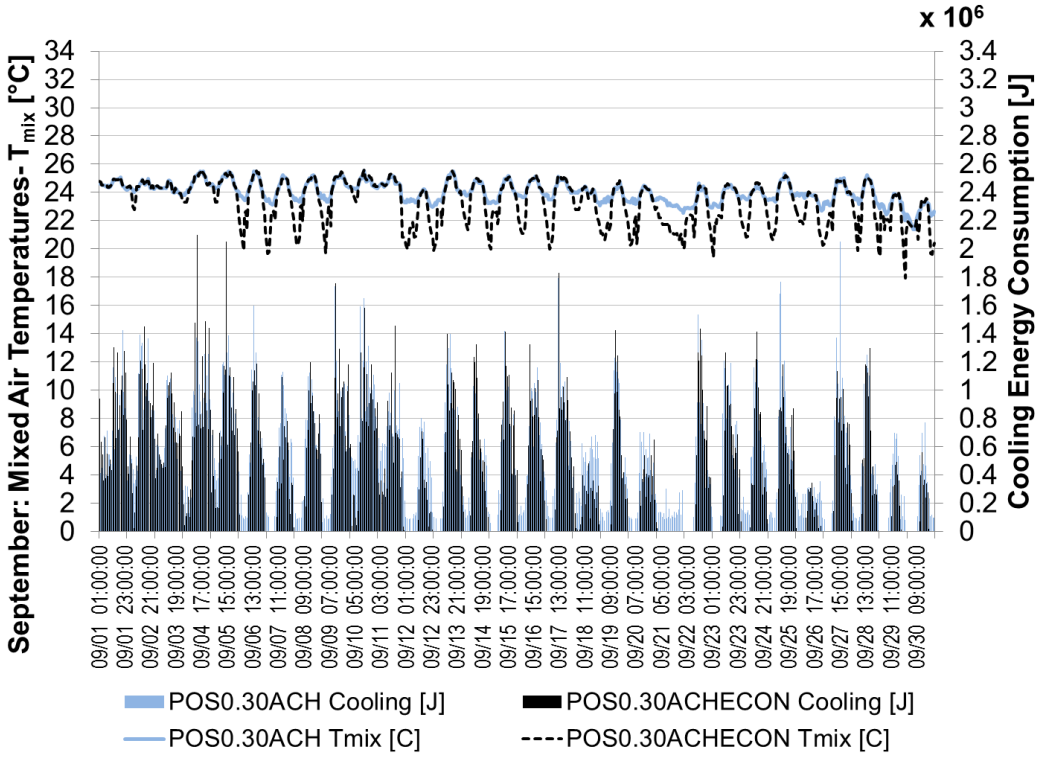

Figure 4.39: The mixed air temperatures (T_{mix}) and the corresponding cooling energy consumption of the Case 1 atrium houses with and without an economizer.

Second, keeping the core of the house at moderate temperatures helped meet the set point temperatures in the surrounding conditioned zones. Fig. 4.41 shows that using the atrium as a plenum removed the zone air temperatures above and below the set points in the living room (LR) and in the kitchen and dining room (KT-DR) zones. Fig. 4.41 also shows that the plenum atrium generally provided a heating effect for the surrounding zones and reduced their heating requirements. This effect was observed more in the bedrooms. Fig. 4.42 summarizes the improvement obtained in the hours that the set points were not met. Fig. 4.43 shows the improvement obtained in comfort conditions of the zones. Third, the atrium partially conditioned with the air returning from the surrounding zones provided a more favorable space to do laundry work and to cook during the cold winter and hot summer days. This way, the heating energy generated by the related home equipment was avoided from the conditioned zones without significantly sacrificing from the comfort of the occupants.

Consequently, this new house with a plenum atrium , i.e. Case 2 (PLPOS0.30ACH), showed 12% less cooling and 21% less heating energy consumption when compared to the case with an unconditioned atrium (POS0.30ACH) while providing improved comfort conditions (see Fig. 4.33). When an economizer was used together with the plenum atrium (PLPOS0.30ACHECON), the heating energy savings appeared to reach 33%, whereas cooling energy savings stayed at 12%. This variation in the heating energy savings was also attributed to the questionably lower supply air temperatures caused by the economizer in the AirflowNetwork model (see Section 4.2.2).

4.2.4 The Atrium House with Occupancy-based Heating and Cooling (Case 3)

The Case 1 atrium house with continuous mechanical ventilation (POS0.30ACH) was added occupancy based heating and cooling as an improvement step to obtain the Case 3 atrium house (i.e. OCPOS0.30ACH) of this study. This new house was divided into four separate scenarios modeled with four separate EnergyPlus files. These scenarios were 1) the cooling scenario of the living area, 2) the heating scenario of the living area, 3) the cooling scenario of the bedrooms and 4) the heating scenario of the bedrooms. Fig. 4.44

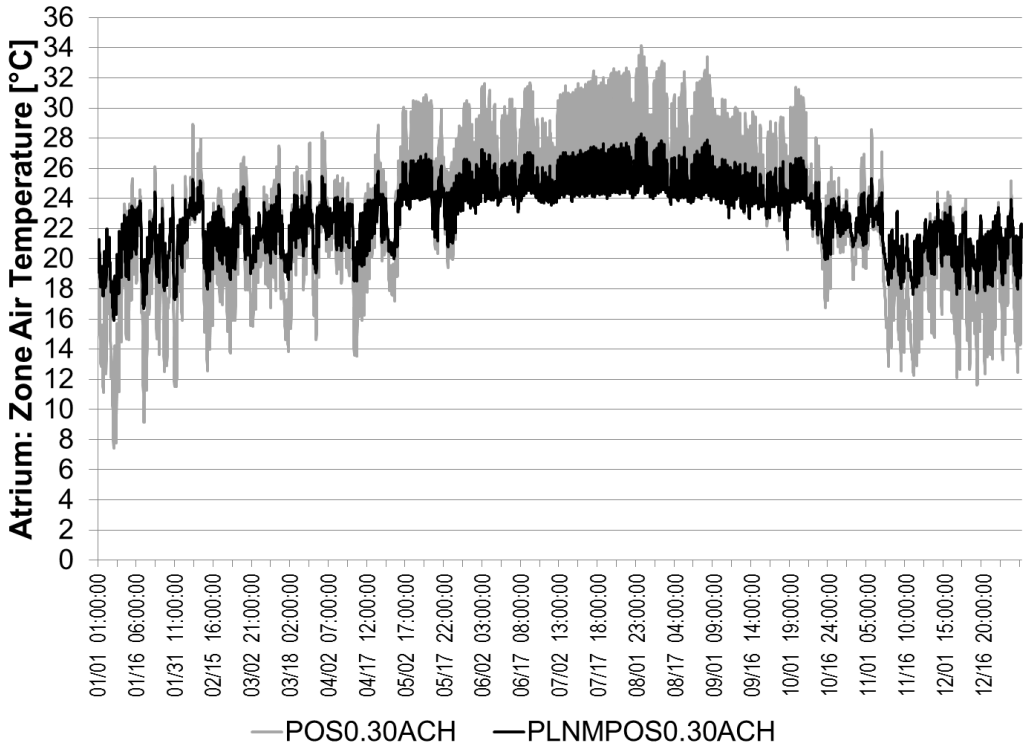

Figure 4.40: The atrium temperatures in the POS0.30ACH and PLPOS0.30ACH cases of the atrium house.

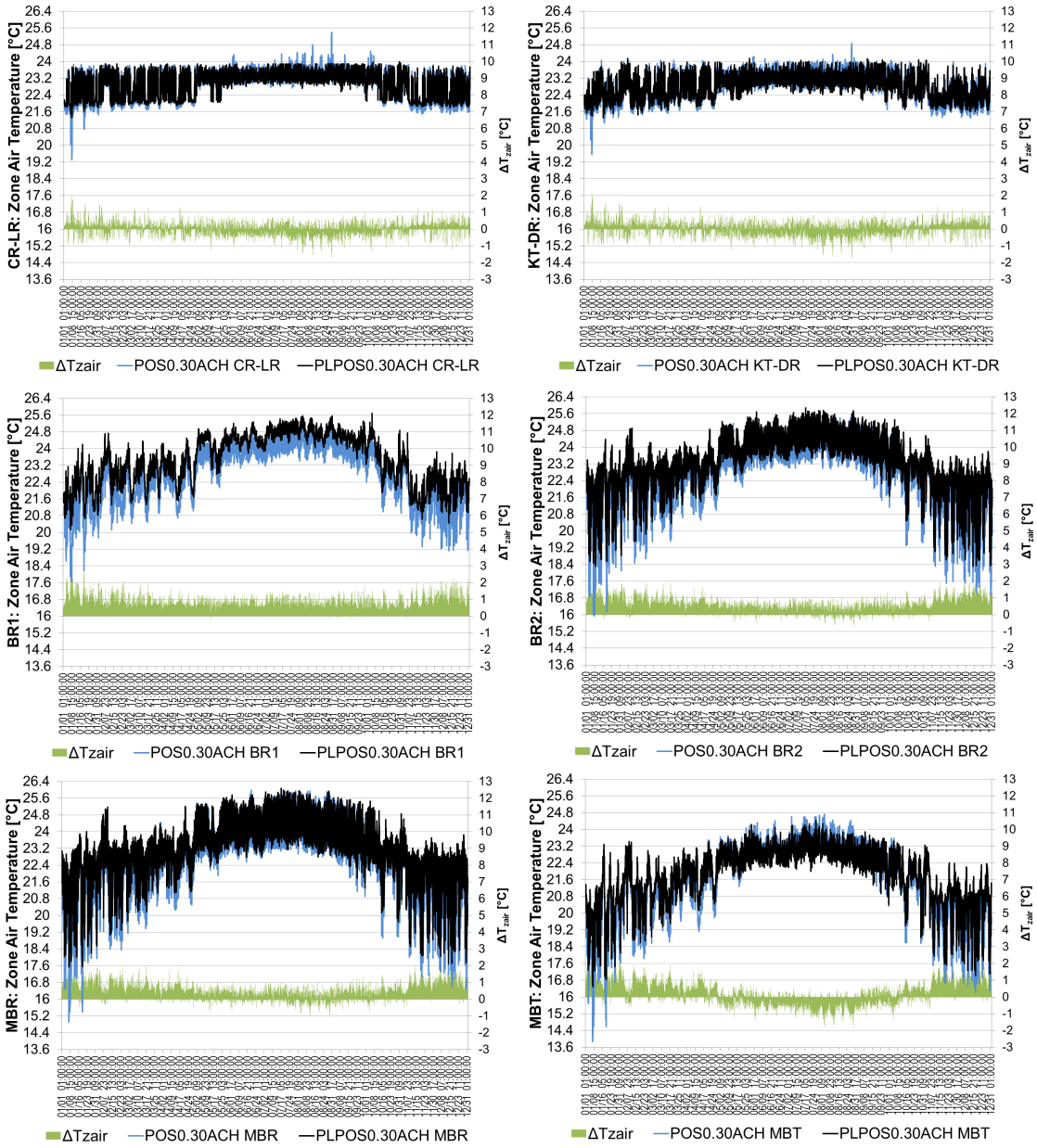

Figure 4.41: POS0.30ACH vs PLPOS0.30ACH: The zone air temperatures. $\triangle T_{zair}$: $T_{zair-PLPOS0.30ACH} - T_{zair-POS0.30ACH}$

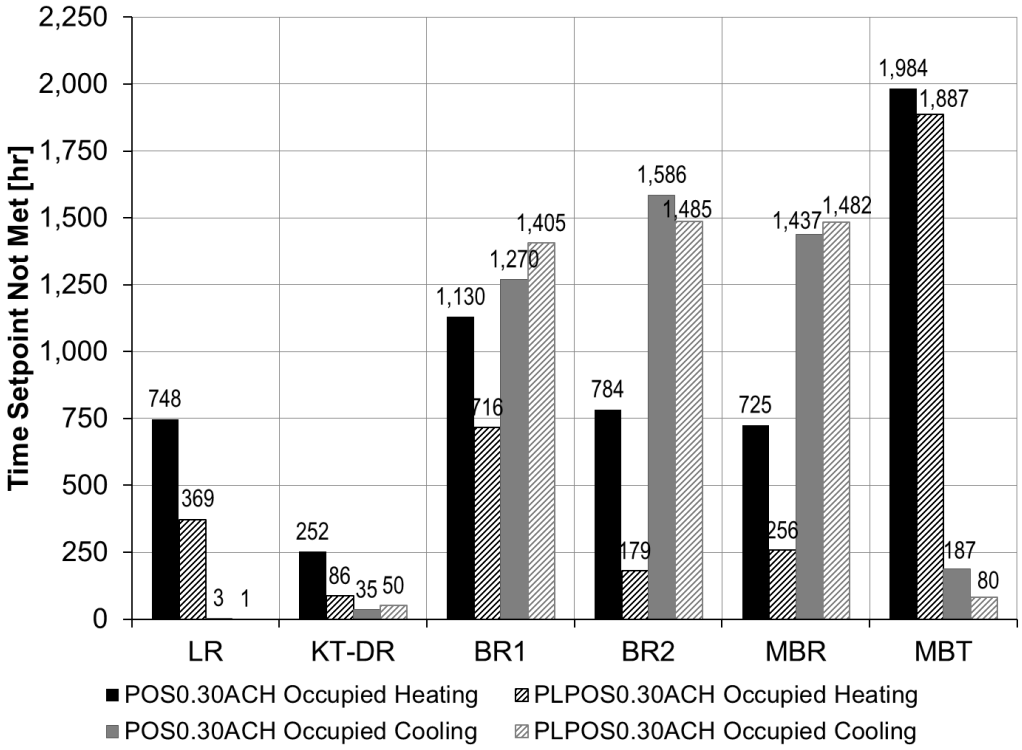

Figure 4.42: POS0.30ACH vs PLPOS0.30ACH: Time set point not met.

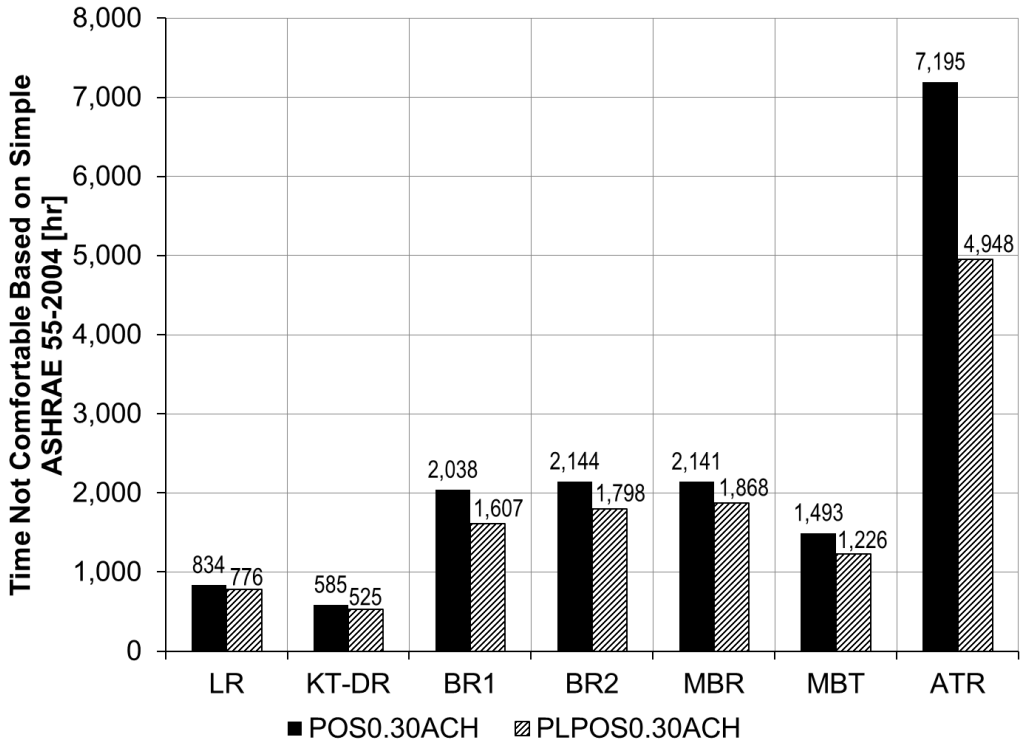

Figure 4.43: POS0.30ACH vs PLPOS0.30ACH: Time not comfortable based on simple ASHRAE 55-2004 with winter or summer clothes.

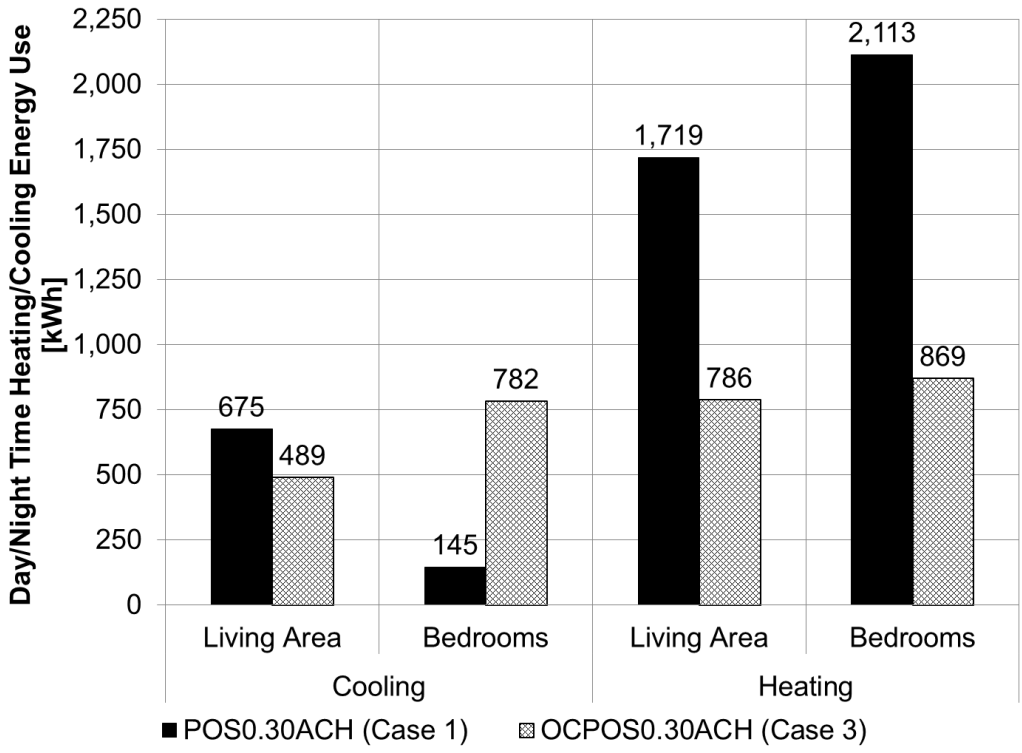

Figure 4.44: OCPOS0.30ACH vs POS0.30ACH: The total heating and cooling energy consumption per scenario.

shows the HVAC energy consumption of the OCPOS0.30ACH atrium house for each of these four scenarios.

It was found that occupancy based conditioning reduced energy consumption in all scenarios except in the cooling scenario of the bedrooms (see Fig. 4.44). In the cooling scenario of the bedrooms, the coil energy consumption increased 5.4 times with the introduction of the occupancy based system. This result was explained with two factors, i.e. the sizing limitation of the EnergyPlus program and the cooling requirement of the bedrooms at nights.

EnergyPlus sized the system airflow rate and the cooling/heating coil capacities for each scenario of the OCPOS0.30ACH system considering the starting hour of the system as the peak hour. This caused a general oversizing of the system equipment in the occupancy based system. It was realized that the oversizing of the equipment will cause the system

to work with lower efficiency, but this limitation of EnergyPlus was accepted in this study for the sake of being consistent in using the EnergyPlus sizing method among the different cases of the study.

The airflow rate ($\dot{v}$) sized for the cooling scenario of the bedrooms was found to be particularly high (0.232 m^3/s). During these hours, the supply air temperatures (T_{sup}) of the system were significantly lower than those of the POS0.30ACH system, because the system was controlled based on the temperatures of the occupied master bedroom rather than the unoccupied living room as in the case of the POS0.30ACH system. This led to higher temperature difference ($\triangle T$) between the mixed air temperature (T_{mix}) and the supply air temperature in the OCPOS0.30ACH system during the cooling hours of the bedrooms. As the energy consumption of the cooling coil (q_{CT}) can be calculated using Eq. 4.4, Eq. 4.5 and Eq. 4.6 for both of these systems, the cooling energy consumption of the bedrooms was found to be higher in the OCPOS0.30ACH system than in the POS0.30ACH system at nights (see Fig. 4.45).

$$q_{CT} = \dot{m}(h_{mix} - h_{sup}) \tag{4.4}$$

$$q_{CT} = \rho \dot{v} C_p (\triangle T) \tag{4.5}$$

$$q_{CT} = \rho \dot{v} C_p (T_{mix} - T_{sup}) \tag{4.6}$$

In all other scenarios of the occupancy based system, $\dot{v}$ of the system was found to be lower in the OCPOS0.30ACH than in the POS0.30ACH (see Fig. 4.45 and Fig. 4.46). In the living area scenarios, this was added to the lower $\triangle T$ values resulting in the 28% (cooling) to 54% (heating) energy savings shown in Fig. 4.44. The occupancy based system (OCPOS0.30ACH) was found to perform better than the POS0.30ACH system in meeting the set points in all scenarios of all the rooms except in the cooling scenario of the kitchen

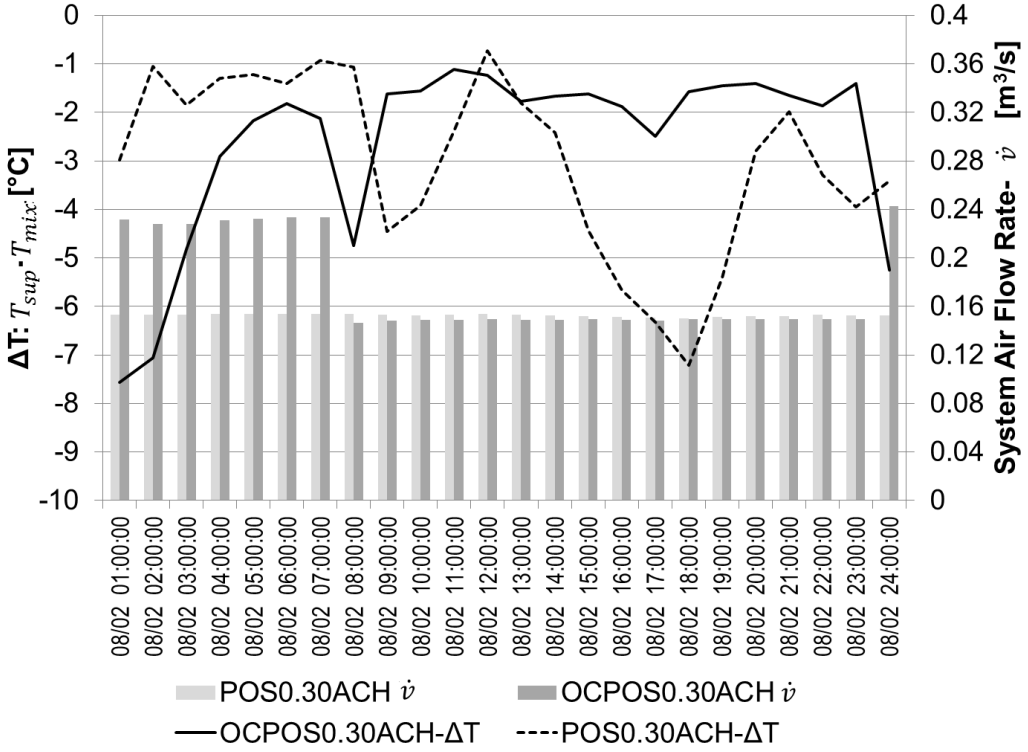

Figure 4.45: OCPOS0.30ACH vs POS0.30ACH: The variation in the $\dot{v}$ and ΔT values of the system on the worst summer day, i.e. August, 2$^{\text{nd}}$.

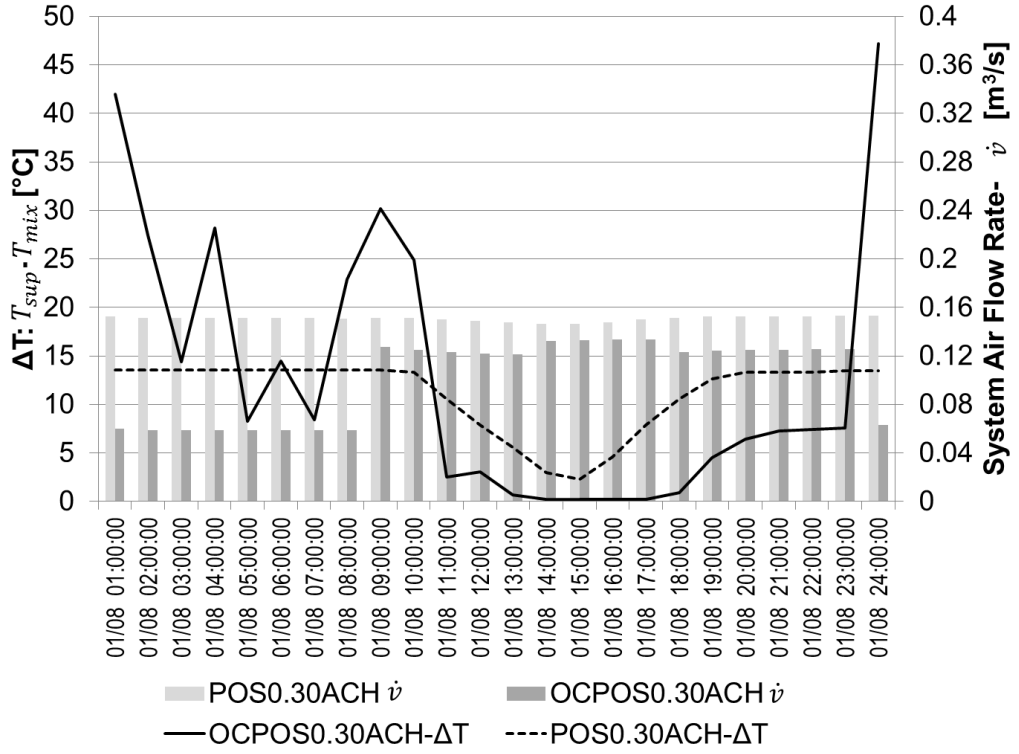

Figure 4.46: POS0.30ACH vs OCPOS0.30ACH: The variation in the $\dot{v}$ and ΔT values of the system on the worst winter day, i.e. January, 8^{th}.

and dining room (KT-DR) (see Fig. 4.47). This was attributed mainly to the higher heating/cooling capacities of the OCPOS0.30ACH system.

With the implementation of the occupancy based system into the positively pressurized baseline atrium house (POS0.30ACH), the distribution of the outside air into the zones changed as well. The Fig. 4.48 showed the mechanical ventilation air exchange rate of each room in the POS0.30ACH and OCPOS0.30ACH models. These values showed that, the occupancy based system pulled the outside air exchange rates of the LR (by 32%) and the KT-DR areas (by 44%) down to more reasonable values (0.3 ACH and 0.4 ACH respectively). The excessive outdoor air in these areas were directed into the poorly ventilated bedrooms increasing their air exchange rate by 57%-94%. The ventilation rate of the main bathroom (MBT) was also increased by 39% with this new system.

Consequently, the implementation of occupancy based system to the positively pres-

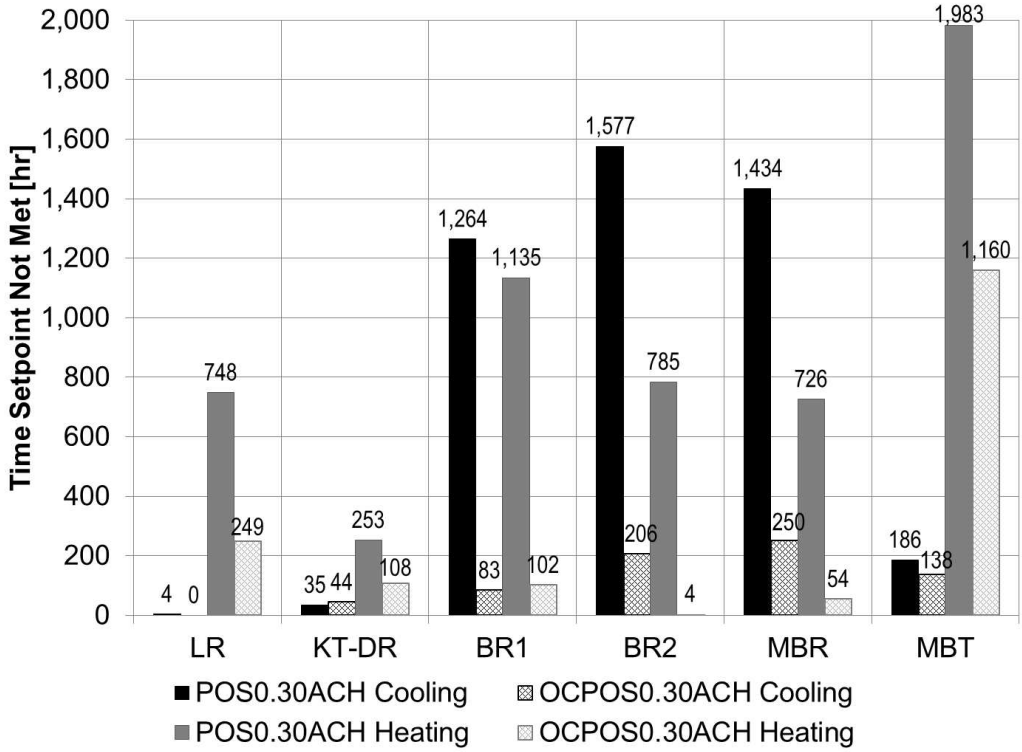

Figure 4.47: POS0.30ACH vs OCPOS0.30ACH: Occupied heating and cooling hours that the set point was not met.

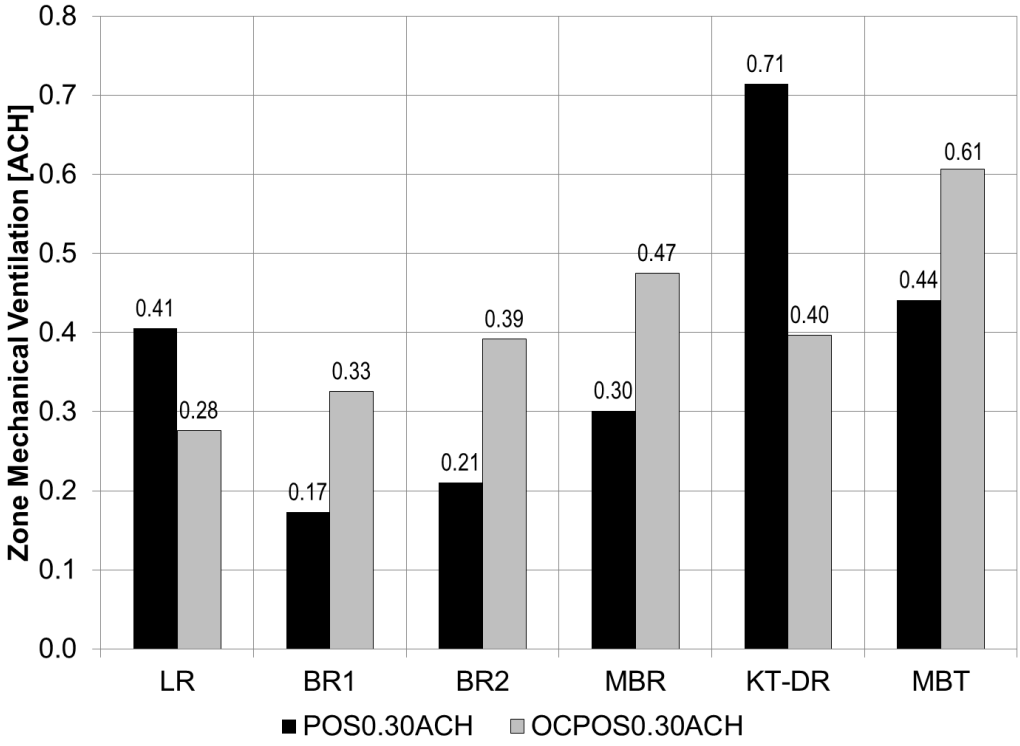

Figure 4.48: POS0.30ACH vs OCPOS0.30ACH: The mechanical ventilation air exchange rate per zone.

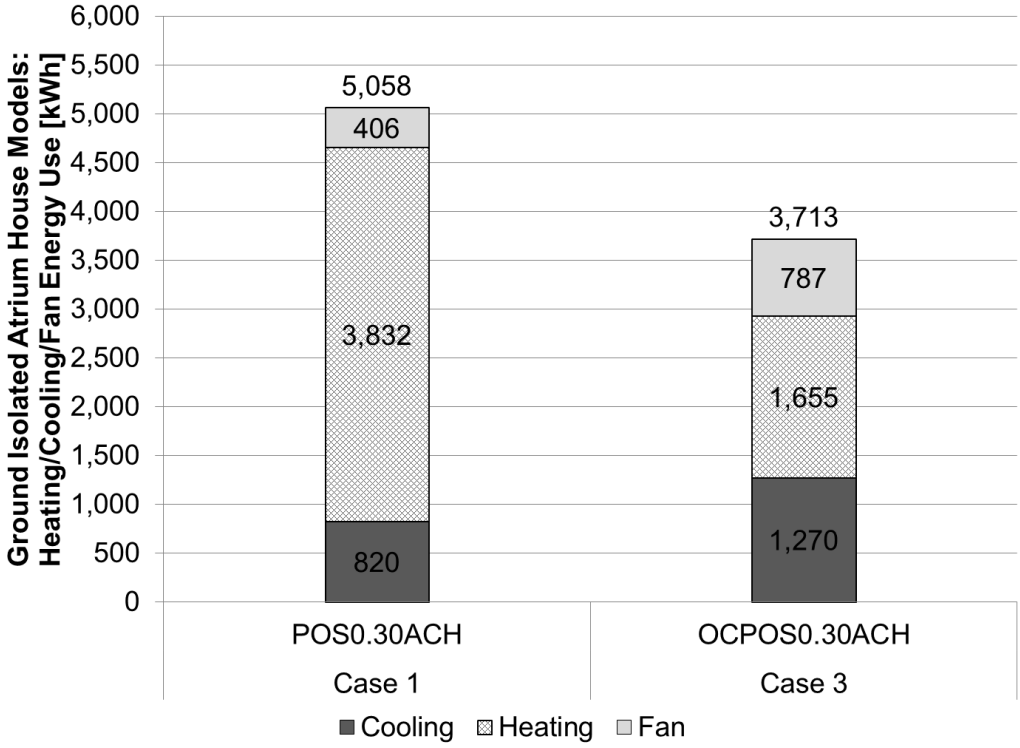

Figure 4.49: OCPOS0.30ACH vs POS0.30ACH: The annual heating, cooling and fan energy consumption.

surized baseline atrium house reduced the annual heating energy consumption by 57% and increased the annual cooling energy consumption by 55% (see Fig. 4.49). This resulted in 26% reduction in total annual HVAC energy consumption.

4.2.5 The Atrium House with Multiple Reuse of Air (Case 4)

The occupancy based system modeled in Section 4.2.4 was further modified by introducing a new airflow design principle, i.e. reuse of air. According to this principle, the air returning from the occupied conditioned rooms were sent to the unoccupied unconditioned rooms. This way, the temperatures of the unoccupied rooms were improved. Fig. 4.50 and Fig. 4.51 show the zone air temperatures of the unoccupied rooms obtained with the OCPOS0.30ACH and MRS0.30ACH systems on the worst summer and worst winter days. Partially conditioning the neighboring unoccupied zones made it easier to maintain the set points in the occupied conditioned zones. Thus, the number of hours that the set points

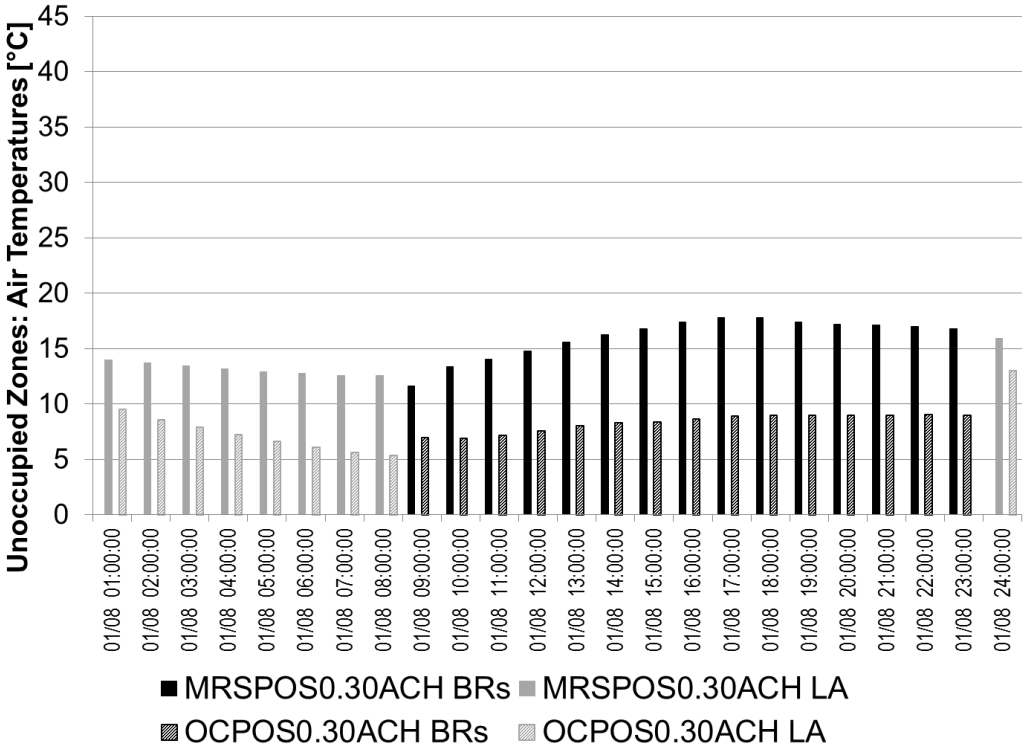

Figure 4.50: MRSPOS0.30ACH vs OCPOS0.30ACH: The temperatures of the unoccupied zones on the worst winter day, i.e. January, 8^{th}.

were not met dramatically decreased with the introduction of the reuse of air principle (see Fig. 4.52). It was observed that humidity conditions of the unoccupied rooms were also significantly improved when they were partially conditioned with the air returning from the occupied conditioned zones (see Fig. 4.53 and Fig. 4.54).

Finally, the cooling energy consumption was reduced by 26%, the heating energy consumption was reduced by 42% and the fan energy consumption was reduced by 51% with the introduction of the "reuse of air" principle to the occupancy based system (OCPOS0.30ACH) (see Fig. 4.55). This corresponded to a total HVAC energy reduction of 37% from the OCPOS0.30ACH case. The total HVAC energy consumption of this final occupancy based system with multiple reuse of air (MRS0.30ACH) was found to be 53% lower than that of the positively pressurized baseline atrium house (ATR POS0.30ACH) and 46% lower than that of the positively pressurized Habitat for Humanity (HFH POS0.30ACH)

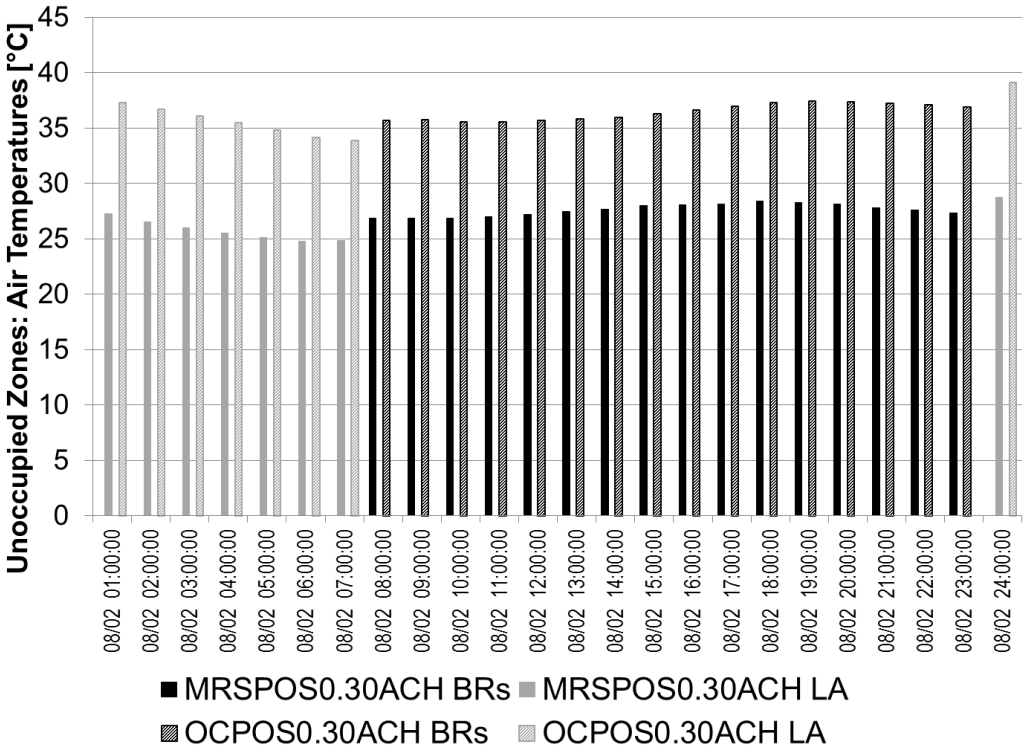

Figure 4.51: MRSPOS0.30ACH vs OCPOS0.30ACH: The temperatures of the unoccupied zones on the worst summer day, i.e. August, 2nd.

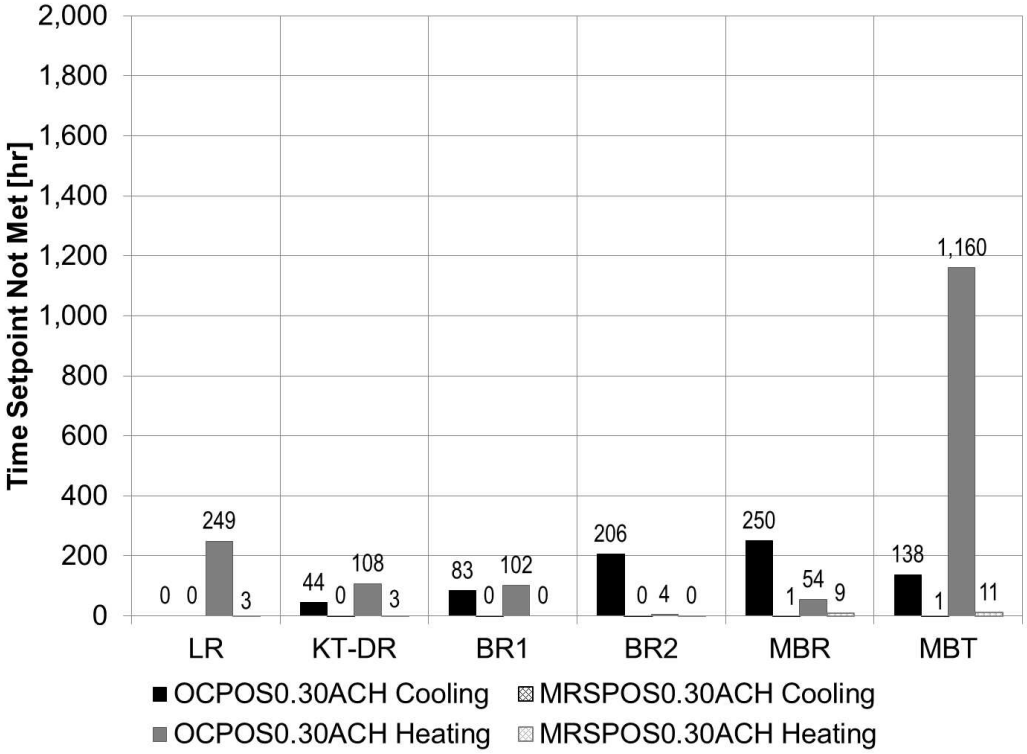

Figure 4.52: MRSPOS0.30ACH vs OCPOS0.30ACH: The number of occupied hours that the set points were not met.

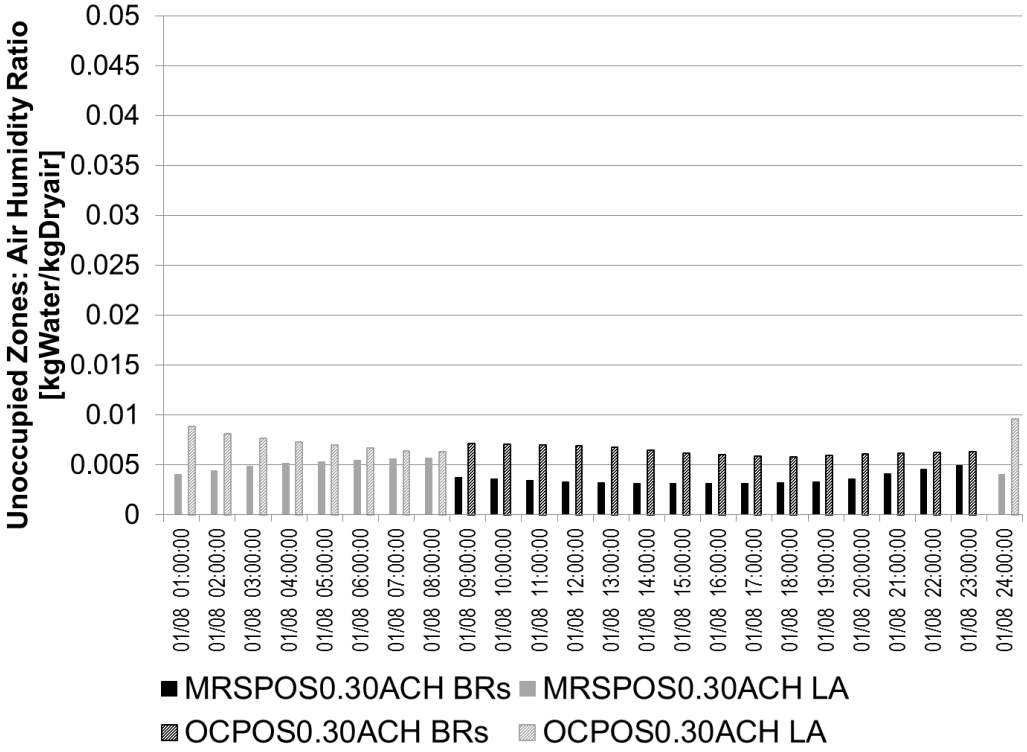

Figure 4.53: MRSPOS0.30ACH vs OCPOS0.30ACH: The humidity ratios of the unoccupied zones on the worst winter day, i.e. January, 8^{th}.

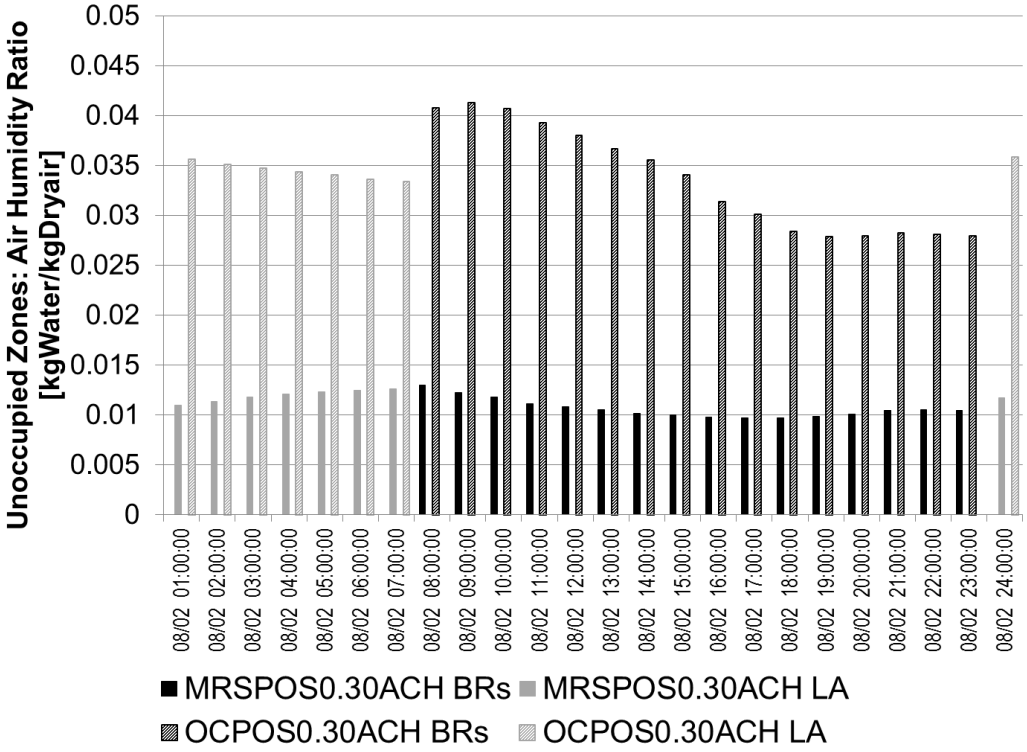

Figure 4.54: MRSPOS0.30ACH vs OCPOS0.30ACH: The humidity ratios of the unoccupied zones on the worst summer day, i.e. August, 2^{nd}.

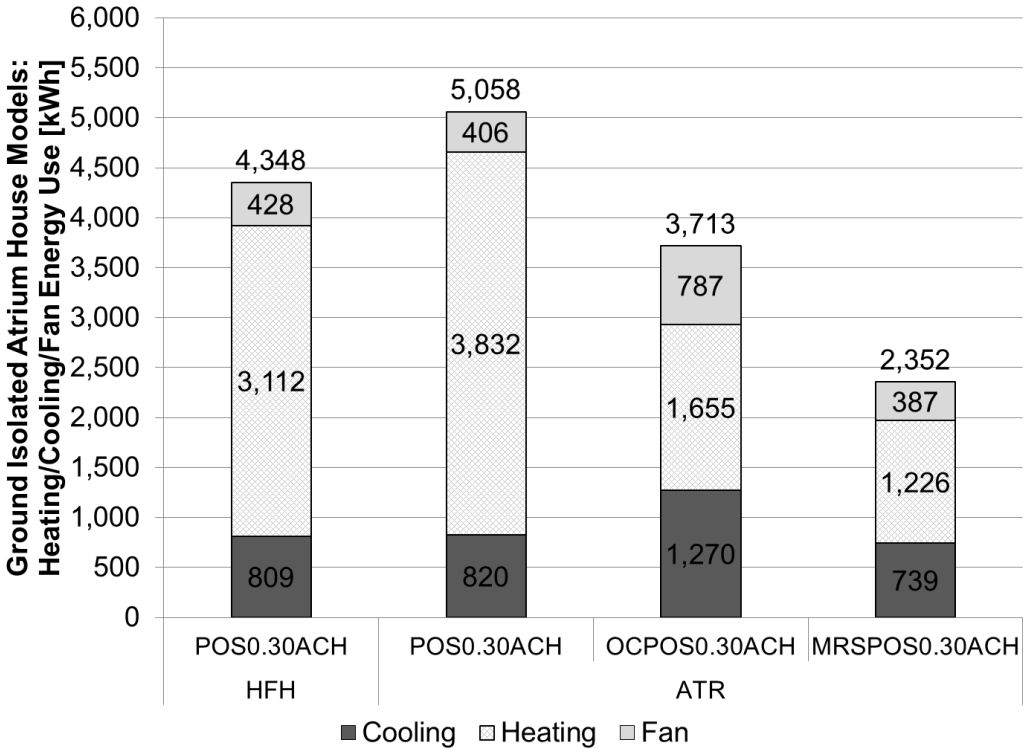

Figure 4.55: MRSPOS0.30ACH vs OCPOS0.30ACH atrium house (ATR) vs POS0.30 ACH atrium and Habitat for Humanity houses (HFH): The annual heating, cooling and fan energy consumption.

house.

The "reuse of air" principle to the occupancy based system (OCPOS0.30ACH) reduced the HVAC energy consumption in all scenarios and in all HVAC categories, i.e. heating, cooling and fan (see Fig. 4.56). The savings per scenario varied between 22% and 49% and the highest savings (49%) occurred in the cooling scenario of the bedrooms. Among the HVAC energy categories, the highest savings (54%) was observed in the fan energy consumption. This showed that, with proper duct design, the "reuse of air" idea does not need to increase fan energy consumption. It was, however, suggested that further validation of duct pressure losses needs to be made to improve this finding.

When the atrium house with multiple reuse of air (MRSPOS0.30ACH) was coupled with the ground to turn it into a slab-on-grade house, it was found that the HVAC en-

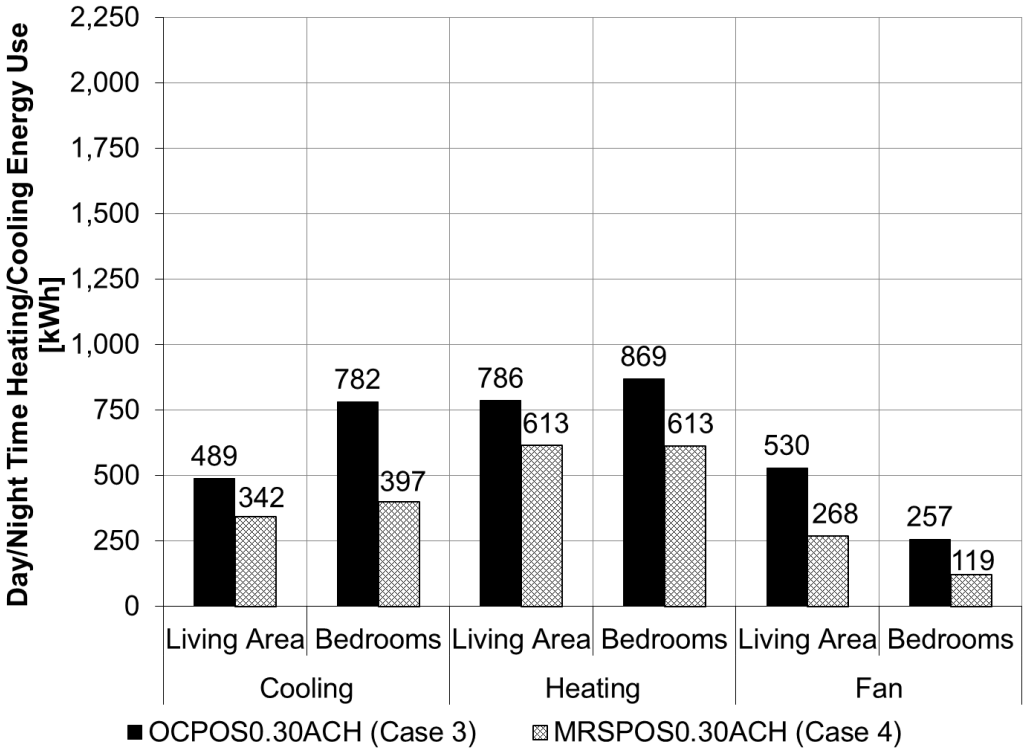

Figure 4.56: MRSPOS0.30ACH vs OCPOS0.30ACH: The total heating and cooling energy consumption per scenario.

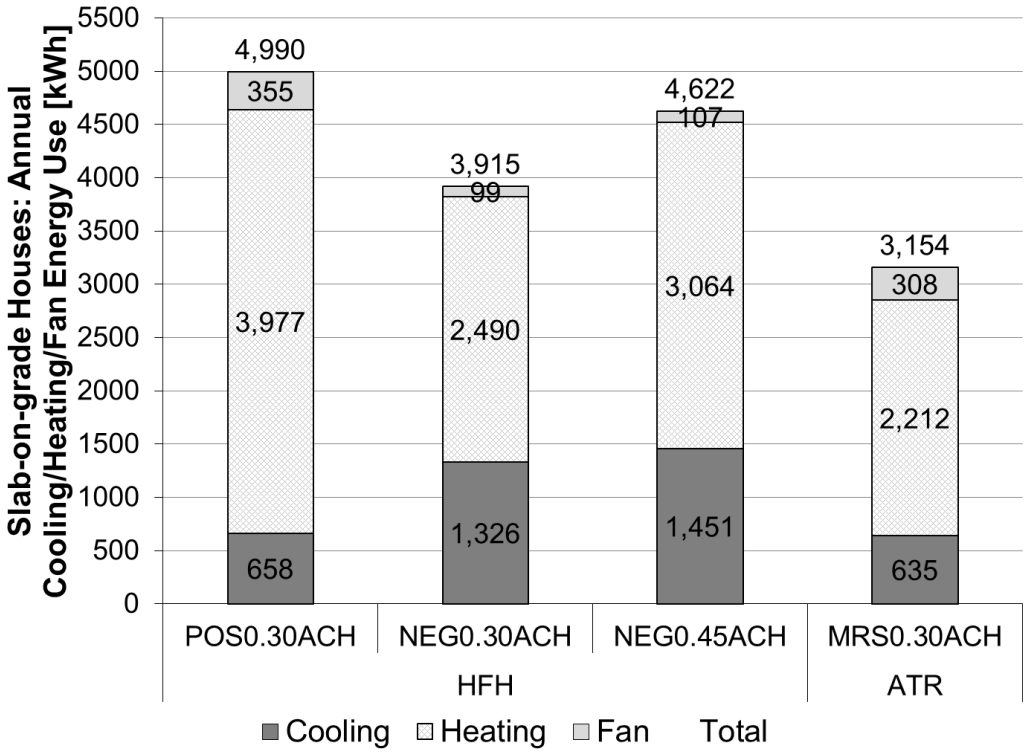

Figure 4.57: MRSPOS0.30ACH atrium house (ATR) vs the Baseline Habitat for Humanity Houses (HFH): The Slab-on-grade annual heating, cooling and fan energy consumption.

ergy savings when compared to the typical Habitat for Humanity baseline houses remained high (see Fig. 4.57). The MRSPOS0.30ACH system showed 44% lower cooling energy consumption and 4% lower cooling energy consumption when compared to the positively pressurized baseline Habitat for Humanity house (HFH POS0.30ACH). This corresponded to 37% lower total HVAC energy consumption with the MRSPOS0.30ACH system. The MRSPOS0.30ACH system also showed 19% lower HVAC energy consumption when compared to the NEG0.30ACH Habitat for Humanity house and 32% lower HVAC energy consumption when compared to the NEG0.45ACH Habitat for Humanity house.

These results showed that the savings that can be obtained from the partial conditioning strategy depends significantly on the ground coupling condition of the house. Depending on the level of heat conduction with the ground, the total HVAC energy savings obtained with the partial conditioning strategy varied between 37% and 53%.

5. SUMMARY AND CONCLUSIONS

This chapter has two primary sections i.e. "slab-on-grade heat transfer" and "partial conditioning." In each of these sections, the objectives, the research methodology and the results regarding the subject are summarized and the conclusions are presented. Based on these conclusions, further research ideas are recommended.

5.1 Slab-on-grade Heat Transfer*

Early studies have shown that the current energy modeling tools calculate dissimilar results for the slab-on-grade heat transfer. This study quantified the discrepancies between DOE-2 and EnergyPlus slab-on-grade heat transfer for low-rise 20m×20m×3m residential buildings with unconditioned attics in four U.S. climates (hot-humid, hot-dry, cold, and temperate). For the modeling of the slab-on-grade heat transfer, Winkelmann's slab-on-grade model was used with DOE-2 and the Slab model was used with EnergyPlus. The reliabilities of these models were then discussed by comparing their results with those of a more detailed TRNSYS slab-on-grade model.

The study included two steps. In the first step, the effect of ground coupling was isolated by modeling empty slab-on-grade sealed boxes at 23°C constant zone air temperature in four U.S. climates with the IECC required insulation configurations. The ground temperatures calculated by Winkelmann's (GCW), Slab (GCS) and TRNSYS (GCT) slab-on-grade models were entered into EnergyPlus and the resulting ground coupling loads were compared. At the second step, load components (i.e. wall heat transfer, ceiling heat transfer to/from an unconditioned attic, windows, doors, shades, lights, equipment and infiltration) were added to these boxes to convert them into fully loaded (with lights, equipment and solar gains) test houses. Discrepancies between the results of the obtained models were then quantified and explained both for the ground isolated and the ground coupled conditions.

For the sealed boxes, the floor heat fluxes of the GCW and GCS models differed from

* Partially reproduced from "EnergyPlus vs DOE-2.1e: The effect of ground coupling on cooling/heating energy requirements of slab-on-grade code houses in four climates of the U.S" by Simge Andolsun, Charles H. Culp, Jeff S. Haberl and Michael Witte, *Energy and Buildings*, 52(2012), 189-206, 2012. Copyright 2012, Elsevier B.V.

those of the GCT slab-on-grade models in the magnitudes, the peak months and the peak-to-peak amplitudes of the floor heat fluxes as follows:

Magnitudes: The GCS models without evaporative transpiration showed much less variation in annual ground coupling loads (2-4 GJ) from those of the GCT models than the GCW models did (4-9 GJ). The GCS models with evaporative transpiration, however, showed significantly (23-74 GJ) higher annual ground coupling loads than those exhibited by the GCT models.

Peak months: For the uninsulated floors in the hot climates, the peaks of the floor heat fluxes in the GCW and GCS models were two months and one month delayed respectively when compared to those of the GCT models. For the insulated floors in the cold climate, however, all three models had identical peak months.

Peak-to-peak amplitudes: The GCS floor heat fluxes showed 1.5 times higher peak-to-peak amplitudes than those of the GCT floor heat fluxes did for all floor configurations and climates. The peak-to-peak amplitudes of the GCW models were 1.4 times higher than those of the GCT models for the uninsulated floors in the hot climates and identical to the GCT models for the insulated floors in the temperate and cold climates.

For the ground isolated fully loaded houses, EnergyPlus results differed from those of DOE-2 by 0-31% in cooling load and by 3-15% in heating load. These differences were caused primarily by the 11-15% higher window solar incidents and 8-15% higher sensible infiltration heat losses that EnergyPlus calculated from identical window 5 inputs and leakage areas respectively.

For the slab-on-grade fully loaded houses, the GCW models calculated 10-13% higher total building loads than the GCT models did. This result was attributed to the fact that the GCW model was based on the results of a 2-D finite difference program that assumed constant zone air temperatures all year. For the same houses, the currently used internally iterated GCS models calculated significantly (18-32%) lower total building loads than those calculated by the GCT models. When EnergyPlus was iterated with Slab externally until the zone air temperatures converged within 0.0001°C, however, very close

(within 9%) total thermal loads were obtained with the GCS models to those calculated by the GCT models. This finding showed that, the convergence of zone air temperatures is significant for the accuracy of the results in the GCS models. The 0.1°C convergence tolerance for zone air temperatures was found to be sufficient in these models to make thermal load estimations within 1% of the fully converged (within 0.0001°C) values. Besides the convergence problem, three other problems were observed with the current Slab model. First, the introduction of evaporative transpiration decreased the total thermal load estimates significantly resulting in 17-60% lower thermal loads than those of the GCT models. Second, the Slab program could not model the vertical R-10 insulation with depths less than 1 m, which was required by IECC for temperate climates. Third, in a few test runs, the Slab program made internal adjustments on the slab thicknesses to meet an internal convergence tolerance value, which resulted in inconsistent thicknesses in the aboveground and belowground models of EnergyPlus.

This study showed that the Slab model produces more reliable slab-on-grade heat transfer values than the Winkelmann's slab-on-grade model (1) if the zone air temperatures converge in EnergyPlus-Slab iterations and (2) if the evaporative transpiration model of Slab is off. The Slab model, however, has significant limitations, convergence problems and inconsistent internal adjustments. Thus, to avoid erroneous results, improvement is needed in the Slab model before it should be used in residential energy code compliance calculations. These findings highlighted the urgent necessity for the implementation of a standardized slab-on-grade heat transfer modeling method into the current energy modeling programs to obtain comparable results from them in energy code compliance calculations.

5.2 Partial Conditioning

Studies have shown that up to 50% overall energy savings can be obtained in affordable houses in Texas through combined application of conventional energy efficiency measures. This study proposes an occupancy based HVAC design strategy for low-income residential buildings in hot and humid climates that will introduce an additional 30%-50% HVAC energy savings. The partial conditioning strategy is based on three primary ideas. These

ideas are 1) using historic courtyard building schemes to provide a shaded buffer zone between conditioned zones, 2) applying occupancy based heating/cooling to save the HVAC energy used during the unoccupied hours and 3) reusing the conditioned air returning from the occupied zones in the unoccupied zones before it is returned to the system in order to avoid too low/high temperatures in the unoccupied zones. The design of this strategy includes design of a central atrium space integrated to the HVAC system and used as a return plenum, i.e. an atrium plenum. It also includes design and modeling of an innovative duct layout that allows for bidirectional airflow between the two sides of the house, i.e. the occupied side and unoccupied side. For the simulation of this strategy, a multizone modeling approach was used for both the aboveground and belowground heat transfer calculations. The AirflowNetwork model of EnergyPlus was used for the aboveground energy and airflow calculations. The TRNSYS Type 1255 slab-on-grade heat transfer model was used to simulate the belowground heat transfer calculations. The aboveground and below ground models were then connected to each other through an iteration process. In this modeling approach, the effects of thermostat location, interior partitions and duct layout were taken into account and the resulting differences in zone air temperatures and infiltration rates between the rooms were monitored.

This part of the study was conducted in four steps: 1) data collection, 2) base-line design and modeling, 3) partial conditioning design and modeling, 4) analyses and recommendations. First, a site visit was held to the Habitat for Humanity houses in Bryan, Texas to collect data on the characteristics of these buildings. Second, a base-line Habitat for Humanity house was designed and modeled using the information collected in the previous step along with multiple other resources including IECC 2012, Building America benchmark definitions, IES and ASHRAE Handbooks and ACCA Manuals. Third, the "partial conditioning" strategy was introduced into the base-line Habitat for Humanity house models to simulate a partially conditioned atrium house.

The baseline building was assumed to be a 994 ft^2, one story high, slab-on-grade Habitat for Humanity house in this study. This building was modeled with three outdoor air

exchange conditions. These conditions were:

1) positively pressurized with mechanical ventilation system that provides 0.3ACH annual average air exchange rate (POS0.30ACH),

2) negatively pressurized with 0.3 ACH annual average infiltration rate (NEG0.30ACH),

3) negatively pressurized with 0.45 ACH annual average infiltration rate (NEG0.45 ACH).

The introduction of the partial conditioning strategy into the baseline Habitat for Humanity house models was conducted in four steps:

1) conversion of the baseline Habitat for Humanity house models into atrium house models:

-resulted in the POS0.30ACH, NEG0.30ACH and NEG0.45ACH atrium house models,

2) using the atrium as a return plenum in the a positively pressurized atrium house model:

-resulted in the PLPOS0.30ACH model,

3) applying occupancy based heating/cooling in the POS0.30ACH baseline atrium house by conditioning only the occupied zones:

-resulted in the OCPOS0.30ACH model,

4) reusing the air returning from the occupied conditioned zones of the OCPOS0.30ACH model in the unoccupied zones before it was returned to the system:

-resulted in the MRSPOS0.30ACH model.

Findings showed that the total HVAC energy consumption of the baseline Habitat for Humanity houses differed from the average by -13% to +11% depending on the outdoor air exchange condition. Mechanical ventilation system with constant airflow rate (POS0.30ACH) provided the opportunity to benefit from the cooler nighttime temperatures in the cooling season; whereas infiltration rates significantly dropped during these hours. This resulted in 50% lower annual cooling energy consumption in the POS0.30ACH model than in the NEG0.30ACH model. In the heating season, this condition had an opposite effect as more outside air entered into the building during the colder night hours

in the mechanically ventilated case than in the negatively pressurized case increasing the annual heating energy consumption by 60%.

For the negatively pressurized models (i.e. NEG0.30ACH and NEG0.45ACH), the baseline atrium houses showed lower (6%-11%) cooling energy consumption and higher (24%-35%) heating energy consumption when compared to the baseline Habitat for Humanity houses. This was caused primary by two reasons. First, the heat gains from the equipment in the conditioned zones was lower in the atrium house. Most of the home equipment that generate heat were located in the atrium in the atrium house; whereas they were in the conditioned rooms in the Habitat for Humanity houses. Second, the atrium house required less electric lighting than the Habitat for Humanity houses due to it improved daylighting design.

When the atrium was used as a return plenum of the HVAC system in the positively pressurized atrium house (PLPOS0.30ACH), the cooling energy consumption decreased by 12% and the heating energy consumption decreased by 21%. This step also reduced the number of occupied uncomfortable hours in the house by 22% and the number of occupied hours that the set points were not met by 21%. When compared to the positively pressurized Habitat for Humanity house model, the model with the occupancy based system

The implementation of occupancy based system into the positively pressurized baseline atrium house (OCPOS0.30ACH) reduced the annual heating energy consumption by 57% and increased the annual cooling energy consumption by 55%. This corresponded to 26% reduction in the total annual HVAC energy consumption. Besides these energy savings, this system also provided 84% reduction in the total occupied hours that the set points were not met. Compared to the positively pressurized Habitat for Humanity house models, the improvement obtained with the OCPOS0.30ACH system in the occupied unmet hours was 39% when the common zones were compared.

With the introduction of the reuse of air idea into the occupancy based system (MRSPOS0.30ACH), the cooling energy consumption was reduced by 26%, the heating energy consumption was reduced by 42% and the fan energy consumption was reduced by 51%.

This corresponded to a total HVAC energy reduction of 37% from the OCPOS0.30ACH model to the MRSPOS0.30ACH model. The final occupancy based system with multiple reuse of air (MRS0.30ACH) used total HVAC energy 53% less than the positively pressurized baseline atrium house and 46% less than the positively pressurized Habitat for Humanity house.

It was found that the quantity of HVAC energy savings that can be obtained from the partial conditioning strategy depends significantly on the ground coupling condition of the house. In hot and humid Texas, the total HVAC energy savings varied between 37% (slab-on-grade with no insulation) and 46% (ground isolated) depending on the insulation condition of the floor.

The primary conclusion of this study is that substantial (37%-46%) reduction can be achieved in the overall HVAC energy consumption of small ($\sim$1,000 ft^2) residences in hot and humid climates while performing better in meeting the temperature set points and more evenly distributing the outside air in the house. The "partial conditioning" is an innovative HVAC design strategy that can meet this challenge.

The experience with EnergyPlus and the design and modeling of the partial conditioning strategy in this study led to identification of a few improvement points and suggestions for further research. These points are as follows:

*Using the multizone AirflowNetwork model of EnergyPlus for the modeling of residential buildings is an effective approach in determining the variations in the temperature and air exchange rates of different rooms. The relationship between the wind speed and the infiltration rates could be studied further by including Computational Fluid Dynamics to improve the wind pressure coefficients for nonrectangular buildings.

*The current energy modeling tools have significant limitations that make the modeling of innovative HVAC system designs like "partial conditioning" a challenge. The flexibility of the modeling tools needs to be improved to allow for new air loop designs that do not necessarily follow the typical order of system components. For instance, a fan blowing air directly into a zone and continuing into a heating coil could act as a preheating system

to be used in the heating season if EnergyPlus allowed. An exhaust fan modeled in the unconditioned atrium could improve the indoor air quality of the atrium and would provide the air exchange requirement of the cooktop unit in the atrium. A flexible air loop model that provides the capability to switch between different duct layouts at different times of the day would also improve the accuracy of the energy estimations for the partial conditioning strategy. Also, zone air splitters could be improved such that they can be used after the air exits of zones. This way, the unoccupied zones can be modeled as separate zones rather than one unified plenum zone in the MRS0.30ACH model resulting in a better representation of reality. Currently, EnergyPlus does not allow for the modeling of any of these conditions.

*The AirflowNetwork:Distribution model used in this study for the modeling of the airflow inside the ducts exhibited significant limitations and reported questionable outputs. One of the most challenging limitation of this model for this study was the "suspected" minimum velocity limit for the airflow in the ducts. This led to compromises in the estimated duct sizes to avoid the program errors. One important questionable output of the model was the airflow rates monitored at the intersection point of the outside air supply duct and the zone return air duct of the air loop. The air flow rate in the main return duct was higher than the sum of the air flow rates in the zone return duct and the outside air supply ducts. The airflow rates reported for these points by the the AirflowNetwork:Distribution model were also found to be significantly different than those reported by the AirloopHVAC model. These issues were reported to the EnergyPlus development team. The team fixed the mass balance at the outdoor air system node with the release of the EnergyPlus version 8.0.0.007. The volume flow rates are, however, still not balanced at the outdoor air node of the AirflowNetwork:Distribution model. The other questionable output of this model was the distribution of outside air into the zones in the mechanically ventilated occupancy based models, i.e. the OCPOS0.30ACH and MRS0.30ACH models. The AirflowNetwork reported that the zone with the lowest peak load received the highest outside air fraction in its supply airflow rate, which was physically not possible since the ducts were sized based on the peak airflow rates of the zones for a given design day. The EnergyPlus development

team has been updated on these points as well for further improvement of the program. In this study, the mechanical ventilation rates of the zones of the OCPOS0.30ACH and MRS0.30ACH models were plotted by turning the AirflowNetwork model off to avoid these reporting errors.

*It was seen that the design of the main bathroom can be critical for more effective implementation of the partial conditioning strategy in atrium houses. In this study, the main bathroom was located distant from the rest of the living area zones and it was modeled attached to the bedrooms. This made it exposed to unoccupied zones during its conditioned hours making the temperature control in this zone harder. Based on the experience gained with this study, it was concluded that locating the bathroom in between the other living area zones (i.e. kitchen, dining room and living room) that it has coinciding occupied hours with could improve the temperatures of this zone. This can also reduce the duct length of the system and add to the overall energy savings by reducing the conduction heat transfer through the ducts and decreasing the fan pressure rise at the design air flow rate of the system.

*The selection of the fittings and minimizing the duct lengths were found to be critical for improving the energy performance of the partial conditioning strategy as these features related to the fan energy consumption. The supply and return diffuser of the zones should be carefully selected to minimize the pressure losses at these critical points. A comprehensive pressure loss study could be conducted including Computational Fluid Dynamics simulations in order to make a more detailed analysis on the performance of the air distribution system in the partially conditioned atrium house.

*The ground coupling condition of a residential building was found to be a critical factor that significantly affects the the quantity of energy savings that can be obtained with the "partial conditioning" strategy. This makes the selection of the modeling method for ground heat transfer very critical in estimation of the energy savings. Thus, the relationship between the performance of the partial conditioning strategy and the ground coupling condition (i.e. slab-on-grade, crawlspace, basement, etc.) needs further studies to discuss

the effectiveness of this strategy in different ground coupling conditions.

*A validation of this study can be conducted in two ways. First, the concepts discussed in this study can be extended to larger residential and also commercial buildings by repeating the same modeling procedure. Second, experimental studies can be conducted on real buildings with and without the partial conditioning strategy in order to compare with the modeling results.

*The cost analysis of the house design proposed in this study cannot at this time be reasonably made. This is because many critical components of the proposed system are currently not available in the market. Thus, the cost estimates will need to wait until the equipment is better defined and close to product available status. When these conditions are met, a life cycle cost estimation of the partially conditioned houses can be a very informative further study.

REFERENCES

[1] United States Environmental Protection Agency, *EPA Green Buildings*, http://www.epa.gov/oaintrnt/projects/ (2013), accessed: 2013-07-16.

[2] The United States Energy Information Administration, *Figure 2.1a Energy consumption estimates by sector overview*, http://www.eia.gov/totalenergy/data/annual/ (2011), accessed: 2013-07-16.

[3] The Environmental Protection Agency, *Inventory of U.S. greenhouse gas emissions and sinks: 1990-2010*, http://www.epa.gov/climatechange/Downloads/ghgemissions/US-GHG-Inventory-2012-Main-Text.pdf (2010), accessed: 2013-07-16.

[4] Energy Efficiency & Renewable Energy United States Department of Energy, *2010 Buildings energy data book*, http://buildingsdatabook.eren.doe.gov/TableView.aspx?table=1.1.9 (2010), accessed: 2013-07-16.

[5] The United States Environmental Protection Agency, *Energy efficiency in affordable housing, a guide to developing and implementing green house gas reduction programs*, http://www.epa.gov/statelocalclimate/documents/pdf/affordable_housing.pdf (2011), accessed: 2013-07-16.

[6] M. Brennan and B. J. Lipman, *Stretched thin: The impact of rising housing expenses on america's owners and renters*, *Proceedings of National Housing Conference* (Center for Housing Policy, 2008).

[7] The United States Department of Housing and Urban Development, *Affordable housing*, http://www.hud.gov/offices/cpd/affordablehousing/ (2013), accessed: 2013-07-16.

[8] The United States Energy Information Administration, *Housing unit characteristics by four most populated states, 2005 million housing units*, http://www.eia.gov/consumption/residential/data/2005/ (2005), accessed: 2013-07-16.

[9] Z. Yu, B. C. M. Fung, F. Haghighat, H. Yoshino, and E. Morofsky, *A systematic procedure to study the influence of occupant behavior on building energy consumption*, Energy and Buildings **43**, 1409 (2011).

[10] A. Al-Mumin, O. Khattab, and G. Sridhar, *Occupants' behavior and activity patterns influencing the energy consumption in the kuwaiti residences*, Energy and Buildings **35**, 549 (2003).

[11] J. Tanimoto, A. Hagishima, and H. Sagara, *A methodology for peak energy requirement considering actual variation of occupants' behavior schedules*, Building and Environment **43**, 610 (2008).

[12] A. F. Emery and C. J. Kippenhan, *A long-term study of residential home heating consumption and the effect of occupant behavior on homes in the pacific northwest constructed according to improved thermal standards*, Energy **31**, 677 (2006).

[13] G. Y. Yun and K. Steemers, *Time-dependent occupant behaviour models of window control in summer*, Building and Environment **43**, 1471 (2008).

[14] T. Leephakpreeda, *Adaptive occupancy-based lighting control via grey prediction*, Building and Environment **40**, 881 (2005).

[15] F. Haldi and D. Robinson, *On the behaviour and adaptation of office occupants*, Building and Environment **43**, 2163 (2008).

[16] L. L. Pan, T. Chen, Q. S. Jia, R. X. Yuan, H. T. Wang, and R. Ding, *An occupant behavior model for building energy efficiency and safety*, *Proceedings of the 2^{nd} International ISCM Symposium and the 12^{th} International EPMESC Conference* (American Institute of Physics, 2010).

[17] D. Beourgeois, *Detailed Occupancy Prediction, Occupancy-sensing Control and Advanced Behavioral Modeling within Whole-building Energy Simulation*, Ph.D. Dissertation, l'Universite Laval, Quebec (2005).

[18] H. B. Rijal, P. Tuohy, M. A. Humphreys, J. F. Nicol, A. Samuel, and J. Clarke, *Using results from field surveys to predict the effect of open windows on thermal comfort and energy use in buildings*, Energy and Buildings **39**, 823 (2007).

[19] C. F. Reinhart, *Lightswitch-2002: A model for manual and automated control of electric lighting and blinds*, Solar Energy **77**, 15 (2002).

[20] M. Mozer, *The neural network house: An environment that adapts to its inhabitants*,

Proceedings of Spring Symposium on Intelligent Environments (American Association for Artificial Intelligence, Stanford University, Palo Alto, California, USA, 1998).

[21] L. Pérez-Lombard, J. Ortiz, and C. Pout, *A review on buildings energy consumption information*, Energy and Buildings **40**, 394 (2008).

[22] L. Pérez-Lombard, J. Ortiz, J. F. Coronel, and I. R. Maestre, *A review of HVAC systems requirements in building energy regulations*, Energy and Buildings **43**, 255 (2011).

[23] *Model Energy Code* (The Council of American Building Officials, Falls Church, Virginia, 1983).

[24] *Energy Policy Act of 1992, PublicLaw 102-486, Title I-Energy Efficiency, Subtitle A-Buildings, Sec. 101. Building Energy Efficiency Standards*, Tech. Rep. (1992).

[25] P. Depecker, C. Menezo, and S. Lepers, *Design of buildings shape and energetic consumption*, Building and Environment **30**, 201 (2001).

[26] W. Pessenlehner and A. Mahdavi, *Building morphology, transparency, and energy performance*, *Proceedings of the Eighth International IBPSA Conference* (Eindhoven, Netherlands, 2003).

[27] R. Ourghi, A. Al-Anzi, and M. Krarti, *A simplified analysis method to predict the impact of shape on annual energy use for office buildings*, Energy Conversion and Management **48**, 300 (2007).

[28] M. R. Atif, D. E. Claridge, L. O. Boyer, and L. O. Degelman, *Atrium buildings: Thermal performance and climatic factors*, ASHRAE Transactions **101**, 454 (1995).

[29] F. A. Mills, *Energy-efficient commercial atrium buildings*, ASHRAE Transactions **100**, 665 (1994).

[30] The United States Energy Information Administration, *Residential energy consumption survey, structural and geographic characteristics by type of housing unit*, `http://www.eia.gov/consumption/residential/data/2009/#undefined` (2009), accessed: 2013-07-16.

[31] K. Labs, J. Carmody, R. Sterling, L. Shen, Y. J. Huang, and D. Parker, *Building*

Foundation Design Handbook, ORNL/Sub/86-72143/1 (Oak Ridge National Laboratory, 1988).

[32] J. Neymark, R. Judkoff, I. Beausoleil-Morrison, A. Ben-Nakhi, M. Crowley, M. Deru, R. Henninger, H. Ribberink, J. Thornton, A. Wijsman, and M. Witte, *The International Energy Agency Building Energy Simulation Test and Diagnostic Method (IEA BESTEST) In-depth Diagnostic Cases for Ground Coupled Heat Transfer Related to Slab-on-grade Construction*, Tech. Rep. NREL/TP-550-43388, National Renewable Energy Laboratory, Golden, Colorado, USA (2008).

[33] *International Energy Outlook 2010*, Tech. Rep., The United States Energy Information Administration, U.S. Department of Energy, Washington, D.C. (2010).

[34] *2012 International Energy Conservation Code* (The International Code Council, Inc., Country Club Hills, IL, U.S.A, 2011).

[35] R. Hendron and C. Engebrecht, *Building America House Simulation Protocols*, Tech. Rep., National Renewable Energy Laboratory (2010).

[36] D. DiLaura, K. Houser, R. Mistrick, and G. Steffy, eds., *The Lighting Handbook* (The Illuminating Engineering Society, 2011), 10th ed.

[37] C. H. Culp and S. Andolsun, *Reducing base load energy use in residential architecture* (ASHRAE Summer Meeting, Salt Lake City, UT, U.S.A., 2008).

[38] The Population Reference Bureau, *World population data sheet*, `http://www.prb.org/Publications/Datasheets/2012/world-population-data-sheet/` (2012), accessed: 2013-07-16.

[39] The United States Census Bureau, *Characteristics of new single family homes completed*, `http://www.census.gov/construction/chars/completed.html` (2011), accessed: 2013-07-16.

[40] The United States Energy Information Administration, *Energy consumption by sector overview*, `http://www.eia.doe.gov/aer/pdf/pages/` (2009), accessed: 2013-07-16.

[41] The National Association of Home Builders, *Characteristics of new single family homes*, `http://www.nahb.org/generic.aspx?genericContentID=64030&fromGSA=1` (2006),

accessed: 2013-07-16.

[42] The Energy Programs Consortium, *Income, energy efficiency and emissions- The critical relationship*, http://www.energyprograms.org/wp-content/uploads/2011/10/02_2008_080226.pdf (2008), accessed: 2013-07-16.

[43] J. McIlvaine, K. Sutherland, K. Schleith, and S. Chandra, *Exploring cost-effective, high performance residential retrofits for affordable housing in the hot humid climate*, *Proceedings of the 17th Symposium for Improving Building Systems in Hot and Humid Climates* (Austin, Texas, 2010).

[44] The National Affordable Housing Network, *The high performance housing partnership (TX)*, http://www.nahn.com/about-us/research-development/ (2000), accessed: 2013-07-16.

[45] J. Haberl, T. Bou-Saada, V. Soebarto, and A. Reddy, *Use of calibrated simulation for evaluation of residential energy conservation options of two Habitat for Humanity houses in houston, Texas*, *Proceedings of the Eleventh Symposium on Improving Building Systems in Hot and Humid Climates* (Forth Forth, TX, 1998).

[46] J. C. Gardner, *The successful design, construction and live-ability of an energy efficient home in a hot and humid climate*, *Proceedings of the Fifteenth Symposium on Improving Building Systems in Hot and Humid Climates* (Orlando, FL, 2006).

[47] S. Kim, *An Analysis of International Energy Conservation Code (IECC) Compliant Single-family Residential Energy Use*, Ph.D. Dissertation, Texas A&M University (2006).

[48] V. Kootin-Sanwu, J. S. Haberl, and B. Kim, *Comfort conditions in a Habitat for Humanity house in central Texas*, *Proceedings of the 12th Symposium on Improving Building Systems in Hot and Humid Climates*, pp. 129–135 (2000).

[49] M. Malhotra, *An Analysis of Off-grid, Off-pipe Housing in Six U.S. Climates*, Ph.D. Dissertation, Texas A&M University (2009).

[50] V. Kootin-Sanwu, *An Analysis of Low Cost, Energy Efficient Housing for Low-income Residents of Hot and Humid Climates*, Ph.D. Dissertation, Texas A&M University

(2004).

[51] K. T. Papakostas and B. A. Sotiropoulos, *Occupational and energy behaviour patterns in Greek residences*, Energy and Buildings **26**, 207 (1997).

[52] J. Reynolds, *Courtyards- Aesthetic, Social and Thermal Delight* (John Wiley & Sons, Inc., New York, USA, 2002).

[53] S. Al-Azzawi, *Indigenous courtyard houses, a comprehensive checklist for identifying, analysing and appraising their passive solar design characteristics*, Renewable Energy **5**, 1099 (1994).

[54] S. Sharples and R. Bensalem, *Airflow in courtyard and atrium buildings in the urban environment: A wind tunnel study*, Solar Energy **70**, 237 (2001).

[55] S. Samant, *A critical review of articles published on atrium geometry and surface reflectances on daylighting in an atrium and its adjoining spaces*, Architectural Science Review **53**, 145 (2010).

[56] C. Hinrichs, *The Architecture of the Courtyard House as Generated by Passive Solar Energy and Other Factors* (Manchester University, Manchester, 1987).

[57] M. A. Mohsen, *Solar radiation and courtyard house forms- I. A mathematical model*, Building and Environment **14**, 89 (1979).

[58] A. S. Muhaisen and M. B. Gadi, *Effect of courtyard proportions on solar heat gain and energy requirement in the temperate climate of Rome*, Building and Environment **41**, 245 (2006).

[59] A.-T. Nguyen, Q.-B. Tran, D.-Q. Tran, and S. Reiter, *An investigation on climate responsive design strategies of vernacular housing in Vietnam*, Building and Environment **46**, 2088 (2011).

[60] T. Kubota, D. T. H. Chyee, and S. Ahmad, *The effects of night ventilation technique on indoor thermal environment for residential buildings in hot-humid climate of Malaysia*, Energy and Buildings **41**, 829 (2009).

[61] J. H. Klote and J. A. Milke, *Principles of Smoke Management*, chap. 5 (ASHRAE, 2002).

[62] L. Deng, *A systematic study of natural ventilation characteristics in tall residential buildings with atrium*, *Proceedings of the Third International Conference on Built Environment and Public Health*, vol. I&II, pp. 490–495 (2009).

[63] J. Li, *Influence of horizontal openings on buoyancy-driven natural ventilation of an atrium in high-rise residential buildings*, *Proceedings of the 6^{th} International Symposium on Heating, Ventilating and Air Conditioning*, vol. I-III, pp. 1224–1231 (2009).

[64] M. H. Zhang, *Effect of atrium size on thermal buoyancy-driven ventilation of high-rise residential buildings: A CFD study*, *Proceedings of the 6^{th} International Symposium on Heating, Ventilating and Air Conditioning*, vol. I-III, pp. 1240–1247 (2009).

[65] A. S. Dili, M. A. Naseer, and T. Z. Varghese, *Passive control methods for a comfortable indoor environment: Comparative investigation of traditional and modern architecture of Kerala in summer*, Energy and Buildings **43**, 653 (2011).

[66] N. Sadafi, E. Salleh, L. C. Haw, and Z. Jaafar, *Evaluating thermal effects of internal courtyard in a tropical terrace house by computational simulation*, Energy and Buildings **43**, 887 (2011).

[67] I. Rajapaksha, H. Nagai, and M. Okumiya, *A ventilation courtyard as a passive cooling strategy in the warm humid tropics*, Renewable Energy **28**, 1755 (2003).

[68] *Design of Low-cost Housing and Community Facilities*, chap. Climate and House Design I, p. 93 (United Nations Department of Economic and Social Affairs, New York, 1971).

[69] *Climatic Design*, Tech. Rep., The Tropical Advisory Service, London (1966).

[70] *ASHRAE Handbook- Fundamentals* (American Society of Heating, Refrigerating and Air-Conditioning Engineers, Inc., Atlanta, GA, 2009).

[71] A. Bagneid, *The Creation of a Courtyard Microclimate Thermal Model for the Analysis of Courtyard Houses*, Ph.D. Dissertation, Texas A&M University (2006).

[72] H. Gordon, *Draft Outline, IEA Task XI*, chap. Atrium Decision (Burt Hill Kosar Rittelmann Associates, 1989).

[73] L. Boyer and K. Song, *Daylighting prediction and sunlighting strategies for atrium design in hot countries*, *ASHRAE Transactions*, vol. 100, pp. 676–682 (1994).

[74] G. Smith, *Materials and systems for efficient lighting and delivery of daylight*, Solar Energy Materials and Solar Cells **84**, 395 (2004).

[75] A. Jain, *Optimising the control strategies for switchable glazing for energy and daylight in an office building*, *Proceedings of the 28th National Passive Solar Conference*, pp. 809–813 (American Solar Energy Society, Austin, Texas, 2003).

[76] S. Selkowitz, *The elusive challenge of daylighted buildings: A brief review 25 years later on*, *Proceedings of the International Daylighting Conference*, pp. 231–235 (Ottawa: Natural Resources Canada, 1998).

[77] S. Robinson-Gayle, M. Kolokotroni, A. Cripps, and S. Tanno, *Etfe foil cushions in roofs and atria*, Construction and Building Materials **15**, 323 (2001).

[78] S. Rouanet and A. Bobkowicz, *First solar daylighting aerogel panels: A green vision comes true!*, *Proceedings of the 28th National Passive Solar Conference*, pp. 821–825 (American Solar Energy Society, Austin, Texas, 2003).

[79] P. Pfrommer, K. Lomas, C. Seale, and C. Kupke, *The radiation transfer through coated and tinted glazing*, Solar Energy **54**, 287 (1995).

[80] W. Y. Hung and W. K. Chow, *A review on architectural aspects of atrium buildings*, Architectural Science Review **44**, 285 (2001).

[81] B. Matusiak and O. Aschehoug, *Daylighting systems for linear atria at high latitudes*, pp. 333–340 (International Daylighting Conference, Ottawa: Natural Resources Canada, 1998).

[82] B. Givoni, *Climate Considerations in Building and Urban Design* (New York: Van Nostrand Reinhold, 1998).

[83] R. McCluney and S. Chandra, *Comparison of window shading strategies for heat gain prevention*, *Proceedings of 9th National Passive Solar Conference* (American Solar Energy Society, 1984).

[84] R. J. Saxon, *Atrium Buildings* (New York: Architectural Press, 1986).

[85] P.-C. Liu, H.-T. Lin, and J.-H. Chou, *Evaluation of buoyancy-driven ventilation in atrium buildings using computational fluid dynamics and reduced-scale air model*, Build-

ing and Environment **44**, 1970 (2009).

[86] J.-T. Lin and Y. Chuah, *A study on the potential of natural ventilation and cooling for large spaces in subtropical climatic regions*, Building and Environment **46**, 89 (2011).

[87] X. Wang, C. Huang, and W. Cao, *Mathematical modeling and experimental study on vertical temperature distribution of hybrid ventilation in an atrium building*, Energy and Buildings **41**, 907 (2009).

[88] T. Ayata and O. Yıldız, *Investigating the potential use of natural ventilation in new building designs in Turkey*, Energy and Buildings **38**, 959 (2006).

[89] J. O. P. Cheung and C.-H. Liu, *CFD simulations of natural ventilation behavior in high-rise buildings in regular and staggered arrangements at various spacings*, Energy and Buildings **43**, 1149 (2011).

[90] A. Laouadi and M. R. Atif, *Comparison between computed and field measured thermal parameters in an atrium building*, Building and Environment **34**, 129 (1999).

[91] O. Gocer, A. Tavil, and E. Ozkan, *Thermal performance simulation of an atrium building*, *Proceedings of eSim 2006 Building Performance Simulation Conference* (Faculty of Architecture, Landscape, and Design, University of Toronto, Canada, 2006).

[92] Y. Pan, Y. Li, and Z. Huang, *Study on energy modeling methods of atrium buildings*, *Proceedings of the Eleventh International IBPSA Conference* (Glasgow, Scotland, 2009).

[93] D. Haltrecht, R. Zmeureanu, and I. Beausoleil-Morrison, *Defining the methodology for the next-generation HOT2000 simulator*, *Proceedings of Building Simulation*, vol. 1, pp. 61–68 (Building Simulation '99, Kyoto, 1999).

[94] C. A. Rundle, M. F. Lightstone, P. Oosthuizen, P. Karava, and E. Mouriki, *Validation of computational fluid dynamics simulations for atria geometries*, Building and Environment **46**, 1343 (2011).

[95] L. Gu, *Airflow network modeling in EnergyPlus*, *Proceedings of the 10th International Building Performance Simulation Association Conference and Exhibition* (Beijing, China, 2007).

[96] G. N. Walton, *AIRNET- A Computer Program for Building Airflow Network Modeling*, Tech. Rep. NISTIR 89-4072, The United States Department of Commence, National Institute of Standards and Technology, National Engineering Laboratory, Center for Building Research, Building Environment Division, Gaithersburg, MD (1989).

[97] H. E. Feustel and A. Rayner-Hooson, *COMIS Fundamentals*, Tech. Rep. LBL-28560, The Applied Science Division, Lawrence Berkeley Laboratory, Berkeley, CA 94720 (1990).

[98] L. Gu and M. V. Swami, *A preliminary computational investigation of radon reduction strategies in a large building*, *Proceedings of the 1993 International Radon Conference* (Florida Solar Energy Center, Cape Canaveral, FL, 1993).

[99] J. L. M. Hensen, *Modeling coupled heat and airflow: Ping-pong vs. onions*, *Proceedings of 16th AIVC conference, Palm Springs* (Palm Springs, USA, 1995).

[100] M. P. Modera and B. Treidler, *Improved modeling of HVAC system/envelope interactions in residential buildings*, *The Proceedings of the ASME International Solar Energy Conference* (1995).

[101] J. Huang, F. Winkelmann, F. Buhl, C. Pedersen, D. Fisher, R. Liesen, R. Taylor, R. Strand, D. Crawley, and L. Lawrie, *Linking the COMIS multizone airflow model with the EnergyPlus building energy simulation program*, *Proceedings of Building Simulation 99*, vol. 2, pp. 1065–1070 (1999).

[102] *A Building Energy Simulation Environment, User Guide Version 8 Series, ESRU Manual U95/1*, University of Strathclyde, Energy System Division, Glasgow, UK (1995).

[103] *EnergyPlus Engineering Reference, the Reference to EnergyPlus Calculations*, Ernest Orlando Lawrence Berkeley National Laboratory, United States Department of Energy (2010).

[104] *EnergyPlus Input Output Reference, the Encyclopedic Reference to EnergyPlus Input and Output*, Ernest Orlando Lawrence Berkeley National Laboratory, United States Department of Energy (2010).

[105] A. Voetzel, F. R. Carrie, and G. Guarracino, *Thermal ventilation modelling of large*

highly-glazed spaces, Energy and Buildings **33**, 121 (2001).

[106] I. Bryn and P.-A. Schiefloe, *Atrium Models for the Analysis of Thermal Comfort and Energy Use*, Tech. Rep., The International Energy Agency Solar Heating and Cooling Programme and Selskapet for Industriell og Teknisk Forskning ved Norges Tekniske Høgskole, Trondheim, Norway (1996).

[107] Y. Jaluria and K. E. Torrance, *Computational Heat Transfer*, p. 366 (Hemisphere, New York, 1986).

[108] H. Pfrommer, *Thermal Modeling of Highly Glazed Spaces*, p. 229 (De Montfort University, Leicester, 1995).

[109] G. Tan and L. R. Glicksman, *Application of integrating multizone model with CFD simulation to natural ventilation prediction*, Energy and Buildings **37**, 1049 (2005).

[110] A. J. Klote, *CFD analysis of atrium smoke control at the newseum*, ASHRAE Transactions **111**, 567 (2005).

[111] H. B. Awbi, *Air movement in naturally ventilated buildings*, *Proceedings of the International Conference Passive and Low Energy Cooling for the Built Environment* (Santorini Island, Greece, 2005).

[112] G. Gan and S. B. Riffat, *CFD modelling of airflow and thermal performance of an atrium integrated with photovoltaics*, Building and Environment **39**, 735 (2004).

[113] P. Haves, P. F. Linden, and G. Carrilho da Graca, *Use of simulation in the design of a large, naturally ventilated office building*, Building Services Engineering Research and Technology **25**, 211 (2004).

[114] S. Kato, S. Murakami, S. Shoya, F. Hanyu, and J. Zeng, *CFD analysis of flow and temperature fields in atrium with ceiling height of 130m*, ASHRAE Transactions **101**, 1144 (1995).

[115] E. Djunaedy, J. L. M. Hensen, and M. G. L. C. Loomans, *External coupling between CFD and energy simulation: Implementation and validation*, ASHRAE Transactions **111** (2005).

[116] J. Gao, X. Zhang, and J. N. Zhao, *Numerical determination of convection coefficient*

for internal surfaces in buildings dominated by thermally stratified flows, Journal of Building Physics **31**, 213 (2008).

[117] Z. Zhai, Q. Chen, P. Haves, and J. H. Klems, *On approaches to couple energy simulation and computational fluid dynamics programs*, Building and Environment **37**, 857 (2002).

[118] Y. Pan, Y. Li, Z. Huang, and G. Wu, *Study on simulation methods of atrium building cooling load in hot and humid regions*, Energy and Buildings **42**, 1654 (2010).

[119] F. Winkelmann, *Daylighting Calculation in DOE-2*, Tech. Rep. LBL-11353, Simulation Research Group, Lawrence Berkeley National Laboratory, Berkeley, CA. (1983).

[120] F. C. Winkelmann and S. Selkowitz, *Daylighting simulation in the DOE-2 building energy analysis program*, Energy and Buildings **8**, 271 (1985).

[121] R. J. Hitchcock and W. L. Carroll, *Delight: A daylighting and electric lighting simulation engine*, *Proceedings of Eight International IBPSA Conference* (Eindhoven, Netherlands, 2003).

[122] S. Selkowitz, J. J. Kim, M. Navvab, and F. Winkelmann, *The DOE-2 and SUPERLITE daylighting programs*, *Proceedings of the* 7^{th} *National Passive Solar Conference*, LBL-14569 (Lawrence Berkeley National Laboratory, Knoxville, TN, 1982).

[123] D. B. Crawley, L. K. Lawrie, F. C. Winkelmann, W. F. Buhl, C. O. Pedersen, R. K. Strand, R. J. Liesen, D. E. Fisher, M. J. Witte, R. H. Henninger, J. Glazer, and D. Shirey, *EnergyPlus: New, capable, and linked*, *Proceedings of the Performance of Exterior Envelopes of Whole Buildings VIII* (ASHRAE, Clearwater Beach, Florida, 2001).

[124] P. G. Loutzenhiser, G. M. Maxwell, and H. Manz, *An empirical validation of daylighting algorithms and associated interactions in building energy simulation programs using various shading devices and windows*, Energy **32**, 1855 (2007).

[125] R. M. Loura, E. Sad de Assis, and V. Goncalves de Souza, *Analysis of EnergyPlus module results- A Brazilian case*, *Proceedings of Eleventh International IBPSA Conference* (Glasgow, Scotland, 2009).

[126] G. Ramos and E. Ghisi, *Analysis of daylight calculated using the EnergyPlus pro-*

gramme, Renewable and Sustainable Energy Reviews **14**, 1948 (2010).

[127] J. Mardaljevic, *Validation of a lighting simulation program under real sky conditions*, Lighting Research & Technology **27**, 181 (1995).

[128] M. Fontoynont, P. Laforgue, R. Mitanchey, M. Aizlewood, J. Butt, W. Carroll, R. Hitchock, H. Erhorn, J. De Boer, M. DirksMöller, L. Michel, B. Paule, J.-L. Scartezzini, and M. R. G. Bodart, *Validation of Daylighting Computer Programs*, Tech. Rep., IEA SHC Task 21/ ECBCS Annex 29 (1999).

[129] J. Du and S. Sharples, *Assessing and predicting average daylight factors of adjoining spaces in atrium buildings under overcast sky*, Building and Environment **46**, 2142 (2011).

[130] C. Reinhart and A. Fitz, *Findings from a survey on the current use of daylight simulations in building design*, Energy and Buildings **38**, 824 (2006).

[131] B. A. Rock and L. L. Ochs, *Slab-on-grade heating load factors for wood-framed buildings*, Energy and Buildings **33**, 759 (2001).

[132] B. A. Rock, *Sensitivity study of slab-on-grade transient heat transfer model parameters*, ASHRAE Transactions **110**, 177 (2004).

[133] B. A. Rock, *A user-friendly model and coefficients for slab-on-grade load and energy calculations*, ASHRAE Transactions:Research pp. 122–136 (2005).

[134] W. P. Bahnfleth, *Three Dimensional Modeling of Heat Transfer from Slab Floors*, Ph.D. Dissertation, University of Illinois (1989).

[135] Y. J. Huang, L. S. Shen, J. C. Bull, and L. F. Goldberg, *Whole-house simulation of foundation heat flows using the DOE-2.1C program*, ASHRAE Transactions **94** (1988).

[136] F. Winkelmann, *Underground surfaces: How to get a better underground surface heat transfer calculation in DOE-2.1E*, Building Energy Simulation User News **23**, 19 (2002).

[137] T. Kasuda and P. R. Achenbach, *Earth temperature and thermal diffusivity at selected stations in the United States*, ASHRAE Transactions **71**, 61 (1965).

[138] E. Clements, *Three Dimensional Foundation Heat Transfer Modules for Whole-building*

Energy Analysis, Master's thesis, Pennsylvania State University (2004).

[139] S. V. Patankar, *Numerical Heat Transfer and Fluid Flow* (Hemisphere Publishing Corporation, New York, USA, 1980).

[140] *TRNSYS 17 A Transient System Simulation Program, Volume 4: Mathematical Reference*, Solar Energy Laboratory and University of Wisconsin-Madison and TRANSSOLAR Energietechnik GmbH and CSTB- Centre Scientifique et Technique du Bâtiment and TESS- Thermal Energy Systems Specialists (2010).

[141] T. P. McDowell, J. W. Thornton, and M. J. Duffy, *Comparison of a ground-coupling reference standard model to simplified approaches*, *Proceedings of Eleventh International IBPSA Conference* (Glasgow, Scotland, 2009).

[142] R. Judkoff and J. Neymark, *The International Energy Agency Building Energy Simulation Test (IEA BESTEST) and Diagnostic Method*, Tech. Rep. NREL/TP-472-6231, National Renewable Energy Laboratory, Golden, Colorado, USA (1995).

[143] R. Judkoff, D. Wortman, B. O'Doherty, and J. Burch, *A Methodology for Validating Building Energy Analysis Simulations*, Tech. Rep. NREL/TP-550-42059, National Renewable Energy Laboratory, Golden, Colorado, USA (2008).

[144] R. Judkoff and J. Neymark, *Home Energy Rating System Building Energy Simulation Test (HERS BESTEST) 1 & 2*, Tech. Rep. NREL/TP-472-7332, National Renewable Energy Laboratory, Golden, Colorado, USA (1995).

[145] F. S. Wang, *Mathematical modeling and computer simulation of insulation systems in belowgrade applications*, *Proceedings of Thermal Performance of the Exterior Envelopes of Buildings*, pp. 456–489 (1979).

[146] RESNET, *Procedures for Verification of International Energy Conservation Code Performance Path Calculation Tools*, Tech. Rep. 07-003, Residential Energy Services Network (2007).

[147] M. Krarti and P. Chuangchid, *Cooler Floor Heat Gain for Refrigerated Structures, Final Report*, ASHRAE Research Project TRP-953 (2002).

[148] M. Deru, R. Judkoff, and J. Neymark, *Proposed IEA BESTEST Ground-coupled Cases*,

IEA Working Document, National Renewable Energy Laboratory, In Conjunction with the International Energy Agency, Solar Heating and Cooling Programme Task 22, Golden, Colorado, USA (2003).

[149] R. H. Henninger and M. J. Witte, *EnergyPlus energy simulation software: Testing and validation*, `http://apps1.eere.energy.gov/` (2011), accessed: 2013-07-16.

[150] S. Spitler, S. Rees, and D. Xiao, *Development of an Analytical Verification Test Suite for Whole Building Energy Simulation Programs- Building Fabric*, Final Report for ASHRAE 1052-RP, Oklahoma State University School Mechanical and Aerospace Engineering, Stillwater, Oklahoma, USA (2001).

[151] A. E. Delsante, A. N. Stokes, and P. J. Walsh, *Application of Fourier transforms to periodic heat flow into the ground under a building*, International Journal of Heat Mass Transfer **26**, 121 (1983).

[152] J. Thornton, *Modeler Report for BESTEST Cases GC10a-GC80c, TRNSYS Version 16.1*, Tech. Rep., Thermal Energy System Specialists, Madison, Wisconsin, USA (2007).

[153] A. Nakhi, *Modeler Report for BESTEST Cases GC10a-GC80c, FLUENT Version 6.0.20*, Tech. Rep., Public Authority for Applied Education and Training, State of Kuwait (2008).

[154] *Fluent 6.3 User's Guide*, Fluent Incorporated, Lebanon, New Hampshire, USA (2007).

[155] M. Crowley, *Modeler Report for BESTEST Cases GC10a-GC80c, MATLAB 7.0.4.365 (R14) Service Pack 2*, Tech. Rep., Dublin Institute of Technology, Dublin, Ireland (2007).

[156] *The MathWorks, Getting Started with MATLAB*, The MathWorks Inc. (2007).

[157] J. Huang, N. Bourassa, F. Buhl, E. Erdem, and R. Hitchcock, *Using EnergyPlus for California title-24 compliance calculations*, *Proceedings of the Second National IBPSA-USA Conference* (Cambridge, MA, U.S.A, 2006).

[158] D. B. Crawley, L. K. Lawrie, C. O. Pedersen, F. C. Winkelmann, M. J. Witte, R. K. Strand, R. J. Liesen, W. F. Buhl, Y. J. Huang, R. H. Henninger, J. Glazer, D. E. Fisher,

D. B. Shirey III, B. T. Griffith, P. G. Ellis, and L. Gu, *EnergyPlus: New, capable, and linked*, Journal of Architectural and Planning Research **21**, 292 (2004).

[159] S. Andolsun and C. H. Culp, *A comparison of EnergyPlus with DOE-2 based on multiple cases from a sealed box to a residential building*, *Proceedings of the Sixteenth Symposium on Improving Building Systems in Hot and Humid Climates* (Plano, TX, U.S.A., 2008).

[160] S. Andolsun, C. H. Culp, and J. Haberl, *EnergyPlus vs DOE-2: The effect of ground coupling on heating and cooling energy consumption of a slab-on-grade code house in a cold climate*, *Proceedings of the Fourth National IBPSA-USA Conference* (New York, U.S.A., 2010).

[161] S. Andolsun, C. H. Culp, J. Haberl, and M. Witte, *EnergyPlus vs DOE-2.1E: The effect of ground coupling on energy use of a code house with basement in a hot-humid climate*, Energy and Buildings **43**, 1663 (2011).

[162] M. Krarti, P. Chuangchid, and P. Ihm, *Foundation heat transfer module for EnergyPlus program*, *Proceedings of the Seventh International IBPSA Conference* (Rio de Janeiro, Brazil, 2001).

[163] R. Sullivan, J. Bull, P. Davis, S. Nozaki, Z. Cumali, and G. Meixel, *Description of an earth-contact modeling capability in the DOE-2.1B*, Energy Analysis Program **91**, 15 (1985).

[164] *ANSI/ASHRAE Standard 140-2007 Standard Method of Test for the Evaluation of Building Energy Analysis Computer Programs* (American Society of Heating, Refrigerating and Air-Conditioning Engineers, Inc., Atlanta, GA, 2008).

[165] *Lecture 24: Ground Heat Transfer. EnergyPlus University Course Teaching Material*, GARD Analytics, University of Illinois at Illinois, National Renewable Energy Laboratory, United States Department of Energy (2003).

[166] *2009 International Energy Conservation Code* (International Code Council, Inc., Country Club Hills, IL, U.S.A, 2009).

[167] M. T. Anello, D. S. Parker, J. R. Sherwin, and K. Richards, *Measured impact of advanced windows on cooling energy use*, *Proceedings of the 2000 ACEEE Summer*

Study, vol. 1, pp. 29–38 (2000).

[168] R. K. Pletzer, J. W. Jones, and B. D. Hunn, *Energy savings resulting from shading devices on single family residences in Austin, Texas*, *Proceedings of the Fourth Annual Symposium on Improving Building Energy Efficiency in Hot and Humid Climate*, pp. 112–121 (1987).

[169] H. E. Feustel, *COMIS- An International Multizone Air-flow and Contaminant Transport Model*, Tech. Rep. LBNL-42182, Lawrence Berkeley National Laboratory, Environmental Energy Technologies Division (1998).

[170] W. T. Grondzik, A. G. Kwok, B. Stein, and J. S. Reynolds, *Mechanical and Electrical Equipment for Buildings* (John Wiley & Sons, Inc., Hoboken, New Jersey, U.S.A, 2010), 11th ed.

[171] *Ventilation and Acceptable Indoor Air Quality in Low-rise Residential Buildings* (American Society of Heating, Refrigerating and Air Conditioning Engineers, Atlanta, GA, 2010).

[172] M. Sherman and J. McWilliams, *Air leakage of U.S. homes: Model prediction*, `http://epb.lbl.gov/publications/pdf/lbnl-62078.pdf` (2007), accessed: 2013-07-16.

[173] *Bathroom vent fan capacity & vent fan noise suggestions*, `http://inspectapedia.com/interiors/Bathroom_Ventilation.htm` (2013), accessed: 2013-07-16.

[174] M. Wassmer, *A Component-based Model for Residential Air Conditioner and Heat Pump Energy Calculations*, Master's thesis, University of Colorado at Boulder (2003).

[175] *Duct Insulation*, Tech. Rep. EPA 430-F-97-028, The United States Environmental Protection Agency, Washington, D.C. (2000).

[176] *ASHRAE Handbook- HVAC Systems and Equipment* (American Society of Heating, Refrigerating and Air-Conditioning Engineers, Inc., Atlanta, GA, 2008).

[177] B. Stein, *Building Technology, Mechanical & Electric Systems* (John Wiley & Sons, Inc., 1997), 2nd ed.

[178] H. Rutkowski, *Residential Duct Systems Manual D* (Air Conditioning Contractors of America, Washington, D.C. 20009, 1995), 2nd ed.

[179] R. G. Huebscher, *Friction equivalents for round, square and rectangular ducts*, ASHVE Transactions **54**, 101 (1948).

[180] *DOE-2 Engineers Manual, Version 2.1A*, Technical Information Center, United States Department of Energy (1982).

[181] G. Walton, *Thermal Analysis Research Program Reference Manual*, The National Bureau of Standards (1983), NBSSIR 83-2655.

[182] D. E. Fisher and C. O. Pedersen, *Convective heat transfer in building energy and thermal load calculations*, ASHRAE Transactions **103** (1997).

[183] H. C. Hottel and A. F. Sarofim, *Radiative Transfer* (McGraw-Hill, New York, 1967).

[184] J. E. Seem, *Modeling of Heat in Buildings*, Ph.D. Dissertation, University of Wisconsin Madison, Solar Energy Laboratory (1987).

[185] R. Perez, P. Ineichen, R. Seals, J. Michalsky, and R. Stewart, *Modeling daylight availability and irradiance components from direct and global irradiance*, Solar Energy **44**, 271 (1990).

[186] H. Kim, J.-C. Baltazar, J. Haberl, and B. Yazdani, *A comparison of building energy code stringency: 2009 IRC versus 2012 IRC for single-family residences in Texas*, `http://www.amarillo.gov/departments/building_safety/pdf/ESL-Comparison_2009-2012.pdf` (2011), accessed: 2013-07-16.